Daily to seasonal environmental variability from giant clams revealed via spatially-resolved geochemical analyses and laboratory culture experiments: Case studies from Recent and Miocene Indo-Pacific *Tridacna* shells

Viola Warter

supervised by

Wolfgang Müller

A thesis submitted for the degree of

Doctor of Philosophy

April 2016

Department of Earth Sciences

Royal Holloway University of London

Egham, UK

Declaration of authorship

I, Viola Warter, hereby declare that this thesis and the work presented in it is entirely my own. Where I have consulted the work of others, this is always clearly stated.

Signed: 

Date:

Everything that happens to us leaves some trace behind; everything contributes imperceptibly to make us what we are.

Johann Wolfgang von Goethe

Acknowledgements

The first two years of this PhD project, conducted under the Initial Training Network *Throughflow*, were funded through the Marie Curie Actions Plan, Seventh Framework Program of the European Union (grant no. 237922). An additional one-off funding received from the Earth Sciences Department, Royal Holloway University of London, partly covered the costs towards the ultra-high resolution LA-ICPMS analysis. I am very grateful for the financial support received through the *Kirsty Brown Memorial Fund* as well as the *University of London Grants for PGR Study Costs,* both of which enabled my research trip to Jerusalem, Israel, where I conducted the so important *Tridacna* culture experiments.

Firstly, I would like to thank my supervisor, Wolfgang Müller, for the continuous guidance and support throughout this PhD process until completion, for introducing me to the field of LA-ICPMS and sharing his expert knowledge. I am also grateful for the opportunity to gain work experience in such an excellent research environment.

I would like to thank Jonathan Erez, for enabling the *Tridacna* culture in Jerusalem and the valuable time spent during our follow-up research meetings. Hagar, Adam, Mathan and Nadav, thanks for the technical support during the culture experiments, but also for your friendliness which made me feel sincerely welcome.

The help of the following persons during analysis and/or sample preparation is greatly acknowledged: Matthew Thirlwall, Christina Manning, Dave Alderton, Nathalie Grassineau, Dave Mattey, Norman Oxtoby, Neil Holloway, Alex Ball and Tomasz Goral. I wish to thank James Hainsworth and Ismael Ferrer from Media Cybernetics for providing the Image-Pro Premier 9.1 software. Thomas Barlow (BGS) is greatly acknowledged for the solution ICPMS analysis of the sweater samples.

I would like to thank the *Throughflow* Team, especially my fellow early stage researchers. You made my start so easy and this project most enjoyable: Amanda, Anja, Elena, Emanuela, Nadia, Nathan, Nick, Vedrana and Vibor. Willem Renema is greatly acknowledged for organizing the final *Throughflow* field trip to East Kalimantan. The *Tridacna* hunt in Indonesia was an unforgettable experience. Thanks to Frank Wesselingh for all his words of encouragement.

A very special thank you goes to Romain Doré, for always being by my side.
Thanks to my friends and family for reminding me what really matters.

Publications

Peer-reviewed journal articles associated with this thesis

Warter, V., Müller, W., Wesselingh, F.P., Todd, J.A., and Renema, W., 2015, Late Miocene seasonal to sub-decadal climate variability in the Indo-West Pacific (East Kalimantan, Indonesia) preserved in giant clams: Palaios, v. 30, p. 66-82.

Warter, V., and Müller, W., 2016, Daily growth and tidal rhythms in Miocene and modern giant clams revealed via ultra-high resolution LA-ICPMS analysis – A novel methodological approach towards improved sclerochemistry: Palaeogeography, Palaeoclimatology, Palaeoecology, doi:10.1016/j.palaeo.2016.03.019.

Journal article in preparation

Warter, V, Erez, J., and Müller, W., in preparation, Environmental vs physiological controls on daily trace element incorporation in *Tridacna crocea* from combined laboratory culturing and ultra-high resolution LA-ICPMS analysis: Intended for submission to Geochimica and Cosmochimica Acta.

Peer-reviewed journal articles relevant to, but not associated with this thesis

Reich, S., Warter, V., Wesselingh, F.P., Zwaan, J. H., Lourens, L., and Renema, W., 2015, Paleoecological significance of stable isotope ratios in Miocene tropical shallow marine habitats (Indonesia): Palaios, v. 30, p. 53-65.

Renema, W., Warter, V., Novak, V., Young, Y., Marshall, N., and Hasibuan, F., 2015, Ages of Miocene fossil localities in the Northern Kutai Basin (East Kalimantan, Indonesia): Palaios, v. 30, p. 26-39.

Journal article in preparation

Marshall, N., Manning, C., Novak, V., Warter, V., Renema, W. Anczkiewicz, R., and Müller, W., in preparation, Navigating the waters of strontium isotope stratigraphy from the Miocene of Borneo.

Abstract

This thesis presents high (weeks-months) and ultra-high (hours-days) resolution time-series proxy records obtained from Miocene, Recent and laboratory cultured giant clam (*Tridacna spp.*) shells.

In order to evaluate the fidelity of two Late Miocene *Tridacna* shells from East Kalimantan (Indonesia) to preserve any palaeoenvironmental variability, a multi-method approach was applied to assess pristine aragonite preservation. Combined usage of XRD, SEM/CL imaging and LA-ICPMS trace elemental screening has proven effective at detecting diagenetic shell alteration. Seasonally-resolved palaeoproxy records obtained from pristine shell aragonite provide insight into tropical sea surface temperature (SST) variability of the Indo-Pacific region during the late Miocene. $\delta^{18}O$ time-series records from two fossil shells indicate an average SST variability of 2.7 ± 2.1 and 4.6 ± 1.7 °C, respectively, which exceeds the modern-day seasonality in the Makassar Strait two- to threefold.

A novel methodological approach of ultra-high resolution LA-ICPMS analysis is introduced, which utilizes the combined capabilities of a rotating rectangular aperture (spot size 4 x 50 µm), the rapid signal washout of a Laurin two-volume laser ablation cell and slow compositional profiling (≤1.5 µm/s) and enables resolution of <10 µm compositional variability in B/Ca, Mg/Ca, Sr/Ca and Ba/Ca preserved within microscopically visible growth increments of both Recent and Miocene *Tridacna* shells. In comparison to a lower-resolution, seasonally resolved Miocene record, the ~10-20 µm element/Ca cycles were determined to be daily in origin, and a further ~14-15 day cyclicity, interpreted to reflect tidal periodicity, is detected in long-term (annual) daily resolved proxy records.

Laboratory culture experiments of *Tridacna crocea*, conducted under controlled environmental conditions including temperature, light level and seawater chemistry, allowed quantifying the temperature and light influence on shell growth rates. Corresponding ultra-high resolution LA-ICPMS analysis of the isotopically labelled cultured shell domains revealed that both temperature and light influence trace elemental incorporation into shell aragonite, yet biophysiology also controls trace element partitioning.

List of acronyms

AC	Alternating current
BSE	Backscattered electron
CITES	Convention on International Trade in Endangered Species
CL	Cathodoluminescence
CL	Confidence level
CRM	Certified reference material
DC	Direct current
DO	Dissolved oxygen
BGS	British Geological Survey
El/Ca	Element/Ca
EMPA	Electron micro probe analysis
ENSO	El Niño Southern Oscillation
ESEM	Environmental scanning electron microscope
FEG	Field emission gun
GEOREM	Geological and environmental reference materials
ICPOES	Inductively-coupled-plasma optical emission spectrometry
IOM	Insoluble organic matrix
IPWP	Indo-Pacific Warm Pool
ITF	Indonesians Throughflow
ITN	Initial Training Network
IRMS	Isotope ratio mass spectrometry
LA	Laser ablation
LA-ICPMS	Laser-ablation inductively-coupled-plasma mass spectrometry
LEC	Light-enhanced calcification
MH	Metal-halide
MPI	Max Planck Institute
MS	Mass spectrometer/mass spectrometry
NBS	National Bureau of Standards Publications
NHM	Natural History Museum
NIST	National Institute of Standards and Technology (US)
ORNL	Oak Ridge National Laboratories
PDB	Pee Dee Belemnite
PS	Photosynthesis

REE	Rare earth element
RF	Radio frequency
RHUL	Royal Holloway University of London
RSD	Relative standard deviation
RSE	Relative standard error
SD	Standard deviation
SE	Secondary electron
SE	Standard error
SEM	Scanning electron microscope
SIMS	Secondary ion mass spectrometry
SIS	Strontium Isotope Stratigraphy
SMOW	Standard mean ocean water
SOM	Soluble organic matrix
SRM	Standard reference material
SSS	Sea surface salinity
SST	Sea surface temperature
SW	Seawater
TIMS	Thermal ionization mass spectrometry
TOF	Time of flight
USGS	United States Geological Survey
UV	Ultra violet
VPDB	Vienna Pee Dee Belemnite
VP	Variable pressure
WEP	Western equatorial Pacific
XRD	X-ray diffraction

Summary

This thesis presents high (weeks-months) and ultra-high (hours-days) resolution time-series proxy records obtained from Miocene, Recent and laboratory cultured giant clam (*Tridacna spp.*) shells. The proxy variables of interest are the element/Ca ratios B/Ca, Mg/Ca, Sr/Ca and Ba/Ca and the stable oxygen isotope composition ($\delta^{18}O$). The overall aim of this thesis is to evaluate whether giant clams faithfully record and preserve any environmental and climate conditions they were exposed to during lifetime within their aragonite shells (Chapter 3). A novel methodological approach for ultra-high resolution LA-ICPMS is introduced, which allows the examination of *daily* trace element variability in giant clams, as well as detecting superimposed tidal periodicities (Chapter 4). Specially-designed laboratory culture experiments in tandem with ultra-high spatially resolved trace element analysis were conducted in order to attempt 1) a better understanding of the combined effects of biophysiological controls and environmental parameters with regards to trace element incorporation and 2) an evaluation of the robustness of the presented proxies to reconstruct environmental/climate variability (Chapter 5).

Thesis outline

Chapter 1 provides background information and sets the spatio-temporal context for this PhD project. It introduces giant clams and their important role as (palaeo)environmental archives and the different geochemical proxies investigated within this thesis. This chapter also gives a general overview of highly-resolved proxy records and in particular, those obtained from bivalve shells. Diagenesis and biophysiological effects are addressed as they represent key impediments towards reliable (palaeo)environmental reconstructions.

Chapter 2 lists and describes the methods used within this work. Because LA-ICPMS plays a major role for this study and is applied in all three applications (Chapters 3, 4 and 5), it is described in-depth.

Chapter 3 investigates the preservation of two Late Miocene *Tridacna* shells from East Kalimantan, Indonesia, using a multi-methodological approach of combined XRD, SEM/CL imaging, and LA-ICPMS trace elemental screening. Age estimates were obtained via strontium isotope stratigraphy (SIS). $\delta^{18}O$ records from pristine aragonite are used to reconstruct mean annual sea surface temperatures (SST) as well as the seasonal SST variability. This chapter is published in Palaios as Warter et al. (2015).

Chapter 4 introduces a novel methodological approach for ultra-high resolution LA-ICPMS analysis, which allows resolving <10 µm *daily* compositional variability in B/Ca, Mg/Ca, Sr/Ca and Ba/Ca, but also to detect longer-term tidal and seasonal cycles in both Miocene and modern giant clam shells. Complementary image processing analysis reveals a close correspondence between the daily and tidal-cyclic growth patterns and the geochemical composition of the shell. This chapter is published in Palaeogeography, Palaeoclimatology, Palaeoecology as Warter and Müller (2016).

Chapter 5 reports results of laboratory culture experiments of *Tridacna crocea*, conducted under tightly monitored and controlled environmental conditions including temperature, light level and seawater chemistry. Ultra-high resolution LA-ICPMS analysis of the isotopically labelled cultured shell portions allows evaluating which environmental factors predominantly trigger daily trace element variability. This chapter presents a manuscript draft aimed for submission to Geochimica and Cosmochimica Acta.

Chapter 6 provides a synopsis of the results obtained in Chapters 3, 4 and 5, evaluates the research findings critically, suggests future research directions and presents overall conclusions.

Chapter 1: Background and Introduction

This chapter provides background information and sets the spatio-temporal context for this PhD project. It introduces giant clams and their important role as (palaeo)environmental archives and the different geochemical proxies investigated within this thesis. This chapter also gives a general overview of highly-resolved proxy records and in particular, those obtained from bivalve shells. Diagenesis and biophysiological effects are addressed as they represent key impediments towards reliable (palaeo)environmental reconstructions.

1.1 Background

1.1.1 The *Throughflow* project and the hotspot of marine biodiversity

This PhD project started as part of the multidisciplinary research program *Throughflow* (http://ipaeg.org/), designed to disentangle the complex relationship between the 'Cenozoic evolution of the Indonesian Throughflow and the origins of the Indo-Pacific marine biodiversity'. The interdisciplinary approach of this Marie-Curie Initial Training Network (ITN) involved seven European institutions and research conducted in close collaboration between palaeontology, geology, stratigraphy, climatology, oceanography, ocean modelling and geochemistry.

The project's name is derived from the last remaining equatorial ocean gateway - the Indonesian Throughflow (ITF) (Fig. 1). Via the modern ITF, heat is transferred from the Pacific into the Indian Ocean and therefore the ITF plays a major role in the global thermohaline circulation (e.g. Kuhnt et al., 2004). Despite its important influence on global weather patterns and oceanic circulations, thus far only limited knowledge about the long-term variability of the ITF exists (Linsley et al., 2010).

South East Asia not only hosts the most diverse extant marine ecosystem, but it is also the area on earth with today's highest diversity of modern marine shallow biota, such as corals, molluscs and foraminifera (e.g. Renema et al., 2008). The exceptional biodiversity of the region probably originated in the Early Neogene (Wilson and Rosen, 1998). Marine biogeographers have named this diversity hotspot, situated in the Indo-West Pacific, the *Coral Triangle* (e.g. Hoeksema, 2007), which includes the waters of Indonesia, Malaysia, Philippines, Papua New Guinea, Solomon Islands and Timor Leste. The development of the extraordinary coral reef diversity in SE-Asia is likely to be the response to long-term environmental changes resulting from the gradual closure of the Indonesian Throughflow during the Oligocene-Miocene transition (Kuhnt et al., 2004; Hall et al., 2011).

Some of the main research results of the *Throughflow* project are published in a Palaios special issue entitled "*Biotic and environmental origins of the Southeast Asian marine biodiversity hotspot: The Throughflow project*" (http://www.bioone.org/toc/palo/30/1-2). This special issue also includes a publication by Warter et al. (2015), presented in Chapter 3 of this thesis, which investigates two Miocene giant clam shells from Bontang, East Kalimantan (Indonesia) with regards to their fidelity as palaeoenvironmental archives. The study further presents detailed information on Late Miocene sea surface temperature (SST) and its seasonal variability.

The study by Reich et al. (2015) examines stable isotope signatures ($\delta^{18}O$ and $\delta^{13}C$) of more than 150 fossil mollusc shells to reconstruct their palaeo-habitats in the Miocene of Java and East Kalimantan.

In Renema et al. (2015) results of strontium isotope stratigraphy (SIS) analyses are presented that - by complementing biostratigraphy - help evaluate ages of fossil assemblages collected from several different localities along the north-eastern margin of the Kutai Basin, Indonesia.
The latter two publications are not presented in this thesis, yet are indirectly associated with it and further provide important background information for this PhD thesis.

1.1.2 The Miocene

The Throughflow project is dedicated to elucidating the origin of the modern biodiversity hotspot in South East Asia. To this end, a fossil perspective of Neogene biodiversity was sought, which also included palaeoenvironmental records from Miocene fossils to ultimately contribute to a more comprehensive understanding of the Miocene climate evolution.
The Miocene (23.03 - 5.33 Ma) is an epoch of major change with respect to the Cenozoic climate history (Flower and Kennett, 1994). During the Eocene/Oligocene transition (~34 Ma), major ice sheets began to develop on East Antarctica. These began to shrink due to rising temperatures during later Oligocene (Zachos et al., 2001). The warming trend continued throughout the Miocene and climaxed in the Middle Miocene Climate Optimum (17-15 Ma), which was concomitant with a significant decrease of the Antarctic ice sheet. Following this climate optimum, gradual climate cooling occurred, leading to the reestablishment of the major Antarctic ice cover by the Late Miocene and permanent Northern Hemisphere glaciation at the Pliocene/Pleistocene transition (Zachos et al., 2008). The Miocene therefore not only clearly interrupts the general long-term cooling trend of the last ~50 Ma, but also sets the foundations for the modern Cenozoic icehouse state.
Whilst the overall Miocene climatic evolution is well documented by benthic foraminifera records (Lear et al., 2000; Zachos et al., 2001, 2008; Billups and Schrag, 2003), the mechanisms causing Miocene climate change are not well understood (Holbourn et al., 2007; Herold et al., 2012). Variations in carbon dioxide concentrations (e.g. Pagani et al., 1999; LaRiviere et al., 2012) and modifications in ocean circulations (Kuhnt et al., 2004; Singh and Gupta, 2010; Hall et al., 2011) are two main parameters which strongly influence climate dynamics.
Atmospheric CO_2 reconstructions for the past 0.8 Ma indicate a strong linkage between pCO_2 and oceanic temperatures (e.g. Hönisch et al., 2009), with the present day atmospheric CO_2 concentration of 400 ppm, being at least 120 ppm higher than at any point in the past 0.8 Ma (Lüthi et al., 2008). However, reaching further back in time, pCO_2 levels and their impact on temperature are poorly understood (Tripati et al., 2009) including suggestions that pCO_2 variability during the Miocene played only a secondary role in forcing climate change (Pagani et al., 1999). This finding is supported by the research of LaRiviere et al. (2012), which provides evidence for a decoupled relationship between atmospheric CO_2 concentrations and sea surface

temperatures (SSTs) during the Late Miocene in the North Pacific open ocean: SST estimates from ODP sediment cores based on both the alkenone unsaturation proxy and $\delta^{18}O$ measurements were up to 5 - 8°C warmer than today, whilst pCO_2, based on alkenone and leaf stomata estimates, remains below pre-industrial values. The authors suggest an oceanic circulation configuration strongly deviating from today, associated with a deeper thermocline and different cloud and vapor feedbacks as possible reasons for the higher temperatures despite the low CO_2 levels.

1.1.3 The Indonesian Throughflow (ITF)

The fossil giant clams investigated in Chapters 3 and 4 are derived from the direct influence area of the Indonesian Throughflow, which connects the Pacific and Indian Ocean and represents today's last remaining low-latitude ocean gateway (Fig. 1). Its gradual closure is considered to be a key initiator for climate change during the Miocene, not only for the South East Asian region but on a global scale (Cane and Molnar, 2001; Kuhnt et al., 2004; Singh and Gupta, 2010).

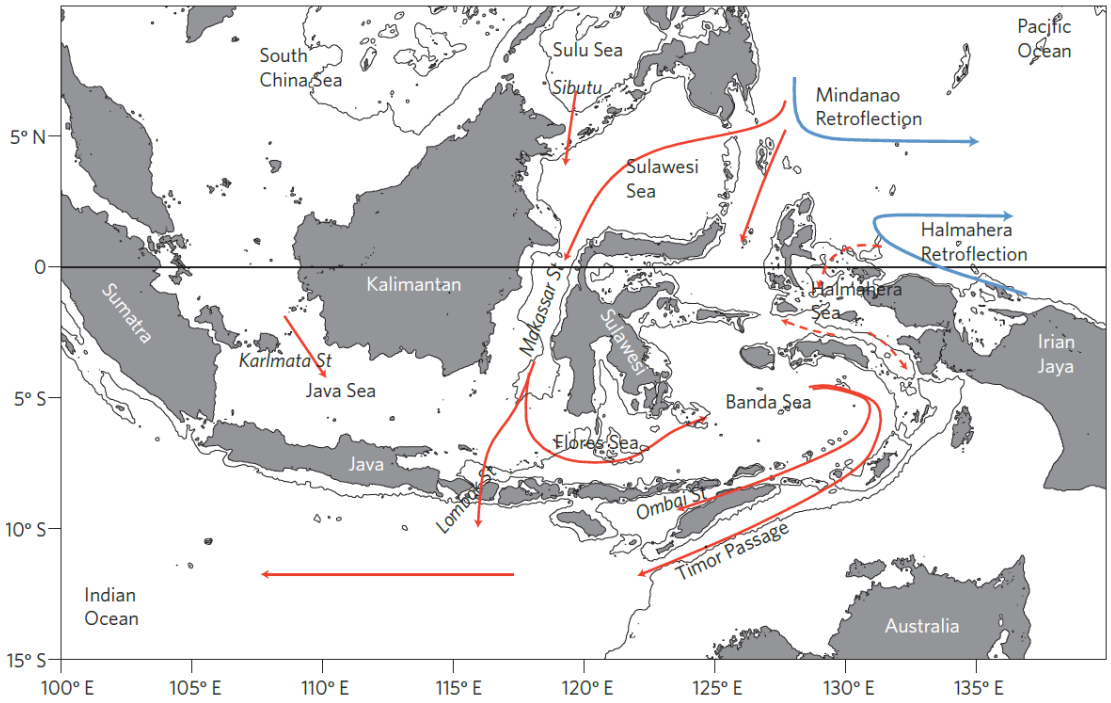

Figure 1. The mean pathways of the Indonesian Throughflow (ITF), indicated by the red arrows (from Sprintall et al., 2014).

The modern ITF exhibits a significant interannual variability, which is closely linked to the geographic extent and position of the West Pacific Warm Pool (Kuhnt et al., 2004) and El Niño–Southern Oscillation (ENSO) patterns (England and Huang, 2005). Its longer-term

palaeo-oceanographic history since the Oligocene/Miocene transition and associated long-term fluctuations in water mass throughflow are strongly controlled by tectonic reorganisation caused by convergence of the Indo-Australian and Philippine-Pacific plates with the stable Asian craton. The collision between the Australian plate and the island arcs on the Pacific plates initiated in the earliest Miocene (Srinivasan and Sinha, 2000; Kuhnt et al., 2004; Hall et al., 2011). Several closures of the ITF might have occurred since then (Srinivasan and Sinha, 2000). The main restriction of the ITF seems to have occurred between the Early and Middle Pliocene (5-3 Ma)(Srinivasan and Sinha, 2000; Cane and Molnar, 2001; Hall et al., 2011), when the continents had moved to their approximate recent position (Robinson et al., 2008). SE Asia is today known as the global centre of marine biodiversity (e.g. Santini and Winterbottom, 2002) and the fossil record provides evidence that this diversity was present at least from Early Miocene on (Renema et al., 2008). However, with respect to the Miocene interval, the interaction between the complex tectonic history of the SE-Asia - Australia collision zone, the corresponding oceanographic modulations of the Indonesian gateway, the associated climate and environmental change and the resulting biotic response are not well understood, even though they must have interplayed (Renema et al., 2008). The current lack of knowledge exists largely because only very few palaeoclimate proxy records from the Miocene ITF area are available. However, high-resolution proxy records provide key input parameters for climate model simulations and hence are essential to quantify palaeoclimate dynamics and to disentangle their causes and effects. One reason for the lack of suitable Miocene climate records is the poor fossil preservation, e.g. in the case of corals (Buick and Ivany, 2004), which restricts the availibility of reliable proxy records for palaeoenvironmental reconstructions. Furthermore, existing palaeoclimate proxy data are derived from the open marine and/or high latitude realm mostly, while low latitude shallow water direct evidence of palaeoclimate is extremely rare.

1.2 Introduction

1.2.1 Giant clams – an overview

Giant clams (family Cardiidae, subfamily Tridacninae, genus *Tridacna/Hippopus*) are the largest living bivalve molluscs. There are currently eleven described species within the genus *Tridacna*: *Tridacna crocea* (Lamarck, 1819), *Tridacna maxima* (Röding, 1798), *Tridacna squamosa* (Lamarck, 1819), *Tridacna squamosina* (Sturany, 1899), *Tridacna derasa* (Röding, 1798), *Tridacna gigas* (Linnaeus, 1758), *Tridacna mbaluvuana/tevoroa* (Ladd, 1934), *Tridacna roseawateri* (Sirenko and Scarlato, 1991), *Tridacna noae* (Röding, 1798), *Tridacna ningaloo* (Penny & Willan, 2014), *Tridacna* costata (Richter et al., 2008) and two species within the genus *Hippopus*: *Hippopus hippopus* (Linnaeus, 1758) and *Hippopus porcellanus* (Rosewater, 1982).

The individual species can vary hugely with regards to their size. The smallest clam is *Tridacna crocea*, which reaches a maximum shell size of 15 cm, the largest is *Tridacna gigas*, with reported shell sizes of over 120 cm (Rosewater, 1965; Fatherree, 2006; Lucas, 2014).

Giant clams have a broad geographic distribution (Fig. 2) throughout the tropical and subtropical regions of the Indo-Pacific Ocean, ranging from 30°E to 120°W (South Africa to beyond French Polynesia) and from 36°N to 30°S (Japan to Australia) (bin Othman et al., 2010). Most species inhabit shallow (< 10 m) and/or only very clear deeper marine waters (e.g. Klumpp and Lucas, 1994).

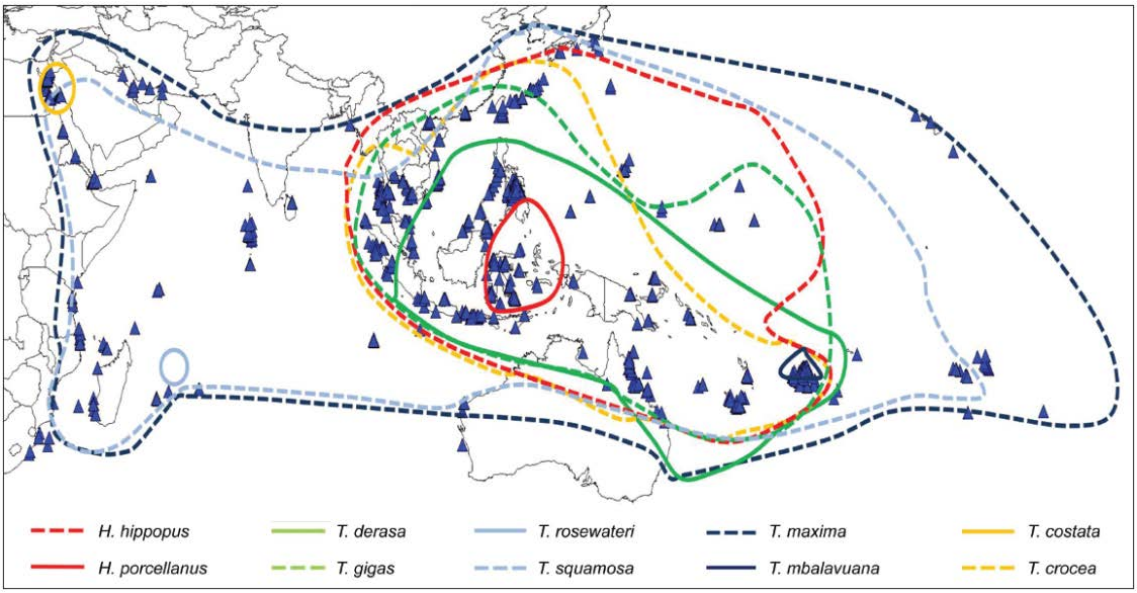

Figure 2. Distribution of giant clams (from bin Othman et al., 2010).

Giant clams can live for several decades to up to more than 100 years (e.g. Rosewater, 1965; Watanabe et al., 2004) and play an important ecological role for coral reef environments. For example they provide shelter for coral reef fish or harbour a variety of epibionts e.g. macroalgae, sponges, tubeworm, bryozoans and corals (Neo et al., 2015). They are a food source for natural predators and their faeces and gametes are consumed by opportunistic feeders (Neo et al., 2015). Apart from making an important contribution to the coral reef carbonate framework, giant clam valves add a topographical relief to the seabed, which alters the water flow resulting in e.g. an increased phytoplankton down-flux (Neo et al., 2015). Furthermore, giant clams potentially counteract eutrophication/hypertrophication through filtration of large amounts of nutrient rich seawater (Neo et al., 2015). Given that clams need several years to reach sexual maturity (e.g. Munro, 1989), the hermaphroditic organisms are especially vulnerable to depletion (Larson et al., 2016). And, although protected under international law (Convention on International Trade in Endangered Species of Wild Fauna and Flora (CITES)),

giant clam stocks are declining rapidly in many countries (e.g. bin Othman et al., 2010; Larson et al., 2016). Local extinctions of several species of giant clams are for instance reported for sites in the Philippines and Indonesia (Lucas, 1994), Malaysia (Tan et al., 1998) and Singapore (Guest et al., 2007). The reason for the rapid decline is most likely a result of overfishing as giant clam biomass is considered a valuable food source on tropical islands, as well as the aquarium trade and habitat destruction (e.g. bin Othman et al., 2010). In China, giant clams have been harvested for centuries for their meat, which is considered to be an aphrodisiac and delicacy. However, in the past few years the illegal trade of carved giant clam shells has taken off (Larson et al., 2016). Of special interest are the shells of largest species, *Tridacna gigas*. Declining stock in the South China Sea has increased the prices for giant clam shells enormously, which encourages local fishers even more to harvest the remaining clams.

Giant clams are, like most bivalve molluscs, filter feeders. But, giant clams also harbour microalgae (dinoflagellate algae: *Symbiodinium spp.*) commonly called zooxanthellae within their mantle tissue (e.g. Klumpp and Lucas, 1994; Ishikura et al., 1999; Jantzen et al., 2008; Lucas, 2014). They form a characteristic tubular system which arises from the gut and terminates in abundant fine 'fingers' projecting up to the surface of the mantle tissue (Lucas, 2014). These symbionts perform photosynthesis and produce translocated photosynthates (e.g. glucose) which act as the main nutrition supply for the giant clams (e.g. Klumpp and Griffiths, 1994; Klumpp and Lucas, 1994; Ishikura et al., 1999; Fatherree, 2006). The mixotroph nature of the giant clams allows them to maintain growth even in low nutrient environments; however Klumpp and Griffiths (1994) also demonstrated that "filter feeding is very important in the nutrition of small (20 - 100 mm) individuals of at least 2 species (*Tridacna gigas* and *Hippopus hippopus)*".

The important role of light for *Tridacna* shell growth has recently been demonstrated by Ip et al. (2015). Their study suggests that light exposure stimulates the zooxanthellae in *Tridacna squamosa* to produce specific signalling molecules, which in turn increase the activity the relevant transporters/enzymes that trigger light-enhanced calcification. Holt et al. (2014) further found that iridescent cells (iridocytes), situated on the surface of the mantle and directly overlying the symbionts *of Tridacna crocea*, distribute photosynthetically productive wavelengths (red and blue portions of the visible light) by lateral and forward-scattering of light into the tissue while back-reflecting non-productive wavelengths (green and yellow portions of the visible light). This selective bi-functional wavelength scattering allows for sufficient solar energy to reach the symbionts, while also preventing any photodamage of mantle tissue and symbionts. Both studies by Ip et al. (2015) and Holt et al. (2014) highlight the importance of light with regards to survival and growth of these highly specialised organisms.

1.2.2 Proxies for environmental conditions

Geochemical signatures recorded in marine biogenic carbonates (e.g. foraminifera tests, coral skeletons, mollusc shells) are increasingly used to obtain information about climate and environmental variability prior to the industrial era and in particular for environmental settings with a limited instrumental data coverage, such as coastal marine environments and mid to high latitude oceans. Isotopic ratios and trace elements commonly used, and also investigated herein, as proxies for (palaeo)environmental reconstruction include:

Oxygen isotopes ($\delta^{18}O$)

The probably best studied proxy of sea surface temperature (SST) and sea surface salinity (SSS) in biogenic carbonates is $\delta^{18}O$ (Urey et al., 1951). Out of the three naturally occurring stable oxygen isotopes (^{16}O, ^{17}O and ^{18}O), the isotope species ^{16}O and ^{18}O have the highest abundances of 99.759 % and 0.204 %, respectively. The $\delta^{18}O$ value refers to the ratio of the heavy ^{18}O isotope relative to the lighter ^{16}O isotope in a sample, which is dictated by mass dependant isotope fractionation, relative to this ratio in a defined standard such as SMOW (Craig and Gordon, 1965).

The isotopic composition of the oxygen isotopes is generally reported as

$$(1)\quad \delta^{18}O = \frac{\frac{^{18}O}{^{16}O}\text{sample} - \frac{^{18}O}{^{16}O}\text{Std}}{\frac{^{18}O}{^{16}O}\text{Std}} \text{ X } 1000\ [‰],$$

where Std denotes an internationally recognized oxygen isotope standard, such as standard mean ocean water (SMOW) or Pee Dee Belemnite (PDB). The measured $\delta^{18}O$ value of biogenic carbonate is comprised primarily of two components: $\delta^{18}O$ seawater ($\delta^{18}O_{sw}$), which is closely related to salinity/ice volume, and isotopic fractionation as a function of SST ($\delta^{18}O_{temp}$). The oxygen isotopic composition of seawater is affected by different environmental processes: Freshwater input (e.g. heavy rainfall, riverine runoff, ice cap melting) leads to an enrichment of the lighter ^{16}O in seawater, resulting in a general lighter $\delta^{18}O_{sw}$ (e.g. Faure and Mensing, 2005). Inversely, increased evaporation (e.g. evaporation > precipitation) leads to a depletion of the light ^{16}O (this isotope evaporates preferentially from the ocean surface into the atmosphere), thus generating a heavier $\delta^{18}O_{sw}$ value (e.g. Faure and Mensing, 2005). These two processes of freshwater input and evaporation have a major influence on the sea surface salinity (SSS) as well; therefore SSS and $\delta^{18}O$ are closely correlated. Saline waters are generally characterized by high $\delta^{18}O$ values.

To isolate $\delta^{18}O_{sw}$ from $\delta^{18}O_{temp}$ an additional proxy is required. Ideally suited is the Sr/Ca (or Mg/Ca) ratio, which mostly reflects only the seawater temperature and is not as dependent on salinity.

Sr/Ca and Mg/Ca

In contrast to $\delta^{18}O$, the Sr/Ca and Mg/Ca ratio in biogenic carbonates are predominantly (palaeo)temperature proxies, reflecting palaeo-SST independent of salinity, and are therefore used to disentangle the SSS from the SST component of the $\delta^{18}O$ record in biogenic carbonates (e.g. McCulloch et al., 1994; Klein et al., 1996; Watanabe et al., 2001). However, a recent publication by Evans et al. (2016) implies that for the planctic foraminifera *Globigerinoides ruber* the sensitivity of the relation between Mg/Ca_{test} and temperature may not remain constant with changing Mg/Ca composition of seawater (Mg/Ca_{sw}). A follow up publication (Evans et al., in press) demonstrates strong controls of seawater pH over the Mg/Ca_{test} chemistry in *Globigerinoides ruber*.

Inorganic precipitation experiments demonstrate that both Mg/Ca and Sr/Ca in aragonite are inversely correlated with temperature (e.g. Kinsman and Holland, 1969; Gaetani and Cohen, 2006). This negative correlation with temperature is due to thermodynamic effects. The substitution of e.g. Sr into the aragonite lattice is an exothermic reaction (Rosenthal and Linsley, 2006). According to Le Chatelier's principle, temperature lowering within an exothermic equilibrium system will shift the equilibrium to the right, thus favouring the reaction products. Therefore, lowered temperatures will lead to an increased strontianite ($SrCO_3$) co-precipitation. Elemental incorporation into the carbonate structure is also controlled by the shell mineralogy. Relatively large cations like Sr^{2+} and Ba^{2+} substitute better for Ca^{2+} in the orthorhombic aragonite structure, while smaller ions such as Mg^{2+} show greater affinity to the rhombohedral calcite lattice (Gotte and Richter, 2009).

The use of Sr/Ca and/or Mg/Ca as (palaeo)temperature proxies, is complicated by the so called 'vital effects', which denote the contribution of biophysiological signals overprinting the actual environmental information recorded in these El/Ca ratios within biogenic carbonates (see 1.2.5 for details).

Ba/Ca

Ba/Ca signals in coral skeletons and planktic foraminifera tests are interpreted as proxies for riverine runoff, i.e. sediment flux, and upwelling of deep, nutrient-rich seawater (e.g. McCulloch et al., 2003; Chen et al., 2011; Hönisch et al., 2011; Grove et al., 2012; Evans et al., 2015). Studies concerned with environmental implications of barium shell composition from modern marine bivalves report very similar high-resolution Ba/Ca profiles, which are characterized by large, sharp, periodically occurring Ba peaks of high intra-shell and even inter-individual reproducibility and suggest a direct link between the presence of phytoplankton blooms/high phytoplankton activity and the Ba/Ca peaks (e.g. Lazareth et al., 2003; Gillikin et al., 2006, 2008; Elliot et al., 2009; Thébault et al., 2009). The mechanism of barium

incorporation into the shell carbonate remains, however, ambiguous (Elliot et al., 2009). Species-specific effects, which might influence barium uptake and incorporation into the shell structure, might also be relevant (Gillikin et al., 2008). The studies by Gillikin et al. (2006) and Poulain et al. (2015) also suggest that Ba/Ca shell ratios are a promising proxy of high-resolution salinity variations in estuarine waters.

B/Ca

Boron isotopes ($\delta^{11}B$) and more recently the B/Ca ratio have been evaluated as promising pH proxies in foraminifera tests and coral skeletons (Pelejero et al., 2005; Douville et al., 2010; Rollion-Bard et al., 2011; Babila et al., 2014; Yu et al., 2015; Liu et al., 2015). The application of boron as pH-proxy is based on the equilibrium reaction between the two dominant species of dissolved boron in seawater, boric acid ($B(OH)_3$) and borate ion ($B(OH)_4^-$). In short, the relative proportion of these two species in an aqueous environment is a function of pH. At low pH, boron exists as $B(OH)_3$ in solution, and at high pH, boron exists as $B(OH)_4^-$. It is assumed that borate is primarily incorporated into the carbonate structure of biogenic carbonates and that the pH determines the amount of this species present within the carbonate (Liu et al., 2015). Further, the isotopic composition of the two boron species is also pH dependant, with the ^{11}B being generally enriched in $B(OH)_3$ relative to $B(OH)_4^-$ (e.g. Rollion-Bard et al., 2011).

Boron as a carbonate system proxy ratio is less well established in the field of palaeoclimate research using bivalve shells (e.g. Liu et al., 2015). Problems arise from biophysiological factors which overprint the environmental information (e.g. McCoy et al., 2011).

1.2.3 Highly-time resolved marine proxy records

Highly time-resolved (palaeo)climate/enviromental records are of special interest, because they can provide detailed insights into natural environmental variability prior to the instrumental era. Those records allow for instance a detailed assessment of seasonal to interannual SST variability, like ENSO (EL Niño Southern Oscillation) or monsoon related changes in SST (e.g. Batenburg et al., 2011). Changes in seasonality seem to play an important role with respect to (abrupt) climate changes (Crowley et al., 1986; Denton et al., 2005; Ayling et al., 2006; Fluckiger et al., 2008). Hence, SST variations, even if recorded over a relative short period (e.g. several years), likely contribute to a better understanding of long-term climate change.

Foraminifera records have traditionally been used to reconstruct palaeotemperature/ice volume for the last ~65 Myr. However, individual specimens are too short-lived to reflect variability of seasonality. Coral skeletons are used as recorders for long-time (palaeo)environmental reconstructions for Pleistocene or younger strata (Alibert and McCulloch, 1997; Gagan et al., 2000; Swart et al., 2002; Corrège et al., 2004; Mishima et al., 2009). However, coral based

proxies from deep-time (e.g. Miocene) strata are still the exception (Mertz-Kraus et al., 2009; Griffiths et al., 2013; Gothmann et al., 2015), also owing to their relatively poor preservation potential (e.g. Buick and Ivany, 2004).

1.2.4 Bivalves as palaeoenvironmental archives

Bivalve-derived geochemical records are increasingly investigated as a potential tool for palaeoenvironmental reconstructions (e.g. Klein et al., 1996; Purton et al., 1999; Freitas et al., 2005; Carré et al., 2006; Elliot et al., 2009; Schöne and Gillikin, 2013).

Indeed, bivalves are perfectly suitable archives of environmental changes for the following reasons:

1) Bivalves have an extremely broad geographic distribution and populate most of the Earth's aquatic habitats ranging from shallow to deep water, including freshwater, estuarine and marine environments. Moreover, bivalves are adapted to tropical, temperate and boreal climates.
2) The first primitive bivalves appeared in the Early Cambrian at about 520 Ma (Dame, 2012). Because bivalves build thick, hard and dense shells, their fossil record is extensive and likely more complete than for other invertebrates.
3) Some bivalve species are extremely long-lived. The ocean quahog *Arctica islandica* for instance has a life span of >500 years (Butler et al., 2013). Such long-lived bivalves are especially suitable for long-term environmental reconstructions.
4) Many bivalves display characteristic growth patterns within their shells. These often result from periodical accretion of carbonate, representing e.g. daily, tidal or seasonal periodicities. As such, bivalves are most suitable candidates for sclerochronology, which is defined as the study of physicochemical properties in periodically growing hard tissues of organisms (Oschmann, 2009).
5) Recent advances in sclerochronology have allowed the construction of so called 'master chronologies' (e.g. Butler et al., 2010), which describes the linking of contemporaneous specimen to produce continuous, long-term, multi-generation records, akin to tree rings chronologies for example.

Giant clams – attractive palaeoenvironmental archives

Owing to their outstanding longevity of several decades to more than one hundred years and large shell sizes of up to 120 cm (e.g. Rosewater, 1965; Watanabe et al., 2004), giant clams are particularly attractive sclerochronological archives and provide an important contribution to palaeoclimate research (Aharon, 1991; Watanabe and Oba, 1999; Watanabe et al., 2004; Aubert et al., 2009; Elliot et al., 2009; Batenburg et al., 2011; Welsh et al., 2011). Carbonate accretion

takes place on a daily basis, which is recorded as microscopic visible daily growth increments in the shell structure (Watanabe and Oba, 1999; Sano et al., 2012; Hori et al., 2015). Because of their high shell growth rates of several mm/year up to several cm/year (e.g. Beckvar, 1981; Aharon, 1991; Elliot et al., 2009), sampling and analysis at sub-seasonal to even daily (e.g. Sano et al., 2012) time resolution is possible. Layers grown during winter can be macroscopically distinguished from those grown during summer months (Aharon, 1991; Elliot et al., 2009; Batenburg et al., 2011; Welsh et al., 2011). The resulting seasonal banding pattern provides a good life-span control. Besides, fortnightly shell growth pattern associated to tidal-cyclic periodicities have been reported (Pannella and MacClintock, 1968).

1.2.5 What complicates palaeoclimate reconstructions

Diagenesis

Reefs are complex environments with diagenetic processes playing a vital role both in their destruction and construction (Tucker and Wright, 1990). Carbonate degradation takes place during biogenic alteration (e.g. bioerosion) or chemical dissolution, whereas carbonate aggradation is due to cementation processes such as precipitation of secondary aragonite or neomorphism including the transformation of aragonite to calcite (Flügel, 1982). Diagenesis is present in a variety of environments like the marine, near surface-meteoric/-vadose or the burial setting (Tucker and Wright, 1990; Flügel, 1982) and occurs ante- and/or post-mortem. Diagenetic processes are a major obstacle for palaeoclimatic reconstructions. They alter and overprint the original carbonate geochemistry, resulting in unreliable pelaeoenvironmental reconstructions (e.g. Hendy et al., 2007; Sayani et al., 2011; Griffiths et al., 2013).

Several advantages of giant clam shells over other biogenic archives such as coral skeletons or foraminifera tests exist: Owing to their dense and relatively thick aragonitic shells, which are less sensitive to diagenetic processes in comparison to e.g. porous coral skeletons, the geochemical composition of *Tridacna* shells might be better preserved over time. However, despite their dense structure, diagenetic processes like neomorphism, cementation and bioerosion can affect the aragonitic shell structure, which might lead to unreliable reconstructions. While the impact of diagenesis on the aragonitic coral geochemistry has been object of numerous studies (McGregor, 2003; Hendy et al., 2007; Nothdurft and Webb, 2009; Hathorne et al., 2011; Sayani et al., 2011), only little research has focused on *Tridacna* shells (Grace & Faylona, 2010; Moir, 1990) or its impact on the original shell geochemistry. Different forms of diagenesis such as recrystallization of aragonite to calcite, secondary aragonite precipitation or dissolution of calcium carbonate under the influence of microorganisms, generate different arteficts of the palaeoclimate record and they often co-occur (e.g. Griffiths et al., 2013). This makes it very difficult to apply corrections. Thus, to obtain reliable

palaeoclimate information from giant clams, pristine mollusc aragonite is required. To check the suitability of a sample, this means checking if the sample has preserved the original carbonate geochemistry, requires a meticulous screening procedure.
An example for such a methodological screening in the case of two Miocene giant clam shells is presented in Chapter 3 (Warter et al., 2015).

The role of biophysiology

"One key requirement for any proxy is that it faithfully records the environmental variable of interest without being influenced by other factors." (Schoepf et al., 2014). However, it has been shown for many calcifying organisms that the incorporation of trace elements into the biogenically produced carbonate depends on the combined effects of biological (physiological) controls and environmental parameters (e.g. Lowenstam, 1981; Weiner and Dove, 2003; Takesue and van Geen, 2004; Gaetani and Cohen, 2006).
Indeed, several studies reveal that species specific physiological effects, the so called 'vital effects', play a major role with regards to Sr and Mg incorporation into bivalve shells (e.g. Klein et al., 1996; Stecher et al., 1996; Purton et al., 1999; Freitas et al., 2005; Gillikin et al., 2005; Carré et al., 2006; Elliot et al., 2009; Foster et al., 2009). The comparison between publications treating possible controls of shell Sr/Ca and Mg/Ca in giant clams equally reveals inconsistent results (e.g., Elliot et al. 2009, Batenburg et al. 2011; Yan et al., 2013, 2014). Moreover, measured element/Ca ratios can vary significantly not only between different species collected contemporaneously from the same site (e.g. Freitas et al., 2005; Gillikin et al., 2005; Yan et al., 2014), but also between different parts (e.g. inner layer, outer layer, hinge) of the very same shell (Elliot et al., 2009), which might be an metabolic artifact and/or related to the bivalve biomineralization process. The latter remains poorly understood (e.g. Weiner and Dove, 2003), which further complicates reliable proxy record interpretations.
To disentangle the role of biophysiological controls with respect to proxy incorporation into the biogenic carbonate of giant clam shells, laboratory culture experiments were designed (Chapter 5). These *Tridacna* culture experiments provide the crucial framework for a better interpretation of highly time-resolved environmental records from giant clams.

References

Aharon, P., 1991, Recorders of reef environment histories - stable isotopes in corals, giant clams and calcareous algae: Coral Reefs, v. 10, p. 71-90.

Alibert, C., and McCulloch, M.T., 1997, Strontium/calcium ratios in modern *Porites* corals from the Great Barrier Reef as a proxy for sea surface temperature: Calibration of the thermometer and monitoring of ENSO: Paleoceanography, v. 12, p. 345-363.

Aubert, A., Lazareth, C.E., Cabioch, G., Boucher, H., Yamada, T., Iryu, Y., and Farman, R., 2009, The tropical giant clam *Hippopus hippopus* shell, a new archive of environmental conditions as revealed by sclerochronological and $\delta^{18}O$ profiles: Coral Reefs, v. 28, p. 989-998.

Ayling, B.F., McCulloch, M.T., Gagan, M.K., Stirling, C.H., Andersen, M.B., and Blake, S.G., 2006, Sr/Ca and $\delta^{18}O$ seasonality in a *Porites* coral from the MIS 9 (339-303 ka) interglacial: Earth and Planetary Science Letters, v. 248, p. 462–475.

Babila, T.L., Rosenthal, Y., and Conte, M.H., 2014, Evaluation of the biogeochemical controls on B/Ca of *Globigerinoides ruber* white from the Oceanic Flux Program, Bermuda: Earth and Planetary Science Letters, v. 404, p. 67-76.

Batenburg, S.J., Reichart, G.J., Jilbert, T., Janse, M., Wesselingh, F.P., and Renema, W., 2011, Interannual climate variability in the Miocene: High resolution trace element and stable isotope ratios in giant clams: Palaeogeography, Palaeoclimatology, Palaeoecology, v. 306, p. 75-81.

Billups, K., and Schrag, D.P., 2003, Application of benthic foraminiferal Mg/Ca ratios to questions of Cenozoic climate change: Earth and Planetary Science Letters, v. 209, p. 181-195.

Beckvar, N., 1981, Cultivation, spawning, and growth of the giant clams *Tridacna gigas*, *T. derasa*, and *T. squamosa* in Palau, Caroline Islands: Aquaculture, v. 24, p. 21-30.

bin Othman, A.S., Goh, G.H.S., and Todd, P.A., 2010, The distribution and status of giant clams (family Tridacnidae) – a short review: Raffles Bulletin of Zoology, v. 58, p. 103-111.

Buick, D.P., and Ivany, L.C., 2004, 100 years in the dark: Extreme longevity of Eocene bivalves from Antarctica: Geology, v. 32, p. 921-924.

Butler, P.G., Richardson, C.A., Scourse, J.D., Wanamaker Jr., A.D., Shammon, T.M., and Bennell. J.D., 2010, Marine climate in the Irish Sea: analysis of a 489-year marine master chronology derived from growth increments in the shell of the clam *Arctica islandica*: Quaternary Science Reviews, v. 29, p. 1614–1632.

Butler, P.G., Wanamaker Jr., A.D., Scourse, J.D., Richardson, C.A., and Reynolds, D.J., 2013, Variability of marine climate on the North Icelandic Shelf in a 1357-year proxy archive based on growth increments in the bivalve *Arctica islandica*: Palaeogeography, Palaeoclimatology, Palaeoecology, v. 373, p. 141-151.

Cane, M.A., and Molnar, P., 2001, Closing of the Indonesian seaway as a precursor to East African aridification around 3–4 million years ago: Nature, v. 411, p. 157-162.

Carré, M., Bentaleb, I., Bruguier, O., Ordinola, E., Barrett, N.T., and Fontugne, M., 2006, Calcification rate influence on trace element concentrations in aragonitic bivalve shells: Evidences and mechanisms: Geochimica et Cosmochimica Acta, v. 70, p. 4906-4920.

Chen, T.R., Yu, K.F., Li, S., Chen, T.G., and Shi, Q., 2011, Anomalous Ba/Ca signals associated with low temperature stresses in *Porites* corals from Daya Bay, northern South China Sea: Journal of Environmental Sciences (China), v. 23, p. 1452-1459.

Corrège, T., Gagan, M.K., Beck, J.W., Burr, G.S., Cabioch, G., and Le Cornec, F., 2004, Interdecadal variation in the extent of South Pacific tropical waters during the Younger Dryas event: Nature, v. 428, p. 927–929.

Crowley, T.J., Short, D.A., Mengel, J.G., and North, G.R., 1986, Role of seasonality in the evolution of climate during the last 100 million years: Science, v. 231, p. 579-584.

Dame, R.F. (ed), 2012, Ecology of Marine Bivalves: An Ecosystem Approach, 2nd edition, Taylor & Francis, London, 283 pages.

Denton, G.H., Alley, R.B., Comer, G.C., and Broecker, W.S., 2005, The role of seasonality in abrupt climate change: Quaternary Science Reviews, v. 24, p. 1159-1182.

Douville, E., Paterne, M., Cabioch, G., Louvat, P., Gaillardet J., Juillet-Leclerc, A., and Ayliffe, L., 2010, Abrupt sea surface pH change at the end of the Younger Dryas in the central sub-

equatorial Pacific inferred from boron isotope abundance in corals (*Porites*): Biogeosciences, v. 7, p. 2445–2459.

Elliot, M., Welsh, K., Chilcott, C., McCulloch, M., Chappell, J., and Ayling, B., 2009, Profiles of trace elements and stable isotopes derived from giant long-lived *Tridacna gigas* bivalves: Potential applications in paleoclimate studies: Palaeogeography, Palaeoclimatology, Palaeoecology, v. 280, p. 132-142.

England, M.H., and Huang, F., 2005, On the interannual variability of the Indonesian Throughflow and its linkage with ENSO: Journal of Climate, v. 18, p. 1435-1444.

Evans, D., Erez, J., Oron, S., and Müller, W., 2015, Mg/Ca-temperature and seawater-test chemistry relationships in the shallow-dwelling large benthic foraminifera *Operculina ammonoides*: Geochimica et Cosmochimica Acta, v. 148, p. 325-342.

Evans, D., Brierley, B., Raymo, M.E., Erez, J., and Müller, W., 2016, Planktic foraminifera shell chemistry response to seawater chemistry: Pliocene–Pleistocene seawater Mg/Ca, temperature and sea level change: Earth and Planetary Science Letters, v. 438, p. 139–148.

Evans, D., Wade, B.S., Henehan, M., Erez, J., and Müller, W., in press, Revisiting carbonate chemistry controls on planktic foraminifera Mg/Ca: implications for sea surface temperature and hydrology shifts over the Paleocene–Eocene Thermal Maximum and Eocene–Oligocene transition: Climates of the Past, v. 12, p. 1–17.

Fatherree, J.W., 2006, Giant clams in the sea and the aquarium: Liquid Medium, Tampa, Florida, 227 pages.

Faure, G., and Mensing, T.M., 2005, Isotopes: Principles and applications: Wiley & Sons, New York, 897 pages.

Flower, B.P., and Kennett, J.P., 1994, The middle Miocene climatic transition: East Antarctic ice-sheet development, deep-ocean circulation and global carbon cycling: Palaeogeography, Palaeoclimatology, Palaeoecology, v. 108, p. 537–555.

Flückiger, J., Knutti, R., White, J.W.C., and Renssen, H., 2008, Modeled seasonality of glacial abrupt climate events: Climate Dynamics, v. 31, p. 633–645.

Flügel, E., 1982, Microfacies of carbonate rocks. Analysis, interpretation and application: Springer-Verlag, Berlin Heidelberg, p. 62-104.

Foster, L.C., 2009, Strontium distribution in the shell of the aragonite bivalve *Arctica islandica*: Geochemistry, Geophysics, Geosystems, v. 10 (3), doi: 10.1029/2007GC001915.

Freitas, P., Clarke, J., Kennedy, H., Richardosn, C., and Abrantes, F., 2005, Mg/Ca, Sr/Ca, and stable isotope ($\delta^{18}O$ and $\delta^{13}C$) ratio profiles from the fan mussel Pinna nobilis: Seasonal records and temperature relationships: Geochemistry, Geophysics, Geosystems, v. 6, doi: 10.1029/2004GC00872.

Gaetani, G.A., and Cohen, A.L., 2006, Element partitioning during precipitation of aragonite from seawater: A framework for understanding paleproxies: Geochimica et Cosmochimica Acta, v. 70, p. 4617-4634.

Gagan, M.K., Ayliffe, L.K., Beck, J.W., Cole, J.E., Druffel, E.R.M., Dunbar, R.B., and Schrag, D.P., 2000, New views of tropical paleoclimates from corals: Quaternary Science Reviews, v. 19, p. 45-64.

Gillikin, D.P., Lorrain, A., Navez, J., Taylor, J.W., André, L., Keppens, E., Baeyens, W., and Dehairs, F., 2005, Strong biological controls on Sr/Ca ratios in aragonitic marine bivalve shells: Geochemistry, Geophysics, Geosystems, v. 6 (5), doi: 10.1029/2004GC000874.

Gillikin, D.P., Dehairs, F., Lorrain, A., Steensmans, D., Baeyens, W., and André, L., 2006, Barium uptake into the shells of the common mussel (*Mytilus edulis*) and the potential for estuarine paleo-chemistry reconstruction: Geochimica et Cosmochimica Acta, v. 70, p. 395-407.

Gillikin, D.P., Lorrain, A., Paulet, Y.M., Andre, L., and Dehairs, F., 2008, Synchronous barium peaks in high-resolution profiles of calcite and aragonite marine bivalve shells: Geo-Marine Letters, v. 28, p. 351-358.

Goodwin, D.H., Flessa, K.W., Schöne, B.R., and Dettman, D.L., 2001, Cross-calibration of daily growth increments, stable isotope variation, and temperature in the Gulf of California bivalve mollusk *Chione cortezi*: Implications for paleoenvironmental analysis: Palaios, v. 16, p. 387-398.

Gothmann, A., Stolarski, J., Adkins, J.F., Schoene, B., Dennis, K.L., Schrag, D.P., Mazur, M., and Bender, M.L., 2015, Fossil corals as an archive of secular variations in seawater chemistry since the Mesozoic: Geochimica et Cosmochimica Acta, v. 160, p. 188-208.

Gotte, T., and Richter, D.K., 2009, Quantitative aspects of Mn-activated cathodoluminescence of natural and synthetic aragonite: Sedimentology, v. 56, p. 483–492.

Griffiths, N., Müller, W., Johnson, K.G., and Aguilera, O.A., 2013, Evaluation of the effect of diagenetic cements on element/Ca ratios in aragonitic Early Miocene (~ 16 Ma) Caribbean corals: Implications for 'deep-time' palaeo-environmental reconstructions: Palaeogeography, Palaeoclimatology, Palaeoecology, v. 369, p. 185-200.

Grove, C.A., Zinke, J., Scheufen, T., Maina, J. Boer, W., Randriamanantsoa, B., and Brummer G.-J.A., 2012, Spatial linkages between coral proxies of terrestrial runoff across a large embayment in Madagascar: Biogeosciences, v. 9, p. 3063-3081.

Guest, J.R., Todd, P.A., Goh, E., Sivalonganathan, B.S., and Reddy, K.P., 2007, Can giant clam (*Tridacna squamosa*) populations be restored on Singapore's heavily impacted coral reefs?: Aquatic Conservation: Marine and Freshwater Ecosystems, v. 18, p. 570-579.

Hall, R., Cottam, M.A. and Wilson, M.E.J., 2011, The SE Asian gateway: History and tectonics of the Australia–Asia collision: Geological Society of London, Special Publications, v. 355, p. 1-6.

Harriss, R.C., 1965, Trace element distribution in molluscan skeletal material I. Magnesium, iron, manganese and strontium: Bulletin of Marine Science, v. 15, p. 265-273.

Hathorne, E.C., Felis, T., James, R.H., and Thomas, A., 2011, Laser ablation ICP-MS screening of corals for diagenetically affected areas applied to Tahiti corals from the last deglaciation: Geochimica et Cosmochimica Acta, v. 75, p. 1490–1506.

Hendy, E.J., Gagan, M.K., Lough, J.M., McCulloch, M., and Demenocal, P.B., 2007, Impact of skeletal dissolution and secondary aragonite on trace element and isotopic climate proxies in *Porites* corals: Paleoceanography, v. 22, doi: 10.1029/2007PA001462.

Herold, N., Huber, M., Müller, R.D., and Seton, M., 2012, Modeling the Miocene climatic optimum: ocean circulation: Paleoceanography, v. 27, doi: 10.1029/2010PA002041.

Hoeksema, B.W., 2007, Delinaetion of the Indo-Malayan centre of maximum marine biodiversity: The coral Triangle. In: Renema W. (Ed.), Biogeography, Time, and Place: Distributions, Barriers, and Islands. Springer, Dordrecht, p. 117-178.

Holbourn, A., Kuhnt, W., Schu;z, M., Flores, J.A., and Andersen, N., 2007, Orbitally-paced climate evolution during the middle Miocene ‘‘Monterey’’ carbon isotope excursion: Earth and Planetary Science Letters, v. 261, p. 534–550.

Holt, A.L., Vahidinia, S., Gagnon, Y.L., Morse, D.E., and Sweeney, A.M., 2014, Photosymbiotic giant clams are transformers of solar flux: Journal of the Royal Society Interface, v. 11, doi.org/10.1098/rsif.2014.0678.

Hönisch, B., Hemming, N.G., Archer, D., Siddall, M., and McManus, F., 2009, Atmospheric carbon dioxide concentration across the Mid-Pleistocene transition: Science, v. 324, p. 1551-1554.

Hönisch, B., Allen, K.A., Russel, A.D., Eggins, S.M., Bijma, J., Spero, H.J., Lea, D.W., and Yu, J., 2011, Planktic foraminifers as recorders of seawater Ba/Ca: Marine Micropaleontology, v. 79, p. 52–57.

Ip, Y.K., Ching, B., Hiong, K.C., Choo, C.Y.L., Boo, M.V., Wong, W.P., and Chew, S.F., 2015, Light induces changes in activities of Na^+/K^+-ATPase, H^+/K^+-ATPase and glutamine synthetase in tissues involved directly or indirectly in light-enhanced calcification in the giant clam, *Tridacna squamosa*: Frontiers in Physiology, doi: 10.3389/fphys.2015.00068.

Ishikura, M., Kato, C., and Maruyama, T., 1997, UV-absorbing substances in zooxanthellate and azooxanthellate clams: Marine Biology, v. 128, p. 649-655.

Jantzen, C., Wild, C., El-Zibdah, M., Roa-Quiaoit, H., Haacke, C., and Richter, C., 2008, Photosynthetic performance of giant clams, *Tridacna maxima* and *T. squamosa*, Red Sea: Marine Biolology, v. 155, p. 211–221.

Kinsman, D.J.J., Holland, H.D., 1969, The coprecipitation of cations with $CaCO_3$: IV. The coprecipitation of Sr^{2+} with aragonite between 16 and 96 °C: Geochimica et Cosmochimica Acta, v. 33, p. 1-17.

Klein, R.T., Lohmann, K.C., and Thayer, C., 1996, Sr/Ca and $^{13}C/^{12}C$ ratios in skeletal calcite of Mytilus trossulus: Covariation with metabolic rate, salinity, and carbon isotopic composition of seawater: Geochimica et Cosmochimica Acta, v. 60, p. 4207-4221.

Klumpp, D.W., and Lucas, J.S., 1994, Nutritional ecology of the giant clams *Tridacna tevoroa* and *T. derasa* from Tonga: influence of light on filter-feeding and photosynthesis. Marine Ecology Progress Series, v. 107, p. 147-156.

Klumpp, D.W., Griffiths, C.L., 1994, Contributions of phototrophic and heterotrophic nutrition to the metabolic and growth requirements of four species of giant clam (Tridacnidae): Marine Ecology Progress Series, v. 115, p. 103-115.

Kuhnt, W., Holbourn, A., Hall, R., Zuvela, M., and Kase, R., 2004, Neogene history of the Indonesian throughflow: Continent-Ocean interactions within East Asian marginal seas, v. 149, p. 299–320.

Ladd, H.S., 1934, Geology of Vitilevu, Fiji: Bernice P. Bishop Mus. Bullettin.

Lamarck, J.B., 1819a, *Tridacna crocea*: In: Histoire naturelle des animaux sans vertèbres présentant les caractères généraux et particuliers de ces animaux, leur distribution, leurs classes, leurs familles, leurs genres, et la citation des principales espèces qui s'y rapportent, v. 6 (1).

Larson, C., 2016, Marine Conservation: Shell trade pushes giant clams to the brink: Science, doi: 10.1126/science.351.6271.323.

LaRiviere, J.P., Ravelo, C.A., Crimmins, A., Dekens, P.S., Ford, H.L., Lyle, M., and Wara, M.W., 2012, Late Miocene decoupling of oceanic warmth and atmospheric carbon dioxide forcing: Nature, v. 486, p. 97-100.

Lazareth, C.E., VanderPutten, E., André, L., and Dehairs, F., 2003, High-resolution trace element profiles in shells of the mangrove bivalve *Isognomon ephippium*: a record of

environmental spatio-temporal variations?: Estuarine, Coastal and Shelf Sciences, v. 57, p. 1103-1114.

Lear, C.H., Elderfield, H., and Wilson, 2000, Cenozois deep-sea temperatures and global ice volumes from Mg/Ca in benthic foraminiferal calcite: Science, v; 287, p. 269-272.

Linnaeus, C., 1758, Systema naturae per regna tria naturae, secundum classes, ordines, species, cum characteribus, differentiis, synonymis, locis: Tomus I, editio decima, reformata. Laurentii Salvii, Stockholm.

Linsley, B.K., Rosenthal, Y., and Oppo, D.W., 2010, Holocene evolution of the Indonesian Throughflow and the western Pacific warm pool: Nature Geoscience, v. 3, p. 578-583.

Liu, Y.-W., Aciego, S.M., and Wanamaker Jr., A.D., 2015, Environmental controls on the boron and strontium isotopic composition of aragonite shell material of cultured *Arctica islandica*: Biogeosciences, v. 12, p. 3351-3368.

Lowenstam, H.A., 1981, Minerals formed by organisms: Science, v. 211, p. 1126-1131.

Lucas, J.S., 1994, The biology, exploitation, and mariculture of giant clams (Tridacnidae): Reviews in Fisheries Science, v. 2, p. 181-223.

Lucas, J.S., 2014, Giant Clams (quick guide): Current Biology, v. 24, p. R183-R184.

Lüthi, D., Le Floch, M., Bereiter, B., Blunier, T., Barnola, J.-M., Siegenthaler, U., Raynaud, D., Jouzel, J., Fischer, H., Kawamura, K., and Sticker, T.S., 2008, High-resolution carbon dioxide concentration record 650,000-800,000 years before present: Nature, v. 453, p. 379-382.

Marshall, J.F., and Mc Culloch, M.T., 2001, Evidence of El Niño and the Indian Ocean Dipole from Sr/Ca derived SSTs for modern corals at Christam Island, eastern Indian Ocean: Geophysical Research Letters, v. 28, p. 3453-3456.

Marshall, J.F, and McCulloch, M., 2002, An assessment of the Sr/Ca ratio in shallow water hermatypic corals as a proxy for sea surface temperature: Geochimica et Cosmochimica Acta, v. 66, p. 3263-3280.

McCoy, S.J., Robinson. L.F., Pfister, C.A., Wootton, J.T., and Shimizu, N., 2011, Exploring B/Ca as a pH proxy in bivalves: relationships between *Mytilus californianus* B/Ca and environmental data from the northeast Pacific: Biogesciences Discussions, v. 8, p. 5587-5616.

McCulloch, M.T., Gagan, M.K., Mortimer, G.E., Chivas, A.R., and Isdale, P.J., 1994, A high-resolution Sr/Ca and $\delta^{18}O$ coral record from the Great Barrier Reef, Australia, and the 1982–1983 El Nino: Geochimica et Cosmochimica Acta, v. 58, p. 2747-2754.

McCulloch, M., Fallon, S., Wyndham, T., Hendy, E., Lough, J., and Barnes, D., 2003, Coral record of increased sediment flux to the inner Great Barrier Reef since European settlement: Nature, v. 421, p. 727-730.

McGregor, H.V., and Gagan, M.K., 2003, Diagenesis and geochemistry of *Porites* corals from Papua New Guinea: implications for paleoclimate reconstruction: Geochimica et Cosmochimica Acta, v. 67, p. 2147-2156.

Mertz-Kraus, R., Brachert, T.C., Jochum, K.P., Reuter, M., and Stoll, B., 2009, LA-ICP-MS analyses on coral growth increments reveal heavy winter rain in the Eastern Mediterranean at 9 Ma: Palaeogeography, Palaeoclimatology, Palaeoecology, v. 273, p. 25-40.

Mishima, M., Kawahata, H., Suzuki, A., Inoue, M., Okai, T., and Omura, A., 2009, Reconstruction of the East China Sea palaeoenvironment at 16 ka by comparison of fossil and modern *Faviidae* corals from the Ryukyus, southwestern Japan: Journal of Quaternary Science, v. 24, p. 928-936

Munro, J.L., 1989, Fisheries for giant clams (Tridacnidae: Bivalvia) and prospects for stock enhancement: In: Caddy, J.F. (Ed.), Marine Invertebrate Fisheries: Their assessment and Management. John Wiley and Sons Inc., New York, p. 541-558.

Neo, M.L., Eckmann, W., Vicentuan, K., Teo, S.L.-M., and Todd, P.A., 2015, The ecological significance of giant clams in coral reef ecosystems: Biologiocal Conversation, v. 181, p. 111-123.

Nothdurft, L.D., and Webb, G.E., 2009, Earliest diagenesis in scleractinian coral skeletons: implications for palaeoclimate-sensitive geochemical archives: Facies, v. 55, p. 161-201.

Oschmann, W., 2009, Sclerochronology: editorial. International Journal of Earth Sciences (Geologische Rundschau), v. 98, p. 1-2.

Pagani, M., Arthur, M.A., and Freeman, K.M., 1999, Miocene evolution of atmospheric carbon dioxide: Paleoceanography, v. 14, p. 273-292.

Pannella, G., and MacClintock, C., 1968, Biological and environmental rhythms reflected in molluscan shell growth. In: Macurda, D.B., Jr., Paleobiological aspects of growth and development: A Symposium: Paleontological Society Memoir, v. 2, p. 64-80.

Pätzold, J., Heinrichs, J.P., Wolschendorf, K., and Wefer, G., 1991, Correlation of stable oxygen isotope temperature record with light attenuation profiles in reef-dwelling *Tridacna* shells: Coral Reefs, v. 10, p. 65-69.

Pelejero, C., Calvo, E., McCulloch, M.T., Marshall, J.F., Gagan, M.K., Lough, J.M., and Bradley, N.O., 2005, Preindustrial to modern interdecadal variability in coral reef pH: Science, doi: 10.1126/science.1113692.

Penny, S.S., and Willan, R.C., 2014, Description of a new species of giant clam (Bivalvia: Tridacnidae) from Ningaloo Reef, Western Australia: Molluscan Research, v. 34, p. 201-211.

Poulain, C., Gillikin, D.P., Thébault, J., Munaron, J.M., Bohn, M., Robert, R., Paulet, Y.-M., and Lorrain, A., 2015, An evaluation of Mg/Ca, Sr/Ca, and Ba/Ca ratios as environmental proxies in aragonite bivalve shells: Chemical Geology, v. 396, p. 42-50.

Purton, L.M.A., Shields, G.A., Brasier, M.D., and Grime, G.W., 1999, Metabolism controls Sr/Ca ratios in fossil aragonitic mollusks: Geology, v. 27, p. 1083-1086.

Reich, S., Warter, V., Wesselingh, F.P., Zwaan, J. H., Lourens, L., and Renema, W., 2015, Paleoecological significance of stable isotope ratios in Miocene tropical shallow marine habitats (Indonesia): Palaios, v. 30, p. 53-65.

Renema, W., Bellwood, D.R., Braga, J.C., Bromfield, K., Hall, R., Johnson, K.G., Lunt, P., Meyer, C.P., McMonagle, L.B., Morley, R.J., O'Dea, A., Todd, J.A., Wesselingh, F.P., Wilson, M.E.J., and Pandolfi, J.M., 2008, Hopping hotspots: Global shifts in marine biodiversity: Science, v. 321, p. 654–657.

Renema, W., Warter, V., Novak, V., Young, Y., Marshall, N., and Hasibuan, F., 2015, Ages of Miocene fossil localities in the Northern Kutai Basin (East Kalimantan, Indonesia): Palaios, v. 30, p. 26-39.

Richter, C., Roa-Quiaoit, H., Jantzen, C., Al-Zibdah, M., and Kochzius, M., 2008, Collapse of a new living species of giant clam in the Red Sea: Current Biology, v. 18, p. 1-6.

Robinson, M.M., Dowsett, H.J., and Chandler, M.A., 2008, Pliocene role in assessing future climate impacts: EOS, v. 89, p. 501-512.

Röding, P.F., 1798, Pars secunda continens conchylia sive testacea univalvia, bivalvia & multivalvia: In Bolten JF (ed.), Museum Boltenianum sive catalogus cimeliorum e tribus regnis naturæ quæ olim collegerat Joa. Fried Bolten. Trapp, Hamburg.

Rollion-Bard, C., Blamart, D., Trebose, J., Tricot, G., Mussi, A., and Cuif, J.-P., 2011, Boron isotopes as pH proxy: A new look at boron speciation in deep-sea corals using ^{11}B MAS NMR and EELS: Geochimica et Cosmochimica Acta, v. 75, p. 1003-1012.

Rosewater, J., 1965, The family Tridacnidae in the Indo-Pacific: Indo-Pacific Mollusca 1, p. 347-396.

Rosenthal, Y., and Linsley, B., 2006, Mg/Ca and Sr/Ca paleothermometery from calcareous marine fossils: In: Encyclopedia of Quaternary Sciences, Elsevier, Amsterdam, 3365 pages.

Sano, Y., Kobayashi, S., Shirai, K., Takahata, N., Matsumoto, K., Watanabe, T., Sowa, K., and Iwai, K., 2012, Past daily light cycle recorded in the strontium/calcium ratios of giant clam shells: Nature Communications, v. 3, doi:10.1038/ncomms1763.

Santini, F., and Winterbottom, R., 2002, Historical biogeography of Indo-western Pacific coral reef biota: is the Indonesian region a centre of origin?: Journal of Biogeography, v. 29, p. 189-205.

Sayani, H.R., Cobb, K.M., Cohen, A.L., Elliott, W.C., Nurhati, I.S., Dunbar, R.B., Rose, K.A., and Zaunbrecher, L.K., 2011, Effects of diagenesis on paleoclimate reconstructions from modern and young fossil corals: Geochimica et Cosmochimica Acta, v. 75, p. 6361–6373.

Schoepf, V., McCulloch, M. T., Warner, M. E., Levas, S. J., Matsui, Y., Aschaffenburg, M. D., and Grottoli, A. G., Short-Term Coral Bleaching Is Not Recorded by Skeletal Boron Isotopes: Plos One, doi:10.1371/journal.pone.0112011, 2014b.

Schöne, B.R., Lega, J., Flessa, K.W., Goodwin, D.H., and Dettman, D.L., 2002, Reconstructing daily temperatures from growth rates of the interdidal bivalve mollusk *Chione cortezi* (northern Gulf of California, Mexico): Palaeogegrapghy, Palaeoclimatology, Palaeoecology, v. 184, p. 131-146.

Schöne, B.R., Zhang, Z., Jacob, D., Gillikin, D.P., Tütken, T., Garbe-Schönberg, D., McConnaughey, T., and Soldati, A., 2010, Effect of organic matrices on the determination of the trace element chemistry (Mg, Sr, Mg/Ca, Sr/Ca) of aragonitic bivalve shells (*Arctica islandica*) – Comparison of ICP-OES and LA-ICP-MS data: Geochemical Journal, v. 44, p. 23-27.

Schöne, B.R., and Gillikin, D.P., 2013, Unraveling environmental histories from skeletal diaries - Advances in sclerochronology: Palaeogegrapghy, Palaeoclimatology, Palaeoecology, v. 373, p. 1-5.

Singh, R.K., and Gupta, A.K., 2010, Deep-sea benthic foraminiferal changes in the eastern Indian Ocean (ODP Hole 757B): their links to deep Indonesian (Pacific) flow and high latitude glaciation during the Neogene: Episodes, v. 33, p. 74–82.

Sirenko, B.I., and Scarlato, O.A., 1991, *Tridacna rosewateri* sp. n: A new species of giant clam from Indian Ocean (Bivalvia: Tridacnidae): La Conchiglia, v. 261, p. 4-9.

Sprintall, J., Gordon, A.L., Koch-Larrouy, A., Lee, T., Potemra, J.T., Pujiana, K., and Wijffels, S.E., 2014, The Indonesian seas and their role in the coupled ocean–climate system, Nature Geoscience, v. 7, p. 487-492.

Srinivasan, M.S., and Sinha, D.K., 2000, Ocean circulation in the tropical Indo-Pacific during early Pliocene (5.6–4.2 Ma): Paleobiogeographic and isotopic evidence: Proceedings of the Indian Academy of Sciences (Earth and Planetary Sciences), v. 109, p. 315–328.

Stecher, H.A., Krantz, D.E., Lord, C.J., Luther, G.W., and Bock, K.W., 1996, Profiles of strontium and barium in *Mercenaria mercenaria* and *Spisula solidissima* shells: Geochimica et Cosmochimica Acta, v. 60, p. 3445-3456.

Sturany, R., 1899, Expedition S.M. Schiff "Pola" in das Rothe Meer, nördliche und südliche Hälfte. 1895/96 und 1897/98. Zoologische Ergebnisse XIV, Lamellibranchiaten des Rothen Meeres. Berichte der Commission für ozeanographische Forschungen. Sonderdruck aus: Denkschriften der mathematisch-naturwissenschaftlichen Klasse der Kaiserlichen Akademie der Wissenschaften, Wien.

Swart, P.K., ELderfield, H., and Greaves, M.J., 2002, A high-resolution calibration of Sr/Ca thermometry using the Caribbean coral Montastraea annularis: Geochemistry Geophysics Geosystems, v. 3, doi: 10.1029/2002GC000306.

Takesue, R. K. and van Geen, A., 2004, Mg/Ca, Sr/Ca, and stable isotopes in modern and Holocene Protothaca staminea shells from a northern California coastal upwelling region: Geochimica and Cosmochimica Acta, v. 68, p. 3845-3861.

Tan, S.-H., Yasin, Z.B., Salleh, I.B., and Yusof, A.A., 1998, Status of giant clams in Pulau Tioman, Malaysia: Malayan Nature Journal, v. 52, p. 205-216.

Thébault, J., Chauvaud, L., L'helguen, S., Clavier, J., Barats, A., Jacquet, S., PechéyranE, C., and Amouroux, D., 2009, Barium and molybdenum records in bivalve shells: geochemical proxies for phytoplankton dynamics in coastal environments?: Limnology and Oceanography, v. 54, p. 1002–1014.

Tripati, A.K., Roberts, C.D., and Eagle, R.A., 2009, Coupling of CO_2 and ice sheet stability over major climate transitions of the last 20 million years: Science, v. 326, p. 1394-1397.

Tucker, M.E., and Wright, V.P., 1990, Diagenetic processes, products and environments: In: Carbonate Sedimentology, Chapter 7, Blackwell Science, Oxford, p. 314-364.

Urey, H.C., Lowenstam, A., Epstein, S., and McKinney, C.R., 1951, Measurement of paleotemperatures and temperatures of the Upper Cretaceous of England, Denmark, and the southeastern United States: GSA Bulletin, v. 62, p. 399-416.

Wanamaker Jr, A.D., Heinemeier, J., Scourse, J.D., Richardson, C.A.., Butler, P.G., Eiríksson, J., and Knudsen, K.L., 2008, Very long-lived mollusks confirm 17th century ad tephra-based radiocarbon reservoir aged for North Icelandic shelf waters: Radiocarbon, v. 50, p. 399-401.

Warter, V., Müller, W., Wesselingh, F.P., Todd, J.A., and Renema, W., 2015, Late Miocene seasonal to sub-decadal climate variability in the Indo-West Pacific (East Kalimantan, Indonesia) preserved in giant clams: Palaios, v. 30, p. 66-82.

Warter, V., and Müller, W., 2016, Daily growth and tidal rhythms in Miocene and modern giant clams revealed via ultra-high resolution LA-ICPMS analysis – A novel methodological approach towards improved sclerochemistry: Palaeogeography, Palaeoclimatology, Palaeoecology, doi:10.1016/j.palaeo.2016.03.019.

Watanabe, T., Winter, A., and Oba, T., 2001, Seasonal changes in sea surface temperature and salinity during the Little Ice Age in the Caribbean Sea deduced from Mg/Ca and $^{18}O/^{16}O$ ratios in corals: Marine Geology, v. 173, p. 21–35.

Watanabe, T., and Oba, T., 1999, Daily reconstruction of water temperature from oxygen isotopic ratios of a modern *Tridacna* shell using a freezing microtome sampling technique: Journal of Geophysical Research, v. 104, p. 20667-20674.

Watanabe, T., Suszuki, A., Kawahata, H., Kan, H., and Ogawa, S., 2004, A 60-year isotopic record from a mid-Holocene fossil giant clam (*Tridacna gigas*) in the Ryukyu Islands: physiological and paleoclimatic implications: Palaeogeography, Palaeoclimatology, Palaeoecology, v. 212, p. 343–354.

Weiner, S., and Dove, P.M., 2003, An overview of biomineralization processes and the problem of the vital effect: Reviews in Mineralogy and Geochemistry, v. 54, p. 1-29.

Welsh, K., Elliot, M., Tudhope, A., Ayling, B., and Chappell, J., 2011, Giant bivalves (*Tridacna gigas*) as recorders of ENSO variability: Earth and Planetary Science Letters, v. 307, p. 266-270.

Wilson, M.E.J. and Rosen, B.R., 1998, Implications of paucity of corals in the Palaeogene of SE Asia: plate tectonics or centre of origin? In: Hall, R., and Holloway, J.D. (Eds.), Biogeography

and Geological Evolution of SE Asia. Backhuys Publishers, Leiden, The Netherlands, p. 165-195.

Yan, H., Shao, D., Wang, Y., and Sun, L., 2013, Sr/Ca profile of long-lived Tridacna gigas bivalves from South China Sea: A new high-resolution SST proxy: Geochimica et Cosmochimica Acta, v. 112, p. 52-65.

Yan, H., Shao, D., Wang, Y., and Sun, L., 2014, Sr/Ca differences within and among three Tridacnidae species from the South China Sea: Implication for paleoclimate reconstruction: Chemical Geology, v. 390, p. 22-31.

Yu, J., Foster, G.L., Elderfield, H., Broecker, W.S., Clark, E., 2010, An evaluation of benthic foraminiferal B/Ca and $\delta^{11}B$ for deep ocean carbonate ion and pH reconstructions: Earth and Planetary Science Letters, v. 293, p. 114-120.

Zachos, J.C., Pagani, M., Sloan, L., Thomas, E., and Billups, K., 2001, Trends,
rhythms, and aberrations in global climate 65Ma to present: Science, v. 292, p. 686-93.

Zachos, J.C., Dickens, G.R., and Zeebe, R.E., 2008, An early Cenozoic perspective on greenhouse warming and carbon-cycle dynamics: Nature, v. 451, p. 279-283.

Chapter 2: Methods

This chapter lists and describes all methods used within this work. The methods specifically relate to the case studies 1, 2 and 3 (Chapters 3, 4 and 5) where details on the methodological approach are outlined accordingly. LA-ICPMS plays a major role for this study and is applied in all three applications and it is therefore described in greater detail.

I acknowledge the following persons for help during analysis:
Matthew Thirlwall and Christina Manning (RHUL) – SIS
Dave Alderton (RHUL) – XRD
Alex Ball and Tomasz Goral (NHM) – SEM
Norman Oxtoby (RHUL) – CL
Dave Lowry, Nathalie Grassineau and Dave Mattey – Stable isotope analysis
Wolfgang Müller – LA-ICPMS

2.1 Strontium isotope stratigraphy (SIS)

SIS was performed on fossil *Tridacna* shells and *Faviidae* scleractinian corals from the Bontang area (East Kalimantan, Indonesia) in order to evaluate their stratigraphic ages and to further investigate the influence of diagenetic alteration on the Sr isotope signature (Chapter 3). Additional SIS work was performed for the research published in Renema et al. (2015) to support the biostratigraphically determined age estimates from twelve fossil localities along the northeastern margin of the Kutai Basin (East Kalimantan, Indonesia).

The strontium isotope ratio of seawater in the open ocean is considered globally uniform and stable at any given time, when measured at an analytical precision of 0.000020 (McArthur et al., 2012), because the Sr residence time is much longer (10^6 years) than the ocean's mixing time (10^3 years) (e.g. Elderfield, 1986; Faure and Mensing, 2005; McArthur et al., 2012). The ability to date and correlate marine (biogenic) carbonates using Sr isotopes relies on the variation in $^{87}Sr/^{86}Sr$ of seawater over time (Fig. 1), which is primarily a function of high $^{87}Sr/^{86}Sr$ terrigenous versus low $^{87}Sr/^{86}Sr$ oceanic crustal input into the oceans (Oslick et al. 1994; Faure and Mensing, 2005). The isotopic evolution of Sr in the oceans can thus be considered as a record of the Earth's geological activity through time. The *Sr isotope seawater curve* (McArthur et al., 2001; McArthur and Howarth, 2004; McArthur et al., 2012) is a compilation of $^{87}Sr/^{86}Sr$ ratios measured on biogenic and inorganic produced marine minerals, mostly carbonates. It covers the whole Phanerozoic Eon and reveals systematic $^{87}Sr/^{86}Sr$ variations, and crucially also multiple recurrences of coinciding ratios at different time intervals. Most favorable conditions for SIS exist for time periods where the marine $^{87}Sr/^{86}Sr$ ratio is changing unidirectionally, as is the case for the post-Eocene era, where the Sr isotope ratios steadily increase to the present $^{87}Sr/^{86}Sr$ ratio of 0.70918 (Fig. 1).

$^{87}Sr/^{86}Sr$ analysis using TIMS

Carbonate powders weighing between 5 - 100 mg were produced using a hand drill (Proxxon GmbH, Niersbach, Germany) fitted with a 1 mm diamond drill bit. Wet geochemistry procedures for Sr purification included dissolution in concentrated HNO_3, acidic redigestion in 4M HNO_3 and exchange chromatography using Eichrom® Sr Spec resin. To improve Sr purification the chromatography step was repeated. Sr was loaded onto degassed single rhenium filaments, preconditioned with H_3PO_4 and tantalum emitter after Birck (1986). $^{87}Sr/^{86}Sr$ ratios were measured on a VG354 multicollector thermal ion mass spectrometer (TIMS) in multidynamic mode (Thirlwall, 1991) at RHUL. Mass fractionation correction for all measured ratios utilized the exponential mass fractionation and the constant $^{86}Sr/^{88}Sr$ ratio of 0.1194 (Steiger and Jäger, 1977). The longterm mean (2011–2012; n = 97) of measured $^{87}Sr/^{86}Sr$ of the international standard NIST SRM 987 is 0.710256 ± 0.000020 (2 SD). All data were corrected

relative to the adopted NIST SRM 987 $^{87}Sr/^{86}Sr$ ratio of 0.710248 (McArthur et al., 2001). Resultant $^{87}Sr/^{86}Sr$ ratios were converted into their respective numerical ages by cross correlation with the strontium isotope data set of the SIS Look-Up Table Version 4: 08/04 (McArthur et al. 2001; McArthur and Howarth 2004). Age minima and maxima were obtained by combining the statistical uncertainty of the SRM 987 long-term reproducibility (0.000020) with the upper and lower confidence limit reported with each Sr isotope ratio in the SIS Look-Up Table.

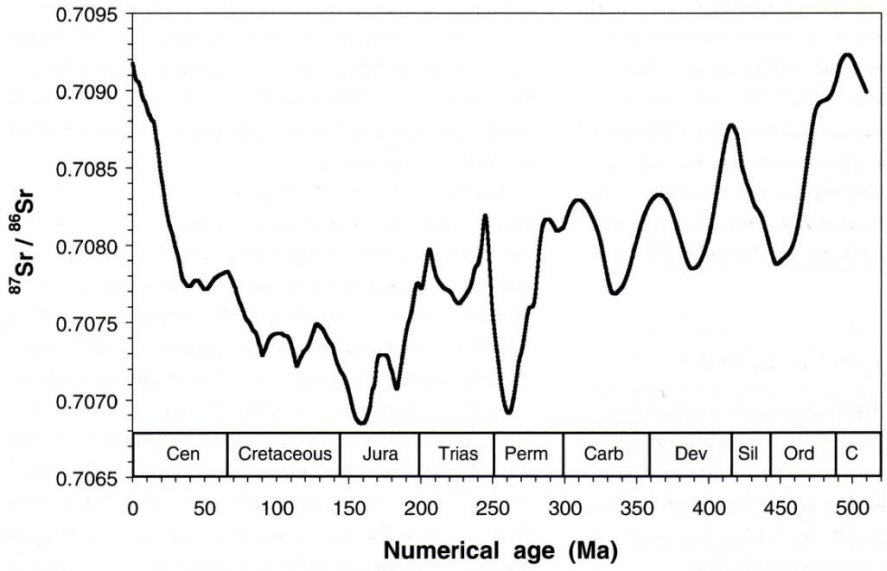

Figure 1. Variation of $^{87}Sr/^{86}Sr$ through the Phanerozoic time (from McArthur and Howarth, 2004).

2.2 X-ray diffraction (XRD)

XRD was conducted to assess the preservation of Miocene *Tridacna* shells by determining the mineralogy of powdered carbonate samples from targeted shell domains (Chapter 3). XRD uses the fact that crystals are made up of a near infinitely repeated regularly ordered three-dimensional atomic network. The internal structure of every crystal, i.e. the atomic arrangement, is reflected in its external morphology in which plane faces intersect at specific angles. X-rays are directed at the sample and - depending on the inter-atomic spacing and crystal face angles - diffracted to a certain degree, which is described by the *Bragg's Law* (Equation 1).

(1) $n\lambda = 2d \sin\theta$,

where n is a positive integer, λ is the wavelength of the characteristic X-rays from the X-ray tube, d is a distance between a set of parallel lattice planes, and θ is a angle between the incident diffracted X-ray beam and an atomic lattice plane in the crystal. The incident angle of the diffracted X-ray beam Tetha (θ), measured as 2θ, contains information about the atomic

arrangement within the crystal. The resulting peak spectra were interpreted by converting the diffraction angles 2θ into interplanar lattice spacings, d, (ångström (Å)) for Cu K-α radiation, via correlation against data tables published e.g. in the Mineral Powder Diffraction File Data book (Joint Committee on Powder Diffraction Standards, 1993).

Powdered samples of targeted shell parts were produced by hand drilling using a Proxxon micro-drill (Proxxon GmbH, Niersbach, Germany) and grinding (using mortar and pestle). XRD analyses were carried out on a Philips PW1830/3020 spectrometer with Cu Kα radiation, operated at 40 kV. Diffraction angles (2θ) between 25° and 37° were scanned, which include the main peaks of the $CaCO_3$ polymorphs calcite and aragonite. The limit of detection was typically better than 3 %. Strikingly, hand-drilling of pristine aragonite resulted in the conversion of meta-stable pristine aragonite to calcite in the case of one of the Miocene shells, while no aragonite-calcite transition occurred when preparing powdered samples via grinding (see details in Chapter 3). This was confirmed through repeated analyses. To avoid polymorphic transitions, careful manual carbonate grinding should be chosen over electric drilling.

2.3 Imaging analysis

2.3.1 Light microscopy

Thin section microscopy under plane-polarized light was carried out to investigate shell preservation and daily incremental growth patterns in modern and fossil giant clams (Chapters 3, 4 and 5). High-resolution transmitted light images were acquired with a Nikon Mikrophot-FX microscope equipped with a Nikon digital camera head (DS-5M) combined with a Nikon digital site controller (DS-L1) at RHUL at 100 – 200x magnification. Microscope images obtained from shell parts of interest were imported into the Resonetics Geostar software as image overlays and X-Y coordinated to facilitate daily growth increment identification (see details in Chapter 5).

2.3.2 Scanning electron microscopy (SEM)

SEM was applied to visually investigate and record the morphology and crystalline structure of pristine and diagenetically altered shell domains of the Miocene giant clams (Chapter 3). Scanning electron microscopy produces contrast images by recording the backscattered electron (BSE) or secondary electron (SE) signals resulting from interactions of a high energy electron beam, which raster scans across the surface of a solid sample. Sample areas with a relatively high atomic number and high packing density, correspond to a higher number of detected BSEs and as a result such areas will appear brighter in the BSE image display compared to areas with a lower atomic coverage and low packing density, respectively.

Uncoated samples were investigated using both, a LEO 1455 variable pressure (VP) SEM (operated at 15 kV) utilizing a solid-state 4 quadrant backscattered electron (BSE) detector and a Quanta 650 ESEM FEG used in VP mode with air as the imaging gas (operated at 7 kV) at the Natural History Museum, London. To enhance visibility of structural morphology, some samples were etched using acetic acid (different concentrations up to 5%, and different reaction times up to 30 min). High-quality digital imaging was performed using the LEO 1455 up to a magnification of 1200 and using the Quanta 650 up to a magnification of 4000.

2.3.3 Cathodoluminescence (CL)

CL microscopy was conducted to investigate the preservation of the Miocene shells (Chapter 3). During CL analysis a beam of high energy electrons is focused onto the sample surface. The electron bombardment results in the emission of photons of characteristic wavelengths typically within the visible portion (400-700 nm) of the electromagnetic spectrum. Certain trace elements, e.g. Mn, are known to promote luminescence in carbonates (e.g. Barbin et al., 1995; England et al., 2006, Gotte and Richter, 2009) and as such this method is ideally suited to screen for diagenetically altered carbonate. Polished thin sections of shell cross sections were examined by cold cathodoluminescence (CL) microscopy using a Technosyn 8200 MkII luminoscope connected to a Nikon Optiphot petrological microscope at RHUL.

2.4 Stable oxygen and carbon isotope analysis

Micromilled sub-samples (300-400 µg) obtained from pristine aragonite of Miocene giant clam shells (Chapter 3) were analyzed for oxygen and carbon isotope ratios using a Micromass Multiflow head space system connected to a GV Instruments Isoprime IRMS at RHUL. The samples were digested in 103 % orthophosphoric acid at 90°C. After a minimum of four hours reaction time, the evolved CO_2 was expanded into the sample loop, and then delivered to the Isoprime mass spectrometer within continuous He-carrier gas flow. Duplicate analyses were performed for each sample and standard. Isotopic ratios were calibrated against the Vienna Pee Dee Belemnite (VPDB) through NBS-19 and LSVEC international standards and an in-house standard (RHBNC calcite). Averaged precision (1SD) of duplicates was 0.03 % for $\delta^{13}C$ and 0.06 % for $\delta^{18}O$.

Powdered aragonite samples were recovered from the inner layer of polished shell cross sections using a semiautomated New Wave micromill fitted with a 300 µm drill bit. Single grooves with a length of 2 mm, depth of 360 µm, and width of 200 µm were milled parallel to existing growth bands in continuous mode. The resulting time-series records obtained for two Miocene *Tridacna* shells consisted of 177 and 88 sub-samples, respectively (Chapter 3).

2.5 Laser-ablation inductively-coupled-plasma mass spectrometry (LA-ICPMS)

2.5.1 Overview

LA-ICPMS is an in-situ analytical method aimed at investigating the chemical and isotopic composition in solid geological, archaeological, environmental, chemical, biological and medical samples (e.g. Durrant and Ward, 1994; Becker, 2002; Liu et al., 2013; Limbeck et al., 2015). The largest application field for this spectrometric technique is geological research (Fig. 2), where LA-ICPMS has been successfully employed since 1985 (Gray, 1985). The popularity of LA-ICPMS has increased dramatically especially over the past 15 years (Fig. 2) also owing to its highly versatile capacities including:

- Fast analysis and no vacuum requirements, which enables a high sample throughput
- Minimal sample preparation requirements: polishing is advised for lateral laser ablation, but not necessary for depth-profiling
- Flexibility in sample size, but must be compatible with the sample chamber
- Ultra-high spatial resolution both in lateral (<5µm, Warter and Müller, 2016) and vertical direction, i.e. depth-profiling (<0.5µm Griffiths et al., 2013), while maintaining sub-ppm detection limits
- Relatively low acquisition- and running costs
- Suitable for bulk and µm-scale compositional analysis
- Multi-element analysis with a wide elemental coverage (Li to U)
- High ionization potential of the Ar plasma enables single mass resolution capability, which is not the case for e.g. SIMS
- Isotope ratio cabability
- Simultaneous analysis of major, minor and trace elements due to linear dynamic range of up to 9 orders of magnitude (e.g. ppt – ppm) owing to analogue/pulse switching capability of the detector
- High sensitivity/low detection capability which enables quantitative characterization at %-level accuracy and precision

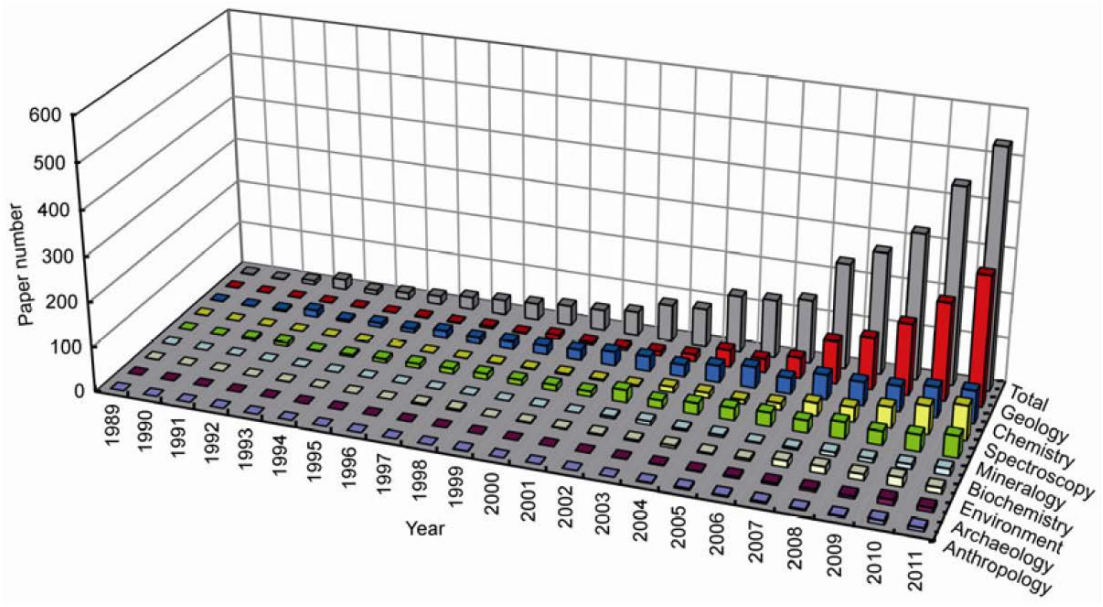

Figure 2. Number of LA-ICPMS applications in different academic fields over the past ~20 years (from Liu et al., 2013).

A major factor for the rapidly increasing popularity is the ability of LA-ICPMS to perform (ultra) high resolution analysis, thanks to controlled laser ablation via short-wavelenghts UV laser beams, improved signal washout due to modifications at the ablation cell and the high performance of the quadrupole mass analyser (see 2.5.2 for details).

Laser ablation can be performed using two different approaches: (1) Lateral profiling, i.e. laser ablation along a defined transect on the sample's surface (2) Depth profiling, which involves static layer by layer removal of material at low laser repetition rates (1 - 2 Hz) to establish a depth-composition relationship (e.g. Eggins et al., 2004; Woodhead and Hergt, 2005; Griffiths et al., 2013; Evans et al., 2015). LA-ICPMS depth profiling has been proven effective in investigating trace elemental variation at sub-µm resolution, because the limiting factor for resolution is depth ablated per individual laser pulse (typically ≤ 0.1 - 0.15 µm) and not the diameter of the laser spot (Griffiths et al., MacDonald et al., 2008; Woodhead et al., 2008). However, the depth range during static spot analysis is physically limited by the laser focal depth and the aspect ratio (depth/diameter) of the laser drilled hole that in turn is controlled by its tapering angle.

Chapters 4 and 5 demonstrate that ultra-high resolution (≤ 4 µm) can also be achieved in lateral LA-ICPMS profiling mode when using a rectangular spot, which allows for very thin compositional (shell growth) bands to be resolved, while maintaining detection of low concentration elements such as Ba and B, besides Mg and Sr, in aragonite. Lateral laser profiling also enables investigating the trace element composition along long distances (several

cm) to produce long-term, ultra-high resolution time-series records. In Chapter 4 we provide the details for our developed novel methodological approach for ultra-high resolution LA-ICPMS analysis.

Comparable in-situ analytical techniques with regards to spatial resolution are (nano)SIMS (secondary ion mass spectrometry) and EMPA (electron micro probe analysis). SIMS allows greater lateral spatial resolution (e.g. 1 µm) and also isotope ratio analysis of light non-metals (e.g. Rollion-Bard et al., 2011). NanoSIMS allows in situ-sampling at 50 nm resolution (Hoppe et al., 2013), however analysis time and running costs are significantly higher. EMPA also offers better lateral spatial resolution (~ 1 µm) compared to LA-ICPMS, however at much lower detection limits (100s of ppm) and higher costs (e.g. Reed, 2005)

2.5.2 Analytical fundamentals

The basic and simplified LA-ICPMS operating principle (e.g. Günther, 1999; Becker, 2002; Liu et al., 2013) is that a high energy-density, pulsed laser beam (GW/m^2), is focused onto the surface of a sample contained in an airtight ablation cell (usually in a He atmosphere), where it ablates the sample. The resulting particle aerosol is transported via an inert carrier gas (He and/or Ar) into the ICP to be ionized by an Ar plasma. Positively charged ions are filtered according to their mass-to-charge ratios by the mass spectrometer before being detected.

A wide range of laser ablation systems exist and similarly there is broad choice with regards to ICPMS instrumentation, including quadrupole, sector-field, time of flight (TOF) and MC-ICPMS; the latter allows high precision isotopic ratio analysis. Quadrupole analyzers are mostly used in ICPMS systems (Becker, 2002). All LA-ICPMS analyses (Chapter 3, 4 and5) were carried out using a 193 nm ArF excimer laser ablation system (RESOlution M-50, formerly Resonetics, now ASI, Canberra, Australia) featuring a two-volume laser ablation cell (Laurin Technic, Australia), which is connected to an Agilent 7500ce quadrupole ICPMS. The LA-ICPMS system was developed at RHUL and is described in detail in Müller et al. (2009).

193 nm ArF excimer laser

The term ‘excimer’ is an abbreviation for ‘excited dimer’. A ‘dimer’, refers to a molecule or structure of two identical sub-units, e.g. Xe_2. The first xenon dimer laser was developed by Basov, Danilychef and Popov in 1970. In modern lasers however, a combination of a noble gas (e.g. Ar, Kr, Xe) and a highly reactive gas (e.g. Fl, Cl) is used and therefore the term ‘excimer’ is misleading. Because noble gases are highly inert and do not usually form chemical compounds, such diatomic molecules can only exist in an excited state, which is achieved by electrical stimulation and/or high pressure (e.g. Stafe et al., 2014). By undergoing spontaneous or stimulated emission, such an (electronically) excited complex, or ‘exciplex’, gives up excess

energy in the ultraviolet range, resulting in a ground state molecule which dissociates back into unbound atoms. The laser operation wavelength depends on the choice of the exciplex. For instance, the wavelengths 193, 248 and 351 nm correspond to ArF, KrF and XeF laser systems, respectively (e.g. Stafe et al., 2014). The choice of the laser system and as such the wavelength strongly depends on the sample material. It is generally accepted that short UV wavelengths are better suited than visible or IR radiation, for controlled ablation of materials which are transparent in the visible spectrum (e.g. Günther et al., 1999). The reason is the absorption behaviour of different materials. Highly transparent materials like glass, carbonate minerals or ice are characterized by a low energy absorption efficiency, which means laser radiation does not interact with the immediate mineral surface only, but surpasses into deeper layers, were absorption occurs at e.g. crystal fractures, inclusion or cleavage planes, causing rupturing and flaking of the crystals (e.g. Günther et al., 1999). The result is uncontrolled ablation with irregular ablation pits or tracks. However, most substances, including carbonates, show a high absorptivity for deep UV radiation (Günther et al., 1999). Jeffries et al. (1998) demonstrated 100 % energy absorbance in calcite for wavelengths ≤ 200 nm. Furthermore, the laser beam wavelengths also influences the particle size distribution of the ablated material. The percentage of small aerosol particles increases with shorter wavelengths, which is beneficial for the aerosol transport and vaporization, atomization and ionization within the ICP source (e.g. Guilling et al., 2003). Hence, the193 nm ArF laser system is perfectly suited for controlled ablation - even at ultra-high resolution - of our aragonite shells.

Two-volume laser cell

The LA-system features a two-volume laser cell (Laurin Technic, Australia). In short, this He-filled 'double' cell consists of a smaller funnel-shaped cell (volume ~1-2 cm^3), which is located stationary within a movable (mounted on a X-Y stage) gas tight cell box (volume ~380 cm^3), which also accommodates the sample holder. Crucially, laser ablation is confined to the small volume cell and the produced sample aerosol is transported in a He stream directly to the ICPMS.

This arrangement has two main advantages, namely the outer sample cell is large enough (50 mm x 50 mm, or larger) to accompany both a sample and two standard mounts, but the effective gas volume at the ablation site (inner cell) is small. A small cell gas volume guarantees rapid signal washout, invariant gas flow and as such uniform sensitivity and reproducible fractionation and no sample cross contamination (e.g. Eggins and Shelley, 2002; Müller et al., 2009).

Argon plasma and interface region

The ablated sample aerosol is introduced into the ICP quartz torch, where an Ar plasma operated at atmospheric pressure and characterized by a high temperature discharge (~6500 - 10000 K), dissociates, atomizes and ionizes the sample. The positively charged ions are directed into the interface region, which is maintained at a vacuum of ~1 Pa with a mechanical roughing pump (e.g. Batsala et al., 2012). The interface region consist of two cones, the sampling and skimmer and cone, and a complex system of electrostatic lenses, which collimate and focus the ion beam (consisting of positively charged ions only) into the quadrupole mass filter, which operates at a high vacuum (0. 01 Pa).

Quadrupole mass spectrometer and detector

In the quadrupole mass filter four round, hyperbolic rods are aligned in a parallel diamond pattern. Opposite pairs of rods are exposed to rapidly changing AC (alternating current) and DC (direct current) voltages, resulting in an electrical potential between opposite rods, which is either negative or positive. The ion beam enters into the path between the four rods. The DC and AC voltages are set to certain values so that only ions of a specific mass-to-charge ratio (m/z) at - a given time - are passed through to the detector (Batsala et al., 2012). A distinguishing factor that allows LA-ICPMS to compete as (ultra) high resolution analysis technique is the capability of the quadrupole MS to sequentially filter masses (m/z) with a resolution of ~1 amu (atomic mass unit: $1.66053886 * 10^{-27}$ kg), therefore different isotopes of the same element can be analysed. Moroeover, the quadropule MS can filter up to 2400 amus per second which highlights that mass filtering happens almost simultaneously.

Once the ions have been separated by their mass-to-charge ratio they are directed to the electron multiplier detector (discrete dynode detector), which is a simultaneous dual mode detector with high speed amplifier providing nine orders (e.g. ppt-ppm) of dynamic range.

2.5.3 Limitations to LA-ICPMS

The limiting factors for ICPMS analysis are mass spectroscopic interferences, such as isobaric, polyatomic or doubly-charged interferences. Isobaric interference refers to isotopes which share the same mass number, e.g. ^{87}Sr - ^{87}Rb, ^{58}Fe - ^{58}Ni and ^{40}Ar - ^{40}Ca - ^{40}K. Polyatomic interference results from the combination of two or more isotopes from different elements, which usually occur in the plasma (Ar plasma gas) and/or in association with the formation of oxides, e.g. ^{31}P - ^{15}N^{16}O and ^{56}Fe - ^{40}Ar^{16}O. To avoid mass interferences it is necessary to carefully select the elements and isotopes to be analyzed, for instance when analysing Sr, the common ^{87}Sr - ^{87}Rb interference can be avoided by analysing ^{88}Sr.

Another source of inaccuracy in the LA-ICPMS analysis of carbonates is the lack of suitable carbonate standards (Evans, 2015). A main requirement for a suitable LA-ICPMS standard is compositional homogeneity on the µm-scale even for elements at low elemental concentration (Evans, 2015; Müller et al., 2015). However, the currently available carbonate standards, either natural or artificial carbonate minerals, don't fulfill these requirements (Müller et al., 2015). As a result, the synthetic glass standards NIST 612 and NIST 610 are used for the calibration of laser ablation data. These glass standards are artificially enriched in trace elements, reasonable homogeneous and available in sufficient quantities, however their significantly different composition leads to "mismatched matrix-derived inaccuracies" (Evans, 2015).

Details on the achieved data accuracy and reproducibility using different LA-ICPMS experimental set-ups and operation conditions can be found in Chapters 3, 4 and 5.

References

Barbin, V., Brand, U., Hewitt, R.A., and Ramseyer, K., 1995, Similarity in cephalopod shell biogeochemistry since carboniferous: evidence from cathodoluminescence: Geobios, v. 26, p. 701–710.

Batsala, M., Chandu, B., Sakala, B., Nama, S., and Domatoti, S., 2012, Inductively coupled plasma mass spectrometry (ICP-MS): International Journal of Research in Pharmacy and Chemistry, v. 2 (3), p. 671-680.

Becker, J.S, 2002, Applications of inductively coupled plasma mass spectrometry and laser ablation inductively coupled plasma mass spectrometry in materials science: Spectrochimica Acta Part B, 57, p. 1805-1820.

Birck, J.L., 1986, Precison K-Rb-Sr isotopic analysis: application to Rb-Sr chronology: Chemical Geology, v. 56, p. 73–83.

Durrant, S.F., and Ward, N.I., 1994, Laser ablation-inductively coupled plasma mass spectrometry (LA-ICP-MS) for the multielemental analysis of biological materials: a feasibility study: Food Chemistry, Analytical Methods Section, v., 49, p. 317-323.

Eggins, S.M., Sadekov, A., and De Deckker, P., 2004, Modulation and daily banding of Mg/Ca in *Orbulina universa* tests by symbiont photosynthesis and respiration: a complication for seawater thermometry? : Earth and Planetary Science Letters, v. 225, p. 411-419.

Eggins, S.M., and Shelley, J.M.G., 2002, Compositional heterogeneity in NIST SRM 610-617 glasses: Geostandards Newsletter, v. 26, p. 269-286.

Elderfield, H., 1986, Strontium Isotope Stratigraphy: Palaeogeography, Palaeoclimatology, Palaeoecology, v. 57, p. 71-90.

England, M.H., and Huang, F., 2005, On the interannual variability of the Indonesian Throughflow and its linkage with ENSO: Journal of Climate, v. 18, p. 1435–1444.

Evans, 2015, Spatially-resolved trace element records in cultured and fossil foraminifera: Cenozoic ocean chemistry, palaeoseasonality and tropical temperature reconstruction: PhD thesis, RHUL.

Evans, D., Erez, J., Oron, S., and Müller, W., 2015, Mg/Ca-temperature and seawater-test chemistry relationships in the shallow-dwelling large benthic foraminifera *Operculina ammonoides*: Geochimica et Cosmochimica Acta, v. 148, p. 325-342.

Faure, G., and Mensing, T.M., 2005, Isotopes: Principles and applications: Wiley & Sons, New York, 897 pages.

Gotte, T., and Richter, D.K., 2009, Quantitative aspects of Mn-activated cathodoluminescence of natural and synthetic aragonite: Sedimentology, v. 56, p. 483–492.

Gray, AL., 1985, Solid sample introduction by laser ablation for inductively coupled plasma source-mass spectrometry. Analyst, v. 110, p. 551-556.

Griffiths, N., Müller, W., Johnson, K.G., and Aguilera, O.A., 2013, Evaluation of the effect of diagenetic cements on element/Ca ratios in aragonitic Early Miocene (~ 16 Ma) Caribbean corals: Implications for 'deep-time' palaeo-environmental reconstructions: Palaeogeography, Palaeoclimatology, Palaeoecology, v. 369, p. 185-200.

Jeffries, T.E., Jackson, S.E. and Longerich, H.P., 1998, Application of a frequency quintupled Nd:YAG source (λ=213 nm) for laser ablation inductively coupled plasma mass spectrometric analysis of minerals: Journal of Analytical Atomic Spectrometry, v. 13, p. 935-940.

Guillong, M., Horn, I., and Günther, D., 2003, A comparison of 266 nm, 213 nm and 193 nm produced from a single solid state Nd:YAG laser for laser ablation ICP-MS: Journal of Analytical Atomic Spectrometry, v. 18, p. 1224-1230.

Günther, D., Jackson, S.E., and Longerich, H.P., 1999, Laser ablation and arc/spark solid sample introduction into inductively coupled plasma mass spectrometers Spectrochimica Acta Part B, v. 54, p. 381-409.

Hoppe, P., Cohen. S., and Meibom, A., 2013, NanoSIMS: Technical aspects and applications in cosmochemistry and biological geochemistry: Geostandards and Geoanalytical Research, v. 37 (2), p. 111-154.

Limbeck, A., Galler, P., Bonta, M., Bauer, G., Nischkauer, W., and Vanhaecke, Frank, 2015, Recent advances in quantitative LA-ICP-MS analysis: challenges and solutions in the life

sciences and environmental chemistry: Analytical and Bioanalytical Chemistry, v. 407, p. 6593-6617.

Liu, Y.S., Hu, Z.C., Li, M., and Gao, S., 2013, Applications of LA-ICP-MS in the elemental analyses of geological samples: Chinese Science Bulletin, v. 58, p. 3863-3878.

McArthur, J.M., Howarth, R.J., and Bailey, T.R., 2001, Strontium isotope stratigraphy: LOWESS version 3: Best fit to the marine Sr-isotope curve for 0–509 Ma and accompanying look-up table for deriving numerical age: Journal of Geology, v. 109, p. 155-170.

McArthur, J.M., and Howarth, R.J., 2004, Strontium isotope stratigraphy, in Gradstein, F.M., Ogg, J.G., and Smith, A.G., eds., A Geological Timescale 2004: Cambridge University Press, Cambridge, U.K., p. 589.

McArthur, J.M., Howarth, R.J., and Shields, G.A., 2012, Strontium Isotope Stratigraphy: In: The Geologic Time Scale 2012, p. 127-144.

MacDonald, J.I., Shelley, J.M.G., Crook, D.A., 2008, A method for improving the estimation of natal chemical signatures in otoliths: Trans. Am. Fish. Soc., v. 137, p. 1674-1682.

Müller, W., Shelley, M., Miller, P., and Broude, S., 2009, Initial performance metrics of a new custom-designed ArF excimer LA-ICPMS system coupled to a two-volume laser-ablation cell: Journal of Analytical Atomic Spectrometry, v. 24, p. 209-214.

Müller, W., Valley, J.W., Warter, V., Kozdon, R., Evans, D., and Orland, I.J, 2015, Natural high-temperature metamorphic calcite as compositionally homogenous microanalytical standard?: Conference abstract, Goldschmidt, Prague.

Oslick, J.S., Miller, K.G., Feigenson, M.D., Wright, J.D., 1994, Oligocene-Miocene strontium isotopes: Stratigraphic revisions and correlations to an inferred glacioeustatic record: Paleoceanography, v. 9(3), p.427-443.

Reed, S.J.B, 2005, Electron microprobe analysis and scanning electron microscopy in Geology (2nd edition): Cambridge University Press, New York.

Renema, W., Warter, V., Novak, V., Young, Y., Marshall, N., and Hasibuan, F., 2015, Ages of Miocene fossil localities in the Northern Kutai Basin (East Kalimantan, Indonesia): Palaios, v. 30, p. 26-39.

Rollion-Bard, C., Blamart, D., Trebosc, J., Grégory, T., Mussi, A., and Cuif, J.-P., 2011, Boron isotopes as pH proxy: A new look at boron speciation in deep-sea corals using ^{11}B MAS NMR and EELS: Geochimica et Cosmochimica Acta, v. 75, p. 1003-1012

Stafe, M., Marcu, A., and Puscas, N.N., 2014, Pulsed laser ablation of solids: Basics, theory and applications: Springer Series in Surface Sciences, v. 53, Heidelberg, 233 pages.

Steiger, R., and Jäger, E., 1977, Subcommission on Geochronology: convention on the use of decay constants in geo- and cosmochronology: Earth and Planetary Science Letters, v. 36, p. 359-362.

Thirlwall, M.F., 1991, Long-term reproducibility of multicollector Sr and Nd isotope ratio analysis: Chemical Geology (Isotope Geochemistry Section), v. 94, p. 85-104.

Warter, V., and Müller, W., 2016, Daily growth and tidal rhythms in Miocene and modern giant clams revealed via ultra-high resolution LA-ICPMS analysis – A novel methodological approach towards improved sclerochemistry: Palaeogeography, Palaeoclimatology, Palaeoecology, doi:10.1016/j.palaeo.2016.03.019.

Woodhead, J.D., and Hergt, J.M., 2005, A preliminary appraisal of seven natural zircon reference materials for *in situ* Hf isotope determination: Geostandards and Geoanalytical Research; v., 29, p. 183-195.

Woodhead, J., Hellstrom, J., Paton, C., Hergt, J., Greig, A., and Maas, R., 2008, A guide to depth-profiling and imaging applications of LA-ICP-MS, in: Laser-ablation-ICP-MS in Earth Sciences: Current practices and outstanding issues: Mineralogical Association of Canada short Course 40, Vancouver, B.C., p.135-145.

Chapter 3: Case study 1

Citation:

Warter, V., Müller, W., Wesselingh, F.P., Todd, J.A., and Renema, W., 2015, **Late Miocene seasonal to sub-decadal climate variability in the Indo-West Pacific (East Kalimantan, Indonesia) preserved in giant clams**: Palaios, v. 30, p. 66-82.

The supplementary electronic data set of the trace element and stable isotope analyses related to this chapter are provided within the appendix.

Author contributions:

Viola Warter designed the research in discussion with Wolfgang Müller, performed the analyses, interpreted the data and wrote the manuscript. Wolfgang Müller helped with the LA-ICPMS analytical set-up. Müller, W., Renema, W., Wesselingh, F.P, and Todd, J.A., conducted the fieldwork and edited the manuscript.

LATE MIOCENE SEASONAL TO SUBDECADAL CLIMATE VARIABILITY IN THE INDO-WEST PACIFIC (EAST KALIMANTAN, INDONESIA) PRESERVED IN GIANT CLAMS

Author(s): VIOLA WARTER, WOLFGANG MÜLLER, FRANK P. WESSELINGH, JONATHAN A. TODD, and WILLEM RENEMA
Source: PALAIOS, 30(1):66-82.
Published By: Society for Sedimentary Geology
URL: http://www.bioone.org/doi/full/10.2110/palo.2013.061

PALAIOS
Emphasizing the impact of life on Earth's history

PALAIOS, 2015, v. 30, 66–82
Research Article
DOI: http://dx.doi.org/10.2110/palo.2013.061

LATE MIOCENE SEASONAL TO SUBDECADAL CLIMATE VARIABILITY IN THE INDO-WEST PACIFIC (EAST KALIMANTAN, INDONESIA) PRESERVED IN GIANT CLAMS

VIOLA WARTER,[1] WOLFGANG MÜLLER,[1] FRANK P. WESSELINGH,[2] JONATHAN A. TODD,[3] AND WILLEM RENEMA[2]
[1]*Royal Holloway University of London, Department of Earth Sciences, Egham, Surrey, TW20 0EX, U.K.*
[2]*Naturalis Biodiversity Center, Department of Geology, P.O. Box 9517, Leiden, 2300 RA, The Netherlands*
[3]*Natural History Museum, Department of Earth Sciences, Cromwell Road, London, SW7 5BD, U.K.*
e-mail: viola.warter@rhul.ac.uk

ABSTRACT: **Two late Miocene *Tridacna* (giant clam) shells from East Kalimantan (Indonesia) were investigated in order to evaluate their potential as subannually resolved paleoenvironmental archives. Via a combination of X-ray diffraction (XRD), laser ablation–inductively coupled plasma–mass spectrometry (LA-ICPMS) trace element analysis, scanning electron microscopy (SEM) and cathodoluminescence (CL) imaging, pristine versus diagenetically altered domains within the shells were identified. LA-ICPMS transects targeting altered aragonite and calcite zones reveal distinct compositional differences in elemental ratios (B/Ca, Mg/Ca, Sr/Ca/ Ba/Ca, Mn/Ca, Al/Ca, La/Ca, Ce/Ca) relative to primary shell aragonite. Pristine shell domains are characterized by an intact banding pattern of alternating dark and light growth bands, with which spatially resolved LA-ICPMS element/Ca and micromilled $\delta^{18}O$ records were aligned. Light $\delta^{18}O$ values correspond to dark growth bands, indicating growth during warm seasons. The Mg/Ca and/or Sr/Ca ratios covary with oscillating stable oxygen isotope profiles. Progressive increase in Mg/Ca with age demonstrates that besides temperature, growth kinetics exert control over Mg incorporation. If interpreted as temperature controlled only, $\delta^{18}O$ from both shells represents average seasonal sea-surface temperature (SST) variability of 2.7 ± 2.1 and 4.6 ± 1.7 °C, respectively. Using published temperature equations and assuming $\delta^{18}O_{sw} = -0.88‰$, corresponding mean annual paleo–sea-surface temperatures of 27.8 ± 0.2 and 28.5 ± 0.2 °C are estimated. Although the fossil *Tridacna* shells were noticeably affected by alteration on their external surfaces, their internal aragonitic structure is, to a large extent, well preserved. These corresponding paleoproxy records provide detailed insight into tropical SST variability of the Indo-Pacific region during the late Miocene.**

INTRODUCTION

The Miocene is an epoch of major change with respect to the Cenozoic climate history (Flower and Kennett 1994). While the overall Miocene climatic evolution is well documented by the stable isotope record derived from oceanic benthic foraminifera tests (Lear et al. 2000; Zachos et al. 2001 2008; Billups and Schrag 2003), the mechanisms causing Miocene climate change are not well understood (Holbourn et al. 2007; Herold et al. 2012).

The Indonesian Throughflow (ITF), a system of currents, surface, and thermocline waters, passes through today's last remaining low-latitude ocean passage, the SE Asian gateway, which connects the Pacific and Indian oceans. It is considered to be a key initiator of climate change during the Miocene and Pliocene, not only for the Southeast Asian region but also on a global scale (Cane and Molnar 2001; Kuhnt et al. 2004; Singh and Gupta 2010). The modern ITF intensity exhibits a significant interannual variability, which is closely linked to the geographic extent and position of the West Pacific Warm Pool (Kuhnt et al. 2004) and El Niño–Southern Oscillation (ENSO) patterns (England and Huang 2005). The paleoceanographic history of the Indonesian Gateway and associated long-term fluctuations in water mass throughflow are strongly controlled by the tectonic reorganization caused by convergence of the Indo-Australian and Philippine-Pacific plates with the stable Asian craton (Hall et al. 2011). Collision between the Australian plate and the island arcs on the Pacific plates initiated in the earliest Miocene (Srinivasan and Sinha 2000; Kuhnt et al. 2004; Hall et al. 2011). The interaction between the complex tectonic history of the Southeast Asia–Australia collision zone, corresponding oceanographic modulations of the Indonesian Gateway, the associated climate and environmental change, and the resulting biotic response during the Miocene are not well understood, even though they must have interplayed (Renema et al. 2008).

Very few paleoclimate proxy records (especially from pre-Quaternary time) from the ITF area exist that give insight into its tectonic and paleocenographic evolution (Kuhnt et al. 2004). However, such records are essential to quantify paleoclimate dynamics and to disentangle their causes and effects. Furthermore, existing paleoclimate proxy data are mostly derived from the open marine and/or high-latitude realm, while direct evidence of paleoclimate from shallow water in low latitudes is rare.

Highly time-resolved paleoclimate records are of special interest, because they allow the assessment of seasonal to interannual sea-surface temperature (SST) variability, like ENSO- or monsoon-related changes in SST. Changes in seasonality play an important role with respect to (abrupt) climate changes (Crowley et al. 1986; Denton et al. 2005; Ayling et al. 2006; Fluckiger et al. 2008). Hence, SST variations (even if recorded over a relatively short period only) might contribute to our understanding of long-term climate change.

Foraminiferan records have traditionally been used to reconstruct paleotemperature/ice volume over the last ~65 myr (Zachos et al. 2001 2008). However, individuals are usually too short-lived to reflect seasonal variability. Coral skeletons are frequently used as paleoenvironmental archives for reconstructions for Pleistocene or younger strata (Alibert and

Published Online: February 2015
 0883-1351/15/030-066/$03.00

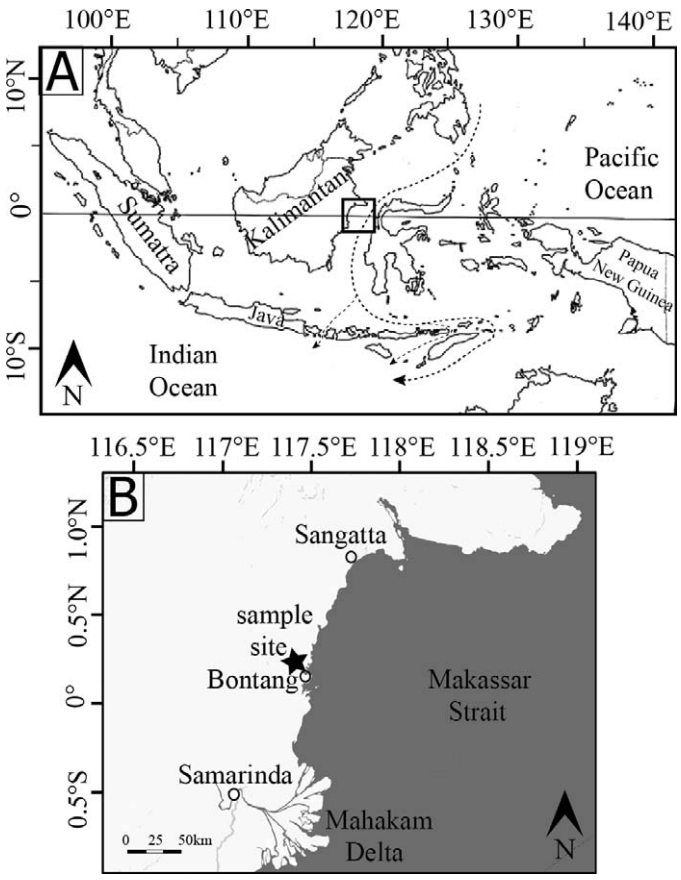

FIG. 1.—Location of study area. **A)** Overview map of the Indo-Pacific study area including the main Throughflow passages (marked by dashed arrows). **B)** Coast of East Kalimantan including Bontang and the nearby sample site with outcrops TF108 and TF109 (marked by star).

McCulloch 1997; Gagan et al. 2000; Quinn and Sampson 2002; Swart et al. 2002; Corrège et al. 2004; Mishima et al. 2009). Coral-based proxies from the Miocene, however, are still rare (Mertz-Kraus et al. 2009; Griffiths et al. 2013). Due to their porous structure and metastable aragonite mineralogy, coral skeletons are highly susceptible to diagenetic processes that affect the original shell geochemistry and challenge their reliability as environmental recorders (McGregor and Gagan 2003; Allison et al. 2007; Hendy et al. 2007; Nothdurft and Webb 2009; Hathorne et al. 2011; Sayani et al. 2011; Griffiths et al. 2013).

Bivalves build a dense shell structure, which makes the shells less prone to diagenetic alteration and thus enhances their preservation potential. Due to their outstanding longevity of up to several decades (Watanabe et al. 2004), giant clams (family Cardiidae, subfamily Tridacninae, genus *Tridacna*) are particularly attractive sclerochronological archives and can provide important contributions to paleoclimatic research (Aharon 1991; Watanabe and Oba 1999; Elliot et al. 2009; Batenburg et al. 2011; Welsh et al. 2011). In contrast to corals, they precipitate their shells in, or close to, isotopic equilibrium (Romanek and Grossman 1989; Aharon 1991; Elliot et al. 2009). Carbonate accretion takes place on a daily basis, which is recorded as microscopically visible growth increments in the shell structure (Aharon and Chappell 1986; Watanabe and Oba 1999; Sano et al. 2012). In the case of giant clams, bands grown during warm periods can usually be distinguished from those secreted during cold months, due to subtle color/density differences (Aharon 1991; Elliot et al. 2009; Welsh et al. 2011) and the resulting banding pattern thus provides a good lifespan control. Furthermore, *Tridacna* shell growth is fast, with growth rates from several mm/yr up to several cm/yr (Beckvar 1981; Aharon 1991; Elliot et al. 2009), which enables sampling and analysis at sub-seasonal time resolution. Moreover, *Tridacna* have a broad geographic distribution throughout the tropical and subtropical regions of the Indo-Pacific Ocean (Harzhauser et al. 2008; Hernavan 2012), and hence, are ideal low-latitude paleoclimate archives. However, well-preserved giant clams from Miocene strata are rare and so are corresponding studies (Batenburg et al. 2011). Despite their dense structure, diagenetic processes like neomorphism and cementation (enhanced by bioerosion) can affect the aragonitic shell structure. Very little work has been done on *Tridacna* shell diagenesis (Moir 1990; Faylona et al. 2011) and its impact on the original shell geochemistry.

Here, we present results from *Tridacna* shells of late Miocene (Tortonian) age from East Kalimantan, Indonesia. Our multi-proxy approach utilizes spatially resolved laser ablation–inductively coupled plasma-mass spectrometry (LA-ICPMS) element/Ca ratios (Mg/Ca, Sr/Ca, Ba/Ca) and microsampled $\delta^{18}O/\delta^{13}C$ records, which are aligned with the shell-banding pattern. Our primary aims are (1) to evaluate the fidelity of Miocene shells as paleoclimate archives by assessing their preservation, (2) to investigate how climate and paleoenvironmental proxy data contained within the shells can be extracted (3) to assess what information they contain about Miocene seasonality.

MATERIAL AND METHODS

The samples were obtained from the eastern coast of Borneo in the Indonesian province of East Kalimantan, close to the city of Bontang (Fig. 1). The two *Tridacna* shells studied herein were collected in December 2010 from outcrops TF108 (0° 11′ 7.08″ N, 117° 26′ 47.04″ E) and TF109 (0° 11′ 11.40″ N, 117° 26′ 40.92″ E). The outcrops are situated in close proximity to each other (~250 m distance) and at equal elevation (within GPS accuracy). A detailed overview of the Bontang area including TF localities 108 and 109 is provided in Renema et al. (2015). Both outcrops (Fig. 1) contain a rich, reef-associated fossil fauna embedded in light-brown, clay-rich Miocene carbonate sediments. Owing to their low permeability, clay-rich sediments provide a natural sealing for carbonate fossils (Pearson et al. 2001) and thus help facilitate excellent fossil preservation.

Biostratigraphic data, based on large benthic foraminifera and calcareous nannoplankton, indicate an early Tortonian (late Miocene) age for the studied strata in the Bontang area (Renema et al. 2015). Stratigraphically, the fossiliferous sediments of TF108 overlie those of TF109, with ~25 m of sediment in between.

The exteriors of both *Tridacna* shells are morphologically and mineralogically altered, resulting in the loss of important morphological features, such as fine details of the ribbing pattern and the hinge area (Fig. 2A, B). Thus, TF109LGS1 (further referred to as LGS1) was not identifiable to the species level. Shell TF108BW4B (further referred to as BW4B) is characterized by general elongate, low egg-shape, subtrigonal outline with widely spaced, low-wavy ribs, resembling those of *Tridacna derasa* (Röding 1798). However, the altered shell exterior prevents confident species identification. Both specimens are reposited in the collections of the Department of Earth Sciences, Natural History Museum, London (NHMUK), with the following registration numbers; PI TB 14531 (BW4B) and PI TB 14532 (LGS1).

To remove organic matter and sediment particles from external shell parts, the *Tridacna* shells were thoroughly cleaned using deionized water and a toothbrush. The valves were then cut along their maximum growth axis, from the umbo to the ventral margin (Fig. 2C, D).

Strontium Isotope Stratigraphy (SIS)

SIS was performed on seven *Tridacna* shells and four associated scleractinian corals (family Faviidae) in order to confirm the biostrati-

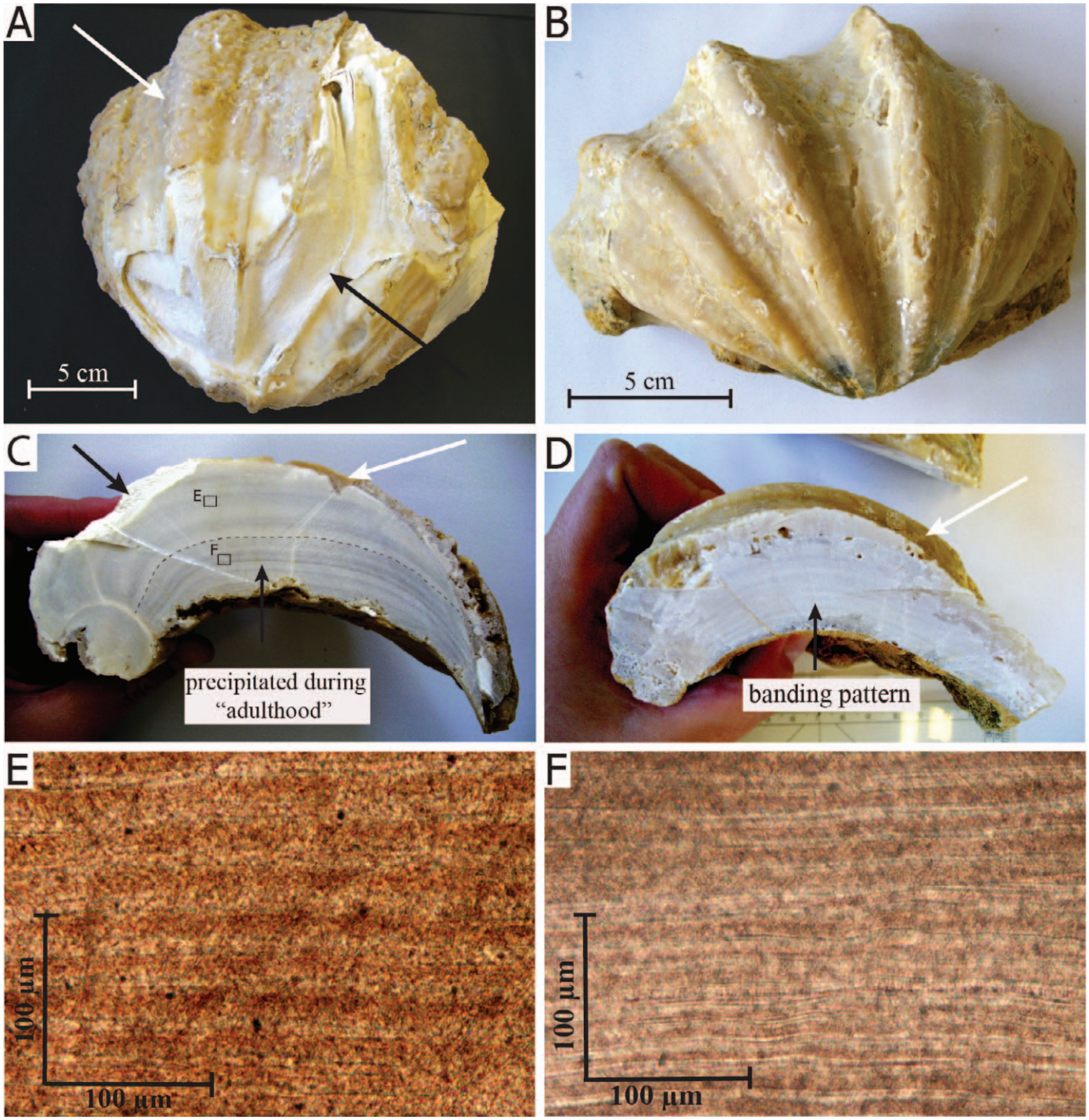

FIG. 2.—Photographs of whole and sectioned valves of BW4B and LGS1 and micrographs of daily growth increments of LGS1. **A)** Valve of LGS1; white arrow indicates presence of calcite, black arrow indicates altered aragonite. **B)** Valve of BW4B with completely recrystallized outer shell layer. **C)** Cross section of LGS1; white arrow indicates calcite, black arrow indicates altered aragonite. Gray dashed line marks the assumed transition between shell bands formed during juvenile phase and those secreted during the adulthood. **D)** Cross section of BW4B; white arrow indicates calcite; internal shell parts reveal a banding pattern. **E)** Daily growth increments of LGS1 secreted during juvenile phase, approximate position indicated in Part C. **F)** Daily growth increments of LGS1 secreted during adulthood, approximate position indicated in Part C.

graphically determined age estimates for the sampled fossil horizons from the Bontang area (Renema et al. 2015). The samples are derived from six different localities (TF 102, 108, 109, 110, 154, and 502), all situated west of the city of Bontang (Fig. 1B) and within a maximum distance of six km to each other.

Carbonate powders weighing between 5–100 mg were produced using a hand drill fitted with a 1 mm drill bit. Wet geochemistry procedures for Sr purification included dissolution in concentrated HNO_3, acidic rediges-tion in 4 M HNO_3 and extraction chromatography using Eichrom® Sr-spec resin (30 mg). Sr was loaded onto degassed single rhenium filaments,

TABLE 1.—*LA-ICPMS operating conditions.*

ICPMS parameters	Agilent 7500ce
RF power	1140–1320 W
Carrier gas flow (Ar)	0.53–0.67 l/min
Sampler, skimmer cones	Ni
Extraction lenses	ce
Monitored masses (m/z)	11, 23, 24, 25, 27, 31, 43, 55, 65, 66, 85, 89, 111, 138, 139, 140, 208, 238
Tuning parameters	$^{232}Th/^{238}U > 95\%$; $^{248}ThO/^{232}Th < 0.5\%$
Laser ablation system	Resolution M-50 (prototype)
He gas flow	850 ml/min
H_2 gas flow	8.5 ml/min
Laser repetition rate	15 Hz
Laser spot size	57 μm

preconditioned with H_3PO_4 and tantalum emitter after Birck (1986). $^{87}Sr/^{86}Sr$ ratios were measured on a VG354 multicollector thermal ion mass spectrometer (TIMS) in multidynamic mode (Thirlwall 1991) at RHUL. Control over mass fractionation for all measured ratios was guaranteed by normalization to the $^{86}Sr/^{88}Sr$ ratio of 0.1194. The long-term mean (2011–2012; n = 97) of measured $^{87}Sr/^{86}Sr$ of the international standard NIST SRM 987 is 0.710256 ± 0.000020 (2 SD). All data were corrected relative to the adopted NIST SRM 987 $^{87}Sr/^{86}Sr$ ratio of 0.710248. Resultant $^{87}Sr/^{86}Sr$ ratios were converted into their respective numerical ages by cross-correlation with the strontium isotope data set of the SIS Look-Up Table Version 4: 08/04 (McArthur et al. 2001; McArthur and Howarth 2004). Age minima and maxima were calculated by combining the statistical uncertainty of the SRM 987 long-term reproducibility (2 SD) with the upper and lower confidence limit reported with each Sr isotope ratio in the SIS Look-Up Table.

Scanning Electron Microscopy (SEM) and Cathodoluninescence (CL) Imaging

SEM was applied to investigate the morphology and crystalline structure of well-preserved and diagenetically altered shell domains. Uncoated samples were investigated using a LEO 1455 variable pressure (VP) SEM (operated at 15 kV) utilizing a solid-state 4 quadrant backscattered electron (BSE) detector and a Quanta 650 ESEM FEG used in VP mode with air as the imaging gas (operated at 7 kV) at the Natural History Museum, London. To enhance visibility of structural morphology, some samples were etched using acetic acid (different concentrations up to 5%, and different reaction times up to 30 min). High-quality digital imaging was performed using the LEO 1455 up to a magnification of 1200× and using the Quanta 650 up to a magnification of 4000×. Polished thin sections of shell cross sections were examined by cold CL microscopy using a Technosyn 8200 MkII luminoscope connected to a Nikon Optiphot petrological microscope at Royal Holloway University of London (RHUL).

X-Ray Diffraction (XRD)

XRD was conducted to determine the mineralogical structure of targeted shell domains. Powdered samples were produced by hand drilling and grinding (using mortar and pestle). Analyses were conducted on a few mg of shell carbonate using a Philips PW1830/3020 spectrometer with Cu Kα radiation, operated at 40 kV. Diffraction angles (2θ) between 25° and 37° were scanned, which include the main peaks of the $CaCO_3$ polymorphs calcite and aragonite. The limit of detection is typically better than 3%.

Laser Ablation–Inductively Coupled Plasma–Mass Spectrometry (LA-ICPMS)

Trace element variability was investigated using LA-ICPMS. Shell cross sections were cut to fit into the LA-ICPMS sample holder (49.5 mm × 27.5 mm × 7 mm) using a water-cooled Jencons Tyslide diamond saw. In order to produce a smooth sample surface and to enhance the visibility of growth increments, sample slabs were polished using silicon carbide paper (Buehler) on a rotating disk. Continuous trace element/Ca ratio profiles were obtained at RHUL using a 193 nm ArF excimer laser ablation system (Resolution M-50 prototype, Resonetics LLC, U.S.A.) featuring a Laurin two-volume laser ablation cell connected to an Agilent 7500ce quadrupole ICPMS (Müller et al. 2009). The LA-ICPMS operating conditions and monitored isotopes are given in Table 1. Shell material was ablated (following the preablated path) using a spot size of 57 μm, ablation speed of 1.8 mm/min and repetition rate of 15 Hz. To ensure a clean sample surface, preablation in two passes was performed (spot diameter of 74 μm, ablation speed of 6 mm/min, repetition rate 25 Hz). ^{43}Ca was used for internal standardization. Data reduction broadly followed Longerich et al. (1996) and was performed using Iolite run under Igor Pro (WaveMetrics, Inc., version 6.22A). NIST SRM 612 (Jochum et al. 2011a) was used as external standard and analyzed before and after each sample. The MPI-DING glasses GOR132-G, GOR128-G, and KL2-G were treated as unknowns and analyzed with each sample. Analytic accuracy was assessed by comparing the measured elemental abundances with the known and certified values of these standards (Jochum et al. 2011b). The samples were analyzed over a period of 6 months. Mean analytical accuracy (%) was 7.0, 4.0, 1.0, 10.5, 2.2, and 7.6 for B, Mg, Sr, Ba, La, and Ce, respectively.

Continuous traverses were analyzed perpendicular to visible growth bands to monitor the variability of trace elemental composition through time (time-series analysis). Ablation was performed from the inner shell edge (formed later in the life of the bivalve/ontogenetically older shell part) to the external rim of the shell (formed earlier in the life of the bivalve/ ontogenetically younger shell part).

Stable Isotope Analysis

Powdered aragonite samples were recovered from polished shell slabs using a semiautomated New Wave micromill fitted with a 300 μm drill bit. Single grooves with a length of 2 mm, depth of 360 μm, and width of 200 μm were milled parallel to existing growth bands in continuous mode. The powdered samples (300–400 μg) were analyzed for carbon and oxygen isotope ratios using a Micromass Multiflow head space system connected to a GV Instruments Isoprime IRMS at RHUL. After digestion in 103% orthophosphoric acid at 90 °C and a minimum of four hours reaction time, the evolved CO_2 was expanded into the sample loop and then delivered to the Isoprime mass spectrometer within continuous He-carrier gas flow. Each sample and standard was analyzed twice. Averaged precision (1 SD) of duplicates was 0.04‰ for $\delta^{18}O$ and 0.03‰ for $\delta^{13}C$. Standards used are NBS-19 and LSVEC international standards and an in-house standard (RHBNC calcite). Isotopic ratios are calibrated against these standards and expressed in conventional delta notation per mil values.

RESULTS

The results of sample imaging, XRD, and (isotope) geochemical analysis are displayed in Figures 2 to 10 and summarized in Tables 2 and 3.

Macroscopic and Microscopic Observations

The two shells studied, BW4B and LGS1, are visually affected by diagenetic alteration in their external shell parts (Fig. 2A, B). LGS1

TABLE 2.—*$^{87}Sr/^{86}Sr$ isotope ratios from 7* Tridacna *shells and 4 coral skeletons and data obtained from altered shell parts of BW4B and LGS1. Reported age estimations are derived from correlation with best fit data from SIS Look-Up Table V4: 08/04 (McArthur et al. 2001; McArthur and Howarth 2004). Errors result from the statistical uncertainty of the SRM 987 external reproducibility (±0.000020) combined with the upper and lower confidence limit of the respective "best fit" data.*

Tridacna/Coral sample	Measured $^{87}Sr/^{86}Sr$ ± 2SD	Resultant age (Ma)	+ error (Ma)	- error (Ma)
TF108BW4B (*Tridacna*)	0.708903 ± 11	9.75	0.39	0.37
TF109LGS1 (*Tridacna*)	0.708921 ± 11	9.16	0.65	0.46
TF08BW6 (*Tridacna*)	0.708921 ± 11	9.16	0.65	0.47
TF109WM (*Tridacna*)	0.708910 ± 09	9.55	0.48	0.38
TF110BW3 (*Tridacna*)	0.708930 ± 10	8.75	1.00	0.57
TF108BW10 (*Tridacna*)	0.708910 ± 12	9.55	0.48	0.38
TF108BW (*Tridacna*)	0.708897 ± 10	9.92	0.38	0.38
TF102BW1 (Coral)	0.708939 ± 11	8.24	0.92	0.71
TF154BW7 (Coral)	0.708903 ± 11	9.75	0.39	0.37
TF102BW2 (Coral)	0.708911 ± 09	9.52	0.50	0.38
TF502NS7 (Coral)	0.708905 ± 10	9.70	0.41	0.37
TF108BW4B calcite	0.708919 ± 11	9.25	0.64	0.43
TF109LGS1 calcite	0.708930 ± 11	8.75	1.00	0.57
TF109LGS1 sec. aragonite	0.708909 ± 11	9.58	0.46	0.38

contains calcified domains and also zones of a relatively porous, friable aragonite microstructure, which is henceforth referred to as altered aragonite (Fig. 2A, C). The outermost shell rim (~5–10 mm) of BW4B is completely recrystallized (Fig. 2B, D). However, both shell cross sections reveal an internal shell structure that to a large extent seems excellently preserved, and which is characterized by a distinct banding pattern, formed by alternating dark-light bands (Fig. 2C, D).

Light observations reveal that bands which appear relatively dark using reflected light illumination are most translucent/least dense, and therefore, appear bright under transmitted light, whereas bands which appear light using a reflected light source are least translucent/most dense, and therefore, appear dark under transmitted light. The literature shows inconsistencies concerning the use of terms such as "dark bands" resulting from observation using either transmitted (e.g., Aharon 1991; Watanabe et al 2004; Welsh et al. 2011) or reflected light illumination (e.g., Aubert et al. 2009; Batenburg et al. 2011). Optical descriptions of the presented shells herein refer to reflected light illumination.

Each dark-light couple likely represents a single year, which has been demonstrated for other *Tridacna* specimens (Aharon 1991; Elliot et al. 2009; Batenburg et al. 2011). Daily growth increments within the annual growth bands have been reported before (Watanabe and Oba 1999; Watanabe et al. 2004; Sano et al. 2012) and similarly can be identified in these late Miocene *Tridacna* shells using petrographic microscopy (Fig. 2E, F).

Both annual and daily growth bands indicate nonlinear growth through the lifetime of the *Tridacna* individual LGS1 (Fig. 2C, E, F), resulting in unevenly spaced time series. This Miocene clam is characterized by a rapid rate of growth and increase in shell thickness when younger (and presumably juvenile or subadult) which abruptly transitions into a phase characterized by much lower rates of shell secretion, that can be inferred to have been secreted during adulthood (Aharon 1991; Jones et al. 1986; Elliot et al. 2009). This is especially obvious when comparing the thickness of daily growth increments obtained from what we have labelled as juvenile and adult shell parts

TABLE 3.—*$\delta^{18}O_{shell}$ maxima, minima, and averaged values and respective calculated paleotemperature data of LGSI and BW4B. For comparison, published data of a Miocene* Tridacna gigas *(Batenburg et al. 2011) and corresponding paleotemperature and paleoseasonality estimates are presented. Paleotemperature/paleoseasonality was assessed using the aragonitic oxygen isotope temperature equation by Grossman and Ku (1986) and assuming $\delta^{18}O_{sw} = -0.88‰$.*

	$\delta^{18}O_{shell}$ min (‰)	$\delta^{18}O_{shell}$ max (‰)	average $\delta^{18}O_{shell}$ (‰)
LGS1	−2.90	−1.46	−2.15
BW4B	−3.00	−1.59	−2.31
Batenburg data	−2.97	−1.72	−2.30
	T (°C) max	T (°C) min	average T (°C)
LGS1	31.28	24.54	27.78
BW4B	31.75	25.13	28.52
Batenburg data	31.60	25.74	28.50
	average $\delta^{18}O_{shell}$ min (‰)	average $\delta^{18}O_{shell}$ max (‰)	
LGS1	−2.66	−1.69	
BW4B	−2.62	−2.05	
Batenburg data	−2.53	−2.09	
	average T (°C) max	average T (°C) min	**average seasonality** T (°C)
LGS1	30.17	25.60	**4.57**
BW4B	29.96	27.27	**2.69**
Batenburg data	29.54	27.47	**2.07**

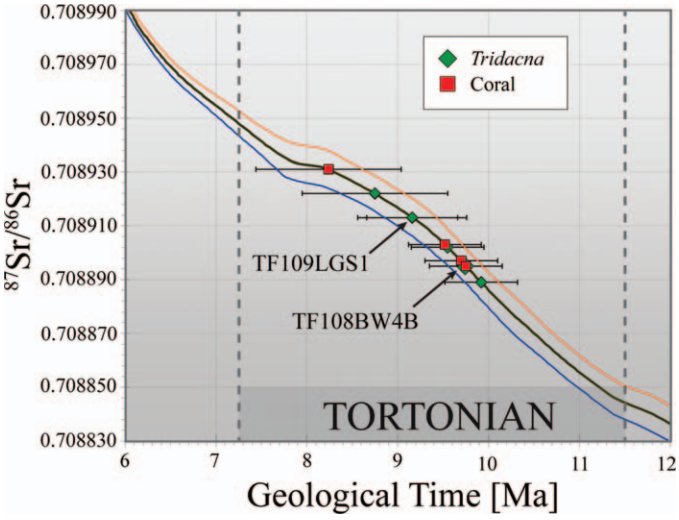

FIG. 3.—$^{87}Sr/^{86}Sr$ data of 7 *Tridacna* shells and 4 coral skeletons from the Bontang area (including results for LGS1 and BW4B) plotted versus the Sr isotope seawater curve based on the best fit data (black curve) from SIS Look-Up Table V4: 08/04 (McArthur et al. 2001; McArthur and Howarth 2004). Note that due to overlapping ratios (see Table 2) not all results can be displayed. Error bars indicate age minima and maxima, which were calculated by combining the statistical uncertainty of the SRM 987 long-term reproducibility (2 SD) with the upper (orange curve) and lower confidence limit (blue curve) reported with each Sr isotope ratio in the SIS Look-Up Table.

(Fig. 2E, F). While a distance of 100 µm corresponds to ~5 dark-light daily couplets in the juvenile shell parts (Fig. 2E), the same distance covers at least 8 dark-light daily couplets in shell parts secreted during the adult stage (Fig. 2F), representing a thickness of presumed individual daily growth increments of ~20 µm during the juvenile phase and ~12 µm during adulthood. A similar ontogenetic trend has been described in other giant clam shells (Aharon 1991; Watanabe et al. 2004; Elliot et al. 2009).

Strontium Isotope Stratigraphy

Seven *Tridacna* shells and four accompanying fossil corals from various localities with slightly different stratigraphic positions within the Bontang area (Renema et al. 2015) were selected for Sr isotope analysis. Resultant $^{87}Sr/^{86}Sr$ ratios with corresponding ages and errors are reported in Table 2 and Figure 3. The $^{87}Sr/^{86}Sr$ ratios of these individuals range between 0.708939 to 0.708897, representing ages of 8.24 to 9.92 Ma. These results clearly place the fossil assemblage into the Tortonian stage (7.25–11.61 Ma) and support biostratigraphically determined ages reported in Renema et al. (2015). The $^{87}Sr/^{86}Sr$ ratios of shells BW4B (0.708903) and LGS1 (0.708921) are identical within standard reproducibility.

To investigate the influence of diagenetic alteration on the Sr isotope ratio, clearly altered shell parts of BW4B (calcite) and LGS1 (calcite and secondary aragonite) were targeted (Table 2). Resultant $^{87}Sr/^{86}Sr$ ratios obtained from pristine aragonite and respective Sr isotope ratios from calcite and secondary aragonite respectively are identical within limits of analytical uncertainty (Table 2).

SEM and CL Imaging

Pristine aragonite consists of a crossed-lamellar, highly ordered structure (Fig. 4A, C, E, H). Single lamellae are relatively short (<10 µm) but elongate, lathlike crystals, that are inclined at nearly right angles (Fig. 4C). The tightly interlocked crystals build a very dense and solid microstructural framework. This kind of shell structure is common for aragonitic shells, including *Tridacna* specimens (Taylor et al. 1973; Moir 1990; Faylona et al. 2011). Pristine aragonite of BW4B shows patchy dissolution, "melted-like" structures (Fig. 4H), which have been reported as a sign of early recrystallization (Faylona et al. 2011).

The altered aragonite of LGS1 reveals a crossed-lamellar arrangement (Fig. 4D), similar to pristine aragonite. However, there are differences in crystal size and morphology and general shell fabric compared to pristine aragonite. The altered aragonite crystals are much larger, up to 20 µm in length (Fig. 4D, F). They are thinner and porous (Fig. 4F), which makes them friable. Furthermore, the crystals are bent, resulting in a disordered, wavelike shell structure containing cavities (Fig. 4D). Diagenetic calcite appears predominantly in the outermost rims of both shells (Fig. 4A) and is characterized by large blocky crystals, which are broken (in a stepwise manner) along their rhombohedral cleavage planes (Fig. 4B, G).

Both light and dark bands are characterized by the crossed-lamellar structure typical for pristine aragonite as described above. The formation of the banding pattern is therefore not due to structural differences. Welsh et al. (2011) suggest that dark (translucent, low-density) shell bands consist of larger crystals relative to bright bands (less translucent, high density), which seems plausible, assuming that tightly joined small crystallites will build a denser shell structure compared to fewer, larger crystallites. However, a significant difference in the size of the individual crystallites within dark and bright bands could not be resolved using SEM.

Cathodoluminescence images of pristine aragonite zones obtained from both shells reveal dark-blue luminescence (Fig. 5A, B). While LGS1 is characterized by a homogeneous blue color, bright patchy "stains" are more frequent in BW4B and additionally a single green luminescing (growth) band can be identified (Fig. 5B). Calcite at the rims of LGS1 and BW4B is characterized by blue to slightly purple luminescence (Fig. 5C, D). Specimen BW4B additionally reveals coexisting calcite zones characterized by distinct brighter, purple-pink luminescence (Fig. 5D). CL imaging did not result in better visibility of the dark-light banding pattern. Macroscopically visible dark and light bands appeared dark and light in CL mode, and no color change or distinct difference of luminescence intensity could be observed.

XRD Analyses

XRD analyses were performed on the Miocene shells, targeting well-preserved as well as altered shell domains. Hand-drilled sample powders obtained from internal shell parts (pristine aragonite) of LGS1 produced major peaks at diffraction angles (2θ) of 26.2° and 27.2°, and minor peaks at angles of 33.2° and 36.2°, all indicating aragonite (Fig. 6A). Altered aragonite from sample LGS1 produced a similar XRD spectrum to that obtained from unaltered crystals (Fig 6A).

Microscopically visible blocky calcite of both shells produced one major peak at 29.4°–29.5° 2θ typical for calcite (Fig. 6A, B). XRD analysis of ground powder recovered from the internal, visibly well preserved shell parts of BW4B revealed 100% aragonite composition (Fig. 6B). Hand-drilled shell powder of BW4B contained about 10% calcite (Fig. 6B), whose significance is discussed below.

LA-ICPMS Profiles

Chemical Signatures of Shell Mineralogical Domains.—LA-ICPMS analysis along a track covering both primary and altered aragonite of sample LGS1 revealed significant geochemical difference between these two domains (Fig. 7). The monitored element/Ca ratios (Mg/Ca, Sr/Ca, Ba/Ca, Mn/Ca, Al/Ca, La/Ca, and Ce/Ca) are either highly elevated or show a pronounced high-frequency variability in the area comprised of altered aragonite. At a distance of ~30 mm from the inner shell edge Mn/Ca, Al/Ca, La/Ca, and Ce/Ca increase up to two orders of

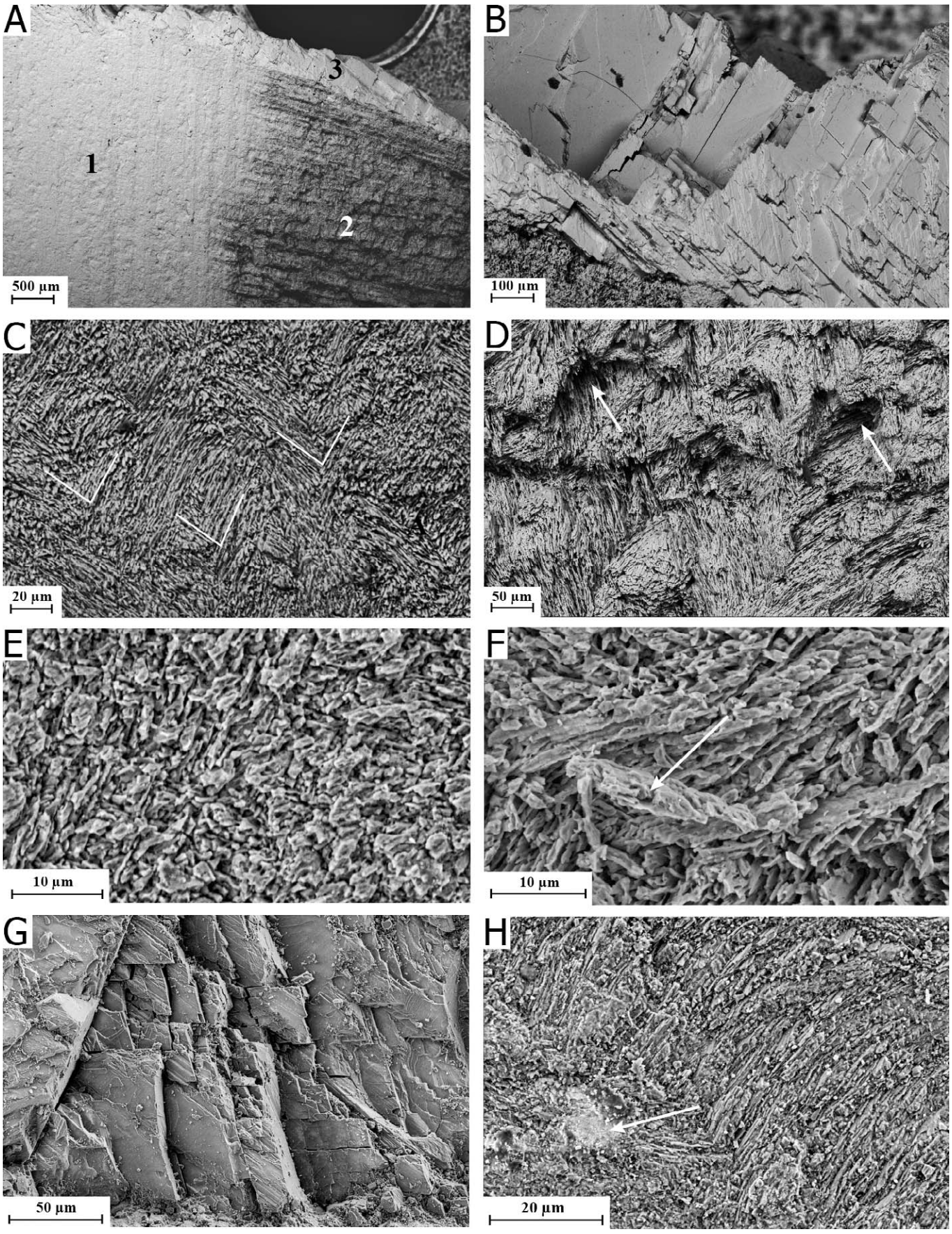
A
1
2
3
500 µm
B
100 µm
C
20 µm
D
50 µm
E
10 µm
F
10 µm
G
50 µm
H
20 µm

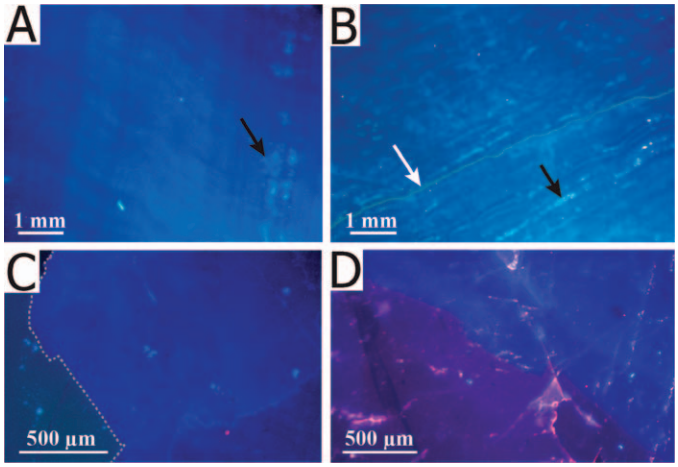

FIG. 5.—Cathodoluminescence images of aragonite and calcite of both shells. **A)** Dark-blue intrinsic luminescence of LGS1 indicates excellent preservation of aragonite. Occurrence of brighter patchy stains indicated by black arrow. **B)** Slightly higher luminescing aragonite of BW4B. Thin green growth band (marked with white arrow) indicates higher Mn^{2+} concentrations in this area. Bright patchy stains marked by black arrow. **C)** Intrinsic blue luminescence of calcite for LGS1, dashed line marks border between thin section and underlying glass slide. **D)** Calcite of BW4B characterized by two different luminescence colors. Blue indicates very low Mn^{2+} contents, whereas elevated Mn^{2+} concentrations activate the pink luminescence.

magnitude. This coincides with the macroscopically visible transition from pristine to altered aragonite (Fig. 7). It is therefore possible to align the trace elemental record with the macroscopic observations. The transition from "normal" aragonitic values to elevated ratios in the altered zone is sharp. From ~32 mm distance from inner shell edge onward Mg/Ca, Sr/Ca, and Ba/Ca ratios are characterized by a noisy high-frequency signal.

The LA-ICPMS profiles obtained from a track that covers pristine aragonite and the adjacent calcitic zone of shell BW4B reveal that aragonite is an order of magnitude enriched in B/Ca, Sr/Ca, and Ba/Ca and depleted in Mg/Ca, Mn/Ca, La/Ca, and Ce/Ca relative to calcite (Fig. 8).

At a distance of ~16 mm from inner shell edge, the laser ablation (LA) track intersects the macroscopically visible border between aragonite and calcite. Almost all monitored elemental ratios reveal a distinct and sharp compositional change at this distance. The two covarying rare earth elemental ratios (La/Ca and Ce/Ca), however, steadily increase from ~14 mm onward.

Mg/Ca.—The Mg/Ca ratio of LGS1 varies from about 0.4 to 1.4 mmol/mol (Fig. 9; see supplemental data). Even though the variation is not regular, an oscillatory pattern can be identified. Alignment of the Mg/Ca record with the shell-banding pattern reveals that high Mg/Ca ratios correspond to dark growth bands, while lower Mg/Ca ratios match with lighter growth bands (Figs. 7, 9). A gentle increase in the Mg/Ca ratio and in amplitude of the Mg/Ca record toward ontogenetically older shell parts (secreted during adulthood) produces oscillations characterized by overall higher Mg/Ca ratios with greater amplitude for the first ~16 mm of the profile.

The Mg/Ca ratio of BW4B ranges from about 0.4 to 1.0 mmol/mol (Fig. 10; see supplemental data). Alignment of the Mg/Ca profile and the banding pattern is possible for the last ~10 mm of the profile, with high Mg/Ca corresponding to dark growth layers (Fig. 10). However, compared to LGS1, the alignment is not as clear and is not constant throughout.

Sr/Ca.—The ratio of Sr/Ca of LGS1 varies from ~1.5 to 3.5 mmol/mol (Fig. 9). Overall, the profile reveals irregular variability. An oscillation pattern or ontogenetic trend as described for Mg/Ca of LGS1 cannot be seen. There is no covariation of ratios with the shell-banding pattern.

The Sr/Ca profile of BW4B ranges from about 1.7 to 2.9 mmol/mol and is characterized by high-amplitude/low-frequency variability (Fig. 10; see supplemental data). A reasonable fit exits between dark growth bands and elevated Sr/Ca ratios (Fig. 10). The Mg/Ca and Sr/Ca ratios covary slightly from ~7 mm distance from inner shell edge onward.

Ba/Ca.—The Ba/Ca values range between about 0.3 to 1.4 µmol/mol and 0.6 to 1.8 µmol/mol for LGS1 and BW4B, respectively (Figs. 9, 10). Corresponding profiles of both *Tridacna* shells are characterized by fine-scale, low-amplitude/high-frequency variability (Figs. 9, 10), that do not correspond with the shell-banding pattern.

Stable Isotope Profiles

$\delta^{18}O$.—The stable isotope profile of LGS1 (Fig. 9) is based on 188 analyses (resolution 200 µm) covering a distance of 37.6 mm. The $\delta^{18}O$ values range from −2.90‰ to −1.46‰ with an average value of −2.15‰ for LGS1 (Table 3). The $\delta^{18}O$ profile reveals pronounced variability and can be aligned with the shell-banding pattern. Dark bands correspond to low oxygen isotope ratios, whereas light bands match with high $\delta^{18}O$ values (Fig. 9).

The Mg/Ca and $\delta^{18}O$ profile of LGS1 are inversely correlated, with high Mg/Ca ratios corresponding to relatively light $\delta^{18}O$ values and low Mg/Ca ratios corresponding to heavy oxygen isotope ratios (Fig. 9). The two profiles correlate in great detail. As for Mg/Ca, a distinct change of amplitude and frequency occurs at ~16 mm distance from the inner shell edge. While the first 16 mm (shell parts secreted during adulthood) are characterized by high-amplitude/low-frequency variability, the final ~10 mm (shell parts secreted during juvenile stage) of the profile reveal low-amplitude/high-frequency variations.

The stable isotope profile of BW4B (Fig. 10) is based on 77 data points recovered from a shell length of 15.4 mm. The $\delta^{18}O$ values oscillate from −3.00‰ to −1.59‰ with an average value of −2.31‰. Alignment with the shell-banding pattern is possible. Light $\delta^{18}O$ values correspond to dark growth bands, while heavy $\delta^{18}O$ values match with light growth bands. Inverse correlation between the Sr/Ca profile and the $\delta^{18}O$ record

←

FIG. 4.—Scanning electron microscope images on the microstructures and diagenetic textures of LGS1 (A–F) and BW4B (G–H). **A)** Overview image of pristine aragonite (=1), altered aragonite (=2), and calcite (=3). **B)** Calcite at the shell rim characterized by typical rhombohedral cleavage planes. **C)** Pristine aragonite after etching in 5% acetic acid for 30 min. Dense, crossed-lamellar structure consisting of short lathlike crystals inclined at an angle of ~90° to each other (indicated with white strokes). **D)** Loosely packed, large and curved altered aragonite crystals which build a very coarse, wavelike structure resulting in cavities (marked by arrows). **E)** High-magnification micrograph of pristine aragonite. **F)** High-magnification micrograph of altered aragonite. Crystals range from 10 to 20 µm, are thin, and porosity (marked by arrow) is present. **G)** Diagenetic calcite at shell rim, which resembles the calcitic structure as described for LGS1 (see Part B). **H)** Pristine aragonite with similar structural characteristics as described for LGS1 (see Part E). Patch of dissolution, which is about 10 µm in diameter and might indicate incipient recrystallization (marked by arrow).

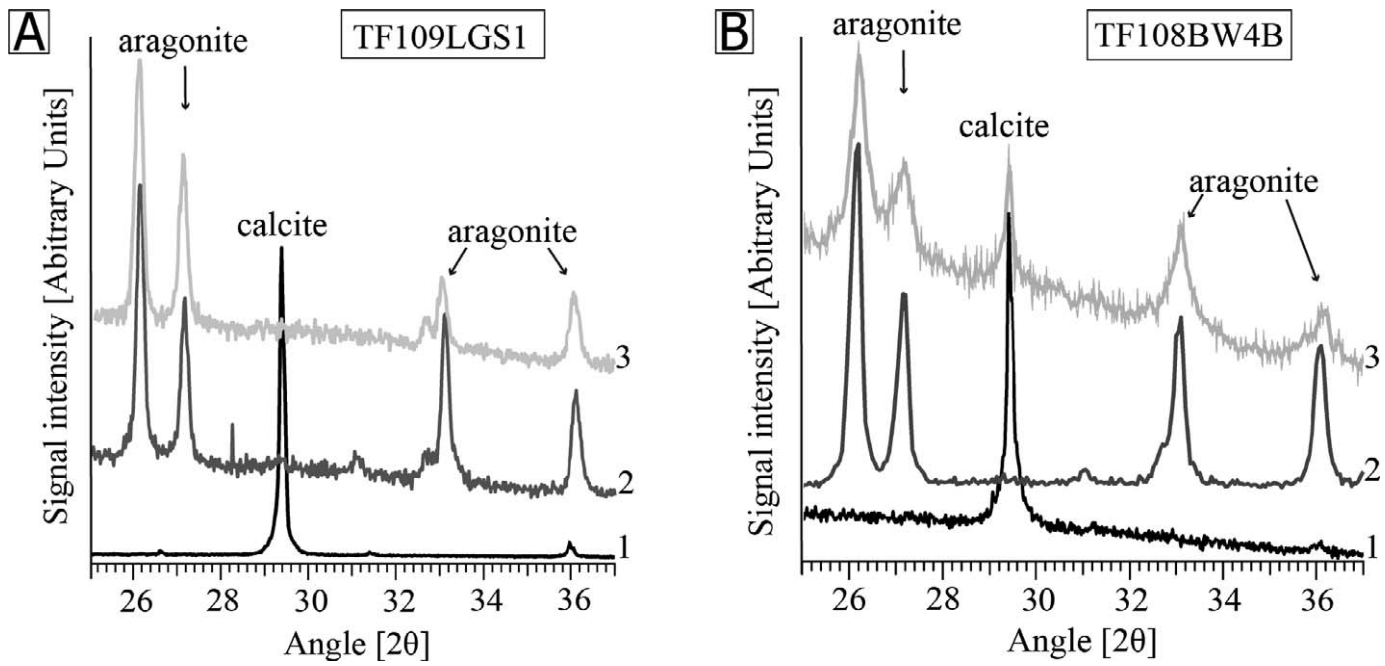

FIG. 6.—XRD spectra obtained from both *Tridacna* shells. **A)** LGS1: 1 = diagenetic calcite with one major peak at a diffraction angle of 29.4°, representing calcite. 2 = pristine aragonite and 3 = altered aragonite, both showing 4 major peaks at 26.2°, 27.2°, 33.2°, and 36.2°, representing aragonite. **B)** BW4B: 1 = diagenetic calcite with one major peak at a diffraction angle of 29.4°. 2 = ground sample from the internal parts of the shell, revealing pure aragonitic composition. 3 = drilled sample from the internal parts of the shell, characterized by peaks indicating the presence of both aragonite and calcite.

exists, however the agreement is not as good as for Mg/Ca and $\delta^{18}O$ in the case of LGS1.

Both shells reveal eight (best visible) dark-light couples that correspond to eight major $\delta^{18}O$ oscillations ($\delta^{18}O$ maxima and minima). These findings imply that both *Tridacna* specimens had lifespans of at least eight years.

$\delta^{13}C$.—The $\delta^{13}C$ values of LGS1 range between 0.32‰ and 2.45‰ with an average of 1.89‰ (Fig. 9). Overall, the profile is characterized by irregular variability, which does not align with the shell-banding pattern. Consequently, $\delta^{13}C$ and $\delta^{18}O$ do not correlate. Just as for the $\delta^{18}O$ signal, the frequency of peaks is higher for shell parts grown during the juvenile phase (from ~16 mm onward).

The $\delta^{13}C$ profile of BW4B shows pronounced oscillations varying from 1.68‰ to 3.2‰ with an average of 2.39‰ (Fig. 10). Eight major $\delta^{13}C$ oscillations (eight major $\delta^{13}C$ maxima and minima) are visible. An apparent negative correlation between $\delta^{13}C$ and $\delta^{18}O$ exists, especially from 4 mm distance from inner shell edge onward. However, a phase lag of a few weeks appears to exist between the two profiles.

DISCUSSION

Evaluation of Preservation and Implications For Retrieving Paleoenvironmental Information

Our multimethod approach combining macroscopic and microscopic observations, SEM/CL imaging, XRD analysis, and LA-ICPMS screening reveals that both shells contain altered zones (calcite and/or altered aragonite) as well as nonaltered parts (pristine aragonite). We exclude the possibility that such mineralogically manifested alteration is the result of changes during shell growth, because these features are not consistently present throughout the shells, but patchy in distribution. Following isochronous growth bands reveals that while at one position of the shell the given growth band is not modified, at another position the same growth band has been diagenetically transformed (Fig. 2C, D). We thus suggest that both calcite and altered aragonite are products of abiotic postmortem recrystallization. As such, alteration or diagenesis is used to refer to any modification of the mineralogy and composition of the original aragonitic biominerals.

SEM studies imply that the original aragonitic microstructure of LGS1 and BW4B is largely excellently preserved. Patchy dissolution features (Fig. 4H) were identified in BW4B, which might indicate incipient recrystallization (Faylona et al. 2011).

Both shells are characterized by dark-blue, dim cathodoluminescence (Fig. 5). Nonluminescent to blue luminescent colors in biogenic carbonates have been interpreted as an indicator for excellent preservation (Barbin et al. 1995; Gotte and Richter 2009; Brand et al. 2012; Wendler et al. 2012). The intrinsic luminescence is due to the absence of Mn^{2+}, which is a major luminescence activator in carbonates (Langlet et al. 2006). Elevated Mn^{2+} concentrations in aragonite result in yellow-green luminescing aragonite (Barbin et al. 1995; Gotte and Richter 2009). The single green band observed in BW4B (Fig. 5B) is therefore interpreted as composed of aragonite with an elevated Mn^{2+} content relative to the surrounding aragonite.

Mn^{2+} activates luminescence in calcite at longer wavelengths (Barbin et al. 1995) and depending on its concentration produces purple, red, or orange colors (Langlet et al. 2006). Blue to weak purple luminescing calcite obtained from the rims of LGS1 (Fig. 5C) indicates a pure $CaCO_3$ composition with only minor Mn^{2+} incorporation into the calcite lattice. Calcite of BW4B shows intrinsic blue luminescence and also areas with a distinct brighter, purple-pink luminescence (Fig. 5D), which indicates elevated Mn^{2+} concentrations in these calcite zones. CL imaging confirms the findings of SEM analysis, showing an excellently preserved original aragonite structure of LGS1 and an overall well preserved aragonitic microstructure of BW4B. The presence of similar XRD spectra for pristine and altered aragonite of LGS1 (Fig. 6A) demonstrates that XRD alone is not a sufficient tool for assessing the preservation state of

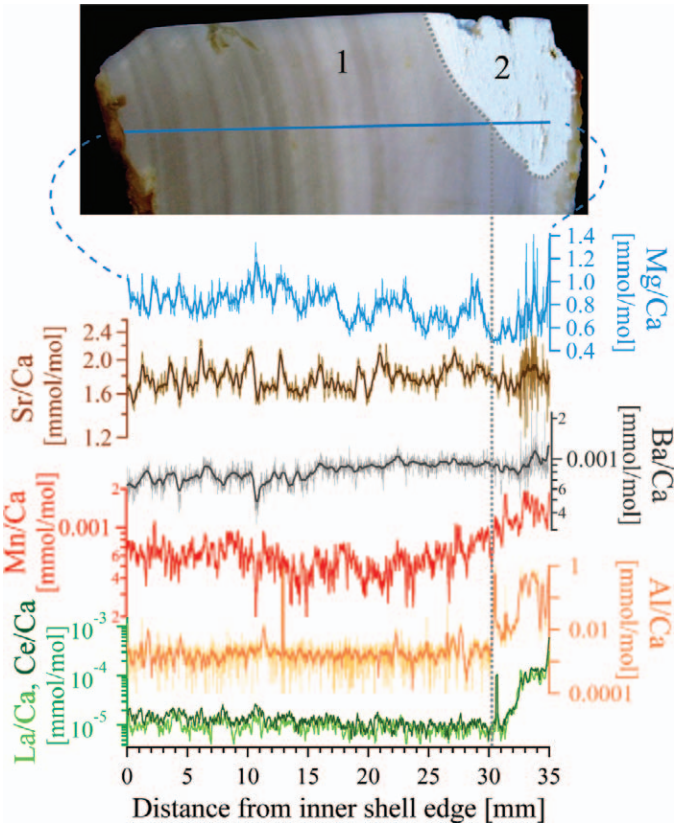

FIG. 7.—Polished thick section of LGS1, with position of laser transect and corresponding trace element profiles (presented on a logarithmic scale). Gray dotted line marks position where the laser-ablation track intersects the border between the well-preserved (=1) and altered aragonite (=2) structure at a distance of ~30 mm from inner shell edge. Smoothing was performed using moving average.

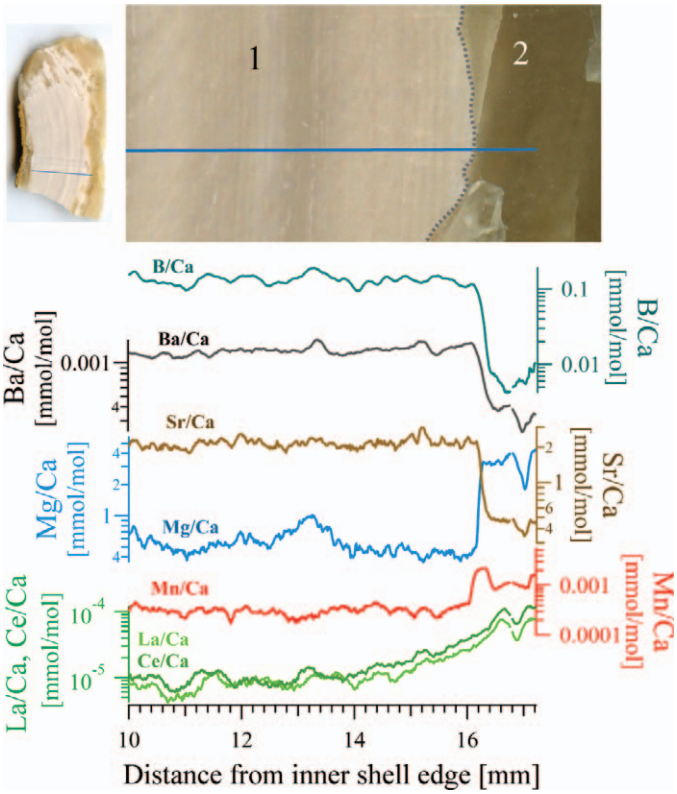

FIG. 8.—Polished thick section of BW4B, with position of laser transect and corresponding trace element profiles (presented on a logarithmic scale). Gray dotted line marks position were the laser-ablation track intersects the border between aragonite (=1) and calcite (=2) at a distance of ~16 mm from inner shell edge. Smoothing was performed using moving average.

aragonite. However, it is suitable to distinguish between the two carbonate polymorphs calcite and aragonite (Fig. 6A, B).

Ground samples obtained from the internal, well-preserved shell parts of BW4B revealed 100% aragonite composition, while hand-drilled samples obtained from the same shell parts contained ~10% of calcite (Fig. 6B). The latter contradicts the macroscopic observations and findings of SEM/CL imaging and LA-ICPMS analysis. None of these methods indicate the presence of calcite in the internal structure. Macroscopically, the banding pattern is preserved (Fig. 2D) and no large blocky crystals could be identified. SEM observations reveal a crossed lamellar structure (Fig. 4H), strikingly similar to that of LGS1 (Fig. 4C) and typical for bivalve aragonite. Cathodoluminescence images are characterized by blue luminescence (Fig. 5B), typical for pure biogenic aragonite. LA-ICPMS profiling does not imply significant compositional changes. Neither distinctively elevated Mg/Ca, La/Ca, Ce/Ca, Mn/Ca, nor significantly depleted Sr/Ca, B/Ca, Ba/Ca ratios, which characterize calcite recrystallization (Fig. 8), were detected. All these results support the interpretation of a well-preserved aragonitic structure in BW4B. Crucially, calcite was only detected in powdered samples produced via hand drilling, but not in those produced by grinding. Potential sample cross-contamination from adjacent calcite zones can be excluded, as repeated measurements were performed on previously cut, well-preserved, internal shell parts only. We conclude that conversion of aragonite to calcite occurred during the drilling process of XRD sampling. Calcite detected in hand-drilled samples from well-preserved internal shell parts can thus be interpreted as a sampling artifact and is not diagenetic in origin. Transformation of marine biogenic aragonite to calcite (up to 6%) due to heat and stress exposure during the drilling process has been reported before (Aharon 1991; Foster et al. 2008). Aharon (1991), who studied a *Tridacna gigas* specimen, additionally reported an offset in $\delta^{18}O$ values due to drilling. On the contrary, Foster et al. (2008) studied fish (cod) otoliths and concluded that micromilling did not affect $\delta^{18}O$ measurements in these specimens. The drilling-induced aragonite to calcite polymorph transition occurs in the case of BW4B, whereas no such sampling artifact is observed for LGS1, which might be related to minor microstructural differences. SEM analysis of BW4B revealed microdissolution features (Fig. 4H), possibly indicating incipient recrystallization. An overall weaker aragonite structure of BW4B might more readily convert during drilling than the more stable structure of LGS1. Even though microsamples for stable isotope analysis were obtained via micromilling (no hand drilling), a possible $CaCO_3$ polymorph transformation introduced by the milling process in case of BW4B cannot be excluded. But, since its $\delta^{18}O$ profile is characterized by a well-defined oscillatory pattern, which correlates with the banding pattern of the shell (Fig. 10), and furthermore, absolute $\delta^{18}O$ values are in good agreement with those of LGS1, we conclude that micromilling did not affect the stable oxygen isotope composition.

Several studies have applied trace elemental screening to coral skeletons in order to investigate the impact of diagenetic alteration on elemental composition and its resultant consequences for paleoenvironmental interpretations (Hendy et al. 2007; Hathorne et al. 2011; Sayani et al. 2011; Griffiths et al. 2013). Similar work focusing on the chemical composition of diagenetically altered shell areas of *Tridacna* are to our knowledge absent. The intrinsic multielemental capability of LA-ICPMS

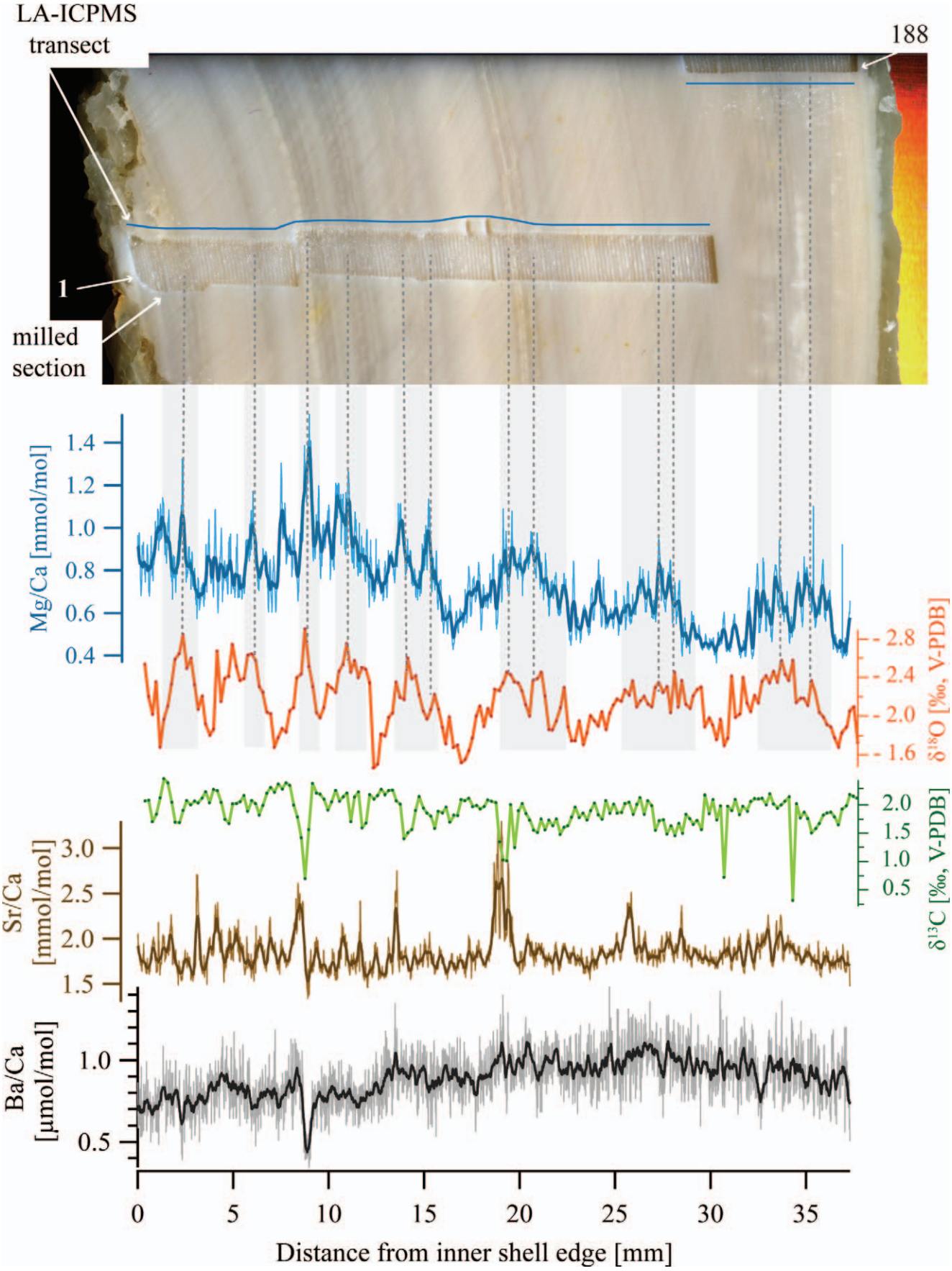
LA-ICPMS
transect
188
1
milled
section
Mg/Ca [mmol/mol]
1.4
1.2
1.0
0.8
0.6
0.4
δ18O [‰, V-PDB]
-2.8
-2.4
-2.0
-1.6
δ13C [‰, V-PDB]
2.0
1.5
1.0
0.5
Sr/Ca
[mmol/mol]
3.0
2.5
2.0
1.5
Ba/Ca
[µmol/mol]
1.0
0.5
0
5
10
15
20
25
30
35
Distance from inner shell edge [mm]

enables to monitor both "proxy" element/Ca ratios (e.g., Mg/Ca, Sr/Ca, Ba/Ca), as well as elements indicative of diagenesis (e.g., Mn, Al, REEs). Mn/Ca, Al/Ca, La/Ca, and Ce/Ca ratios change together with microstructures at about 30 mm distance from the inner shell edge (border between pristine aragonite to altered aragonite). The diagenetic monitor element/Ca ratios are distinctively enriched in altered aragonite relative to pristine aragonite. Elevated Mn concentrations in bivalve and brachiopod shells have been interpreted as an indication for diagenetic alteration (Grossman et al. 1996; Gomez-Alday and Elorza 2003). The elevated Al concentrations of the altered aragonite domain likely reflect the abundance of aluminum-bearing minerals in the cavities of this structure. Owing to the high porosity of the altered aragonite structure, the incorporation of interstitial minerals is facilitated. Indeed, XRD analysis of altered aragonite powder revealed the possible existence of diaspore (δ-AlO(OH)). This aluminum hydroxide is a typical weathering product of aluminosilicates in tropical regions and its occurrence is compatible with the clay-rich sediments in which the shells were found. Thus, the measured traces (<1%) of diaspore likely explain the enhanced Al concentrations detected via LA-ICPMS.

Significant compositional differences for the proxy element/Ca ratios Mg/Ca, B/Ca, Ba/Ca, and Sr/Ca were observed when comparing pristine aragonite versus diagenetic calcite (Fig. 8). While B/Ca, Sr/Ca, and Ba/Ca are strongly depleted, Mg/Ca is strongly enriched in diagenetic calcite compared to the pristine aragonite. Using proxy data obtained from those calcite zones for paleoenvironmental studies would result in unreliable inferences. All these ratios are prominent paleoenvironmental proxies (Mg/Ca, Sr/Ca: temperature; B/Ca: salinity/pH; Ba/Ca: runoff/upwelling, primary productivity). Calculating paleotemperature from those zones using, e.g., Mg/Ca and Sr/Ca would result in positive temperature anomalies.

Elemental incorporation into the carbonate structure is mainly controlled by the shell mineralogy. Relatively large cations like Sr^{2+} and Ba^{2+} substitute better for Ca^{2+} in the orthorhombic aragonite structure, while smaller ions such as Mg^{2+} show affinity to the rhombohedral calcite lattice (Gotte and Richter 2009). The behavior of Mg and Sr in the different carbonate polymorphs was documented by Harriss (1965), who compiled analyses of molluscan shell material of 95 different species. He reported overall lower Mg concentrations in aragonite (several hundred ppm) versus calcite (several thousand ppm), while Sr generally was found in higher concentrations in aragonite (frequency maximum at 2500 ppm) compared to calcite (frequency minimum at 1500 ppm). Diagenetic calcite cements in Miocene aragonitic coral skeletons have been found to be enriched in Mg/Ca and depleted in Sr/Ca relative to pristine aragonite by a factor of 15 to 20 (Griffiths et al. 2013).

To evaluate the impact of alteration on the Sr isotope ratio, diagenetic calcite from BW4B and calcite and secondary aragonite from LGS1 were compared with the respective ratios obtained from pristine zones. Due to the considerable Sr concentration changes documented by the LA-ICPMS, significant differences in the Sr isotope ratio between the different carbonate polymorphs were expected. However, considering the estimates of analytical uncertainty, pristine and altered zones show near identical $^{87}Sr/^{86}Sr$ ratios (Table 2). Two hypotheses are possible to explain this: (1) The effect of diagenetic alteration on the Sr isotope composition was small, hence the $^{87}Sr/^{86}Sr$ ratio has not resolvably been modified (considering the measuring inaccuracy and the error of the Sr isotope seawater curve). Simple loss of Sr without later admixture of isotopically different Sr also does not change the initially acquired $^{87}Sr/^{86}Sr$ isotope composition. (2) Diagenetic alteration either affected the living specimen (recrystallization from the same $^{87}Sr/^{86}Sr$ pool) or occurred relatively early postmortem, at a time interval that cannot be resolved in regard to the current measurement uncertainty for our geochronological dating (~ <1 Ma).

Ba/Ca Profiles: Lack of Phytoplankton Blooms?

Several recent studies treat environmental implications of barium shell geochemistry on modern marine bivalves (e.g., Gillikin et al. 2006, 2008; Elliot et al. 2009; Thébault et al. 2009). All report very similar high-resolution Ba/Ca profiles, which are characterized by large, sharp, periodically occurring Ba peaks of high intrashell and even interindividual reproducibility.

Ba/Ca signals in coral skeletons and planktic foraminifera are interpreted as proxies for riverine runoff (sediment flux) and upwelling of deep, nutrient-rich water (e.g., McCulloch et al. 2003; Chen et al. 2011; Hönisch et al. 2011; Grove et al. 2012). Studies on Ba/Ca variability in bivalve shells suggest a direct link between the presence of phytoplankton blooms/high phytoplankton activity and the Ba/Ca peaks (e.g., Lazareth et al. 2003; Gillikin et al. 2006, 2008; Elliot et al. 2009; Thébault et al. 2009); however, the mechanism of barium incorporation into the shell carbonate remains ambiguous (Elliot et al. 2009). Species-specific effects, which might influence barium uptake and incorporation into the shell structure, might also be relevant (Gillikin et al. 2008).

The Ba/Ca records preserved in the presented Miocene *Tridacna* shells discussed herein are different from modern profiles as described above. No pronounced Ba/Ca peaks can be identified, and overall these records are characterized by irregular variability (Figs. 9, 10). The low Ba/Ca variability in our specimens may indicate a lack of plankton blooms and/or stable euhaline conditions at the time of shell formation; however, the length of the *Tridacna* records is too short to exclude the presence of interseasonal variations in local primary productivity.

Seasonality Derived from LA-ICPMS and Stable Isotope Time-Series Profiles

Tridacna secrete their aragonitic structure in or close to isotopic equilibrium (Romanek and Grossman 1989; Aharon 1991; Elliot et al. 2009). The measured shell $\delta^{18}O$ is comprised primarily of two components: (1) $\delta^{18}O$ seawater ($\delta^{18}O_{sw}$), which is closely related to salinity/ice volume and (2) fractionation as a function of SST ($\delta^{18}O_{temp}$) (e.g., Aharon 1991). In regions with constant salinity, shell $\delta^{18}O$ can be interpreted as being temperature controlled.

Much of the coastline of East Kalimantan is subjected to riverine influence from the Mahakam delta, a fluvio-deltaic system that already existed during the Miocene. Salinity variation (e.g., reduced salinity due to fluvial runoff) negatively impacts on the relationship between corals and their symbionts (e.g., Moberg et al. 1997; Mayfield and Gates 2007), for which the occurrence of coral reefs is usually taken to indicate stable euhaline conditions. Since our studied shells were collected within a rich and diverse fossil coral community, we assume that shell formation took place under relatively constant sea-surface salinity (SSS) conditions.

←

FIG. 9.—Polished thick section of LGS1 used for stable isotope analysis, with positions of micromilled section and laser transect, and respective stable isotope and LA-ICPMS profiles. Micromilled section as indicated by arrows ranges from sample 1 (innermost shell edge) and sample 188 (outermost shell edge). Blue line represents laser-ablation track. Gray bars and dotted lines indicate good agreement between $\delta^{18}O$ and Mg/Ca and alignment with the shell-banding pattern. Smoothing of LA-ICPMS data was performed using the moving average.

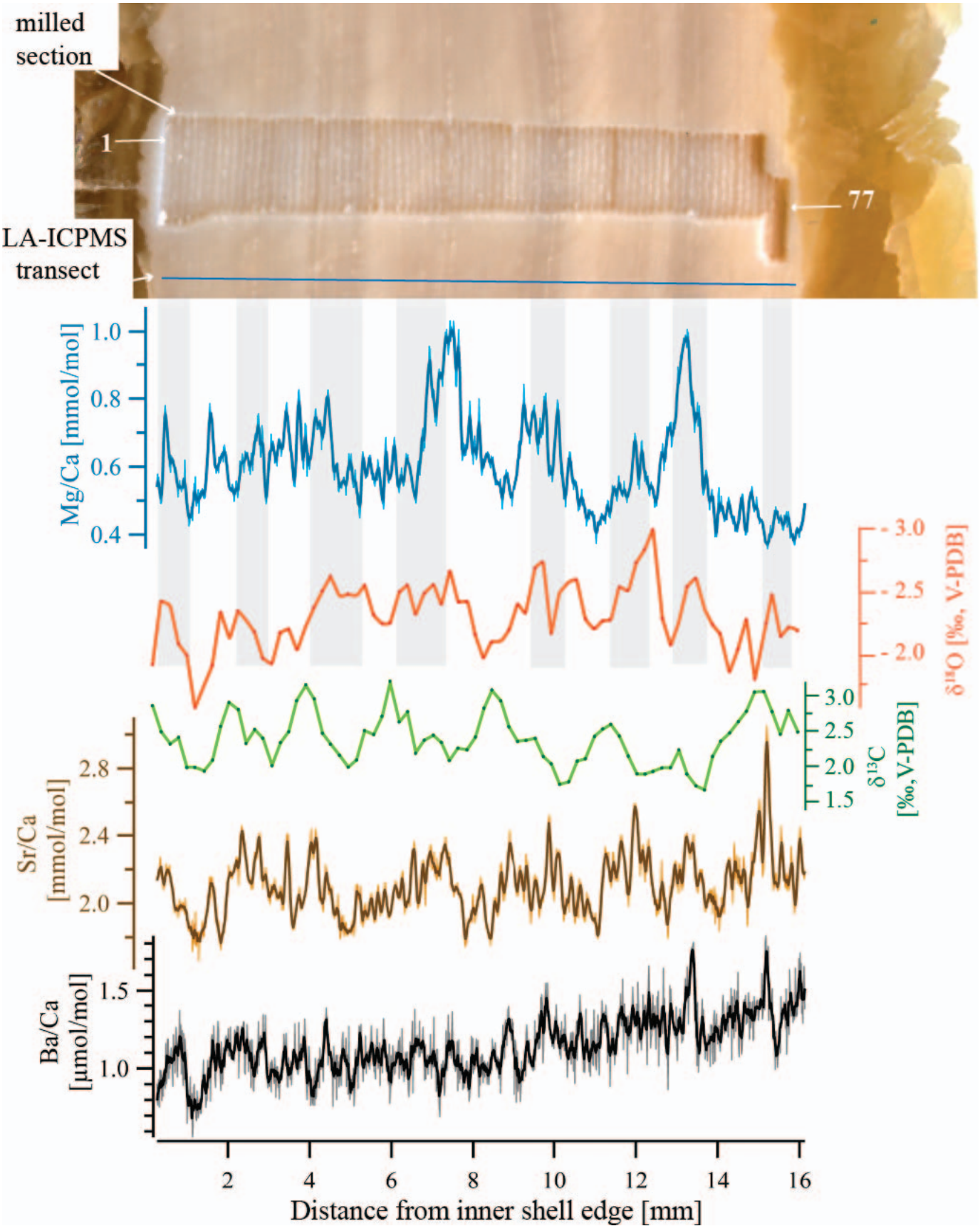
milled section
1
77
LA-ICPMS transect
Mg/Ca [mmol/mol]
1.0
0.8
0.6
0.4
δ18O [‰, V-PDB]
-3.0
-2.5
-2.0
δ13C [‰, V-PDB]
3.0
2.5
2.0
1.5
Sr/Ca [mmol/mol]
2.8
2.4
2.0
Ba/Ca [µmol/mol]
1.5
1.0
2
4
6
8
10
12
14
16
Distance from inner shell edge [mm]

In contrast to $\delta^{18}O$, the Mg/Ca and Sr/Ca ratio in biogenic carbonates are predominantly paleotemperature proxies only, reflecting paleo-SST independent of salinity, and therefore used to deconvolve the SSS from the SST component of the $\delta^{18}O$ record in biogenic carbonates (e.g., McCulloch et al. 1994; Klein et al. 1996; Watanabe et al. 2001; Lear et al. 2002; Ren et al. 2002). The good qualitative agreement of Mg/Ca with the stable oxygen isotope records of LGS1 (Fig. 9) suggests that $\delta^{18}O_{shell}$ mainly reflects SST.

Interpreted as such, light $\delta^{18}O$ values reflect warm SSTs (warm seasons) and heavy $\delta^{18}O$ values cold SSTs (cold seasons), respectively. Eight dark-light couples can be assigned to eight $\delta^{18}O$ minima and maxima in both shells and are interpreted as annual couples (Figs. 9, 10). However, smaller-scale variations in the stable isotope profile exist (especially for shell parts formed during adulthood) and can be aligned with respective scale sub-growth bands. Superimposed on a yearly temperature cycle, minor variations in temperature might occur related to complex and varied monsoon systems, variations in the position of the Intertropical Convergence Zone (ITCZ) and/or multiscale variability of the proto-warm pool in the western equatorial Pacific, which could have caused small scale variations in the $\delta^{18}O$ profile and the banding pattern. However, we cannot entirely exclude that these variations are annual in nature as well, in which case the observed (minimal) lifespan of the specimens is longer. Because pristine aragonite has been replaced (by calcite or altered aragonite) at the inner- and outermost shell edges in both shells, the observed eight years must be interpreted as a minimum estimate of the true lifespan.

Mg/Ca correlates well with the $\delta^{18}O$ variations in LGS1 (Fig. 9). Relatively high Mg/Ca ratios correspond to relatively light $\delta^{18}O$ signals and, like the $\delta^{18}O$ record, can be aligned with the darker growth bands within the shell-banding pattern (Fig. 9). This inverse correlation between the Mg/Ca and $\delta^{18}O$ record together with the positive correlation of Mg/Ca in biogenic carbonates with temperature (e.g., Batenburg et al. 2011; Welsh et al. 2011; Quinn and Sampson 2002) suggests that low density dark bands were formed during warm seasons (reflecting warm SSTs), while high density light bands were secreted during cold seasons (reflecting cold SSTs), respectively. This is in agreement with results from other studies on *Tridacna* shells (e.g., Aharon 1991; Watanabe et al. 2004; Batenburg et al. 2011; Welsh et al. 2011). However, there is apparently no universal mechanism in band formation of marine bivalves. Aubert et al. (2009) showed that dark bands in shells of the modern tridacnine *Hippopus hippopus* were secreted during winter periods. Studies on the clam *Mercenaria mercenaria* even indicate significant latitudinal variation regarding growth band formation (Jones and Quitmyer 1996). Modern shells from the northeastern coast of the United States typically form dark bands during the winter season, whereas in the lower latitudes (U.S. south east coast) these form during summer to early fall (Jones and Quitmyer 1996). Moreover, $\delta^{18}O$ records from a Pliocene *Mercenaria campechiensis* from the northeast U.S. show that dark bands correlate with the warmest temperatures of the annual cycle, revealing an opposite pattern to that seen in modern *Mercenaria mercenaria* shells from the same area (Jones and Quitmyer 1996).

The overall gradual rise of Mg/Ca and the increase in amplitude of the oscillations with age of LGS1 (Fig. 9) indicate that Mg/Ca partitioning in the *Tridacna* shells seems to be influenced not only by temperature but also physiologically via the growth rate. Such an ontogenetic trend in Mg/Ca has been reported for modern *Tridacna* shells (Romanek and Grossman 1989; Elliot et al. 2009). Without correction for this ontogenetic trend, quantitative temperature estimates using Mg/Ca are problematic. Nevertheless, the Mg/Ca variations can be utilized to identify seasonal cycles, which is demonstrated by the good inverse correlation between Mg/Ca and $\delta^{18}O$, which exists throughout the whole length of the profiles (Fig. 9). The $\delta^{18}O$ oscillation amplitude changes with shell growth rate changes, similar as seen in the Mg/Ca ratio variability. Shell parts secreted during adulthood are characterized by high amplitude/low frequency variability, while those formed during juvenile stage show low amplitude/high frequency variations. The changes in amplitude are relatively small and we cannot exclude that these are due to environmental changes rather than a biological control. However, similar findings for modern *Tridacna maxima* from the Samoan Islands have been reported (Romanek and Grossman 1989).

Three broad, low amplitude/high frequency oscillations in specimen LGS1 (Fig. 9) can be assigned (given the above above-mentioned interpretation) to three years in the lifetime of the juvenile *Tridacna.* Contrary to the pattern seen in LGS1, an ontogenetic trend of the $\delta^{18}O$ record related to changes in growth rate was not seen in BW4B, which conforms to visual observations of the banding pattern in this individual. No clear correlation between Mg/Ca and the stable oxygen isotope record of BW4B was found (Fig. 10). It is not clear why the Mg/Ca and $\delta^{18}O$ records agree well in case of LGS1, while this does not apply for the corresponding records of BW4B. Species-specific effects, which partly control biomineralization and thus the incorporation of environmental signals into the shell structure, should be considered. Visual examination reveals a weak correlation between Sr/Ca and $\delta^{18}O$. The two records are inversely correlated (light $\delta^{18}O$ agree with high Sr/Ca ratios), which implies that high Sr/Ca ratios reflect warmer seawater temperatures. However, Sr/Ca in modern *Tridacna gigas* specimen from the South China Sea has been reported to be negatively correlated with temperature, implying a positive correlation between $\delta^{18}O$ and Sr/Ca (Yan et al. 2013). Another study demonstrated the ability of Sr/Ca to reflect the daily light cycle and reported negative correlation between Sr/Ca and temperature on a yearly basis (Sano et al. 2012), contrary to our observations.

Temperature Seasonality Estimates

Calculations of SSTs based on the $\delta^{18}O$ data were performed using the commonly accepted aragonitic oxygen isotope temperature equation by Grossman and Ku (1986), $T\ ^{\circ}C = 21.8 - 4.69\ (\delta^{18}O_{shell} - \delta^{18}O_{sw})$, where $\delta^{18}O_{shell}$ is the measured oxygen isotope composition of the (mollusk) shell, and $\delta^{18}O_{sw}$ the oxygen isotope composition of ambient seawater. Usage of this empirical equation enables the conversion of the measured $\delta^{18}O$ values ($\delta^{18}O_{shell}$) into absolute paleotemperatures. However, the stable oxygen isotope composition of the ambient seawater ($\delta^{18}O_{sw}$) at the time of shell formation of the two *Tridacna* shells can only be estimated. We used a $\delta^{18}O_{sw}$ of −0.88‰, similar to Batenburg et al. (2011) for a late–middle Miocene *Tridacna gigas.* Assuming a $\delta^{18}O_{sw}$ for an ice-free greenhouse world of −1.2‰ (Lear et al. 2000) or −1.0‰ (Zachos 1994), and a modern $\delta^{18}O_{sw}$ of −0.28‰ (Lear et al. 2000) for today's icehouse conditions, this value can be considered as a reasonable estimate for the late Miocene climate, characterized by a reestablished major Antarctic ice cover and gradual onset of the Northern Hemisphere glaciation.

The $\delta^{18}O_{shell}$ maxima, minima, and averaged values and the respective calculated paleotemperature data of LGS1 and BW4B are presented in

←

FIG. 10.—Polished thick section of BW4B used for stable isotope analysis, with respective stable isotope and LA-ICPMS profiles. Micromilled section and position of laser track are marked by arrows. Milled sample 1 was recovered from innermost shell edge, while sample 77 was obtained from outermost shell edge. Smoothing of LA-ICPMS data was performed using the moving average.

Table 3. For comparison, we added the $\delta^{18}O$ data of the late to middle Miocene *Tridacna gigas* published in Batenburg et al. (2011) and the respective (calculated) paleotemperatures/paleoseasonality. Using the equation by Grossman and Ku (1986) and assuming $\delta^{18}O_{sw} = -0.88‰$ results in average temperatures of 27.8 °C for LGS1 and 28.5 °C for BW4B (Table 3); using $\delta^{18}O_{sw}$ of −1.2‰, −1.0‰, or −0.5‰ instead of −0.88‰ shifts the absolute paleotemperatures by −1.2, −0.6, or +1.8 °C. The measurement uncertainty produces errors of ±0.2 °C. Our results are very similar to the average temperature of 28.5 °C calculated for the *Tridacna gigas* dataset (Table 3). The good agreement between stable oxygen isotope data of our *Tridacna* shells with those obtained by another independent study confirms our findings toward a well-preserved aragonite microstructure that contains the original geochemical signature. The present day SST yearly average in the Makassar Strait is about 28.5 to 29.5 °C (Chen et al. 2005; Tangdong et al. 2005) and therefore only slightly higher than the estimated temperatures from the Miocene $\delta^{18}O$ records.

The modern Indo-Pacific Warm Pool (IPWP), which influences tropical Pacific climate and ocean circulations and which determines the SST in the Makassar Strait today, did not appear until about 4 Ma (Li et al. 2006). However, a proto–warm pool existed in the western equatorial Pacific (WEP) from the early late Miocene onward (Li et al. 2006; Nathan and Leckie 2009). It is possible that the slight difference between the modern and estimated Miocene SST conditions (apart from uncertain $\delta^{18}O_{sw}$) is due to these different warm pool regimes. Mg/Ca paleotemperature estimates using late Miocene foraminiferan tests from the WEP generated temperatures ranging from 27.3 to 28.2 °C (Nathan and Leckie 2009). The authors suggest that late Miocene surface waters were slightly cooler and more saline than today. Owing to the uncertain $\delta^{18}O_{sw}$ values, these quantitative paleotemperature reconstructions have a built-in error and therefore a more achievable objective is to calculate average temperature seasonality. Assuming eight years of growth and a constant $\delta^{18}O_{sw}$ and using the $\delta^{18}O$ maximum and minimum for each of the eight years, an average seasonality of 4.6 ± 1.7 °C (2 SD) and 2.7 ± 2.1 °C (2 SD) for LGS1 and BW4B has been calculated for the late Miocene. For comparison, we also assessed the seasonality of the Miocene *Tridacna gigas* dataset by Batenburg et al. (2011), which gives an estimated seasonality of 2.1 ± 2.7 °C (2 SD). Even though the *Tridacna gigas* data overall show higher SST fluctuations, the calculated average seasonality is slightly lower, compared to the data of the two presented *Tridacna* shells. The high standard deviation might reflect high and low ENSO periods within the 15 years of growth of this specimen. Overall, the reported variations of all three $\delta^{18}O$ profiles consistently exceed modern seasonal variability in the Makassar Strait, which is <1.5 °C (Tangdong et al. 2005).

It is not possible to decipher the causes of these relatively high seasonality estimates at the current state of knowledge. Several regional factors possibly influenced late Miocene seasonal variability, such as the East Asian monsoon system, seasonal shifts in ocean currents, changes in the upwelling regime, or the incipient restriction of the Indonesian Seaway from late Miocene onward with the development of the WEP proto–warm pool and possible onset of ENSO-type climate variability (Batenburg et al. 2011). Furthermore, local $\delta^{18}O_{sw}$ modifications due to fluvial runoff, upwelling, or evaporation/precipitation processes must be considered. The good qualitative agreement between the Mg/Ca and the stable oxygen isotope profiles in case of LGS1 suggests that $\delta^{18}O_{shell}$ mainly mirrors SST. The occurrence of the *Tridacna* shells within a rich and diverse fossil coral assemblage and the absence of characteristic peaks in the Ba/Ca profiles possibly indicate relatively constant SSS conditions during shell formation and thus seawater uninfluenced by major (variations in) upwelling and/or riverine runoff.

Few model simulations exist that could potentially help in predicting late Miocene seasonality. Galoetti et al. (2010) suggested evidence for Pacific ENSO-type interannual variability during the late Miocene, which is, owing to strong Pacific-Mediterranean teleconnections during this time interval, recorded in varved evaporitic successions from the Mediterranean. According to Huber and Caballero (2003), the Eocene "hothouse" climate experienced Pacific ENSO variability, even greater in amplitude than today. Their modeled predictions are confirmed by recorded ENSO timescale variability in varved sediments from lakes situated within teleconnected regions. Paleoclimate reconstructions using fossil *Nummulites* from Java indicate an annual seasonal temperature shift of 5–6 °C for the middle Eocene, which indicates ~2 °C greater than modern seasonality at this locality (Evans et al. 2013).

CONCLUSIONS

The interiors of both Miocene *Tridacna* shells discussed herein are to a large extent excellently preserved, which could not be expected from their external appearance. Besides well-preserved pristine aragonite, altered aragonitic and calcitic domains were identified. The latter two deviate strongly in their trace elemental composition from pristine aragonite zones. We demonstrate that element/Ca ratios obtained from diagenetically altered zones should not be used as paleoproxies for reconstructions of primary paleoenvironmental conditions during the time of shell formation. Combined usage of XRD, SEM/CL imaging, and LA-ICPMS trace elemental screening has proven effective at detecting diagenetic shell alteration. The good agreement between stable oxygen isotope data and trace elemental records and the overall good alignment with visible growth bands provides evidence for an intact late Miocene geochemical inventory within pristine shell aragonite.

Based on the $\delta^{18}O$ time-series records, average SST paleotemperatures ranging from 27.8 to 28.5 °C were obtained (for $\delta^{18}O_{sw} = -0.88‰$), which indicates slightly cooler late Miocene SST conditions in the Makassar Strait compared with present day. Assuming a lifespan of eight years, the shells reflect a seasonal SST variability of 2.7 ± 2.1 to 4.6 ± 1.7 °C, which exceeds modern-day seasonality in the Makassar Strait two- to threefold.

Despite presenting less than decade-long continuous paleorecords, analysis of these shells contributes to the scarce, seasonally resolved, contiguous tropical SST record for the Miocene. Our reconstructed Miocene SST seasonality provides key input parameters for climate models and allows better assessment of the dynamics of the Miocene tropics. To extend existing records and to ensure that seasonal and subdecadal climate variability is recognized, new and longer records, possibly even from visually altered specimen, are required.

ACKNOWLEDGMENTS

Special thanks to all Throughflow members for help with fieldwork and discussions, Norman Oxtoby for help with CL-imaging, and to Alex Ball and Tomasz Goral (Science Facilities, NHMUK) for help with SEM work. Thanks are extended to the following people at RHUL: Dave Alderton (XRD), Dave Lowry, Nathalie Grassineau and Dave Mattey (stable isotope analysis), Matthew Thirlwall and Christina Manning (TIMS analysis), and Neil Holloway (thin sections). The authors want to thank Sietske Batenburg and an anonymous reviewer for their detailed and constructive reviews, which significantly helped to improve this manuscript, as well as associate editor Ken Johnson for review supervision and helpful comments. This study was conducted under research license 0266/SIP/FRP/XI/2010 issued by RISTEK (Kementerian Riset Dan Teknologi Republik Indonesia) with special thanks to Professor F. Hasibuan and the team of the Indonesian Badan Geologi–Pusat Survei Geologi. As part of the Throughflow Initial Training Network, this work was funded by the Marie Curie Actions Plan, Seventh Framework Program of the European Union (grant no. 237922).

SUPPLEMENTAL MATERIAL

Data is available from the PALAIOS Data Archive: http://www.sepm.org/pages.aspx?pageid=332.

REFERENCES

Aharon, P., 1991, Recorders of reef environment histories: stable isotopes in corals, giant clams and calcareous algae: Coral Reefs, v. 10, p. 71–90.

Aharon, P., and Chappell, J., 1986, Oxygen isotopes, sea-level changes and the temperature history of a coral-reef environment in New Guinea over the last 105 years: Palaeogeography, Palaeoclimatology, Palaeoecology, v. 56, p. 337–379.

Alibert, C., and McCulloch, M.T., 1997, Strontium/calcium ratios in modern *Porites* corals from the Great Barrier Reef as a proxy for sea surface temperature: Calibration of the thermometer and monitoring of ENSO: Paleoceanography, v. 12, p. 345–363.

Allison, N., Finch, A.A., Webster, J.M., and Clague, D.A., 2007, Palaeoenvironmental records from fossil corals: the effects of submarine diagenesis on temperature and climate estimates: Geochimica et Cosmochimica Acta, v. 71, p. 4693–4703.

Aubert, A., Lazareth, C.E., Cabioch, G., Boucher, H., Yamada, T., Iryu, Y., and Farman, R., 2009, The tropical giant clam *Hippopus hippopus* shell, a new archive of environmental conditions as revealed by sclerochronological and $\delta^{18}O$ profiles: Coral Reefs, v. 28, p. 989–998.

Ayling, B.F., McCulloch, M.T., Gagan, M.K., Stirling, C.H., Andersen, M.B., and Blake, S.G., 2006, Sr/Ca and $\delta^{18}O$ seasonality in a *Porites* coral from the MIS 9 (339–303 ka) interglacial: Earth and Planetary Science Letters, v. 248, p. 462–475.

Barbin, V., Brand, U., Hewitt, R.A., and Ramseyer, K., 1995, Similarity in cephalopod shell biogeochemistry since carboniferous: evidence from cathodoluminescence: Geobios, v. 26, p. 701–710.

Batenburg, S.J., Reichart, G.J., Jilbert, T., Janse, M., Wesselingh, F.P., and Renema, W., 2011, Interannual climate variability in the Miocene: high resolution trace element and stable isotope ratios in giant clams: Palaeogeography, Palaeoclimatology, Palaeoecology, v. 306, p. 75–81.

Beckvar, N., 1981, Cultivation, spawning, and growth of the Giant Clams *Tridacna gigas*, *T. derasa*, and *T. squamosa* in Palau, Caroline Islands: Aquaculture, v. 24, p. 21–30.

Billups, K., and Schrag, D.P., 2003, Application of benthic foraminiferal Mg/Ca ratios to questions of Cenozoic climate change: Earth and Planetary Science Letters, v. 209, p. 181–195.

Birck, J.L., 1986, Precison K-Rb-Sr isotopic analysis: application to Rb-Sr chronology: Chemical Geology, v. 56, p. 73–83.

Brand, U., Jiang, G.Q., Azmy, K., Bishop, J., and Montanez, I.P., 2012, Diagenetic evaluation of a Pennsylvanian carbonate succession (Bird Spring Formation, Arrow Canyon, Nevada, USA), 1: Brachiopod and whole rock comparison: Chemical Geology, v. 308–309, p. 26–39.

Cane, M.A., and Molnar, P., 2001, Closing of the Indonesian seaway as a precursor to east African aridification around 3–4 million years ago: Nature, v. 411, p. 157–162.

Chen, M.T., Huang, C.C., Pflaumann, U., Waelbroeck, C., and Kucera, M., 2005, Estimating glacial western Pacific sea-surface temperature: methodological overview and data compilation of surface sediment planktic foraminifer faunas: Quaternary Science Reviews, v. 24, p. 1049–1062.

Chen, T.R., Yu, K.F., Li, S., Chen, T.G., and Shi, Q., 2011, Anomalous Ba/Ca signals associated with low temperature stresses in *Porites* corals from Daya Bay, northern South China Sea: Journal of Environmental Sciences (China), v. 23, p. 1452–1459.

Corrège, T., Gagan, M.K., Beck, J.W., Burr, G.S., Cabioch, G., and Le Cornec, F., 2004, Interdecadal variation in the extent of South Pacific tropical waters during the Younger Dryas event: Nature, v. 428, p. 927–929.

Crowley, T.J., Short, D.A., Mengel, J.G., and North, G.R., 1986, Role of seasonality in the evolution of climate during the last 100 million years: Science, v. 231, p. 579–584.

Denton, G.H., Alley, R.B., Comer, G.C., and Broecker, W.S., 2005, The role of seasonality in abrupt climate change: Quaternary Science Reviews, v. 24, p. 1159–1182.

Elliot, M., Welsh, K., Chilcott, C., McCulloch, M., Chappell, J., and Ayling, B., 2009, Profiles of trace elements and stable isotopes derived from giant long-lived *Tridacna gigas* bivalves: potential applications in paleoclimate studies: Palaeogeography, Palaeoclimatology, Palaeoecology, v. 280, p. 132–142.

England, M.H., and Huang, F., 2005, On the interannual variability of the Indonesian Throughflow and its linkage with ENSO: Journal of Climate, v. 18, p. 1435–1444.

Evans, D., Müller, W., Oron, S., and Renema, W., 2013, Eocene seasonality and alkaline earth reconstruction using shallow-dwelling large benthic foraminifera: Earth and Planetary Science Letters, v. 381, p. 104–115.

Faylona, M.G.P.G., Lazareth, C.E., Semah, A.M., Caquineau, S., Boucher, H., and Ronquillo, W.P., 2011, Preliminary study on the preservation of giant clam (Tridacnidae) shells from the Balobok Rockshelter archaeological site, South Philippines: Geoarchaeology: An International Journal, v. 26, p. 888–901.

Flower, B.P., and Kennett, J.P., 1994, The middle Miocene climatic transition: East Antarctic ice-sheet development, deep-ocean circulation and global carbon cycling: Palaeogeography, Palaeoclimatology, Palaeoecology, v. 108, p. 537–555.

Fluckiger, J., Knutti, R., White, J.W.C., and Renssen, H., 2008, Modeled seasonality of glacial abrupt climate events: Climate Dynamics, v. 31, p. 633–645.

Foster, L.C., Andersson, C., Høie, H., Allison, N., Finch, A.A., and Johansen, T., 2008, Effects of micromilling on $\delta^{18}O$ in biogenic aragonite: Geochemistry, Geophysics, Geosystems, v. 9, doi: 10.1029/2007GC001911.

Gagan, M.K., Ayliffe, L.K., Beck, J.W., Cole, J.E., Druffel, E.R.M., Dunbar, R.B., and Schrag, D.P., 2000, New views of tropical paleoclimates from corals: Quaternary Science Reviews, v. 19, p. 45–64.

Galoetti, S., von der Heydt, A., Huber, M., Bice, D., Dijkstra, H., Jilbert, T., Lanci, L., and Reichart, G.-J., 2010, Evidence for active El Niño Southern Oscillation variability in the late Miocene greenhouse climate: Geology, v. 38, p. 419–422.

Gillikin, D.P., Dehairs, F., Lorrain, A., Steensmans, D., Baeyens, W., and André, L., 2006, Barium uptake into the shells of the common mussel *(Mytilus edulis)* and the potential for estuarine paleo-chemistry reconstruction: Geochimica et Cosmochimica Acta, v. 70, p. 395–407.

Gillikin, D.P., Lorrain, A., Paulet, Y.M., Andre, L., and Dehairs, F., 2008, Synchronous barium peaks in high-resolution profiles of calcite and aragonite marine bivalve shells: Geo-Marine Letters, v. 28, p. 351–358.

Gomez-Alday, J.J., and Elorza, J., 2003, Diagenesis, regular growth and records of seasonality in inoceramid bivalve shells from mid-Maastrichtian hemipelagic beds of the Bay of Biscay: Geologie En Mijnbouw, v. 82, p. 289–301.

Gotte, T., and Richter, D.K., 2009, Quantitative aspects of Mn-activated cathodoluminescence of natural and synthetic aragonite: Sedimentology, v. 56, p. 483–492.

Griffiths, N., Müller, W., Johnson, K.G., and Aguilera, O.A., 2013, Evaluation of the effect of diagenetic cements on element/Ca ratios in aragonitic early Miocene (~ 16 Ma) Caribbean corals: implications for "deep-time" palaeo-environmental reconstructions: Palaeogeography, Palaeoclimatology, Palaeoecology, v. 369, p. 185–200.

Grossman, E.L., and Ku, T.-L., 1986, Oxygen and carbon isotope fractionation in biogenic aragonite: temperature effects: Chemical Geology, Isotope Geochemistry Section, v. 59, p. 59–74.

Grossman, E.L., Mii, H.S., Zhang, C.L., and Yancey, T.E., 1996, Chemical variation in Pennsylvanian brachiopod shells: diagenetic, taxonomic, microstructural, and seasonal effects: Journal of Sedimentary Research, v. 66, p. 1011–1022.

Grove, C.A., Zinke, J., Scheufen, T., Maina, J. Boer, W., Randriamanantsoa, B., and Brummer G.-J.A., 2012, Spatial linkages between coral proxies of terrestrial runoff across a large embayment in Madagascar: Biogeosciences, v. 9, p. 3063–3081.

Hall, R., Cottam, M.A., and Wilson, M.E.J., 2011, The SE Asian gateway: History and tectonics of the Australia–Asia collision: Geological Society of London, Special Publications, v. 355, p. 1–6.

Harriss, R.C., 1965, Trace element distribution in molluscan skeletal material I. Magnesium, iron, manganese and strontium: Bulletin of Marine Science, v. 15, p. 265–273.

Harzhauser, M., Mandic, O., Piller, W.E., Reuter, M., and Kroh, A., 2008, Tracing back the origin of the Indo-Pacific mollusc fauna: Basal Tridacninae from the Oligocene and Miocene of the Sultanate of Oman: Palaeontology, v. 51, p. 199–213.

Hathorne, E.C., Felis, T., James, R.H., and Thomas, A., 2011, Laser ablation ICP-MS screening of corals for diagenetically affected areas applied to Tahiti corals from the last deglaciation: Geochimica et Cosmochimica Acta, v. 75, p. 1490–1506.

Hendy, E.J., Gagan, M.K., Lough, J.M., McCulloch, M., and Demenocal, P.B., 2007, Impact of skeletal dissolution and secondary aragonite on trace element and isotopic climate proxies in *Porites* corals: Paleoceanography, v. 22, doi: 10.1029/2007PA001462.

Hernavan, U.E., 2012, Taxonomy of Indonesian giant clams (Cardiidae, Tridacninae): Biodiversitas, v. 13, p. 118–123.

Herold, N., Huber, M., Müller, R.D., and Seton, M., 2012, Modeling the Miocene climatic optimum: ocean circulation: Paleoceanography, v. 27, doi: 10.1029/2010PA002041.

Holbourn, A., Kuhnt, W., Schulz, M., Flores, J.A., and Andersen, N., 2007, Orbitally-paced climate evolution during the middle Miocene "Monterey" carbon-isotope excursion: Earth and Planetary Science Letters, v. 261, p. 534–550.

Hönisch, B., Allen, K.A., Russel, A.D., Eggins, S.M., Bijma, J., Spero, H.J., Lea, D.W., and Yu, J., 2011, Planktic foraminifers as recorders of seawater Ba/Ca: Marine Micropaleontology, v. 79, p. 52–57.

Huber, M., and Caballero R., 2003, Eocene El Niño: Evidence for robust tropical dynamics in the "hothouse": Science, v. 299, p. 887–881.

Jochum, K.P., Weis, U., Stoll, B., Kuzmin, D., Yang, Q.C., Raczek, I., Jacob, D.E., Stracke, A., Birbaum, K., Frick, D.A., Gunther, D., and Enzweiler, J., 2011a, Determination of reference values for NIST SRM 610–617 glasses following ISO guidelines: Geostandards and Geoanalytical Research, v. 35, p. 397–429.

Jochum, K.P., Wilson, S.A., Abouchami, W., Amini, M., Chmeleff, J., Eisenhauer, A., Hegner, E., Iaccheri, L.M., Kieffer, B., Krause, J., McDonough, W.F., Mertz-Kraus, R., Raczek, I., Rudnick, R.L., Scholz, D., Steinhoefel, G., Stoll, B., Stracke, A., Tonarini, S., Weis, D., Weis, U., and Woodhead, J.D., 2011b, GSD-1G and MPI-DING reference glasses for *in situ* and bulk isotopic determination: Geostandards and Geoanalytical Research, v. 35, p. 193–226.

Jones, D.S., and Quitmyer, J.R., 1996, Marking time with bivalve shells: oxygen isotopes and season of annual increment formation: PALAIOS, v. 11, p. 340–346.

Jones, D.S., William, D.F., and Romanek, C.S., 1986, Life history of symbiont-bearing giant clams from stable isotope profiles: Science, v. 231, p. 46–48.

Klein, R.T., Lohmann, K.C., and Thayer, C.W., 1996, Bivalve skeletons record sea-surface temperature and $\delta^{18}O$ via Mg/Ca and $^{18}O/^{16}O$ ratios: Geology, v. 24, p. 415–418.

Kuhnt, W., Holbourn, A., Hall, R., Zuvela, M., and Kase, R., 2004, Neogene history of the Indonesian throughflow: Continent-ocean interactions within East Asian marginal seas, v. 149, p. 299–320.

Langlet, D., Alunno-Bruscia, M., Rafelis, M., Renard, M., Roux, M., Schein, E., and Buestel, D., 2006, Experimental and natural cathodoluminescence in the shell of *Crassostrea gigas* from Thau lagoon (France): ecological and environmental implications: Marine Ecology Progress Series, v. 317, p. 143–156.

Lazareth, C.E., Vander Putten, E., André, L., and Dehairs, F., 2003, High-resolution trace element profiles in shells of the mangrove bivalve *Isognomon ephippium*: a record of environmental spatio-temporal variations?: Estuarine, Coastal and Shelf Sciences, v. 57, p. 1103–1114.

Lear, C.H., Elderfield, H., and Wilson, P.A., 2000, Cenozoic deep-sea temperatures and global ice volumes from Mg/Ca in benthic foraminiferal calcite: Science, v. 287, p. 269–272.

Lear, C.H., Rosenthal, Y., and Slowey, N., 2002, Benthic foraminiferal Mg/Ca-paleothermometry: a revised core-top calibration: Geochimica et Cosmochimica Acta, v. 66, p. 3375–3387.

Li, Q., Li, B., Zhong, G., McGowran, B., Zhou, Z., Wang, J., and Wang, P., 2006, Late Miocene development of the western Pacific warm pool: planktonic foraminifer and oxygen isotopic evidence: Palaeogeography, Palaeoclimatology, Palaeoecology, v. 237, p. 465–482.

Longerich, H.P., Gunther, D., and Jackson, S.E., 1996, Elemental fractionation in laser ablation inductively coupled plasma mass spectrometry: Fresenius Journal of Analytical Chemistry, v. 355, p. 538–542.

Mayfield, A., and Gates, R., 2007, Osmoregulation in anthozoan-dinoflagellate symbiosis: Comparative Biochemistry and Physiology A, 147, 1–10.

McArthur, J.M., and Howarth, R.J., 2004, Strontium isotope stratigraphy, *in* Gradstein, F.M., Ogg, J.G., and Smith, A.G., eds., A Geological Timescale 2004: Cambridge University Press, Cambridge, U.K., p. 589.

McArthur, J.M., Howarth, R.J., and Bailey, T.R., 2001, Strontium isotope stratigraphy: LOWESS version 3: Best fit to the marine Sr-isotope curve for 0–509 Ma and accompanying look-up table for deriving numerical age: Journal of Geology, v. 109, p. 155–170.

Mcculloch, M.T., Gagan, M.K., Mortimer, G.E., Chivas, A.R., and Isdale, P.J., 1994, A high-resolution Sr/Ca and $\delta^{18}O$ coral record from the Great Barrier Reef, Australia, and the 1982–1983 El Nino: Geochimica et Cosmochimica Acta, v. 58, p. 2747–2754.

Mcculloch, M.T., Fallon, S., Wyndham, T., Hendy, E., Lough, J., and Barnes, D., 2003, Coral record of increased sediment flux to the inner Great Barrier Reef since European settlement: Nature, v. 421, p., 727–730.

McGregor, H.V., and Gagan, M.K., 2003, Diagenesis and geochemistry of *Porites* corals from Papua New Guinea: implications for paleoclimate reconstruction: Geochimica et Cosmochimica Acta, v. 67, p. 2147–2156.

Mertz-Kraus, R., Brachert, T.C., Jochum, K.P., Reuter, M., and Stoll, B., 2009, LA-ICP-MS analyses on coral growth increments reveal heavy winter rain in the Eastern Mediterranean at 9 Ma: Palaeogeography, Palaeoclimatology, Palaeoecology, v. 273, p. 25–40.

Mishima, M., Kawahata, H., Suzuki, A., Inoue, M., Okai, T., and Omura, A., 2009, Reconstruction of the East China Sea palaeoenvironment at 16 ka by comparison of fossil and modern *Faviidae* corals from the Ryukyus, southwestern Japan: Journal of Quaternary Science, v. 24, p. 928–936.

Moberg, F., Nystrom, M., Kautsky, N., Tedengren, M., and Jarayabhand, P., 1997, Effects of reduced salinity on the rates of photosynthesis and respiration in the hermatypic corals *Porites lutea* and *Pocillopora damicornis*: Marine Ecology Progress Series, v. 157, p. 53–59.

Moir, B.G., 1990, Comparative studies of "fresh" and "aged" *Tridacna-gigas* shell: Preliminary investigations of a reported technique for pretreatment of tool material: Journal of Archaeological Science, v. 17, p. 329–345.

Müller, W., Shelley, M., Miller, P., and Broude, S., 2009, Initial performance metrics of a new custom-designed ArF excimer LA-ICPMS system coupled to a two-volume laser-ablation cell: Journal of Analytical Atomic Spectrometry, v. 24, p. 209–214.

Nathan, S.A., and Leckie, R.M., 2009, Early history of the Western Pacific Warm Pool during the middle to late Miocene (~ 13.2–5.8 Ma): role of sea-level change and implications for equatorial circulation: Palaeogeography, Palaeoclimatology, Palaeoecology, v. 274, p. 140–159.

Nothdurft, L.D., and Webb, G.E., 2009, Earliest diagenesis in scleractinian coral skeletons: implications for palaeoclimate-sensitive geochemical archives: Facies, v. 55, p. 161–201.

Pearson, P.N., Ditchfield, P. W., Singano, J., Harcourt-Brown, K.G., Nicholas, C.J., Olsson, R.K., Shackleton, N.J., and Hall, M.A., 2001, Warm tropical sea surface temperatures in the Late Cretaceous and Eocene epochs: Nature, v. 413, p. 481–487.

Quinn, T.M., and Sampson, D.E., 2002, A multiproxy approach to reconstructing sea surface conditions using coral skeleton geochemistry: Paleoceanography, v. 17, doi: 10.1029/2000PA000528.

Ren, L., Lindley, B.K., Wellington, G.M., Schrag, D.P., and Hoegh-Guildberg, O., 2002, Deconvolving the $\delta^{18}O$ seawater component from subseasonal coral $\delta^{18}O$ and Sr/Ca at Rarotonga in the southwestern subtropical Pacific for the period 1726–1997: Geochimica Et Geocosmica Acta, 67, p. 1609–1621.

Renema, W., Bellwood, D.R., Braga, J.C., Bromfield, K., Hall, R., Johnson, K.G., Lunt, P., Meyer, C.P., McMonagle, L.B., Morley, R.J., O'Dea, A., Todd, J.A., Wesselingh, F.P., Wilson, M.E.J., and Pandolfi, J.M., 2008, Hopping hotspots: Global shifts in marine biodiversity: Science, v. 321, p. 654–657.

Renema, W., Warter, V., Novak, V., Young, Y., Marshall, N., and Hasibuan, F., 2015, Ages of Miocene fossil localities in the Northern Kutai Basin (East Kalimantan, Indonesia): PALAIOS, v. 30, p. 26–39.

Romanek, C.S., and Grossman, E.L., 1989, Stable isotope profiles of *Tridacna maxima* as environmental indicators: PALAIOS, v. 4, p. 402–413.

Sano, Y., Kobayashi, S., Shirai, K., Takahata, N., Matsumoto, K., Watanabe, T., Sowa, K., and Iwai, K., 2012, Past daily light cycle recorded in the strontium/calcium ratios of giant clam shells: Nature Communications, v. 3, doi: 10.1038/NCOMMS1763.

Sayani, H.R., Cobb, K.M., Cohen, A.L., Elliott, W.C., Nurhati, I.S., Dunbar, R.B., Rose, K.A., and Zaunbrecher, L.K., 2011, Effects of diagenesis on paleoclimate reconstructions from modern and young fossil corals: Geochimica et Cosmochimica Acta, v. 75, p. 6361–6373.

Singh, R.K., and Gupta, A.K., 2010, Deep-sea benthic foraminiferal changes in the eastern Indian Ocean (ODP Hole 757B): their links to deep Indonesian (Pacific) flow and high latitude glaciation during the Neogene: Episodes, v. 33, p. 74–82.

Srinivasan, M.S., and Sinha, D.K., 2000, Ocean circulation in the tropical Indo-Pacific during early Pliocene (5.6–4.2 Ma): Paleobiogeographic and isotopic evidence: Proceedings of the Indian Academy of Sciences (Earth and Planetary Sciences), v. 109, p. 315–328.

Swart, P.K., Elderfield, H., and Greaves, M.J., 2002, A high-resolution calibration of Sr/Ca thermometry using the Caribbean coral Montastraea annularis: Geochemistry Geophysics Geosystems, v. 3, doi: 10.1029/2002GC000306.

Tangdong, Q., Du, J., Strachan, J., Meyers, G., and Slingo, J., 2005, Sea surface temperature and its variability in the Indonesian region: Oceanography, v. 18, p. 50–61.

Taylor, J.D., Kennedy, W.J., and Hall, A., 1973, The Shell Structure and Mineralogy of the Bivalvia II, Lucininacea–Clavagellacea, Conclusions: Bulletin of the British Museum (Natural History), Zoology, v. 22, p. 255–294.

Thébault, J., Chauvaud, L., L'Helguen, S., Clavier, J., Barats, A., Jacquet, S., Pechéyran, C., and Amouroux, D., 2009, Barium and molybdenum records in bivalve shells: geochemical proxies for phytoplankton dynamics in coastal environments?: Limnology and Oceanography, v. 54, p. 1002–1014.

Thirlwall, M.F., 1991, Long-term reproducibility of multicollector Sr and Nd isotope ratio analysis: Chemical Geology (Isotope Geochemistry Section), v. 94, p. 85–104.

Watanabe, T., and Oba, T., 1999, Daily reconstruction of water temperature from oxygen isotopic ratios of a modern *Tridacna* shell using a freezing microtome sampling technique: Journal of Geophysical Research, v. 104, p. 20667–20674.

Watanabe, T., Winter, A., and Oba, T., 2001, Seasonal changes in sea surface temperature and salinity during the Little Ice Age in the Caribbean Sea deduced from Mg/Ca and $^{18}O/^{16}O$ ratios in corals: Marine Geology, v. 173, p. 21–35.

Watanabe, T., Suzuki, A., Kawahata, H., Kan, H., and Ogawa, S., 2004, A 60-year isotopic record from a mid-Holocene fossil giant clam (*Tridacna gigas*) in the Ryukyu Islands: physiological and paleoclimatic implications: Palaeogeography, Palaeoclimatology, Palaeoecology, v. 212, p. 343–354.

Welsh, K., Elliot, M., Tudhope, A., Ayling, B., and Chappell, J., 2011, Giant bivalves (*Tridacna gigas*) as recorders of ENSO variability: Earth and Planetary Science Letters, v. 307, p. 266–270.

Wendler, J.E., Wendler, I., Rose, T., and Huber, B.T., 2012, Using cathodoluminescence spectroscopy of Cretaceous calcareous microfossils to distinguish biogenic from early-diagenetic calcite: Microscopy and Microanalysis, v. 18, p. 1313–1321.

Yan, H., Shao, D., Wang, Y., and Sun, L., 2013, Sr/Ca profile of long-lived *Tridacna gigas* bivalves from South China Sea: a new high-resolution SST proxy: Geochimica et Cosmochimica Acta, v. 112, p. 52–65.

Zachos, J.C., 1994, From the greenhouse to the icehouse: a Southern Ocean perspective of Paleogene climate: Oceanus, v. 36, p. 57–61.

Zachos, J.C., Pagani, M., Sloan, L., Thomas, E., and Billups, K., 2001, Trends, rhythms, and aberrations in global climate 65 Ma to present: Science, v. 292, p. 686–93.

Zachos, J.C., Dickens, G.R., and Zeebe, R.E., 2008, An early Cenozoic perspective on greenhouse warming and carbon-cycle dynamics: Nature, v. 451, p. 279–283.

Received 18 June 2013; accepted 25 February 2014.

Chapter 4: Case study 2

Citation:

Warter, V., and Müller, W., 2016, **Daily growth and tidal rhythms in Miocene and modern giant clams revealed via ultra-high resolution LA-ICPMS analysis – A novel methodological approach towards improved sclerochemistry**: Palaeogeography, Palaeoclimatology, Palaeoecology, doi:10.1016/j.palaeo.2016.03.019.

This chapter includes three pages of supplementary material.
The complete data set of all here presented LA-ICPMS profiles is provided as electronic supplementary material within the appendix.

Author contributions:

Viola Warter designed the research in discussion with Wolfgang Müller, performed the analyses, interpreted the data and wrote the manuscript. Wolfgang Müller helped design the procedure for the ultra-high resolution LA-ICPMS analysis and edited the manuscript.

Palaeogeography, Palaeoclimatology, Palaeoecology xxx (2016) xxx–xxx

Contents lists available at ScienceDirect

Palaeogeography, Palaeoclimatology, Palaeoecology

journal homepage: www.elsevier.com/locate/palaeo

Daily growth and tidal rhythms in Miocene and modern giant clams revealed via ultra-high resolution LA-ICPMS analysis — A novel methodological approach towards improved sclerochemistry

Viola Warter *, Wolfgang Müller

Department of Earth Sciences, Royal Holloway University of London, Egham, Surrey TW20 0EX, United Kingdom

ARTICLE INFO

Article history:
Received 3 September 2015
Received in revised form 14 March 2016
Accepted 18 March 2016
Available online xxxx

Keywords:
Tridacna spp.
Miocene
Daily cycles
Tidal periodicity
Ultra-high resolution LA-ICPMS
Image processing

ABSTRACT

We present a novel approach for ultra-high resolution laser-ablation inductively-coupled-plasma mass spectrometry (LA-ICPMS) analysis, which not only allows us to clearly resolve <10 μm (daily) compositional variability in B/Ca, Mg/Ca, Sr/Ca and Ba/Ca, but also to detect long-term tidal and seasonal cycles in both Miocene and modern *Tridacna* (giant clam) shells. Daily element/Ca variability preserved within microscopically visible growth increments is resolved by utilizing the combined capabilities of a rotating rectangular aperture (spot size on target 4 × 50 μm), the rapid signal washout of a Laurin two-volume laser ablation cell and slow compositional profiling (≤1.5 μm/s). Striking co-variation between oscillating cycles in B/Ca, Mg/Ca, Sr/Ca and Ba/Ca is discernible, yet also tantalizingly, sub-daily shifts between these element/Ca ratios can be observed. In comparison to a lower-resolution, seasonally-resolved δ^{18}O–Mg/Ca record (Warter et al., 2015), the ~10–20 μm element/Ca cycles are determined to be daily in origin, and a further ~14–15 day cyclicity is superimposed on the daily cycles. The latter is interpreted to reflect (Miocene) tidal periodicity. Changes in pixel intensity during thin section observation associated with micro- and macroscopically visible low and high density bands have been quantified via image processing analysis. This reveals close correspondence to the measured trace elemental cyclicity, indicating a coupling between the geochemical composition of the shell and the incremental growth pattern. A comparison between the elemental and image processing results reveals that ultra-high-resolution LA-ICPMS analysis surpasses the latter in detecting environmental rhythms, including daily and tidal cycles. Highly-resolved LA-ICPMS analysis is a viable alternative to nanoSIMS and opens up routine investigation of long-term (deep-time) paleoenvironmental records at daily resolution.

1. Introduction

Biogenic carbonates with recognizable growth bands, such as mollusk shells, coral skeletons or fish otoliths, are of special interest for (paleo)environmental research (e.g. Alibert and McCulloch, 1997; Epplé et al., 2006; Meibom et al., 2007; Mertz-Kraus et al., 2009; Patterson, 1999; Schöne et al., 2002; Schöne and Gillikin, 2013; Stott et al., 2010; Vanhove et al., 2011; Yan et al., 2014b). Annual to sub-daily growth bands preserved in the biomineralized hard tissues of organisms, represent an accretionary record of (past) environmental conditions and may serve as direct lifespan control. Owing to their extraordinary size of more than one meter, longevity of more than 100 years and rapid shell growth rates of several mm/year, giant clams (family Cardiidae, subfamily Tridacninae, genus *Tridacna*) are particularly attractive sclerochronological archives for the tropical and subtropical regions of the Indo Pacific and have been extensively studied in the past ~30 years (e.g. Aharon, 1983, 1991; Batenburg et al., 2011; Elliot et al., 2009; Sano et al., 2012; Warter et al., 2015; Welsh et al., 2011; Yan et al., 2013, 2015). The occurrence of a well-visible seasonal banding pattern within the aragonitic shell of *Tridacna* spp. is well-known and facilitated numerous studies on seasonal environmental variability (e.g. Batenburg et al., 2011; Elliot et al., 2009; Pätzold et al., 1991; Warter et al., 2015; Yan et al., 2014a). Less-utilized is the fact that *Tridacna* spp. secrete their shells daily, recorded as microscopically visible daily growth increments in the shell structure (Aharon and Chappell, 1986; Hori et al., 2015; Sano et al., 2012; Warter et al., 2015; Watanabe and Oba, 1999). Thus, environmental changes – reflected as variations in the shell's geochemical inventory – are continuously recorded in chronological order and at extremely high, possibly even hourly, temporal resolution.

Spatially-resolved geochemical analysis of successively secreted carbonate, via laser-ablation inductively-coupled-plasma mass spectrometry (LA-ICPMS), secondary ion mass spectrometry ((nano)SIMS) or electron micro probe analyzer (EMPA), enables retrieval of the trace elemental and isotopic inventory in chronological order, resulting in so-called time-series records. To ensure the accuracy of such time-series

* Corresponding author.
E-mail addresses: viola.warter@rhul.ac.uk (V. Warter), w.muller@es.rhul.ac.uk (W. Müller).

http://dx.doi.org/10.1016/j.palaeo.2016.03.019
0031-0182/

analysis, it is crucial to reliably identify and characterize daily or annual growth bands within the carbonate structure. To translate the detected (trace) elemental ratio variability into a temporal context of days, months or years, the usage of a second independent geochemical proxy, e.g. $\delta^{18}O$, might be necessary.

Owing to its potential for rapid and accurate high-resolution *in situ* trace element analysis at relatively low costs and minimal sample preparation requirements, LA-ICPMS has become a routine analytical tool in a wide area of research applications. Apart from analysis by discrete adjacent spots, compositional trace elemental variability in biogenic carbonates can be assessed using two different methodological approaches: (1) Lateral profiling, i.e. laser ablation along a defined transect on the sample's surface, typically oriented perpendicular to the accretionary growth direction and (2) Depth profiling, which involves static layer by layer removal of material at low laser repetition rates (1–2 Hz) to establish a depth-composition relationship (e.g. Eggins et al., 2004; Evans et al., 2015; Griffiths et al., 2013). The choice of sampling approach strongly depends on the size/thickness of the biogenic carbonate sample which depends on the growth rate and the overall lifespan of the organism, and the desired spatial/temporal resolution as well as the desired profile length, which determines the covered 'time window'. Traditionally, LA-ICPMS lateral profiling is performed to produce long-term, up to centennial, time-series records with relatively low spatial and thus low temporal resolution of weeks to years (e.g. McCulloch et al., 2003). Lateral profiling therefore is suited for thick/large biogenic samples on the mm-scale, which exhibit well-defined annual growth layers, such as specific mollusk shells and coral skeletons (e.g. Alibert and McCulloch, 1997; Batenburg et al., 2011; Elliot et al., 2009; Gagan et al., 2000). On the other hand, LA-ICPMS depth profiling is the better approach for investigating trace elemental variation at (sub-)μm resolution, because the limiting factor for resolution is depth ablated per individual laser pulse (typically ≤0.1–0.15 μm) and not the diameter of the laser spot (Griffiths et al., 2013; MacDonald et al., 2008; Woodhead et al., 2008). It has been shown that it is possible to resolve daily compositional variability in planktonic foraminifera and fish otoliths using LA-ICPMS depth profiling (Eggins et al., 2004; MacDonald et al., 2008). This indicates that LA-ICPMS compares well with other high resolution methods, such as (nano)SIMS, which has been successfully employed to resolve daily compositional variability in foraminifera tests (Vetter et al., 2013), fish otoliths (Weidel et al., 2007), mollusk shells (Hori et al., 2015; Sano et al., 2012) and coral skeletons (Meibom et al., 2007). While LA-ICPMS depth profiling in principle allows highly spatially-resolved sampling, the depth range during static spot analysis is limited by the laser focal depth and the aspect ratio (depth/diameter) of the laser-drilled hole that in turn is controlled by its tapering angle. The achieved resolution via lateral profiling is determined by the utilized spot size. To maximize resolution along growth increments a rectangular spot should be used which facilitates substantially better spatial and thus temporal resolution compared to a round spot, while maintaining similar signal sensitivities (see details in Section 3.2).

Our primary aims are: (1) Introducing our methodology for ultra-high resolution LA-ICPMS analysis to the sclerochronology community to highlight that LA-ICPMS as the more rapid and inexpensive method compared to nanoSIMS is well-capable of resolving <10 μm compositional cycles such as the growth increments in the aragonitic structure of giant clams. (2) Confirming that the presented μm scale (trace) elemental cyclicity can be characterized as *daily*, for which we utilize a Miocene specimen that has been extensively characterized in an earlier study (Warter et al., 2015). (3) Demonstrating that the chemical composition of the shell varies with the microscopically visible (micro)growth pattern. To this end we present complementary image processing results that link light intensity with measured trace elemental ratios. (4) Showcasing how long-term (annual) ultra-high resolution LA-ICPMS analysis reveals periodicities and their respective frequencies in giant clam shells.

2. Materials and study sites

2.1. Fossil *Tridacna* spp.

The presented Miocene *Tridacna* shells, LGS1 and BW4B, were sampled from the eastern coast of Borneo in the Indonesian province of East Kalimantan (0° 11′ 11.40″ N, 117° 26′ 40.92″ E; 0° 11′ 7.08″N, 117° 26′ 47.04″E), close to the city of Bontang (Fig. 1). The exteriors of both shells are altered, resulting in the loss of characteristic morphological features such as the fine details of the ribbing pattern and hinge area. Consequently, neither of the shells was identifiable to species level. A previous study (Warter et al., 2015) demonstrated that the interiors of both *Tridacna* shells are to a large extent excellently preserved,

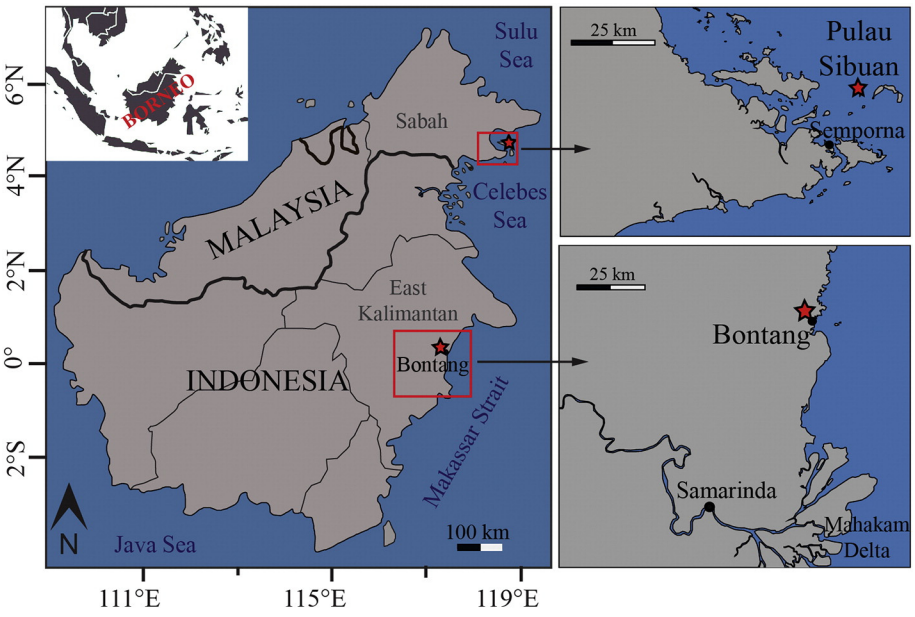

Fig. 1. Sampling locations. Overview map of South East Asia (inset) and maps of Borneo with the sampling locations in East Kalimantan, Indonesia and Sabah, Malaysia (marked by stars).

Please cite this article as: Warter, V., Müller, W., Daily growth and tidal rhythms in Miocene and modern giant clams revealed via ultra-high resolution LA-ICPMS analysis — A novel ..., Palaeogeogr. Palaeoclimatol. Palaeoecol. (2016), http://dx.doi.org/10.1016/j.palaeo.2016.03.019

with evidence for an intact Miocene geochemical inventory within pristine shell aragonite. Strontium Isotope Stratigraphy (SIS) indicates an age of 9.16 ± 0.55 Ma for LGS1 and 9.75 ± 0.38 Ma for BW4B, respectively, which places both samples into the Tortonian stage (Late Miocene) and supports biostratigraphic data from the Bontang area (Renema et al., 2015). Macroscopically, the shell cross sections reveal a distinct banding pattern of alternating dark and light growth bands (Fig. 2). Alignment of micromilled stable oxygen isotope data and LA-ICPMS element/Ca ratios with the shell banding pattern demonstrates that each macroscopically visible dark/bright couple can be characterized as one annual cycle (Warter et al., 2015). Microscopically, sub-mm patterns within seasonal bands can be detected, which are best visible under transmitted illumination of polished thin sections (Fig. 2). A recurring alternation of relatively broad, dark, i.e. least translucent, dense 'bands' with relatively fine, bright, i.e. more translucent, less dense 'lines' can be observed. Each couple comprising one broad band and thin line can be described as one growth unit. Regarding terminology we refer to Rosenberg (1975) who defines the period of the increment as the "time represented between the beginning of a unit of structure or composition, and the beginning of the next adjacent unit" and we further use the term 'growth increment' to denote a couple of an adjacent broad dark band and thin bright line. It has been shown that shell growth rates of *Tridacna* spp. decrease as a function of age (e.g. Elliot et al., 2009; Warter et al., 2015). This ontogenetic trend is also reflected in the microgrowth pattern. In the case of LGS1 for example, the growth increments visible in the micrograph labeled as J (juvenile) are on average 20 μm thick, while those visible in the micrograph labeled as A (adult) are only ~10 μm thick (Fig. 2).

2.2. Modern *Tridacna squamosa*

The investigated modern *Tridacna* shell, SB1, is a *Tridacna squamosa* and was collected with permission from Sabah Parks in October 2012, at Pulau Sibuan (4° 39′ 04.00″ N, 118° 39′ 32.00″ E), an island close to the city Semporna in the Malaysian State of Sabah, located in the Celebes Sea (Fig. 1). Macroscopic examination of the shell reveals evidence for bioerosion (Fig. 2), most likely caused by shell-boring organisms such as sponges (e.g. Govan, 1992; Nava and Carballo, 2008). Similar to the Miocene shells, individual daily microgrowth increments, identifiable in the thin section, are subject to an ontogenetic growth rate trend, with on average thicker increments in shell parts secreted early in life of the organism and thinner increments for shell parts secreted later in life of the organism (Fig. 2). The growth increments visible in the micrograph labeled as J (juvenile) are on average about 20 μm thick, while those visible in the micrograph labeled as A (adult) are significantly thinner than 10 μm.

3. Methodology

3.1. Sample preparation

The *Tridacna* shells were thoroughly cleaned using deionized water and a tooth brush to remove organic matter and sediment particles from the external shell parts. The valves were then cross-sectioned along the maximum growth axis, from the umbo to the ventral margin, using a water-cooled Jencons Tyslide diamond saw, to expose internal

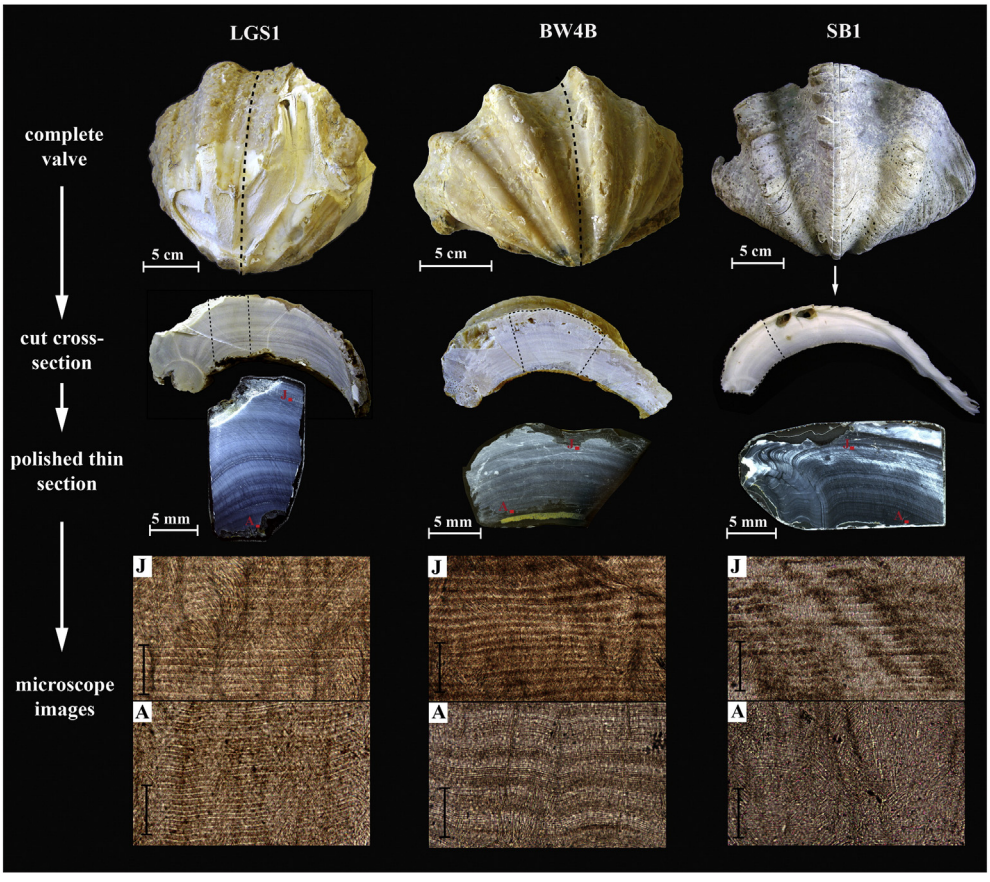

Fig. 2. Photographs of whole and sectioned valves, polished thin sections and transmitted light microscope images of the studied shells LGS1, BW4B and SB1. From top to bottom: Complete valves: The black dashed lines on LGS1 and BW4B mark the approximate cut position for cross-sectioning, while the exact cut position of SB1 is indicated. Cut cross-sections: the dashed polygons mark the area represented by the thin sections. Polished thin sections: the red squares mark the approximate area of microscopic examination in 'juvenile' or 'adult' shell areas, labeled as 'J' or 'A', respectively (scale bars represent 100 μm).

Please cite this article as: Warter, V., Müller, W., Daily growth and tidal rhythms in Miocene and modern giant clams revealed via ultra-high resolution LA-ICPMS analysis — A novel ..., Palaeogeogr. Palaeoclimatol. Palaeoecol. (2016), http://dx.doi.org/10.1016/j.palaeo.2016.03.019

growth increments. From opposite surfaces ~30 μm thick polished sections without cover (Fig. 2) were prepared and used for both microscopic examination of the (micro)growth pattern and LA-ICPMS analysis.

3.2. Ultra-high resolution LA-ICPMS analysis

Daily trace element variability in the giant clams was investigated using a 193 nm ArF excimer laser ablation system (RESOlution M-50, formerly Resonetics, now ASI, Canberra, Australia) featuring a two-volume laser ablation cell (Laurin Technic, Australia), which is connected to an Agilent 7500ce quadrupole ICPMS (Müller et al., 2009). Instrument tuning on the standard reference material NIST SRM 612 (Jochum et al., 2011) was performed to ensure optimal sensitivity (maximum signal to background ratio), while minimizing oxide formation ($^{248}ThO/^{232}Th < 0.5\%$) and doubly charged ion production ($Ca^{2+}/Ca^{+} < 0.5\%$) and to yield near-equal response for thorium and uranium ($^{232}Th/^{238}U > 95\%$) to minimize elemental fractionation. The LA-ICPMS operating conditions are given in Table 1.

The laser ablation system is equipped with a rotating rectangular aperture-slit mask, which is perfectly suited for the analysis of 'layered' samples, such as growth patterns in mollusk shells, coral skeletons, fish otoliths, teeth, wood samples or speleothems. To resolve daily compositional variability in the presented giant clams, the double-slit assembly was set up to a resultant rectangular laser spot of 4 × 50 μm on the sample surface. To maximize resolution, the long direction of the slit was carefully aligned parallel to visible daily growth increments in the thin sections. The area, covered by a 4 × 50 μm rectangular spot is equivalent to the area covered by a 16 μm round spot. This highlights that the slit option offers – at equal signal sensitivity – substantially better spatial/temporal resolution, namely four-fold herein, compared to the circular spot, and is thus preferably used for 'layered' samples with unidirectional compositional variability, while maintaining detection of low concentration elements such as Ba and B, besides Mg and Sr, in aragonite. Crucially, the rectangular aperture-slit mask can be rotated 360°, which enables the user to accurately follow layer orientation and to correct for non-parallel growth. The precision of the slit alignment and with it the success of the ultra-high resolution LA-ICPMS analysis strongly depends on the visibility and distinctness of individual growth patterns. To guarantee maximal visibility, ultra-high resolution LA-ICPMS analysis was performed on thin sections under transmitted light illumination.

To achieve ultra-high spatial/temporal resolution, laser ablation was performed in continuous profiling mode and at very slow speed (≤1.5 μm/s). The total ICPMS sweep time was kept short (≤350 ms) by analyzing only six elements (m/z ^{11}B, ^{24}Mg, ^{43}Ca, ^{88}Sr, ^{89}Y and ^{138}Ba) with dwell times ranging between 5 and 100 ms (Table 1). Combining a slow scan speed, e.g. 1 μm/s, with a short total sweep time, e.g. 350 ms, means that each data point advances by 0.35 μm as a running average of at best 4 μm spatial resolution. To investigate the effect of the X–Y stage speed on the achieved resolution, trace elemental profiles obtained at different scan speeds are compared (Fig. 3). Three parallel laser transects were ablated at varying scan speeds of 1.0, 3.0 and 5.0 μm/s in the Miocene shell LGS1 (Fig. 3). The comparison of the resulting LA-ICPMS profiles reveals that compositional variability is best resolved when using a very slow stage speed of ≤1.5 μm/s. An increase of the scan speed in the order of 2 μm/s, reduces the number of data points by half, resulting in fewer data points per cycle and thus in a decrease of the resolved detail. At a scan speed of ≥3 μm/s both peak and trough amplitudes appear dampened, which can be attributed to a loss of detail due to signal washout issues.

The depth of the laser ablation transect also strongly depends on the employed scan speed. At a repetition rate of 15 Hz and a scan speed of 1 μm/s, one pulse equals a distance of 0.06667 μm. In order to ablate a distance of 4 μm, 60 pulses are required, resulting in a maximum depth of the trench of ~6 μm, when assuming 0.1 μm (Griffiths et al., 2013) depth removal per pulse. For comparison, using the same repetition rate but a higher scan speed of 1.5 μm/s creates a trench that is only ~4 μm deep. A conventional 30-μm thin section allows several repeated scans along the same path, even when applying a very slow scan speed. As both signal rise and washout time are twice as fast without the 'squid' smoothing device and smoothing is only critical for laser repetition rates <10 Hz (Müller et al., 2009), the squid was not fitted, which therefore allows thinner compositional bands to be resolved.

Data reduction broadly followed Longerich et al. (1996) and was performed using Iolite (Paton et al., 2011) run under Igor Pro (WaveMetrics, Inc.). The isotope ^{43}Ca was used for internal standardization, NIST SRM 612 (Jochum et al., 2011) was used as external standard and analyzed before and after each sample.

Lacking sufficiently homogenous matrix-matched carbonate minerals as microanalytical standards (pressed powder pellet USGS MACS-3 (Wilson et al., 2008) is rather inhomogenous), the MPI-DING glasses GOR132-G, GOR128-G and KL2-G (GEOREM preferred values: http://georem.mpch-mainz.gwdg.de) were utilized as secondary standards and analyzed alongside every sample for accuracy and precision evaluation. In total, 36 standard analyses were performed over a period of eight months; each transect consisted of on average 180 individual data points, equivalent to an ablation distance of ~0.1 mm. Mean analytical accuracy and corresponding external precision (accuracy [%] ± 1 RSD [%]) for all three MPI-DING glasses was 6.95 ± 6.73, 11.09 ± 3.32, −0.66 ± 1.11, −5.61 ± 3.93 and 5.10 ± 4.80, for B, Mg, Sr, Y and Ba, respectively. These external precision data compare well with the reported 95% confidence level (CL) uncertainties of 12.43, 1.09, 3.17, 4.15, 4.83 for B, Mg, Sr, Y and Ba, especially when considering the small spot size utilized (~16 μm circular equivalent). The typical mean internal precision for one standard analysis of the MPI-DING glasses GOR132-G, GOR128-G and KL2-G, expressed as 2 relative SE [%] was 3.94, 1.22, 1.38, 3.47 and 2.87 for B, Mg, Sr, Y and Ba, respectively. It is not possible to assess the precision/reproducibility by repeat analysis of the *Tridacna* shells owing to their compositional heterogeneity on the sub-μm scale. Typical limits of detection for the elements B, Mg, Sr, Y and Ba were 0.18, 0.20, 0.015, 0.019 and 0.009 ppm.

Table 1
LA-ICPMS operating conditions.

ICPMS	Agilent 7500ce
RF Power	1100–1150 W (optimized daily)
Sampling depth	4.5 mm
Carrier gas flow (Ar)	0.47–0.68 l/min
Sampler, skimmer cones	Ni
Extraction lenses	ce
Tuning Parameters	$^{232}Th/^{238}U > 95\%$ $^{248}ThO/^{232}Th < 0.25\%$
Monitored masses (m/z)	11, 24, 43, 88, 89,138
Total sweep time	350 ms
Individual dwell times (ms)	^{11}B: 100; ^{24}Mg: 60; ^{43}Ca: 50; ^{88}Sr: 50; ^{89}Y: 5; ^{138}Ba: 80
Laser Ablation System	**RESOlution M-50 (prototype)**
He gas flow	850 ml/min
N_2/H_2 gas flow	6/8.5 ml/min
Laser repetition rate	15 Hz (same for preablation)
Laser spot size	50 × 4 μm
Scan speed (X–Y stage)	≤1.5 μm/s (preablation: 2 mm/min)
Transport tubing	Nylon-6
Fluence (energy density)	5-5.5 J/cm^2

3.3. Image processing analysis

High resolution transmitted light images of the thin sections were acquired with a Nikon Mikrophot-FX microscope equipped with a Nikon digital camera head (DS-5M) combined with a Nikon digital site controller (DS-L1) at RHUL at 100–200× magnification. Digital images of the complete shell thin sections were created using an EPSON Perfection V500 Photo flatbed scanner in reflective mode at 4800 dpi. To detect and measure individual growth increments, we used the

Please cite this article as: Warter, V., Müller, W., Daily growth and tidal rhythms in Miocene and modern giant clams revealed via ultra-high resolution LA-ICPMS analysis — A novel ..., Palaeogeogr. Palaeoclimatol. Palaeoecol. (2016), http://dx.doi.org/10.1016/j.palaeo.2016.03.019

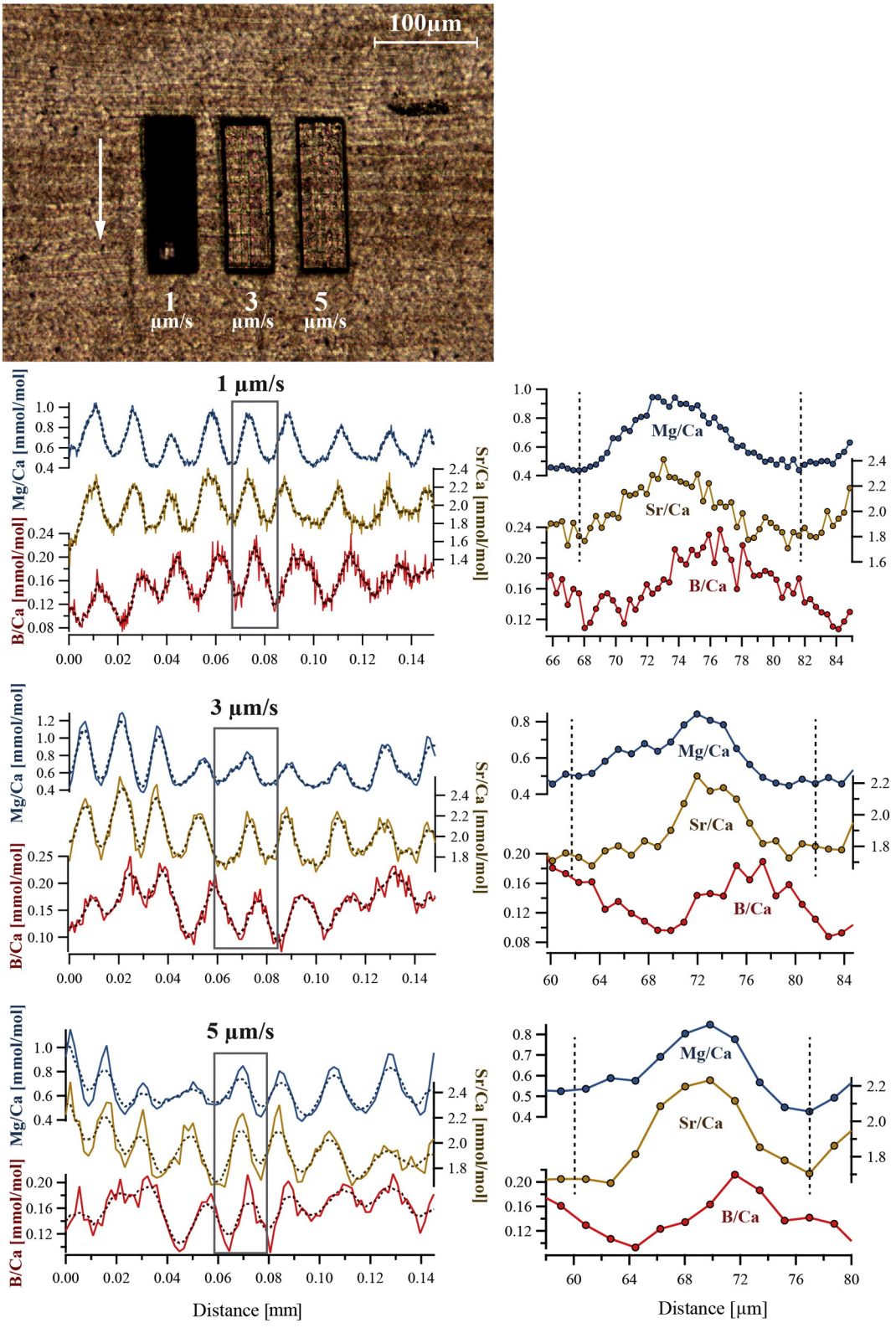

Fig. 3. B/Ca, Mg/Ca and Sr/Ca and profiles of the Miocene shell LGS1 acquired at variable X–Y stage scan speeds of 1.0, 3.0 and 5.0 µm/s. The micrograph illustrates the ablated shell area with the three visible ablation transects; the ablation direction is indicated by the arrow. The gray rectangle within each profile set marks the daily trace elemental variability of one daily cycle presented in enlarged view and with individual data points visible. The black dashed lines within the enlarged profiles mark one day of growth estimated from the Mg/Ca and Sr/Ca variability. Data smoothing was performed using a 5 point moving average, the smoothed profiles are presented as dashed lines.

'Caliper/Line Profile tool' of the Image-Pro Premier 9.1 package provided by Media Cybernetics. This tool allows the user to create any arbitrary transect across the image. At every point along this defined transect, the pixel intensity of the image is measured, resulting in a line profile plot, which displays the pixel intensity values in RGB. Aligning the transect perpendicular to the shell banding pattern results in a wavy oscillatory pattern of the line profile spectrum, where sharp peaks in the profile represent thin/bright layers with high pixel intensity and broad

Please cite this article as: Warter, V., Müller, W., Daily growth and tidal rhythms in Miocene and modern giant clams revealed via ultra-high resolution LA-ICPMS analysis — A novel ..., Palaeogeogr. Palaeoclimatol. Palaeoecol. (2016), http://dx.doi.org/10.1016/j.palaeo.2016.03.019

valleys represent wide/dark bands with low pixel intensity, respectively (see Sections 4.1 and 4.2 for details). The pixel intensity line profile helps to define single increments where they are not easily identified with the naked eye and allows for a systematic unbiased analysis of the banding pattern. To achieve the best comparison between the image processing and the trace element analysis, image processing was performed parallel and as close as possible to visible LA-ICPMS tracks. For ideal comparison between results of the image processing and the ultra-high resolution LA-ICPMS analysis, pixel intensity measurements could be performed before laser ablation takes place.

4. Results

The results of both LA-ICMPS analysis and image processing are displayed in Figs. 4 to 8 and supplementary Figs. S1–S3. The complete data set of all here presented LA-ICPMS profiles is provided as electronic supplementary material (Table S1–S6). Ablation of all transects was performed (unless otherwise specified) in direction of growth ('dog'), i.e. towards more recently precipitated shell parts. All laser ablation transects were aligned perpendicular to microscopically well-visible growth increments, with the length direction of the rectangular slit oriented parallel to isochronous growth increments. Yttrium has been co-acquired as an element indicative of diagenetic alteration. For the modern shell SB1, the concentrations for Y fall below the limit of detection (LOD: 0.019 ppm). In the case of the Miocene shells LGS1 and BW4B the concentration are below 0.3 ppm and 0.1 ppm, respectively and do not show significant variability.

4.1. Daily to weekly time-series records

Significant variability for the proxy element/Ca ratios B/Ca, Mg/Ca, Sr/Ca and Ba/Ca, resembling clear compositional cycles, can be observed throughout each of the presented profiles (e.g. Fig. 4). The elemental ratios of the LA-ICPMS profile of LGS1 vary from 0.10–0.24 mmol/mol (B/Ca), 0.45–1.49 mmol/mol (Mg/Ca), 1.41–2.49 mmol/mol (Sr/Ca) and 0.49–1.41 μmol/mol (Ba/Ca). The corresponding results for SB1 vary from 0.04–0.23 mmol/mol (B/Ca), 0.55–1.30 mmol/mol (Mg/Ca), 1.15–2.35 mmol/mol (Sr/Ca) and 0.50–6.98 μmol/mol (Ba/Ca). The transitions between peak and trough ratios are smooth, resulting in a cyclic pattern. In the following the term 'daily cycle' will be used to describe the oscillatory trace elemental variability. Following this terminology, the nine cycles in the LA-ICPMS profile of LGS1 (Fig. 4A), correspond to nine days of growth and the fourteen cycles in the LA-ICPMS profile of SB1 (Fig. 4B), correspond to fourteen days of growth. The average length of a daily cycle for LGS1 and SB1 is about 15 ± 4 μm and 11 ± 5 μm, respectively. Zooming into individual daily cycles allows an assessment of the achieved resolution. Fig. 4C highlights one daily growth cycle spanning a width of ~18 μm, which consists of ~30 individual data points. Fig. 4D highlights one daily growth cycle spanning a width of ~9 μm, which consists of at least ~15 individual data points. Both examples demonstrate that sub-daily resolution is achievable using ultra-high resolution LA-ICPMS analysis and that the achieved time resolution – under constant ablation conditions – depends on the thickness of individual growth increments.

Striking co-variation between the LA-ICPMS profiles for B/Ca, Mg/Ca, Sr/Ca and partly Ba/Ca is discernible, yet also tantalizingly, systematic sub-daily shifts of up to several μms between these element/Ca ratios can be observed (Fig. 4). In order to quantify both correlations and shifts between the element/Ca ratios, we chose the best-resolved Sr/Ca as basis to which the other element/Ca ratios are compared. Rather than using all data points, we use maxima and minima defined by Sr/Ca and compare the equivalent positions for the other element/Ca ratios to reveal potential shifts among the geochemical proxies. The means of five adjacent data points (two either side of maximum or minimum)

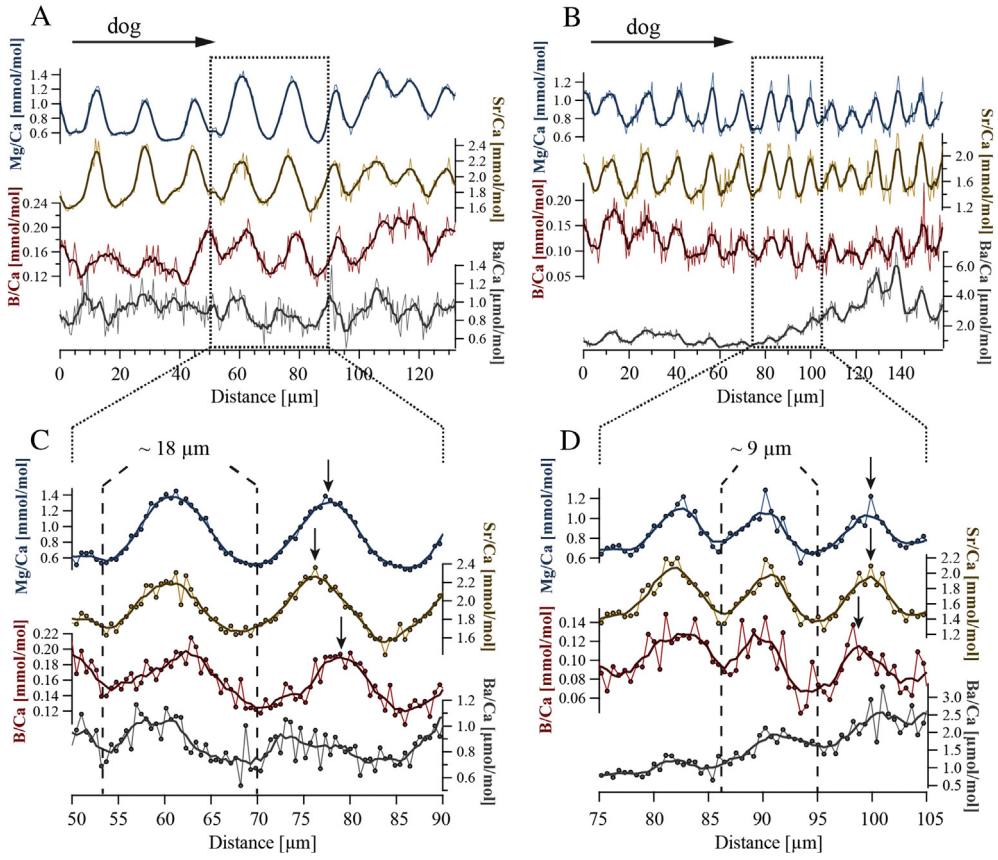

Fig. 4. Daily resolved LA-ICPMS profiles of B/Ca, Mg/Ca, Sr/Ca and Ba/Ca in A) the Miocene shell LGS1 and B) the modern shell SB1. The gray dotted squares mark the profiles enlarged in C) and D). The arrows indicate the phase shift between peak ratios for B/Ca, Mg/Ca and Sr/Ca. Data smoothing was performed using a 5 point moving average. Dog: direction of growth.

Please cite this article as: Warter, V., Müller, W., Daily growth and tidal rhythms in Miocene and modern giant clams revealed via ultra-high resolution LA-ICPMS analysis — A novel ..., Palaeogeogr. Palaeoclimatol. Palaeoecol. (2016), http://dx.doi.org/10.1016/j.palaeo.2016.03.019

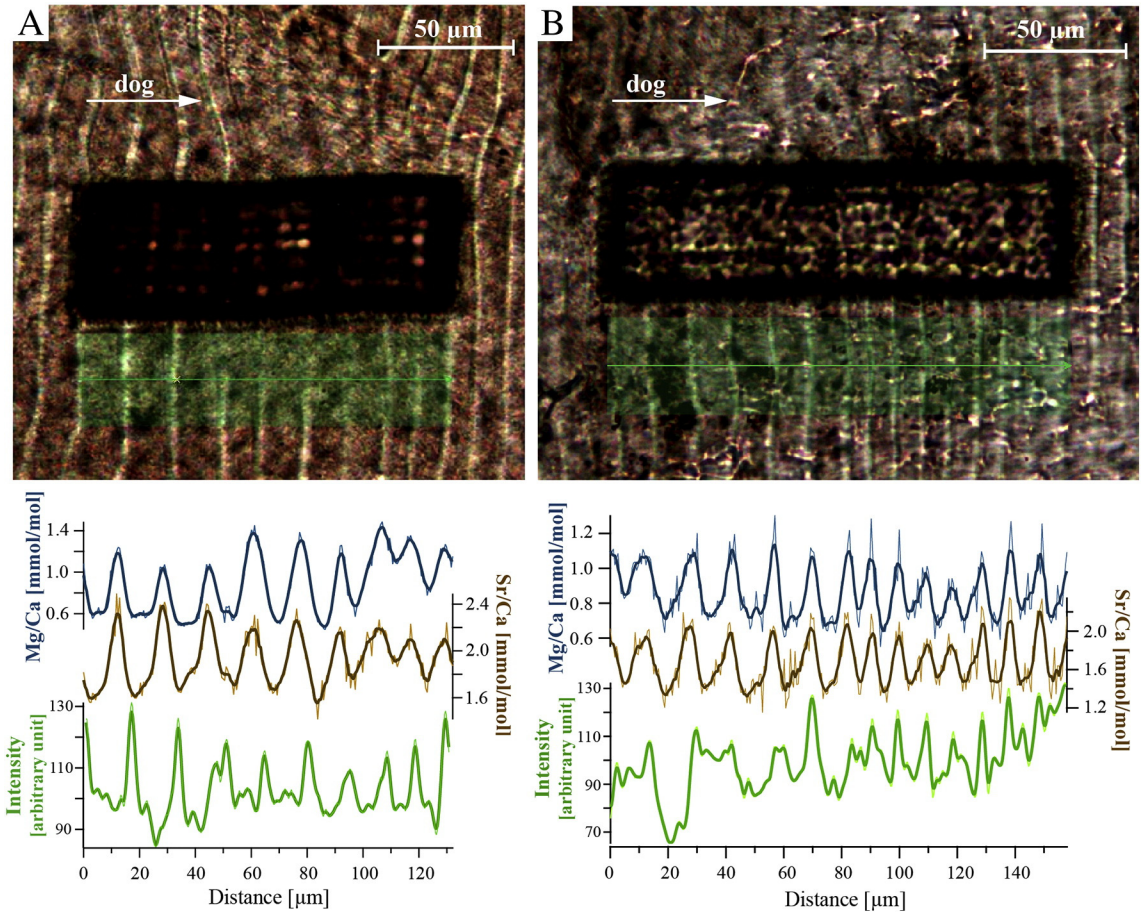

Fig. 5. Mg/Ca and Sr/Ca LA-ICPMS profiles and corresponding pixel intensity profiles aligned with daily growth increments in thin section microscope images of A) LGS1 and B) SB1. The dark brown rectangles represent the ablated shell area, the transparent green rectangles mark the area of the microscope image on which image processing was performed. Data smoothing on trace element and pixel intensity data was performed using a 5 point moving average. (For interpretation of the references to color in this figure legend, the reader is referred to the web version of this article.)

are presented. All correlations reveal a positive relationship. Regarding LGS1 (Fig. S1A) there is a strong correlation between Sr/Ca and Mg/Ca ($R^2 = 0.71$), a weak correlation between Sr/Ca and B/Ca ($R^2 = 0.10$) and a strong correlation ($R^2 = 0.50$) between Sr/Ca and Ba/Ca. Equivalent analyses for SB1 (Fig. S1B) reveal a very strong correlation between Sr/Ca and Mg/Ca ($R^2 = 0.90$), a strong correlation between Sr/Ca and B/Ca ($R^2 = 0.45$) and a weak correlation ($R^2 = 0.13$) between Sr/Ca and Ba/Ca. The results of the correlations analysis are in line with the visual observations from Fig. 4 that Sr/Ca and Mg/Ca daily cycles correlate best. The compositional cycles are best developed for Sr/Ca and Mg/Ca, compared to which the daily cycles of the B/Ca and Ba/Ca profiles are more irregular in shape and noisy, which can be attributed to the lower Ba and B concentrations. The average offset for peak and trough ratios in LGS1 between Sr/Ca and Mg/Ca, B/Ca and Ba/Ca are 0.45 µm, 2.51 µm and −1.58 µm, respectively. The average offset for peak and trough concentrations in SB1 between Sr/Ca and Mg/Ca, B/Ca and Ba/Ca are −0.17 µm, 0.12 and −0.06 µm, respectively. The absolute numbers for the phase shift for SB1 are on average smaller, because other than for LGS1, the phase shift is not uniform positive or negative, and therefore the numbers cancel out.

The daily resolved LA-ICPMS trace elemental records of LGS1 and SB1 were aligned with the shell banding pattern to investigate whether a relation between the microscopically visible growth pattern and the geochemical composition of the shell exists. Only the clearly resolved Mg/Ca and Sr/Ca profiles are presented (Fig. 5). The comparison between the LA-ICPMS profiles with the incremental growth pattern reveals that peak element/Ca ratios overall correspond to relatively thin and bright, most translucent growth lines, while low element/Ca ratios match with the relatively broad and dark, least translucent growth bands, respectively (Fig. 5). This indicates a coupling between the geochemical composition of the shell and the incremental growth pattern. The resulting pixel intensity curves are broadly similar to the oscillatory pattern of the daily resolved LA-ICPMS profiles. In case of the Miocene shell LGS1 (Fig. 5A), the nine peaks/troughs in pixel intensity can be matched with the nine peaks/troughs in element/Ca ratios. However, the direct comparison reveals an offset between the pixel intensity profile and the trace elemental profiles. The offset can be explained by the fact that the position, thickness and visibility of individual growth increments change within a few µms, which becomes evident when comparing different areas of the micrographs (Fig. 5A). The correlation between the Sr/Ca profile and the light intensity data (Fig. S1A) reveals no relationship ($R^2 = 0.06$). By rejection of the outlier marked by the dashed circle (Fig. S1A), the correlation becomes moderately negative ($R^2 = 0.25$). In case of the modern shell SB1 (Fig. 5B), the pixel intensity curves are, especially for the first ~80 µm, more irregular compared to the trace element cycles, which again might be related to changes of the growth pattern within the shell on the µm scale. However, the match between peak and trough values is higher compared to the results of the Miocene shell, which is reflected by the moderately positive correlation ($R^2 = 0.21$) between Sr/Ca and the corresponding pixel intensity data (Fig. S1B). Overall, the pixel intensity cycles are not as well-defined as are the Mg/Ca and Sr/Ca profiles and consequently it is not as easy to distinguish between individual daily cycles. This highlights the strength of LA-ICPMS over such image processing methods for e.g. sclerochronological analysis.

Please cite this article as: Warter, V., Müller, W., Daily growth and tidal rhythms in Miocene and modern giant clams revealed via ultra-high resolution LA-ICPMS analysis — A novel ..., Palaeogeogr. Palaeoclimatol. Palaeoecol. (2016), http://dx.doi.org/10.1016/j.palaeo.2016.03.019

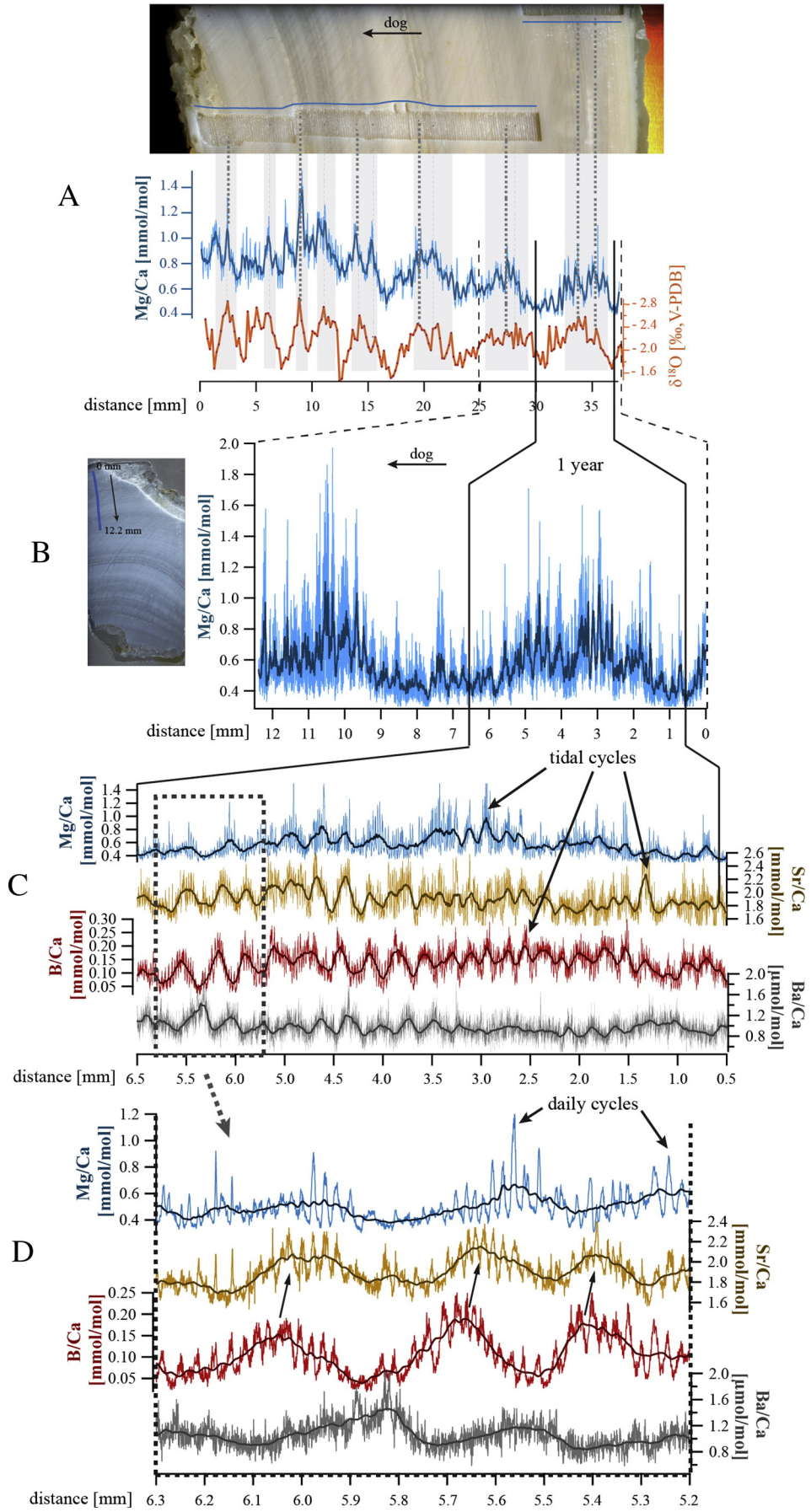

Please cite this article as: Warter, V., Müller, W., Daily growth and tidal rhythms in Miocene and modern giant clams revealed via ultra-high resolution LA-ICPMS analysis — A novel ..., Palaeogeogr. Palaeoclimatol. Palaeoecol. (2016), http://dx.doi.org/10.1016/j.palaeo.2016.03.019

4.2. Annual time-series records

Long-term (up to two years) daily resolved LA-ICPMS profiles are presented in order to (1) prove that the trace element compositional cyclicity described under 4.1 can indeed be described as 'daily' and (2) demonstrate that environmental rhythms exist superimposed on daily growth cycles that can be detected using long-term, highly resolved LA-ICPMS analysis.

A low resolution LA-ICPMS-derived Mg/Ca profile (spot size: 57 μm, repetition rate: 15 Hz, ablation speed: 30 μm/s) and its corresponding $\delta^{18}O$ profile (sampling resolution of micro-milling: 200 μm) of the Miocene clam LGS1 are presented in Fig. 6A (Warter et al., 2015). The Mg/Ca and oxygen isotope profile are inversely correlated (Fig. 6A), both of which reveal eight major oscillations that are aligned with the seasonal banding pattern of the shell and have been interpreted to represent eight years of growth. Approximately two years of growth (~12 mm) during the early ontogenetic stage of Miocene LGS1 were analyzed at ultra-high resolution (Fig. 6B) parallel to the track shown in Fig. 6A. The comparison between the relatively low resolution and the ultra-high-resolution profile not only reveals that the annual cycles can also be recognized using highly resolved LA-ICPMS analysis but close examination shows well-recognizable, smaller scale oscillations within the B/Ca, Mg/Ca, Sr/Ca and Ba/Ca profiles (Fig. 6C). These smaller scale variations are most regularly developed for the B/Ca profile and have ~300–400 μm wavelengths. Approximately 24 of these cycles can be counted within one year of shell growth (Fig. 6C) and each is composed of on average 14–15 daily cycles, thus the counted 24 cycles are equivalent to ~one year of growth (Fig. 6D). Those fortnightly cycles will be further referred to as 'tidal cycles' (see Section 5.3 for details). It is the change in elemental ratios of the daily cycles which determines the overall shape of an individual tidal cycle. Maxima/minima of tidal cycles consist of an accumulation of daily cycles characterized by high/low elemental ratios. The element/Ca ratios in LGS1 vary from 0.02–0.35 mmol/mol (B/Ca), 0.23–1.97 mmol/mol (Mg/Ca), 1.34–3.20 mmol/mol (Sr/Ca) and 0.37–2.27 μmol/mol (Ba/Ca). The transition between highest and respectively lowest trace elemental ratios within one tidal cycle is smooth, resulting in a cyclic pattern of a 100–150 point moving average (Fig. 6C, D). The number of daily cycles within each tidal cycle varies (±2 days, between about 12 to 16 days), but for well-defined, regularly shaped tidal cycles the average is 14 to 15 daily cycles (Fig. 6D). Counting uncertainties arise from (1) the section defined as one tidal cycle and (2) the differentiation of all individual daily cycles within one tidal cycle. The existence and detectability of such ~14–15 day cyclicity greatly facilitates age estimations, as not each individual daily cycle needs to be counted.

Similar to the daily cycles, a systematic out-of-phase shift between the peaks/troughs of tidal cycles for Mg/Ca, Sr/Ca, B/Ca and Ba/Ca in the range of up to several hundreds of μms exists (Fig. 6C, D). This is especially clear when comparing Sr/Ca with Ba/Ca and B/Ca with Ba/Ca in Fig. 6D. The latter two are offset to each other by up to 250 μm and seem to anticorrelate. The correlations of the tidal-cyclic peak and trough data of the Sr/Ca profile with the corresponding values for B/Ca, Mg/Ca and Ba/Ca ratios (based on a 50 point moving average data set and using the averages of nine adjacent data points) are illustrated in supplementary Fig. S2A. All correlations reveal a weak positive relationship with R^2 values ranging from 0.11 for Sr/Ca versus Mg/Ca, 0.27 for Sr/Ca versus B/Ca and 0.17 for Sr/Ca versus Ba/Ca.

The results of the long-term, daily resolved LA-ICPMS analysis of the second Miocene sample BW4B are presented in Fig. 7. The about 6.5 mm long ablation transect covers the shell part secreted ontogenetically earliest (Fig. 7A). The corresponding profiles for B/Ca, Mg/Ca, Sr/Ca and Ba/Ca profiles reveal well-recognizable, smaller scale oscillations, also resembling tidal cycles. The elemental/Ca ratios in BW4B vary from 0.02–0.30 mmol/mol (B/Ca), 0.20–1.58 mmol/mol (Mg/Ca), 1.35–5.29 mmol/mol (Sr/Ca) and 0.69–3.22 μmol/mol (Ba/Ca). The Ba/Ca tidal cycles appear to be most regularly developed (Fig. 7A, B). However, daily cycles within the tidal cycles are best discernible for Mg/Ca and Sr/Ca (Fig. 7B). A systematic out-of-phase shift between peaks/troughs of the tidal cycles for B/Ca, Mg/Ca, Sr/Ca and Ba/Ca is discernible. It appears that Mg/Ca and B/Ca on the one hand and Sr/Ca and Ba/Ca on the other correlate best. The correlation of the LA-ICPMS profiles illustrated in Fig. 7B indeed reveals a strong positive correlation between Sr/Ca and Ba/Ca ($R^2 = 0.47$), whereas the correlation for Sr/Ca with B/Ca is weak ($R^2 = 0.25$) and no correlation exists between Sr/Ca and Mg/Ca ($R^2 = 0.07$). The correlations are illustrated in supplementary Fig. S2B.

The results of the long-term, daily resolved LA-ICPMS analysis of the modern shell SB1 are presented in supplementary Fig. S3. An about 3 mm long ablation transect covers the middle part of the inner shell layer, which is characterized by a pronounced banding pattern. The corresponding element/Ca ratios vary from 0.04–0.32 mmol/mol (B/Ca), 0.38–2.99 mmol/mol (Mg/Ca), 0.72–3.42 mmol/mol (Sr/Ca) and 0.15–4.20 μmol/mol (Ba/Ca). Compared to the Miocene trace element profiles, these modern profiles for Mg/Ca, Sr/Ca and B/Ca appear 'flat' and lack the oscillatory cycles with the typical 14–15 day tidal periodicity (Fig. S3). The Ba/Ca profile is characterized by unsystematically large, sharp peaks in Ba/Ca ratios, which are up to five-fold higher than the average ratios (Fig. S3). Similar profiles have been described before in modern marine bivalves, including *Tridacna* spp. and have been linked to periods of high phytoplankton activity, i.e. phytoplankton blooms (e.g. Elliot et al., 2009; Gillikin et al., 2006, 2008; Lazareth et al., 2003).

The smoothed tidal-cyclic B/Ca and Sr/Ca records of the first 6.5 mm of the Miocene shell LGS1 were compared with the macroscopically visible shell banding pattern to investigate whether a relation between the growth pattern and the geochemical composition of the shell exists (Fig. 8A). The alignment was performed using a scanned image of the thin section (reflected light mode), which renders the most translucent/least dense bands appear dark and vice versa. An accurate alignment of the LA-ICPMS data with the incremental growth pattern is not straightforward due to the complexity of the growth pattern, the curvature of the laser ablation track and the fact that Sr/Ca and B/Ca cycles are out-of-phase, but overall the highest element/Ca ratios correspond to relatively dark, most translucent growth bands and vice versa (Fig. 8A). Image processing analysis performed on the same scanned image parallel to the LA-ICPMS transect provides a more quantitative assessment. The comparison reveals a similarity between the oscillatory pattern of the high resolution LA-ICPMS profiles and the pixel intensity profile, which is especially obvious within the final 3 mm (distance of 3.5–6.5 mm) of the profiles, where the banding pattern of alternating dark and bright bands is best developed (Fig. 8A). Troughs of pixel intensity under reflected light illumination (corresponding to peaks of light intensity under transmitted light illumination) co-vary with maxima in trace elemental ratios, indicating that the least dense, most translucent shell bands are enriched in trace

Fig. 6. Low versus highest resolution LA-ICPMS profiles of the Miocene shell LGS1. A) Polished thick section of LGS1 with position of both laser ablation transect (blue line) and micromilled section with the corresponding 'low resolution' LA-ICPMS and oxygen isotope profiles (modified from Warter et al. (2015)). The arrow marks the direction of growth (dog). B) Thin section of LGS1 used for highest resolution LA-ICPMS analysis, where the blue line marks the position of the laser ablation transect; the ablation direction corresponds the direction of growth as indicated by the black arrow. Data smoothing of the corresponding Mg/Ca record was performed using a 50 point moving average. C) Enlarged view of the first annual cycle reveals periodic cycles with 300–400 μm wavelengths in Mg/Ca, Sr/Ca, B/Ca and Ba/Ca. Data smoothing was performed using a 150 point moving average. D) Enlarged view on three 'tidal cycles' marked by the dotted rectangle in C. Each cycle consists of smaller-scale, daily cycles. The phase shift between Sr/Ca and B/Ca is indicated by the black arrows. Data smoothing was performed using a 100 point moving average. All high resolution profiles (B, C, D) are presented with reversed x-axis to facilitate comparison with the low resolution profile in A. (For interpretation of the references to color in this figure legend, the reader is referred to the web version of this article.)

Please cite this article as: Warter, V., Müller, W., Daily growth and tidal rhythms in Miocene and modern giant clams revealed via ultra-high resolution LA-ICPMS analysis — A novel ..., Palaeogeogr. Palaeoclimatol. Palaeoecol. (2016), http://dx.doi.org/10.1016/j.palaeo.2016.03.019

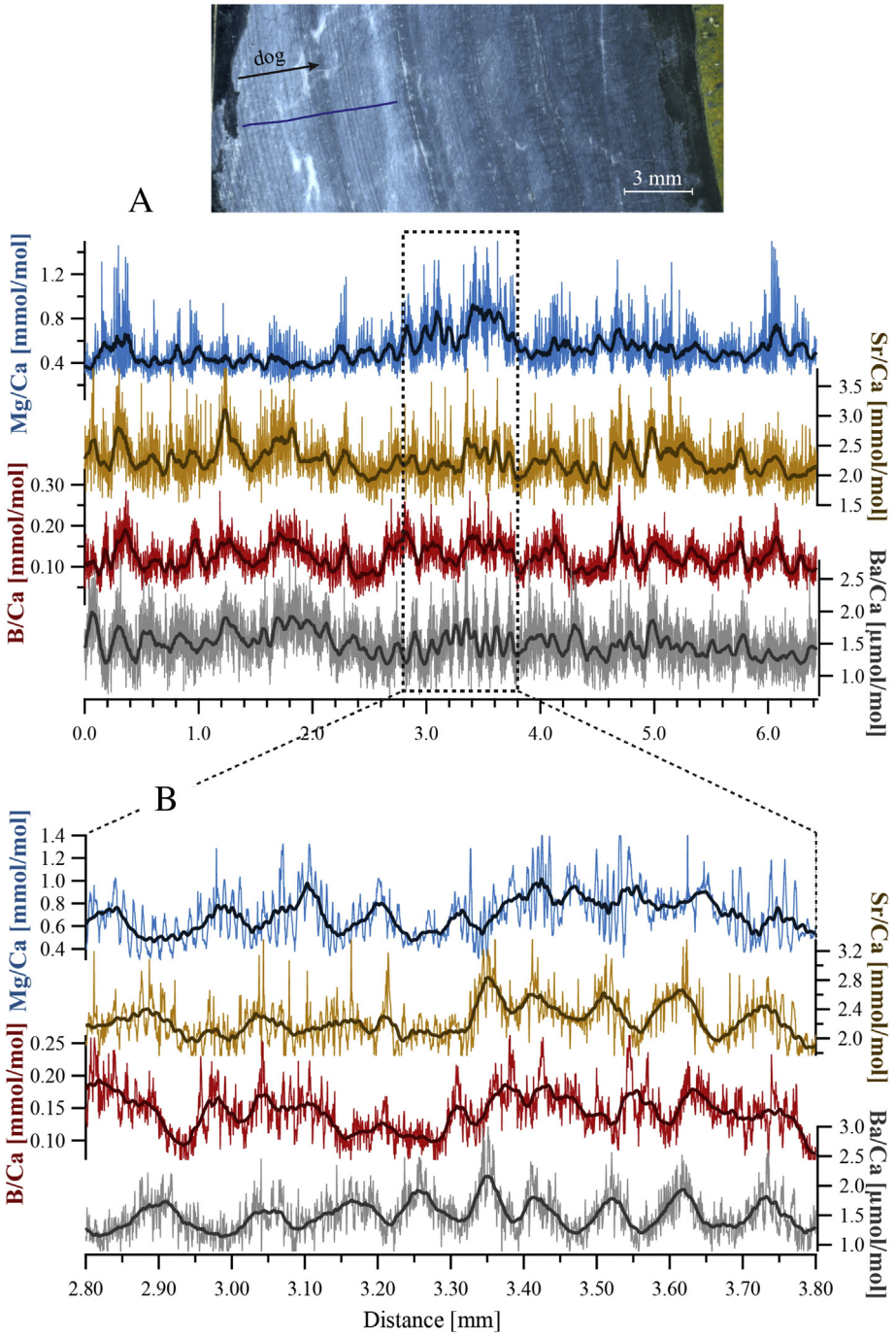

Fig. 7. Long-term, tidal-cyclic LA-ICPMS profiles of the Miocene shell BW4B. A) Thin section of BW4B used for highest resolution LA-ICPMS analysis. The blue line marks the position of the laser ablation transects. Data smoothing of the corresponding trace elemental records was performed using a 100 point moving average. B) Enlarged view on approximately nine to ten tidal cycles marked by the dotted rectangle in A. Data smoothing was performed using a 50 point moving average. (For interpretation of the references to color in this figure legend, the reader is referred to the web version of this article.)

elements. However, by comparing the tidal-cyclic pattern obtained from the pixel intensity profile with the equivalent B/Ca and Sr/Ca variability, it becomes clear that the element/Ca cycles in general are better defined and more regularly shaped and thus more easily detectable and discernible.

The Ba/Ca profile of the Miocene shell BW4B was chosen for alignment with the banding pattern, because its tidal-cyclic pattern is most regularly developed. The comparison between the smoothed Ba/Ca profile with the incremental growth pattern reveals that, equivalent to the results obtained from LGS1, peak ratios correspond to relatively dark, most translucent bands, whereas trough ratios match with bright, least translucent growth bands (Fig. 8B). Strikingly, at a distance of 3.0 to 3.8 mm, eight Ba/Ca tidal cycles, each only ~100 µm thick, can be identified and matched with eight fine, but prominent dark bands. The complementary image processing analysis reveals that, equivalent to the result of LGS1, troughs of pixel intensity (reflected light source) overall co-vary with maxima in Ba/Ca concentration, indicating that the least dense, most translucent shell bands are enriched in this trace element and vice versa. However, it is obvious that the Ba/Ca tidal cycles generally are better developed and provide more detail. This is especially obvious when comparing the pixel intensity profile and the Ba/Ca profile for the above described profile between 3.0 to 3.8 mm. The Ba/Ca spikes clearly mirror the fine banding pattern, although the intensity profile lacks detail.

Please cite this article as: Warter, V., Müller, W., Daily growth and tidal rhythms in Miocene and modern giant clams revealed via ultra-high resolution LA-ICPMS analysis — A novel ..., Palaeogeogr. Palaeoclimatol. Palaeoecol. (2016), http://dx.doi.org/10.1016/j.palaeo.2016.03.019

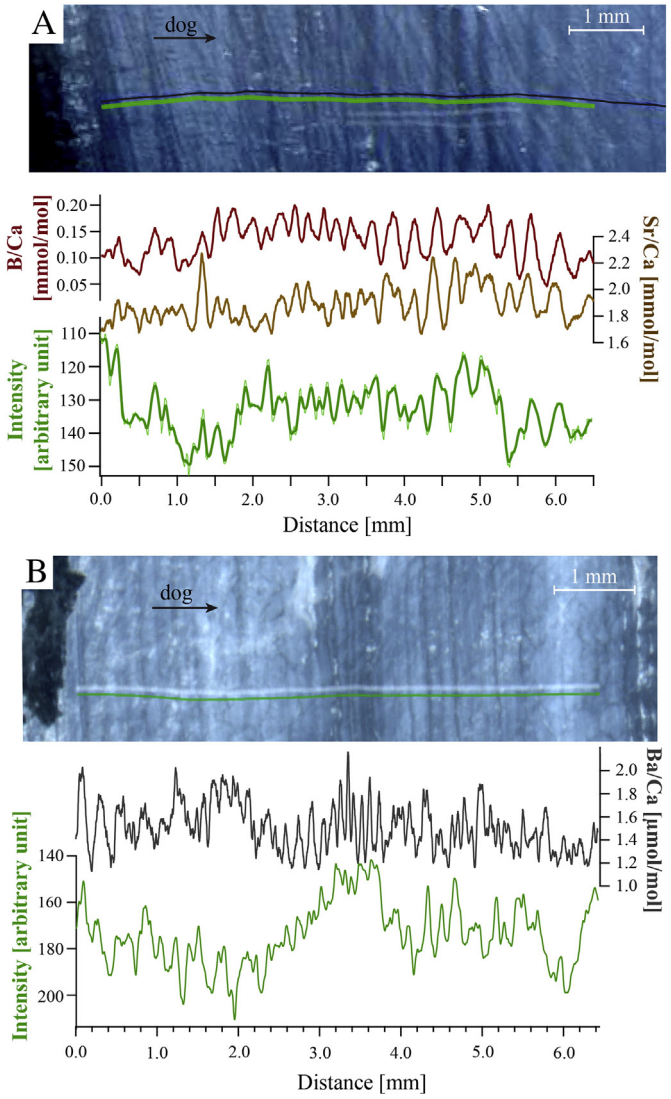

Fig. 8. A) B/Ca and Sr/Ca smoothed tidal-cyclic profiles and pixel intensity profile aligned with the macroscopically visible shell banding pattern from a scanned image (reflected light) of thin section LGS1. The black line within the micrograph represents the ablated shell part; the green line marks the position where the image processing analysis has been performed. Data smoothing was performed using a 150 and 10 point moving average for the trace elemental and pixel intensity data, respectively. B) Smoothed tidal-cyclic Ba/Ca record and pixel intensity profile aligned with the macroscopically visible shell banding pattern from a scanned image (reflected light source) of the thin section of BW4B. The white line within the micrograph represents the ablated shell part; the green line marks the position where the image processing analysis has been performed. Data smoothing for Ba/Ca was performed using 50 point moving average. Pixel intensity data in A and B are presented unsmoothed and with reversed y-axis to facilitate direct comparison with the trace elemental data.

The direct comparison between the trace elemental and pixel intensity profiles presented here reveals that the ultra-high resolution LA-ICPMS analysis is better suited than image processing analysis in the routine detection of environmental rhythms like the presented daily and tidal cyclicity.

5. Discussion

5.1. LA-ICPMS versus nanoSIMS for resolving daily trace elemental variability in giant clam shells

This study expands upon earlier nanoSIMS work by Sano et al. (2012) and Hori et al. (2015), who successfully extracted daily compositional variability in modern (Mg/Ca, Sr/Ca) and Holocene giant clams (Mg/Ca, Sr/Ca, Ba/Ca) via discrete spot analysis at 2 µm resolution.

Here, we utilize a different methodological approach – ultra-high resolution LA-ICPMS – and extend the (trace) elemental suite to also include B and Y, besides Mg, Sr, Ba and Ca. By utilizing a rotating rectangular laser spot (4 × 50 µm) and aligning the long direction of the slit parallel to visible daily increments, our achieved spatial resolution equals 4 µm, given the interplay between X–Y stage scan speed, LA cell washout, ICPMS sweep time and laser repetition rate (see Section 3.2 for details). However, continuous lateral profiling at a laser repetition rate of 15 Hz and very slow scan speed (1.5 µm/s) combined with a short total ICPMS sweep time (350 ms) allows for continuous data acquisition at nominal intervals of ~0.5 µm. The resulting data density using this methodological approach is greater than that of nanoSIMS analysis performed with a 2 µm spot at 2 µm intervals. Owing to this increase in data coverage, peaks and troughs within each daily cycle are composed of more individual data points and therefore appear smoother than those presented by Sano et al. (2012) and Hori et al. (2015).

Our methodology to obtain accurate, ultra-high resolution analysis of giant clams offers advantages over nanoSIMS such as significantly faster analysis (cf. Sano et al., 2005) at lower cost with less sample preparation (e.g. no vacuum requirements) and routine analysis of boron with its importance as carbonate system proxy (Yu et al., 2010). Ultra-high resolution LA-ICPMS further facilitates long-tem, i.e. monthly to annual, records to be obtained which help to detect periodicities, superimposed on the daily compositional variability, such as potential tidal and seasonal cycles.

5.2. Possible controls on daily trace element variability

Both Sano et al. (2012) and Hori et al. (2015) link the daily Sr/Ca variability, detected in modern *Tridacna derasa* and fossil *Tridacna gigas* shells, to the daily light cycle, i.e. the variation of insolation intensity. Other published research focuses, owing to trace elemental analysis at relatively lower resolution, on seasonally resolved Sr/Ca variations in diverse bivalve species. Those studies also link Sr/Ca variability to organism physiology, e.g. growth rate, ontogenetic age and metabolism and not exclusively to environmental controls (e.g. Carré et al., 2006; Freitas et al., 2005; Gillikin et al., 2005; Klein et al., 1996; Purton et al., 1999; Stecher et al., 1996). However, due to the relationship between sea surface temperature (SST) and shell growth rate (e.g. Aubert et al., 2009; Goodwin et al., 2001; Pätzold et al., 1991; Schöne et al., 2002), shell Sr/Ca may be indirectly coupled to the seawater temperature (e.g. Gillikin et al., 2005; Stecher et al., 1996). Yan et al. (2013) presented ICPOES derived Sr/Ca profiles of modern and fossil *T. gigas* shells with well-defined annual cycles, which are negatively correlated with SST and concluded that *Tridacna* Sr/Ca is a potential SST proxy, similar to findings from coral-based climate records (e.g. Marshall and McCulloch, 2002; Wei et al., 2000). Elliot et al. (2009), in contrast, found that temperature, growth rate and metabolic rates have no or very little control on LA-ICPMS derived Sr/Ca ratios in the investigated modern *T. gigas* shells and these results are corroborated by studies of Batenburg et al. (2011) and Warter et al. (2015), who did not report a clear link between SST and Sr/Ca in modern and fossil *Tridacna* shells. This shows that published results on possible controls of shell element/Ca in bivalves, including giant clams, are equivocal. Moreover, measured element/Ca ratios can vary significantly not only between different species but also for the same species collected from the same site (e.g. Freitas et al., 2005; Gillikin et al., 2005; Yan et al., 2014c). What is more, these vary even between different parts (e.g. inner layer, outer layer, hinge) of the very same shell (Elliot et al., 2009). Further complications arise from residual organic matrices within the shell that occur both at inter- and intracrystalline locations and which may influence the trace metal content of the shell (e.g. Foster et al., 2009;

Please cite this article as: Warter, V., Müller, W., Daily growth and tidal rhythms in Miocene and modern giant clams revealed via ultra-high resolution LA-ICPMS analysis — A novel ..., Palaeogeogr. Palaeoclimatol. Palaeoecol. (2016), http://dx.doi.org/10.1016/j.palaeo.2016.03.019

Schöne et al., 2010), at least in modern shells. Dreier et al. (2014) compared the organic content of a modern and a Pleistocene *Tridacna maxima* shell and found a substantial loss of bulk organic shell matrix in the fossil giant clam, probably due to degradation of shell organics during the fossilization process. With regards to our Miocene (9–10 Ma) samples it is thus likely that their organic content is very small with resultant negligible influence on the geochemical signature of the shell.

While in situ sampling via LA-ICPMS, (nano)SIMS or EMPA involves analysis of the bulk shell content, including inorganic carbonate, soluble (SOM) and insoluble organic matrix (IOM), the wet-chemical sample pre-treatment for ICPOES analysis will separate the IOM (e.g. Schöne et al., 2010), which leaves the inorganic shell fraction and SOM for analysis. Schöne et al. (2010) compared ICPOES and LA-ICPMS data and demonstrated that LA-ICPMS derived element/Ca ratios obtained from a modern *Arctica islandica* shell are significantly influenced by the trace elemental signature of the IOM, which also shows a heterogeneous distribution across the shell. The authors recommend the use of ICPOES derived data, at the expense of lower sampling resolution, for paleoenvironmental reconstructions. Yan et al. (2013) presented highly reproducible *T. gigas* Sr/Ca profiles with well-defined annual cycles obtained via ICPOES. Their corresponding comparative LA-ICPMS derived Sr/Ca profiles, however, do not reveal clear annual variability and are not reproducible. Crucially, the absolute values do not match the corresponding ICPOES-derived data set either, casting some uncertainty on the validity of the overall comparison. The authors argued that the organic shell content, the sampling method and experimental errors might account for the differences between the data sets. At present, the only techniques that enable resolving shell composition at the scale of daily incremental growth (for *Tridacna* species ca. 5–25 μm) involve in situ sampling via LA-ICPMS, (nano)SIMS or EMPA, by means of which it is not possible to determine the trace elemental contribution of the organic components towards the whole biomineral.

The asynchronous offsets between B/Ca, Mg/Ca, Sr/Ca and Ba/Ca observed within the daily and tidal profiles (e.g. Figs. 4 and 6) are intriguing. Branson et al. (2015) performed synchrotron X-ray analysis of foraminiferal calcite and found μm-scale cyclic Mg and B concentration distributions, characterized by a systematic offset between Mg and B, similar to our findings. The authors argued that the asynchronous banding in the foraminiferal calcite could be driven biologically, by fluctuations of the bulk fluid chemistry at the site of mineralization or through purely chemical oscillatory trace element zoning.

Spero et al. (2015) cultured planktic foraminifera and detected, similar to Branson et al. (2015), μm-scale cyclic Mg banding within the calcite tests of *Orbulina universa* using LA-ICPMS depth profiling. What is more, the authors demonstrated that high Mg bands are precipitated during the night, while low Mg bands are precipitated during the day and concluded that the daily Mg variability is linked to a diurnal cycle in foraminifer physiology related to light. The authors hypothesized that a light-induced variation of the Mg^{2+} uptake by mitochondria and/or diurnal variations in either mitochondrial density or activity may account for the daily cyclic Mg/Ca variability observed in *O. universa*.

With regards to the results of the modern and fossil giant clams presented here, it is not yet possible to reliably identify the mechanisms that cause the oscillatory μm-scale trace elemental variability and/or the out-of-phase shift between the element/Ca ratios. Instrumental records of the daily SST- or light cycle are not available for our modern shell because its exact habitat location during lifetime is unknown. Thus, it is not possible to isolate the relative contributions of environmental factors from physiological and/or biochemical controls. Moreover, the process of biomineralization in bivalve shells including *Tridacna* spp. is poorly understood (e.g. Lowenstam, 1981; Weiner and Dove, 2003), yet key to a detailed knowledge of the relationship between environmental factors and (bio)chemical processes and their relative influence on shell composition.

However, Warter et al. (in prep.) will report results of laboratory culture experiments on *Tridacna crocea*, conducted under tightly monitored and controlled environmental conditions such as temperature, light level and seawater chemistry. Preliminary results indicate that light levels play a role with regards to the daily trace elemental incorporation into the biogenic carbonate structure of giant clams (cf. Hori et al. (2015) and Sano et al. (2012)).

5.3. Tidal rhythms revealed via ultra-high resolution LA-ICPMS analysis

Numerous sclerochronological studies demonstrated that molluscs from tidally-influenced habitats are characterized by tidally-controlled growth patterns in their shells and concluded that tidally-induced environmental changes, such as changes of the sea level, can influence bivalve shell growth and as such the appearance of the shell growth pattern (e.g. Carré et al., 2005; Hallmann et al., 2009; House and Farrow, 1968; Goodwin et al., 2001; Miyaji et al., 2007; Richardson, 1987). The studies report a systematic change in daily increment widths associated with the fortnightly tidal periodicity (e.g. Miyaji et al., 2007; House and Farrow, 1968). Narrow increments and distinct growth lines are deposited during spring tides, often related to growth cessation during aerial exposure (e.g. Carré et al., 2005) and wider increments, with less distinct growth lines are deposited during neap tides (e.g. Goodwin et al., 2001; Hallmann et al., 2009). Pannella and MacClintock (1968) equally detected a recurrent tidal-cyclic pattern with a clear 14-day periodicity within the shell of a *T. squamosa* shell.

The long-term (>1 year) ultra-high resolution LA-ICPMS analysis presented here reveals the existence of ~14–15 day recurrent periodic pattern for B/Ca, Mg/Ca, Sr/Ca and Ba/Ca in both Miocene shells (Figs. 6 and 7). As explained above, the best known source for such fortnightly rhythms detected within bivalve shells are tidally-controlled environmental changes and therefore the term 'tidal cycle' is chosen to describe the observed oscillatory trace element variability that exists superimposed on daily growth cycles. It is elemental ratio variability not the width of the daily cycles, which determines the overall shape of an individual tidal cycle. Maxima/minima of each tidal cycle consist of an accumulation of daily cycles characterized by relatively high/low elemental ratios. Direct comparison between the results obtained via LA-ICPMS and those from the image processing analysis reveals a link between the geochemical composition of the shell and its tidal-cyclic growth pattern. Highest element/Ca ratios of each tidal cycle match with troughs of pixel intensity under reflected light illumination (Fig. 8), which correspond to peaks of light intensity under transmitted light illumination. As for the daily cycles, so far we cannot unequivocally explain the causes of the tidal-cyclic trace element variability detected within the Miocene shells and to our knowledge no study exists which investigates tidal cyclic trace elemental variability in bivalve shells at similar resolution. Potential factors are changes in shell growth rates related to exogenous factors such as sea level fluctuations and corresponding fluctuation in light intensity, varying seawater current and nutrient availability as well as endogenous metabolic (e.g. Richardson, 1987; Schöne and Gillikin, 2013; Ramón and Richardson, 1992) controls. The fact that both Miocene shells, contemporaneous within error and from the same locality, show tidal periodicities, whereas the modern shell from a different sample location does not, might indicate that the modern specimen was not exposed to a tidally-controlled environmental setting that influenced its shell chemistry.

6. Conclusions

Our novel approach for ultra-high resolution LA-ICPMS analysis enables resolution of <10 μm compositional variability in B/Ca, Mg/Ca, Sr/Ca and Ba/Ca preserved within microscopically visible daily growth increments in the aragonitic structure of modern and Miocene giant clams. LA-ICPMS allows significantly faster and less cost intensive analysis compared to nanoSIMS and compares well with the results by Sano et al. (2012) and Hori et al. (2015), who resolved daily

Please cite this article as: Warter, V., Müller, W., Daily growth and tidal rhythms in Miocene and modern giant clams revealed via ultra-high resolution LA-ICPMS analysis — A novel ..., Palaeogeogr. Palaeoclimatol. Palaeoecol. (2016), http://dx.doi.org/10.1016/j.palaeo.2016.03.019

compositional trace elemental variability in giant clam shells via discrete spot analysis at 2 μm resolution.

Striking co-variation between compositional daily cycles in B/Ca, Mg/Ca, Sr/Ca and Ba/Ca is discernible, yet also tantalizingly, sub-daily shifts between these element/Ca ratios can be observed. Systematic correlations of peak and trough data from daily resolved LA-ICPMS profiles suggest a strong positive correlation between Sr/Ca and Mg/Ca, but less so with B/Ca and Ba/Ca. Year-long, daily resolved LA-ICPMS records of B/Ca, Mg/Ca, Sr/Ca and Ba/Ca, reveal the existence of a Miocene tidal cyclicity, superimposed on the daily cycles, which is characterized by a fortnightly recurrent periodic pattern. Light intensity profiles obtained via image processing analysis show close correspondence to measured trace elemental ratios, implying a coupling between the geochemical composition of the shell and the incremental growth pattern. Direct comparison between the results of the trace element and image processing analysis, however, reveals that the ultra-high resolution LA-ICPMS analysis excels in detecting environmental rhythms such as our daily and tidal cyclicity. The existence and detectability of an ~14–15 day tidal periodicity within (trace) elemental records might help to improve and facilitate age estimations, where conventional sclerochronological methods are limited. Even though it is not the central aim of this study, the possibility to obtain long-term, daily resolved (trace) element profiles allows investigation of daily trace elemental variability changes through time, which might also make an important contribution towards studies on the history of the Earth's rotation.

The successful acquisition of proxy data at ultra-high resolution in tandem with laboratory culture experiments (Warter et al., in prep.), where environmental conditions such as temperature, light level and seawater chemistry are tightly monitored and controlled, provide the crucially needed framework towards a better understanding of the controls on trace elemental incorporation into the biogenic carbonate structure of giant clams.

Supplementary data to this article can be found online at http://dx.doi.org/10.1016/j.palaeo.2016.03.019.

Acknowledgments

A special thanks to all people and authorities involved in the sampling of the modern *Tridacna squamosa* shell, namely Aaron Hunter (Curtin University, Perth) and Jasmin Saw (SEAaRL - Universiti Teknologi PETRONAS, Malaysia) for collecting and exporting the specimen (funded by URIF, UTP, CITES Permit Certificate DOF(S)1611), Datuk Ali Lamri and Maklarin Lakim at Sabah Parks for permission to work on Pulau Sibuan, Tun Sakaran Marin Park, and Willem Renema (Naturalis Biodiversity Center, Leiden, Netherlands) for importing the specimen. Thanks to all Throughflow members, in particular Fauzie Hasibuan and the team of the Indonesian Badan Geologi, for help with fieldwork and the collection of the Miocene Tridacna shells. We are grateful to James Hainsworth and Ismael Ferrer from Media Cybernetics for providing the Image-Pro Premier 9.1 software. We further wish to thank Neil Holloway (RHUL) for thin section preparation. The comments of two anonymous reviewers and guest editor Paul Butler helped to improve this manuscript considerably and are gratefully acknowledged. This work was partly funded through the Marie Curie Actions Plan, Seventh Framework Program of the European Union (grant no. 237922) as well as RHUL Earth Sciences.

References

Aharon, P., 1983. 140,00-yr isotope climate record from raised coral reefs New Guinea. Nature 304, 720–723.

Aharon, P., 1991. Recorders of reef environment histories — stable isotopes in corals, giant clams and calcareous algae. Coral Reefs 10, 71–90.

Aharon, P., Chappell, J., 1986. Oxygen isotopes, sea-level changes and the temperature history of a coral-reef environment in New Guinea over the last 105 years. Palaeogeogr. Palaeoclimatol. Palaeoecol. 56, 337–379.

Alibert, C., McCulloch, M.T., 1997. Strontium/calcium ratios in modern Porites corals from the Great Barrier Reef as a proxy for sea surface temperature: calibration of the thermometer and monitoring of ENSO. Paleoceanography 12, 345–363.

Aubert, A., Lazareth, C.E., Cabioch, G., Boucher, H., Yamada, T., Iryu, Y., Farman, R., 2009. The tropical giant clam *Hippopus hippopus* shell, a new archive of environmental conditions as revealed by sclerochronological and $\delta^{18}O$ profiles. Coral Reefs 28, 989–998.

Batenburg, S.J., Reichart, G.J., Jilbert, T., Janse, M., Wesselingh, F.P., Renema, W., 2011. Interannual climate variability in the Miocene: high resolution trace element and stable isotope ratios in giant clams. Palaeogeogr. Palaeoclimatol. Palaeoecol. 306, 75–81.

Branson, O., Kaczmarek, K., Redfern, S.A.T., Misra, S., Langer, G., Tyliszczak, T., Bijima, J., Elderfield, H., 2015. The coordination and distribution of B in foraminiferal calcite. Earth Planet. Sci. Lett. 416, 67–72.

Carré, M., Bentaleb, I., Blamart, D., Ogle, N., Cardenas, F., Zevallos, S., Kalin, R.M., Ortlieb, L., Fontugne, M., 2005. Stable isotopes and sclerochronology of the bivalve Mesodesma donacium: potential application to Peruvian paleoceanographic reconstructions. Palaeogeogr. Palaeoclimatol. Palaeoecol. 228, 4–25.

Carré, M., Bentaleb, I., Bruguier, O., Ordinola, E., Barrett, N.T., Fontugne, M., 2006. Calcification rate influence on trace element concentrations in aragonitic bivalve shells: evidences and mechanisms. Geochim. Cosmochim. Acta 70, 4906–4920.

Dreier, A., Loh, W., Blumenberg, M., Thiel, V., Hause-Reitner, D., Hoppert, M., 2014. The isotopic biosignatures of photo- vs. thiotrophic bivalves: are they preserved in fossil shells? Geobiology 12 (5). http://dx.doi.org/10.1111/gbi.12093.

Eggins, S.M., Sadekov, A., De Deckker, P., 2004. Modulation and daily banding of Mg/Ca in *Orbulina universa* tests by symbiont photosynthesis and respiration: a complication for seawater thermometry? Earth Planet. Sci. Lett. 225, 411–419.

Elliot, M., Welsh, K., Chilcott, C., McCulloch, M., Chappell, J., Ayling, B., 2009. Profiles of trace elements and stable isotopes derived from giant long-lived *Tridacna gigas* bivalves: Potential applications in paleoclimate studies. Palaeogeogr. Palaeoclimatol. Palaeoecol. 280, 132–142.

Epplé, V.M., Brey, T., Witbaard, R., Kuhnert, H., Pätzold, J., 2006. Sclerochronological records of *Arctica islandica* from the inner German bight. The Holocene 15, 763–769.

Evans, D., Erez, J., Oron, S., Müller, W., 2015. Mg/Ca-temperature and seawater-test chemistry relationships in the shallow-dwelling large benthic foraminifera *Operculina ammonoides*. Geochim. Cosmochim. Acta 148, 325–342.

Foster, L.C., Allison, N., Finch, A.A., Andersson, C., 2009. Strontium distribution in the shell of the aragonite bivalve *Arctica islandica*. Geochem. Geophys. Geosyst. 10 (3). http://dx.doi.org/10.1029/2007GC001915.

Freitas, P., Clarke, J., Kennedy, H., Richardosn, C., Abrantes, F., 2005. Mg/Ca, Sr/Ca, and stable isotope ($\delta^{18}O$ and $\delta^{13}C$) ratio profiles from the fan mussel *Pinna nobilis*: seasonal records and temperature relationships. Geochem. Geophys. Geosyst. 6 (4). http://dx.doi.org/10.1029/2004GC00872.

Gagan, M.K., Ayliffe, L.K., Beck, J.W., Cole, J.E., Druffel, E.R.M., Dunbar, R.B., Schrag, D.P., 2000. New views of tropical paleoclimates from corals. Quat. Sci. Rev. 19, 45–64.

Gillikin, D.P., Lorrain, A., Navez, J., Taylor, J.W., André, L., Keppens, E., Baeyens, W., Dehairs, F., 2005. Strong biological controls on Sr/Ca ratios in aragonitic marine bivalve shells. Geochem. Geophys. Geosyst. 6 (5). http://dx.doi.org/10.1029/2004GC000874.

Gillikin, D.P., Dehairs, F., Lorrain, A., Steensmans, D., Baeyens, W., André, L., 2006. Barium uptake into the shells of the common mussel (*Mytilus edulis*) and the potential for estuarine paleo-chemistry reconstruction. Geochim. Cosmochim. Acta 70, 395–407.

Gillikin, D.P., Lorrain, A., Paulet, Y.M., Andre, L., Dehairs, F., 2008. Synchronous barium peaks in high-resolution profiles of calcite and aragonite marine bivalve shells. Geo-Mar. Lett. 28, 351–358.

Goodwin, D.H., Flessa, K.W., Schöne, B.R., Dettman, D.L., 2001. Cross-calibration of daily growth increments, stable isotope variation, and temperature in the Gulf of California bivalve mollusk *Chione cortezi*: implications for paleoenvironmental analysis. Palaios 16, 387–398.

Govan, H., 1992. Predators of maricultured tridacnid clams. Proceedings of the Seventh International Coral Symposium vol. 2, pp. 749–753.

Griffiths, N., Müller, W., Johnson, K.G., Aguilera, O.A., 2013. Evaluation of the effect of diagenetic cements on element/Ca ratios in aragonitic Early Miocene (~16 Ma) Caribbean corals: implications for 'deep-time' palaeo-environmental reconstructions. Palaeogeogr. Palaeoclimatol. Palaeoecol. 369, 185–200.

Hallmann, N., Burchell, M., Schöne, B.R., Irvine, G.V., Maxwell, D., 2009. High-resolution sclerochronological analysis of the bivalve mollusk *Saxidomus gigantea* from Alaska and British Columbia: techniques for revealing environmental archives and archaeological seasonality. J. Archaeol. Sci. 36, 2353–2364.

Hori, M., Sano, Y., Ishida, A., Takahata, N., Shirai, K., Watanabe, T., 2015. Middle Holocene daily light cycle reconstructed from the strontium/calcium ratios of a fossil giant clam shell. Sci. Rep. 5 http://dx.doi.org/10.1038/srep08734.

House, M.R., Farrow, G.E., 1968. Daily growth banding in the shell of the cockle, Cardium edule. Nature 219 (5161), 1384–1386.

Jochum, K.P., Weis, U., Stoll, B., Kuzmin, D., Yang, Q.C., Raczek, I., Jacob, D.E., Stracke, A., Birbaum, K., Frick, D.A., Günther, D., Enzweiler, J., 2011. Determination of reference values for NIST SRM 610-617 glasses following ISO guidelines. Geostand. Geoanal. Res. 35, 397–429.

Klein, R.T., Lohmann, K.C., Thayer, C., 1996. Sr/Ca and $^{13}C/^{12}C$ ratios in skeletal calcite of *Mytilus trossulus*: covariation with metabolic rate, salinity, and carbon isotopic composition of seawater. Geochim. Cosmochim. Acta 60, 4207–4221.

Lazareth, C.E., VanderPutten, E., André, L., Dehairs, F., 2003. High-resolution trace element profiles in shells of the mangrove bivalve *Isognomon ephippium*: a record of environmental spatio-temporal variations? Estuar. Coast. Shelf Sci. 57, 1103–1114.

Longerich, H.P., Günther, D., Jackson, S.E., 1996. Elemental fractionation in laser ablation inductively coupled plasma mass spectrometry. Fresenius J. Anal. Chem. 355, 538–542.

Lowenstam, H.A., 1981. Minerals formed by organisms. Science 211, 1126–1131.

MacDonald, J.I., Shelley, J.M.G., Crook, D.A., 2008. A method for improving the estimation of natal chemical signatures in otoliths. Trans. Am. Fish. Soc. 137, 1674–1682.

Marshall, J.F., McCulloch, M., 2002. An assessment of the Sr/Ca ratio in shallow water hermatypic corals as a proxy for sea surface temperature. Geochim. Cosmochim. Acta 66, 3263–3280.

McCulloch, M., Fallon, S., Wyndham, T., Hendy, E., Lough, J., Barnes, D., 2003. Coral record of increased sediment flux to the inner Great Barrier Reef since European settlement. Nature 421, 727–730.

Meibom, A., Mostefaoui, S., Cuif, J.-P., Dauphin, Y., Houlbreque, F., Dunbar, R., Constantz, B., 2007. Biological forcing controls the chemistry of reef-building coral skeleton. Geophys. Res. Lett. 34 http://dx.doi.org/10.1029/2006GL028657.

Mertz-Kraus, R., Brachert, T.C., Jochum, K.P., Reuter, M., Stoll, B., 2009. LA-ICP-MS analyses on coral growth increments reveal heavy winter rain in the Eastern Mediterranean at 9 Ma. Palaeogeogr. Palaeoclimatol. Palaeoecol. 273, 25–40.

Miyaji, T., Tanabe, K., Schöne, B.R., 2007. Environmental controls on daily shell growth of *Phacosoma japonicum* (Bivalvia: Veneridae) from Japan. Mar. Ecol. Prog. Ser. 336, 141–150.

Müller, W., Shelley, M., Miller, P., Broude, S., 2009. Initial performance metrics of a new custom-designed ArF excimer LA-ICPMS system coupled to a two-volume laser-ablation cell. J. Anal. At. Spectrom. 24, 209–214.

Nava, H., Carballo, J.L., 2008. Chemical and mechanical bioerosion of boring sponges from Mexican Pacific coral reefs. J. Exp. Biol. 211, 2827–2831.

Pannella, G., MacClintock, C., 1968. Biological and environmental rhythms reflected in molluscan shell growth. In: Macurda Jr., D.B. (Ed.)Paleobiological Aspects of Growth and Development: A Symposium vol. 2. Paleontological Society Memoir, pp. 64–80.

Paton, C., Hellstrom, J., Paul, B., Woodhead, J., Hergt, J., 2011. Iolite: freeware for the visualization and processing of mass spectrometric data. J. Anal. At. Spectrom. http://dx.doi.org/10.1039/c1ja10172b.

Patterson, W.P., 1999. Oldest isotopically characterized fish otoliths provide insight to Jurassic continental climate of Europe. Geology 27, 199–202.

Pätzold, J., Heinrichs, J.P., Wolschendorf, K., Wefer, G., 1991. Correlation of stable oxygen isotope temperature record with light attenuation profiles in reef-dwelling *Tridacna* shells. Coral Reefs 10, 65–69.

Purton, L.M.A., Shields, G.A., Brasier, M.D., Grime, G.W., 1999. Metabolism controls Sr/Ca ratios in fossil aragonitic mollusks. Geology 27, 1083–1086.

Ramón, M., Richardson, C.A., 1992. Age determination and shell growth of *Chamelea gallina* (Bivalvia: Veneridae) in the western Mediterranean. Mar. Ecol. Prog. Ser. 89, 15–23.

Renema, W., Warter, V., Novak, V., Young, Y., Marshall, N., Hasibuan, F., 2015. Ages of Miocene fossil localities in the Northern Kutai Basin (East Kalimantan, Indonesia). PALAIOS 30, 26–39.

Richardson, C.A., 1987. Tidal bands in the shell of the clam *Tapes philippinarum* (Adam and Reeve, 1850). Proc. R. Soc. Lond. B 230, 367–387.

Rosenberg, G.D., 1975. A comment on terminology: the increment and the series. In: Rosenberg, G.D., Runcorn, S.K. (Eds.), Growth Rhythms and the History of the Earth's Rotation. Wiley and Sons, London Edition, pp. 1–8.

Sano, Y., Shirai, K., Takahata, N., Hirata, T., Sturchio, N.C., 2005. Nano-SIMS analysis of Mg, Sr, Ba and U in natural calcium carbonate. Anal. Sci. 21, 1091–1097.

Sano, Y., Kobayashi, S., Shirai, K., Takahata, N., Matsumoto, K., Watanabe, T., Sowa, K., Iwai, K., 2012. Past daily light cycle recorded in the strontium/calcium ratios of giant clam shells. Nat. Commun. 3 http://dx.doi.org/10.1038/NCOMMS1763.

Schöne, B.R., Gillikin, D.P., 2013. Unraveling environmental histories from skeletal diaries — advances in sclerochronology. Palaeogeogr. Palaeoclimatol. Palaeoecol. 373, 1–5.

Schöne, B.R., Lega, J., Flessa, K.W., Goodwin, D.H., Dettman, D.L., 2002. Reconstructing daily temperatures from growth rates of the interdidal bivalve mollusk *Chione cortezi* (northern Gulf of California, Mexico). Palaeogeogr. Palaeoclimatol. Palaeoecol. 184, 131–146.

Schöne, B.R., Zhang, Z., Jacob, D., Gillikin, D.P., Tütken, T., Garbe-Schönberg, D., McConnaughey, T., Soldati, A., 2010. Effect of organic matrices on the determination of the trace element chemistry (Mg, Sr, Mg/Ca, Sr/Ca) of aragonitic bivalve shells (*Arctica islandica*) — comparison of ICP-OES and LA-ICP-MS data. Geochem. J. 44, 23–27.

Spero, J.H., Eggins, S.M., Russell, A.D., Vetter, L., Kilburn, M.R., Hönisch, B., 2015. Timing and mechanism for intratest Mg/Ca variability in a living planktic foraminifer. Earth Planet. Sci. Lett. 409, 32–42.

Stecher, H.A., Krantz, D.E., Lord, C.J., Luther, G.W., Bock, K.W., 1996. Profiles of strontium and barium in *Mercenaria mercenaria* and *Spisula solidissima* shells. Geochim. Cosmochim. Acta 60, 3445–3456.

Stott, K.J., Austin, W.E.N., Sayer, M.D.J., Weidman, C.R., Cage, A.G., Wilson, R.J.S., 2010. The potential of *Arctica islandica* growth records to reconstruct coastal climate in North West Scotland, UK. Quat. Sci. Rev. 29, 1602–1613.

Vanhove, D., Stassen, P., Speijer, R.P., Steurbaut, E., 2011. Assessing paleotemperature and seasonality during the Early Eocene Climatic Optimum (EECO) in the Belgian Basin by means of fish otolith stable O and C isotopes. Geol. Belg. 14 (3–4), 143–158.

Vetter, L., Kozdon, R., Mora, C.I., Eggins, S.M., Valley, J.W., Hönisch, B., Spero, H.J., 2013. Micron-scale intrashell oxygen isotope variation in cultured planktic foraminifers. Geochim. Cosmochim. Acta 107, 267–278.

Warter, V., Müller, W., Wesselingh, F.P., Todd, J.A., Renema, W., 2015. Late Miocene seasonal to sub-decadal climate variability in the Indo-West Pacific (East Kalimantan, Indonesia) preserved in giant clams. Palaios 30, 66–82. http://dx.doi.org/10.2110/palo.2013.061.

Watanabe, T., Oba, T., 1999. Daily reconstruction of water temperature from oxygen isotopic ratios of a modern *Tridacna* shell using a freezing microtome sampling technique. J. Geophys. Res. 104, 20667–20674.

Wei, G., Sun, M., Lia, X., Nie, B., 2000. Mg/Ca, Sr/Ca and U/Ca ratios of a porites coral from Sanya Bay, Hainan Island, South China Sea and their relationships to sea surface temperature. Palaeogeogr. Palaeoclimatol. Palaeoecol. 162, 59–74.

Weidel, B.C., Ushikubo, T., Carpenter, S.R., Kita, N.T., Cole, J.J., Kitchell, J.F., Pace, M.L., Valley, J.W., 2007. Diary of a bluegill (*Lepomis macrochirus*): daily $\delta^{13}C$ and $\delta^{18}O$ records in otoliths by ion microprobe. Can. J. Fish. Aquat. Sci. 64, 1641–1645.

Weiner, S., Dove, P.M., 2003. An overview of biomineralization processes and the problem of the vital effect. Rev. Mineral. Geochem. 54, 1–29.

Welsh, K., Elliot, M., Tudhope, A., Ayling, B., Chappell, J., 2011. Giant bivalves (*Tridacna gigas*) as recorders of ENSO variability. Earth Planet. Sci. Lett. 307, 266–270.

Wilson, S.A., König, A.E., Orklid, R., 2008. Development of microanalytical reference material (MACS-3) for LA-ICP-MS analysis of carbonate samples. Geochim. Cosmochim. Acta 72, A1025.

Woodhead, J., Hellstrom, J., Paton, C., Hergt, J., Greig, A., Maas, R., 2008. A guide to depth-profiling and imaging applications of LA-ICP-MS. Laser-Ablation-ICP-MS in Earth Sciences: Current Practices and Outstanding Issues. Mineralogical Association of Canada Short Course 40, Vancouver, B.C., pp. 135–145.

Yan, H., Shao, D., Wang, Y., Sun, L., 2013. Sr/Ca profile of long-lived *Tridacna gigas* bivalves from South China Sea: a new high-resolution SST proxy. Geochim. Cosmochim. Acta 112, 52–65.

Yan, H., Wang, Y., Sun, L., 2014a. High resolution oxygen isotope and grayscale records of a medieval fossil giant clam (*Tridacna gigas*) in the South China Sea: physiological and paleoclimatic implications. Acta Oceanol. Sin. 33, 18–25.

Yan, H., Sun, L., Shao, D., Wang, Y., Wei, G., 2014b. Higher sea surface temperature in the northern South China Sea during the natural warm periods of late Holocene than recent decades. Chin. Sci. Bull. http://dx.doi.org/10.1007/s11434-014-0317-3.

Yan, H., Shao, D., Wang, Y., Sun, L., 2014c. Sr/Ca differences within and among three Tridacnidae species from the South China Sea: implication for paleoclimate reconstruction. Chem. Geol. 390, 22–31.

Yan, H., Soon, W., Wang, Y., 2015. A composite sea surface temperature record of the northern South China Sea for the past 2500 years: a unique look into seasonality and seasonal climate changes during warm and cold periods. Earth Sci. Rev. 141, 122–135.

Yu, J., Foster, G.L., Elderfield, H., Broecker, W.S., Clark, E., 2010. An evaluation of benthic foraminiferal B/Ca and $\delta^{11}B$ for deep ocean carbonate ion and pH reconstructions. Earth Planet. Sci. Lett. 293, 114–120.

Please cite this article as: Warter, V., Müller, W., Daily growth and tidal rhythms in Miocene and modern giant clams revealed via ultra-high resolution LA-ICPMS analysis — A novel ..., Palaeogeogr. Palaeoclimatol. Palaeoecol. (2016), http://dx.doi.org/10.1016/j.palaeo.2016.03.019

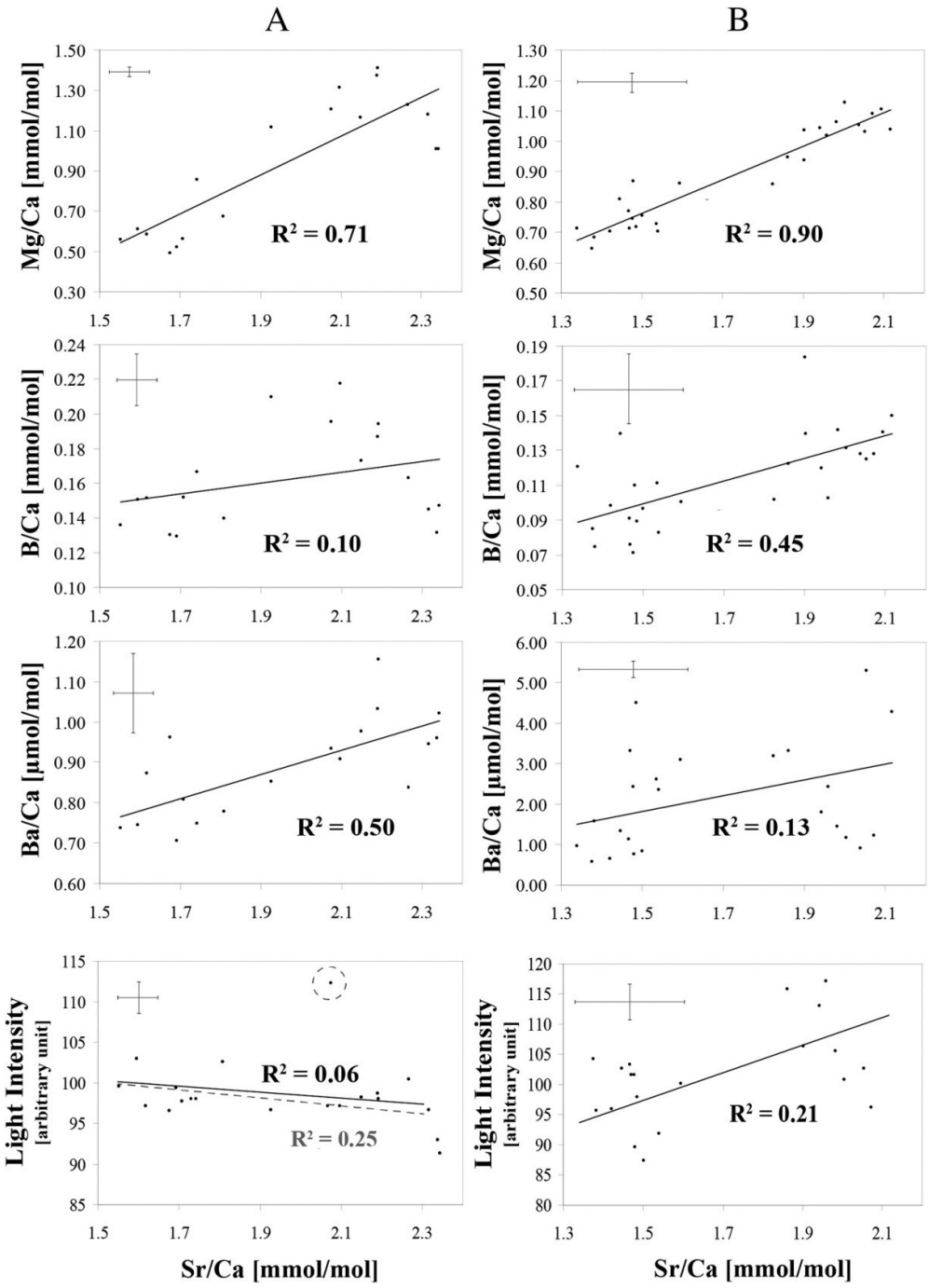

Fig. S1.

Correlations of LA-ICPMS daily peak and trough data of the Sr/Ca profiles with the corresponding values for B/Ca, Mg/Ca and Ba/Ca ratios and light intensity data from the image processing analysis. All data are presented as a mean of each five adjacent data points with the average ± 1SD illustrated by the error bar. A) Correlations for the Miocene shell LGS1. The gray dashed line represents the resulting trendline excluding the outlier marked by the dashed circle. B) Correlations for the modern shell SB1.

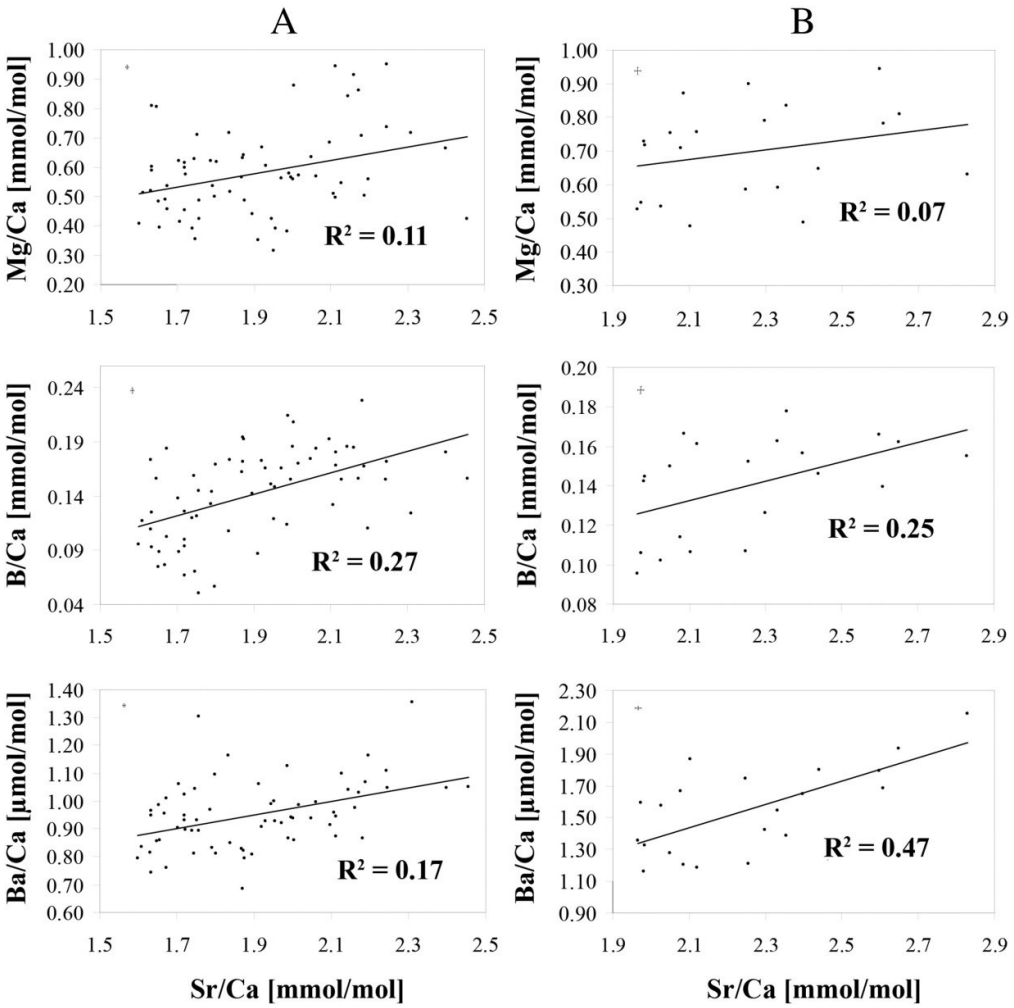

Fig. S2.

Correlations of LA-ICPMS tidal-cyclic peak and trough data of the long-term Sr/Ca profiles with the corresponding ratios for B/Ca, Mg/Ca and Ba/Ca. All data are presented as a mean of each nine adjacent data points with the average ± 2SD illustrated by the error bar. A) Correlations for the Miocene shell LGS1. B) Correlations for the Miocene shell BW4B.

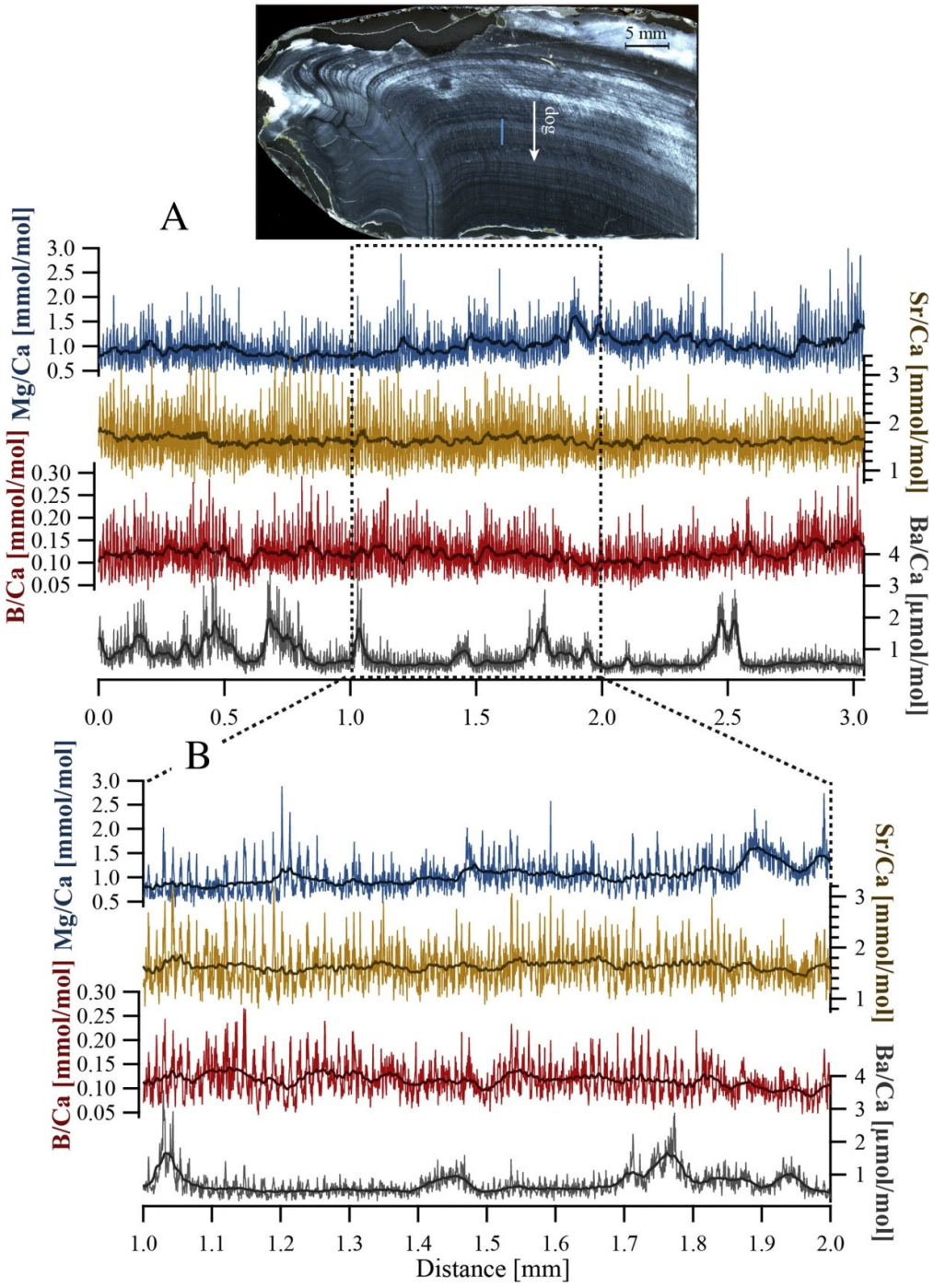

Fig. S3.

Long-term, highest resolution LA-ICPMS profiles of the modern shell SB1. A) Shell thin section with the position of the laser transect marked by the blue line and corresponding trace element profiles. Data smoothing was performed using a 50 point moving average; dog: direction of growth. B) Enlarged view on the profile marked by the dotted rectangle in A. Data smoothing was performed using a 50 point moving average.

Chapter 5: Case study 3

Citation:

Warter, V, Erez, J., and Müller, W., in preparation, **Environmental vs physiological controls on daily trace element incorporation in *Tridacna crocea* from combined laboratory culturing and ultra-high resolution LA-ICPMS analysis**: Intended for submission to Geochimica and Cosmochimica Acta.

Author contributions:

Viola Warter designed the research and interpreted the data in discussion with Jonathan Erez and Wolfgang Müller, performed the culture experiments and LA-ICPMS analyses and wrote the manuscript. Thomas Barlow (BGS) performed the solution ICPMS analysis. Wolfgang Müller edited the manuscript.

Environmental vs physiological controls on daily trace element incorporation in *Tridacna crocea* from combined laboratory culturing and ultra-high resolution LA-ICPMS analysis

Viola Warter[a]*, Jonathan Erez[b] and Wolfgang Müller[a]

[a]Department of Earth Sciences, Royal Holloway University of London, Egham, Surrey, TW20 0EX, United Kingdom

[b]Earth Science Institute, The Hebrew University of Jerusalem, Israel

[*]Corresponding author

Abstract

Laboratory culture experiments have been performed to investigate the effect of varying temperatures and light levels on organism physiology and shell geochemistry of the giant clam *Tridacna crocea* at daily time-resolution. We find that both temperature and light strongly influence shell growth rates, which range from ~3 to 20 mg/day. Besides demonstrating light enhanced calcification, we also observe growth inhibition during culture in constant darkness. Ultra-high resolution LA-ICPMS analysis (Warter and Müller, 2016) in tandem with a ^{135}Ba spiking technique enables to unequivocally identify newly secreted, cultured aragonite and to investigate its trace elemental composition (B/Ca, Mg/Ca, Sr/Ca, Ba/Ca) at (sub) daily resolution. Overall, average El/Ca ratios reveal an inverse relation with temperature and light. Strikingly, an increasing trend in all El/Ca ratios is observed in the direction of shell growth, which is interpreted as metabolically controlled, possibly related to organism 'stress'. Daily, cyclic trace element variability, best developed in Mg/Ca and B/Ca, can be clearly resolved at ~5-15 µm in relatively fast growing shells, which experienced a diurnal light cycle but *constant* temperatures. Therefore, we exclude temperature as a controlling factor responsible for daily trace element variability. We further demonstrate that high El/Ca ratios correspond to growth during night time, i.e. low light intensities. Our findings in general corroborate field observations from Sano et al. (2012) that variations in light intensity account for daily trace element variability in giant clams. We further hypothesize that *Tridacna* physiology and biochemistry is controlled by a circadian rhythm, which is initiated by the external factor light, but endogenously mediated by the giant clam and/or its photosynthetic symbionts.

5.1 Introduction

Bivalve-derived trace elemental records are increasingly investigated as a potential tool for palaeoenvironmental reconstructions (e.g. Klein et al., 1996; Purton et al., 1999; Freitas et al., 2005; Carré et al., 2006; Elliot et al., 2009; Schöne et al., 2010). Of special interest are highly time-resolved proxy records from long-lived species because they can provide detailed insight of natural environmental variability prior to the instrumental era. Bivalves can be considered as excellent (palaeo)environmental archives owing to their remarkably broad biogeographic distribution, their abundant fossil record which dates back to the early Cambrian (e.g. Dame., 2012) and their unrivalled longevity, e.g. > 500 years in the case of the ocean quahog *Arctica islandica* (Butler et al., 2013). Furthermore, due to their high shell preservation potential, bivalves are ideal recorders for 'deep-time' climate variability (e.g. Buick and Ivany, 2004; Batenburg et al., 2011, Warter et al., 2015), a clear advantage over corals, which in general are more prone to diagenetic alteration because of the high porosity of the skeleton (Ivany et al., 2004).

In contrast to coral-based climate research, where Sr/Ca, Mg/Ca and B/Ca have been shown to be promising and reliable poxies for past sea surface temperature (SST) variability (e.g. Sinclair et al., 1998, Wei et al., 2000; Marshall and McCulloch, 2001), published results on the possible controls of bivalve Sr/Ca and Mg/Ca, including giant clams, are equivocal. For example, Yan et al. (2013) presented ICPOES derived Sr/Ca profiles of modern and fossil *Tridacna gigas* shells with well-defined annual cycles, which are negatively correlated with SST, in concordance to findings from coral-based climate records (e.g. Wei et al., 2000; Marshall and McCulloch, 2001, 2002), and concluded that *Tridacna* Sr/Ca is a potential SST proxy. Elliot et al. (2009), in contrast, found that temperature, growth rate and metabolic rates have no or very little control on LA-ICPMS derived Sr/Ca ratios in the investigated modern *Tridacna gigas* shells and these results are corroborated by studies of Batenburg et al. (2011) and Warter et al. (2015), who did not report a clear link between SST and Sr/Ca in modern and fossil *Tridacna* shells. Various studies link Sr/Ca and Mg/Ca variability to organism physiology, e.g. growth rate, ontogenetic age and metabolism and not exclusively to environmental controls (e.g. Klein et al., 1996; Stecher et al., 1996; Purton et al., 1999; Freitas et al., 2005; Gillikin et al., 2005; Carré et al., 2006; Warter et al., 2015). However, due to the relationship between SST and shell growth rate (e.g. Pätzold et al., 1991; Goodwin et al., 2001; Schöne et al., 2002; Aubert et al., 2009), shell Sr/Ca and Mg/Ca may be indirectly coupled to the seawater temperature (e.g. Stecher et al., 1996; Gillikin et al., 2005). Moreover, measured element/Ca ratios can vary significantly not only between different species but also for the same species collected from the same site (e.g. Freitas et al., 2005; Gillikin et al., 2005; Yan et al., 2014), but these vary even between different parts of the very same shell, e.g. inner layer, outer layer and hinge (Elliot et al., 2009). Further

complications arise from residual organic matrices within the shell that occur both inter- and intracrystalline and which may influence the trace metal content of the shell (e.g. Foster et al., 2009; Schöne et al., 2010). This applies primarily to modern shells, which however are invariably necessary to perform proxy calibrations. Finally, the process of biomineralization in bivalve shells is still poorly understood (e.g. Lowenstam, 1981; Weiner and Dove, 2003), yet key to a detailed knowledge of the relationship between environmental factors and (bio)chemical processes and their relative influence on shell composition.

Owing to their extraordinary size of up to more than one meter (e.g. Watanabe et al., 2004; Rosewater, 1965), longevity of more than 100 years and rapid shell growth rates from several mm/year to several cm/year (Bonham, 1965, Beckvar, 1981; Aharon, 1991; Elliot et al., 2009), giant clams (family Cardiidae, subfamily Tridacninae, genus *Tridacna*) are particularly attractive sclerochronological archives for the tropical and subtropical regions of the Indo Pacific and have been extensively studied in the past ~30 years (e.g. Aharon, 1983; Aharon, 1991; Elliot et al., 2009; Batenburg et al., 2011; Welsh et al., 2011; Sano et al., 2012; Hori et al., 2015; Warter et al., 2015; Yan et al., 2015). The bivalves secrete their shells daily, recorded as microscopically visible daily growth increments in the shell structure. Thus, environmental changes - reflected as variations in the shell's geochemical inventory - are continuously recorded in chronological order and at extremely high temporal resolution.

Giant clams are mixotroph, capable of photosynthesis via their symbiosis with zoozanthellae (dinoflagellate algae*: Symbiodinium Spp.*) and – like most bivalve molluscs – capable of filter feeding (e.g. Kunzmann et al., 2008). Translocated photosynthates produced by the symbionts provide the main nutrition supply for the organisms (e.g. Klump and Lucas, 1994; Klumpp and Griffiths, 1994; Fatherree, 2006), allowing them to maintain growth even in low nutrient environments. The critical role of light for *Tridacna* shell growth has recently been demonstrated by Ip et al. (2015). Their study suggests that light exposure stimulates the zooxanthellae in *Tridacna squamosa* to produce specific signalling molecules, which in turn increase the activity of relevant transporters/enzymes that trigger light-enhanced calcification.

Recent studies have succeeded in resolving daily trace element variability within modern and fossil giant clams via nanoSIMS (Sano et al., 2012, Hori et al., 2015) and ultra-high resolution LA-ICPMS (Warter and Müller, 2016). Both Sano et al. (2012) and Hori et al. (2015) link the daily variability in Sr/Ca to changes of insolation. Warter and Müller (2016) further demonstrate striking co-variation between daily oscillating cycles in B/Ca, Mg/Ca, Sr/Ca and Ba/Ca. Both Sano et al. (2012) and Warter and Müller (2016) suggest to perform laboratory culture experiments to disentangle possible external controls on trace elemental incorporation into the biogenic carbonate structure.

This study is the first to present daily resolved trace element records from laboratory cultured giant clams. By culturing *Tridacna crocea* under different, but constant temperature (23, 25, 27, 29°C) and light regimes (diurnal light cycle, simulated shading, constant light exposure and darkness), the temperature and light effect on each proxy (B/Ca, Mg/Ca, Sr/Ca, Ba/Ca) can be assessed. To unequivocally identify shell parts grown under culture conditions, the culture solution was isotopically enriched in ^{135}Ba. Alkalinity, DO (dissolved oxygen) and pH measurements were performed to monitor shell growth rates and the photosynthetic performance of each individual organism and the associated changes in seawater chemistry.
Our primary aims are: (1) Introducing our laboratory experimental set-up, which has proven effective in culturing *Tridacna crocea* organisms over a longer period (~17 days). (2) Highlighting the effectiveness of the ^{135}Ba shell labelling in tandem with ultra-high resolution LA-ICPMS to identify shell parts secreted under culture conditions. (3) Investigating the effect of the external environmental parameters - temperature and light - on calcification rate and the trace element incorporation into the aragonite structure of giant clams.

5.2 Materials and Methods

5.2.1 Culture organism - *Tridacna crocea*

Tridacna crocea (Lamarck, 1819) is the smallest giant clam species and reaches a maximum length of 15 cm (Rosewater, 1965; Yonge, 1982). It is also called 'boring clam', owing to its ability to burrow into rock, e.g. solid limestone and coral heads (e.g. Hammer and Jones, 1976; Fatheree, 2006). *Tridacna crocea* is of particular interest to the aquarium trade because of its iridescent mantle colouration (Fig. 1E). In nature, the species predominantly inhabits shallow waters of subtidal and intertidal environments such as inner reef flats and lagoonal areas (Hammer and Jones, 1976; Hart et al., 1998, Fatheree, 2006), where they are often periodically exposed above sea level for several hours. Their geographic distribution within the Indo-Pacific realm ranges from the west coast of the Malaysian Peninsula and eastwards to Fiji, as far north as the southern islands of Japan and a southern limit in Northern Australia (Fatheree, 2006). Like all species of the *Tridacna* genus, *Tridacna crocea* are mixotroph, capable of filter feeding, but they also receive energy/food from their microalgal symbionts, zooxanthellae, which live within the soft mantle tissue and perform photosynthesis. Holt et al. (2014) discovered that iridescent cells (iridocytes), which are situated on the surface of the mantle and which directly overlie the symbionts of *Tridacna crocea*, distribute the photosynthetically productive wavelengths, namely the red and blue portions of the visible light, by lateral and forward-scattering into the tissue while eliminating via back-reflecting the non-productive wavelengths, i.e. the green and yellow portions of the visible light. This selective bi-functional wavelength scattering allows for sufficient photosynthetically relevant electromagnetic radiation to reach the

symbionts, while also preventing any photodamage of mantle tissue and symbionts. Photodamage here denotes to photoinhibition, i.e. the overall decrease of photosynthesis efficiency (e.g. Han et al., 2000), due to high irradiance levels and resulting photo-oxidative stress and damage to proteins and membranes. The study by Holt et al. (2014) further highlights the importance of light with regards to survival and growth of these highly specialised organisms.

5.2.2 *Tridacna* culture – Experimental set-up

All culture experiments were performed at the aquatic lab at the Institute of Earth Sciences, Hebrew University of Jerusalem, Israel. *Tridacna crocea* (Fig. 1) were purchased from an aquarium supplier in Tel Aviv, according to whom the specimens were derived from a Vietnamese aquaculture facility. The exact sampling location and earlier life history is, however, unknown. The organisms were transferred into the seawater aquarium at the Hebrew University Jerusalem approximately two weeks prior to the culture work and fed with phytoplankton suspension (1-2 µm, Brightwell Aquatics PhytoGreen-S) every three to four days. No food was supplied during the culture period.

For the main experiment (VW3) six organisms were chosen. Each individual was cultured separately in a 700 ml volume flow-through chamber (Fig. 1) over a period of 16.5 days. The chambers were sealed airtight via an O-ring and headspace free, to prevent air exchange between chamber seawater and the surrounding atmosphere. A peristaltic pump consisting of six individual channels was used to supply each chamber with the 'reservoir' seawater (see below for details). The chambers were magnetically stirred and placed into constant (± 0.2°C) temperature baths. Four different temperature regimes of 23°C, 25°C, 27°C and 29°C were utilized (Fig. 1B). All organisms were exposed to an approximate twelve hour diurnal light cycle, simulated using a light system consisting of two metal-halide (MH) lamps and one additional light source. The two main MH lamps were switched on from 08:00 to 19:00, while the smaller light was in use from 06:00 to 21:00 to ensure a gradual transition from day to night time and vice versa. Temperature and light intensities were measured at least once per day. Light measurements were performed at the top of the chambers, as such the actual light exposure of each organism was slightly lower, owing to its position on the base of the sample chamber. Light levels during daytime were on average 162 ± 7 µmol photons/m^2/s for the experimental chambers 1 - 3. Chamber 4 within the 29°C bath received 79 % (129 ± 7 µmol photons/m^2/s) of the light relative to chambers 1-3, owing to its position relative to the light sources. Two chambers within the 27°C regime were used to simulate shading and thus constitute the variable light experiment at constant temperature (Fig. 1C). Shading was simulated using dark net cloth, which does not change the wavelength of the receiving light.

One of the chambers received 42 % (68 ± 6 µmol photons/m^2/s) of the light, the other one 14 % (22 ± 3 µmol photons/m^2/s) relative the normal (chambers 1-3) light regime. The experimental chambers were labelled as follows: 1 = 23°C, 100% light; 2 = 25°C, 100 % light; 3 = 27 °C, 100% light; 4 = 29°C, 79% light; 5 = 27°C, 42% light; 6 = 27°C, 14% light (Fig. 1).

A separate experiment (VW4) was performed to evaluate growth under constant light exposure (no diurnal cycle) and constant darkness. Two organisms were cultured for 3.5 days at constant 27°C. The light intensity received by chamber 7 was 220 ± 4 µmol photons/m^2/s, which is ~26% higher compared to the light levels received by chambers 1-3. Complete darkness in case of chamber 8 was simulated by covering the complete sample chamber in black, light blocking foil.

At the end of the culture period, the organisms were sacrificed and the soft mantle tissue was carefully removed from the shells using a sharp scalpel and immediately stored in a freezer. All bivalve shells were immersed in dilute (8 %) NaOCl under ultrasonic agitation for several hours to remove traces of organic tissue, then thoroughly rinsed in deionised water and air-dried.

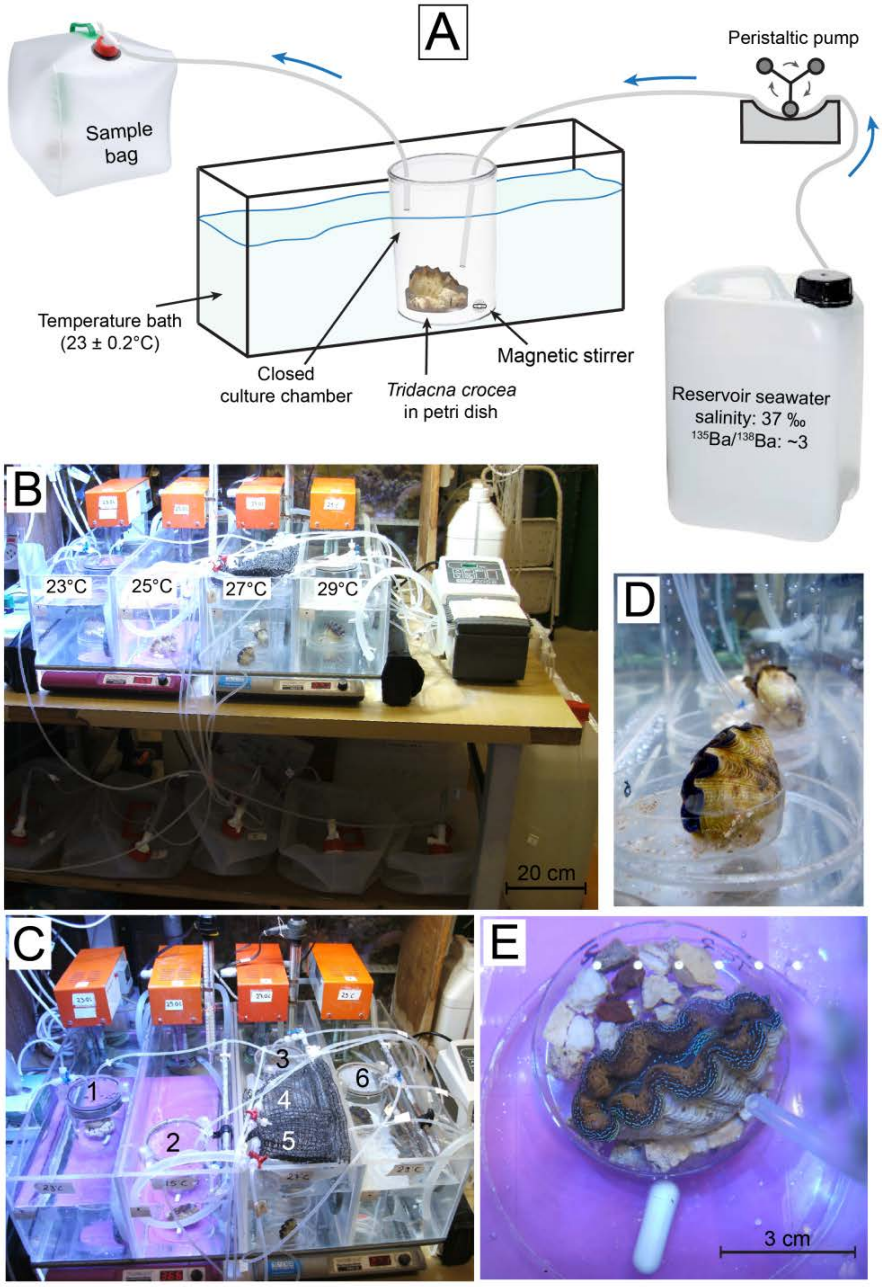

Figure 1. Experimental set-up of the *Tridacna crocea* culture experiment VW3. A) Schematic drawing of the experimental through-flow set-up showing a temperature bath with closed culture chamber connected via a peristaltic pump to the seawater reservoir and sample bag. The blue arrows indicate the direction of water flow. B) Front photograph of the culturing set-up at the aquatic lab of the Hebrew University Jerusalem. Four different culture temperature regimes are created using four different culture baths. C) Photograph from top showing one sample chamber each within the temperature baths set to 23°C, 25°C, 29°C and 3 chambers within the 27°C temperature bath. Chambers 4 and 5 were chosen to simulate shading using a net cloth. D) View from side onto the *Tridacna crocea* culture organisms. E) View from top onto a *Tridacna crocea* with exposed mantle tissue.

5.2.3 Seawater reservoir and sampling strategy

Seawater collected from the Gulf of Eilat (Gulf of Aqaba) was used as culture solution. Its natural salinity of 40.65 ‰ was adjusted to 37.0 ‰ using deionised water. To clearly identify shell parts grown during culture, the culture reservoir seawater was 'spiked' with ^{135}Ba - enriched $BaCl_2$ (Oak Ridge National Laboratories (ORNL), 93.38 % ^{135}Ba). Given the low Ba concentration in bivalve aragonite (ppb - ppm), we deliberately achieved a $^{135}Ba/^{138}Ba$ ratio that deviates considerably from the natural ratio (~0.092), to facilitate detection via ultra-high resolution LA-ICPMS. The resulting $^{135}Ba/^{138}Ba$ ratio of the culture solution is about 30-fold higher compared to the natural ratio (see 3.2).

Each chamber or organism received the same reservoir seawater. Water flow was set for ~260 ml/hour. Seawater flowing out from the culture chambers was collected in individual airtight sealed sample bags (Fig. 1). The collecting period was 24 hours to measure the alkalinity change for a 24 hours culturing period, or was optionally sampled separately in the morning and in the evening, to receive day and night seawater data, respectively. After each sampling period, the dissolved oxygen (DO in mg/L), alkalinity and pH of each of sample bag was measured. Water samples were stored in airtight sealed 30 ml plastic syringes. After sub-sampling, all seawater samples were mixed thoroughly to create a new 'recycled' seawater reservoir, aerated for ca. 15 minutes to increase the oxygen saturation, and then fed to the chambers for the following 24 hour period. The sampling strategy for the short-term experiment VW4 was identical to VW3. However, a newly prepared batch of seawater solution was used and no aeration was performed after 24 hours.

5.2.4 Alkalinity measurements

To estimate shell growth over time, we measured and compared the alkalinities of the reservoir seawater for each 24 hour culture period as well as the seawater obtained from sample bags 1 – 8. Alkalinity measurements were performed by titration with 0.025 mol/L HCl using an automated Metrohm/Brinkmann 716 DMS Titrino, at the Hebrew University of Jerusalem. The reported data are averages of duplicate/triplicate measurements by Gran titration. Triplicates were measured if the difference between duplicates was greater than 1.2 µeq/kg. Mean analytical accuracy (%), assessed through analysis of the certified reference material Batch 138 (sterilised natural seawater) provided by the Scripps Institution of Oceanography (University of California, San Diego), was 0.097. The reproducibility, assessed over a period of two weeks (n = 130) and expressed as 2 SD, was 2.4 µeq/kg.

5.2.5 Analysis of the seawater reservoirs for VW3 and VW4 via solution ICPMS

Solution analysis of the reservoir seawater samples was carried out using an Agilent 7500cx ICPMS at the Inorganic Geochemistry Facility of the British Geological Survey (BGS Keyworth, UK) to determine element concentrations and the barium isotopic composition. All samples were diluted 30-fold to bring Na in solution to approximately 333 ppm. The reported $^{135}Ba/^{138}Ba$ ratios are mass bias corrected, based on the difference between the measured and true (natural) $^{135}Ba/^{138}Ba$ ratio in SRM 1640a, using the preferred isotope abundances in de Laeter et al. (2003). Average internal precision (%) based on in total six analyses per sample (n = 18) expressed as 2 relative SE [%] was 4.68, 0.90, 1.24, 1.84 and 3.43 for B, Mg, Ca, Sr and Ba, respectively.

A synthetic, in-house seawater quality control standard (BGS seawater QC) was prepared to match the concentrations (analysed at 30-fold dilution) of the major elements Na, Mg, Ca, S, Sr and K in the samples. The certified reference materials (CRM) NASS-4 (seawater standard), SLRS-2 (riverine water standard) and SRM 1640a (fresh water standard) were analysed for evaluation of accuracy and reproducibility. Triplicate analyses were performed in the case of NASS-4 and duplicates were measured in the case of SLRS-2 and SRM 1640a, respectively. NASS-4 was diluted in the same way as the seawater samples (30-fold); SLRS-2 and SRM 1640a were not diluted and analysed neat. The seawater standard NASS-4 has become obsolete today, and because the seawater was bottled decades ago, this standard cannot be considered as 'fresh'. Therefore, measured values are used for evaluation of reproducibility only. Mean analytical accuracy (for SLRS-2 and SRM 1640a) and corresponding external precision (for SLRS-2, SRM 1640a and NASS-4) was 4.39 ± 5.85, -1.69 ± 1.48, -7.45 ± 1.81, -0.58 ± 1.5 and -2.28 ± 4.12 for B, Mg, Ca, Sr and Ba (accuracy [%] ± 1 RSD [%]).

5.2.6 Sample preparation for LA-ICPMS analysis

The left valve of each bivalve was cross-sectioned along the maximum growth axis, from the umbo to the ventral margin, using an IsoMet 5000 water-cooled precision saw by Buehler equipped with a 0.6 mm thick diamond blade. Thin sections (~50 µm) without cover were prepared and used for both microscopic examination of the growth pattern and ultra-high resolution LA-ICPMS analysis (Fig. 2A). High resolution transmitted light images of the thin sections were acquired with a Nikon Mikrophot-FX microscope equipped with a Nikon digital camera head (DS-5M) combined with a Nikon digital site controller (DS-L1) at RHUL at 100 - 200 x magnification (Fig. 2B, D). Digital images of the complete shell thin sections (Fig. 2A) were created using an EPSON Perfection V500 Photo flatbed scanner in reflective mode at 4200 dpi.

5.2.7 Ultra-high resolution LA-ICPMS analysis

Ultra-high resolution laser-ablation inductively-coupled-plasma mass spectrometry (LA-ICPMS) was performed using a 193 nm ArF excimer laser ablation system (RESOlution M-50, formerly Resonetics, now ASI, Canberra, Australia) featuring a two-volume laser ablation cell (Laurin Technic, Australia), connected to an Agilent 7500ce quadrupole ICPMS (Müller et al., 2009). To resolve daily compositional variability in the presented giant clams we apply the methodological approach for ultra-high resolution LA-ICPMS analysis presented by Warter and Müller (2016), with the following modifications: x 35 demagnification; 3 x 50 µm resultant rectangular laser spot on target; 1.0 µm/s ablation speed (Table 1). LA-ICPMS analysis was performed on thin sections under transmitted light illumination, but to further improve daily growth increment identification, high-resolution microscope images of the shell areas of interest were imported into the Resonetics Geostar software as image overlays and X-Y coordinated (Fig. 2C, D). Laser ablation was performed against the direction of growth (Fig. 2B).

The total ICPMS sweep time was kept short (≤350 ms) by analysing only six elements (m/z: ^{11}B, ^{24}Mg, ^{43}Ca, ^{88}Sr, ^{135}Ba,^{138}Ba) with dwell times ranging between 30 - 90 ms (Table 1). Combining the slow scan speed of 1 µm/s with a short total sweep time of 350 ms means that each data point advances by 0.35 µm as a running average of 3 µm spatial resolution.

Instrument tuning on the standard reference material NIST SRM 612 (Jochum et al., 2011) was performed to ensure optimal sensitivity (maximum signal to background ratio), while minimizing oxide formation (^{248}ThO/^{232}Th <0.5%) and doubly charged ion production (Ca^{2+}/Ca^{+} <0.5%) and to yield near-equal response for thorium and uranium (^{232}Th/^{238}U >95%); the LA-ICPMS operating conditions are given in Table 1.

Data reduction broadly followed Longerich et al. (1996) and was performed using Iolite. 2.4 (Paton et al., 2011) run under Igor Pro (WaveMetrics, Inc.). The isotope ^{43}Ca was used for internal standardization, NIST SRM 610 and SRM 612 (Jochum et al., 2011) were used as external (calibration) standards. Owing to the modified Ba-isotopic composition, Ba data reduction was performed using a custom-made EXCEL spreadsheet, where the effective ^{138}Ba abundance is based on the measured ^{135}Ba/^{138}Ba ratio. Because of both limited precision of Ba isotope ratios and the large observed differences, only linear mass bias correction was conducted, which is based on the difference between measured and true ^{135}Ba/^{138}Ba ratios in NIST SRM612, using the preferred isotope abundances in de Laeter et al. (2003).

The MPI-DING glasses GOR132-G, GOR128-G and KL2-G (GEOREM preferred values: http://georem.mpch-mainz.gwdg.de) were analysed as secondary standards alongside each sample for accuracy and precision evaluation. In total, twelve standard analyses were performed over a period of three days; each transect consisted of on average 110 individual data points, equivalent to an ablation distance of 0.11 mm. Best accuracies were obtained when calibrating

B, Sr and Ba against NIST SRM 612 and Mg against NIST SRM 610. Mean analytical accuracy and corresponding external precision (accuracy [%] ± 1 RSD [%]) for all three MPI-DING glasses was -18.25 ± 8.93, -3.03 ± 2.18, 0.59 ± 1.79, -5.90 ± 6.66 for B, Mg, Sr and Ba, respectively. The typical mean internal precision for one standard analysis of the MPI-DING glasses GOR132-G, GOR128-G and KL2-G, expressed as 2 relative SE [%] was 3.88, 2.12, 2.37 and 1.77 for B, Mg, Sr and Ba, respectively. It is not possible to assess the precision/reproducibility by repeat analysis of the *Tridacna* shells owing to their compositional heterogeneity on the sub-µm scale.

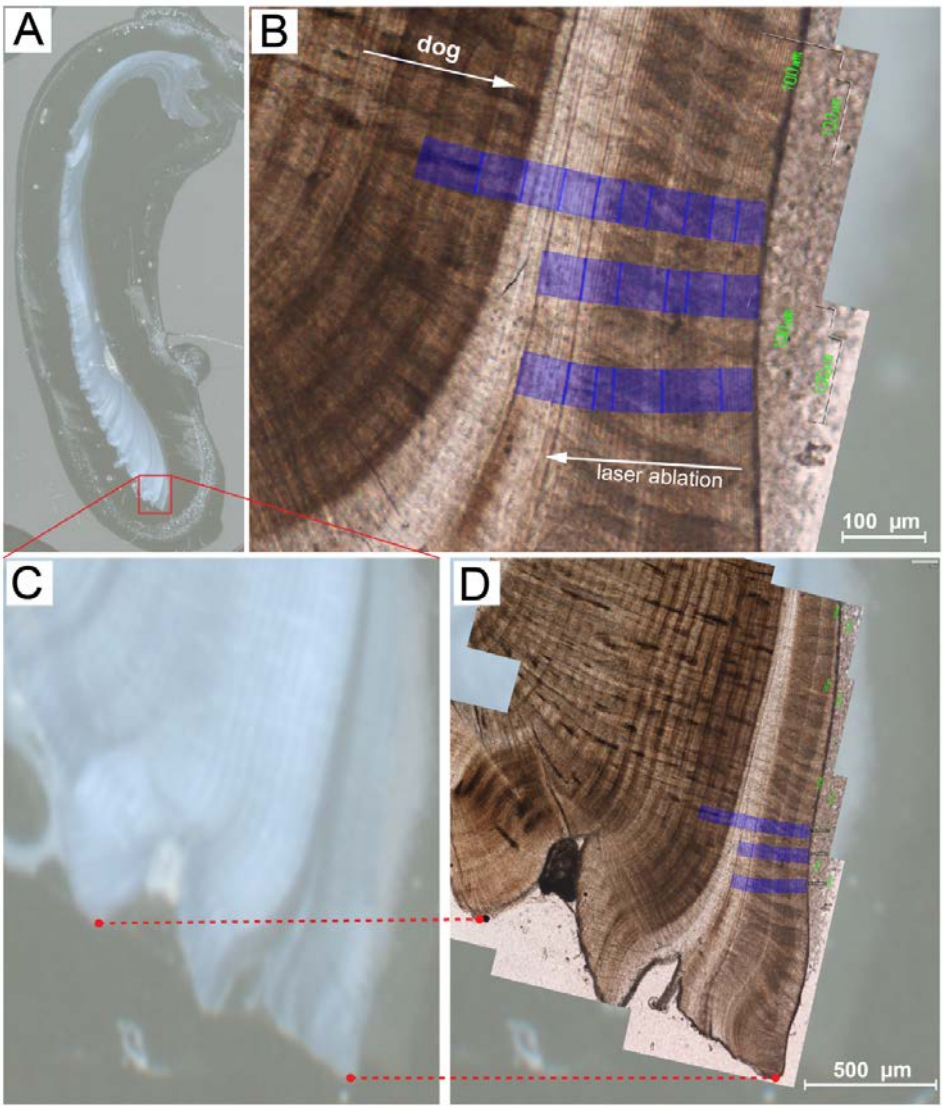

Figure 2. High resolution digital and microscope images of the outer layer shell of sample 6. A) Scanned image of the complete shell thin section. B) Zoom onto 3 parallel laser ablation tracks, marked in blue). C) Close-up image of the shell section highlighted by the red rectangle in A. D) Microscope image, which overlies the scanned image illustrated in C. The dotted red lines connect distinct shell features, which are used as 'anchor points' for the X-Y image coordination in Resonetics Geostar.

Table 1. LA-ICPMS operating conditions.

ICPMS	**Agilent 7500ce**
RF Power	1120 - 1220 W (optimized daily)
Sampling depth	4.5 mm
Carrier gas flow (Ar)	0.61 - 0.68 l/min
Sampler, skimmer cones	Ni
Extraction lenses	ce
Tuning Parameters	$^{232}Th/^{238}U$ ~90 % ; $^{248}ThO/^{232}Th$ ~0.25 %
Monitored masses (m/z)	11, 23, 24, 31, 43, 57, 66, 88, 89,135, 138
Total sweep time	~350 ms
Individual dwell times (ms)	^{11}B: 75; ^{24}Mg: 35; ^{43}Ca: 35; ^{88}Sr: 30; ^{135}Ba: 90; ^{138}Ba: 80
Laser Ablation System	**RESOlution M-50 (prototype)**
He gas flow	850 ml/min
H_2 gas flow	8.5 ml/min
Laser repetition rate	15 Hz (same for preablation)
Laser spot size	2.9 x 50 µm
Scan speed (X-Y stage)	1.0 µm/s (preablation: 2 mm/min)
Transport tubing	Nylon-6
Fluence (energy density)	5 - 5.5 J/cm^2

5.3 Results

All results of the carbonate chemistry of the seawater reservoirs and samples, and LA-ICPMS trace element analyses are displayed in Figures 3 to 9 and summarized in Tables 2 and 3.

5.3.1 Reservoir seawater alkalinity and calcification rates

In the case of both culture experiments, VW3 and VW4, the reservoir seawater 'recycling strategy' (see 5.2.3 for details) resulted in a gradual, linear depletion of the measured reservoir seawater alkalinities with time (Fig. 3). The total alkalinity depletion of the culture solution over a period of ~17 days in the case of experiment VW3 was 0.339 meq/kg. The alkalinity depletion after 3 days of culture of the experiment VW4 was 0.057 meq/kg.

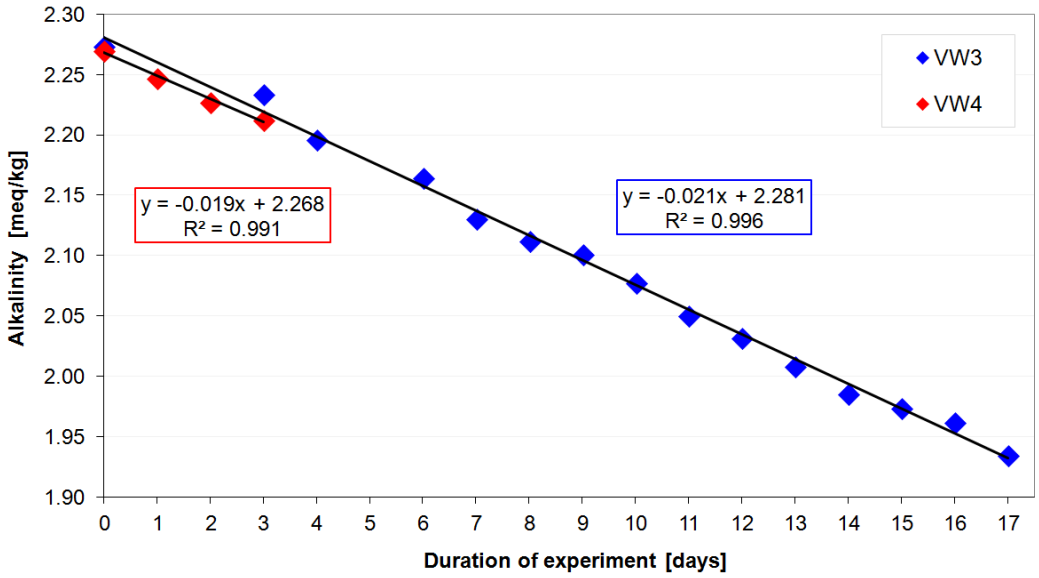

Figure 3. Alkalinity reduction of the reservoir seawater through time for the experiments VW3 and VW4. The linear trendlines indicate a very high correlation ($R^2 \sim 1$) for both data sets. Data points are larger than the analytical uncertainty (2 SD) of 2.4 µeq/kg.

Regular alkalinity measurements of samples 1-6 (here referred to the individual seawater samples) were performed for experiment VW3. Alkalinity measurements were performed each day for samples 7 and 8 in the case of the short-term experiment VW4. Delta alkalinities for a 24 hour period were calculated by subtracting the sample alkalinities from the respective alkalinity of the reservoir seawater, which was provided to each *Tridacna crocea* during the 24 hour period. Knowing the delta alkalinity and the daily seawater throughflow volume allows estimating the calcification rate per day for each organism. Figure 4A presents the cumulative calcification rates (µg/day) as normalised to the total shell weight of the organisms 1, 2, 3 and 4, cultured at 23, 25, 27 and 29°C, respectively. It should be considered that organisms 1-3 received 100 % light intensity, but organism 4, due to its relative position to the light source,

received only 79 % of the light intensity. Fig 4B shows the cumulative calcification rates for the organism 3, 5 and 6, all cultured at constant 27°C, but with variable day-time light intensities of 100, 42 and 14 %, respectively. All organisms calcified throughout the culture period and both temperature and light level influence the growth rate distinctively. The temperature experiment (Fig. 4A) reveals that highest growth rates can be observed for the *Tridacna crocea* cultured at 29°C, while the organism cultured at 23°C shows the lowest growth rates, with the 27°C and 25°C temperature experiments lying in between. The shading experiment (Fig. 4B) reveals that the highest growth rates can be observed for the organism cultured at 100 % and the lowest for the organism which received 14 % light intensity only. Surprisingly, the organism cultured at a light intensity of 42 % shows similar calcification rates to the organism cultured at 100 % light intensity. The average weight increases (%) shown throughout the entire culture period confirm a strong positive relation between temperature and growth rate on the one hand and light intensity and growth rate on the other hand (Fig. 4C, D).

Figure 5 illustrates the cumulative calcification rate curves of the organisms 7 and 8, cultured under the constant light and constant darkness regimes at 27°C. Whereas organism 7, cultured in constant light exposure, displays a highly linear calcification rate, organism 8, cultured in constant darkness, did not calcify noticeably; the overall negative slope of the linear indicates aragonite dissolution. The comparison of daily shell weight increases between sample 3 (27°C, diurnal light cycle) and sample 7 (27°C, constant light) reveals that the organism which was exposed to a 'natural' diurnal light cycle, calcified almost twice as much, namely 0.110 % versus 0.063 %, than the organism that was exposed to constant light (Table 2). It must be stressed that organism 7 (27°C, constant light regime) received ~36 % higher light intensities, namely 220 ± 4 µmol photons/m^2/s, compared to organism 1-3 (27°C, diurnal light cycle regime).

Sample 6 (27°C; 14 % light intensity) is characterized by a four-fold lower calcification rate compared to sample 3, and strikingly, approaches that of organism 1, cultured at 4°C lower temperatures.

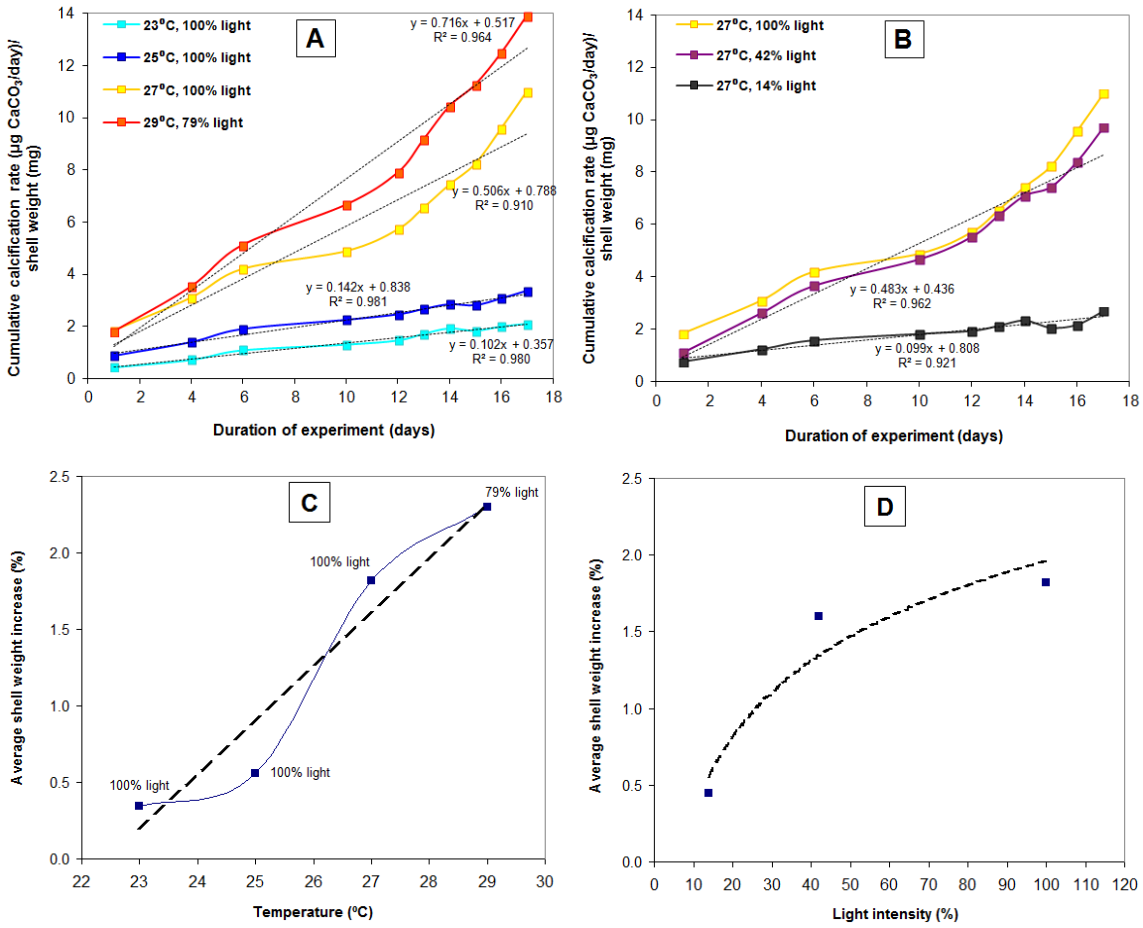

Figure 4. Effect of culture temperature and light intensity on shell growth rates for experiment VW3. A, B) Cumulative calcification rates for A) variable temperature regimes; diurnal light cycle and B) variable light intensities (simulated shading); diurnal light cycle. C, D) Estimated shell weight increase as a function of C) temperature and D) light intensity.

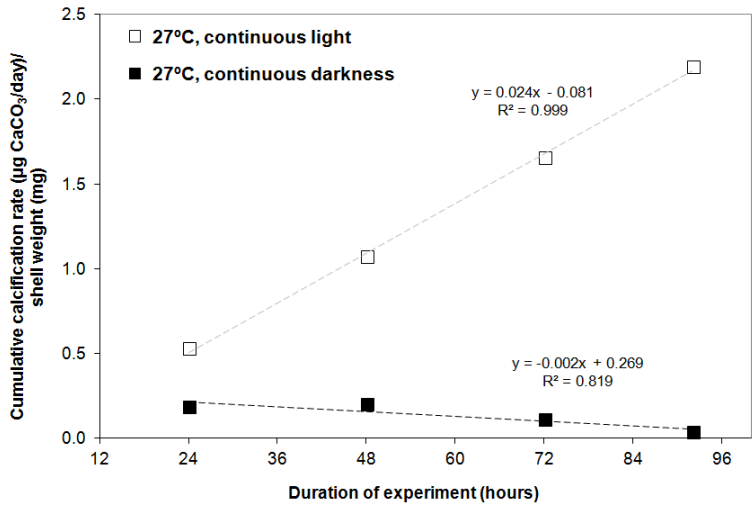

Figure 5. Cumulative calcification rates of *Tridacna* cultures both under constant light (open squares) and co constant darkness (closed squares). The negative slope of the constant darkness regime indicates carbonate dissolution.

Table 2. Calcification rate estimates from the carbonate chemistry of the seawater samples for both experiments VW3 (samples 1 – 6) and VW4 (samples 7 and 8). Light intensity data are given in µmol photons/m^2/s.

Sample number	Culture duration [days]	Light cycle	Culture conditions T [°C] ; Light intensity	Total calcification [mg CaCO3]	Total shell weight increase [%]	Calficication rate/day [mg CaCO3/day]	Shell weight increase/day [%]
1	16.5	diurnal	23 ± 0.2 ; 160 ± 5	43.725	0.344	2.650	0.021
2	16.5	diurnal	25 ± 0.2 ; 166 ± 9	65.579	0.556	3.974	0.034
3	16.5	diurnal	27 ± 0.2 ; 161 ± 6	221.896	1.817	13.448	0.110
4	16.5	diurnal	29 ± 0.2 ; 129 ± 7	324.199	2.301	19.648	0.139
5	16.5	diurnal	27 ± 0.2 ; 68 ± 6	185.668	1.601	11.253	0.097
6	16.5	diurnal	27 ± 0.2 ; 22 ± 3	48.674	0.445	2.950	0.027
7	3.5	constant	27 ± 0.2 ; 220 ± 4	48.884	0.219	13.967	0.063
8	3.5	constant	27 ± 0.2 ; 0	0.755	0.004	0.216	0.001

5.3.2 Ultra-high resolution LA-ICPMS

^{135}Ba shell labelling to identify growth under culture conditions

The seawater reservoir solutions for both experiments, VW3 and VW4, were isotopically enriched in ^{135}Ba to label shell parts grown during the culture period. The barium isotope composition of the both starting reservoir seawater solutions of experiment VW3 and VW4 was 2.820 ± 0.081 (2SD) and 3.012 ± 0.092 (2SD), respectively. The LA-ICPMS-derived ^{135}Ba/^{138}Ba ratios of the outer layer shell portions of the cultured *Tridacna* shells 1-7 are 2.998 ± 0.201 (2SD) (Table 2), which matches the barium isotopic composition of both starting reservoir seawater solutions. The ^{135}Ba/^{138}Ba ratio of shell 8, characterized by only ~2 µm shell growth under culture in constant darkness, is 1.081 ± 0.065 (2SE) (Table 3).

Table 3. LA-ICPMS-derived ^{135}Ba/^{138}Ba ratios and average El/Ca obtained from the cultured shells 1 – 8. Light intensities were measured in µmol photons/m^2/s.

Sample number	Culture conditions T [°C] ; Light intensity	n		^{135}Ba/^{138}Ba	B/Ca [mmol/mol	Mg/Ca [mmol/mol	Sr/Ca [mmol/mol	Ba/Ca [µmol/mol
1	23 ± 0.2 ; 160 ± 5	**48**	**average**	**3.029**	**0.163**	**0.625**	**2.266**	**2.014**
			2 SE	0.232	0.016	0.043	0.157	0.163
2	25 ± 0.2 ; 166 ± 9	**111**	**average**	**2.976**	**0.167**	**0.243**	**1.883**	**1.371**
			2 SE	0.208	0.005	0.011	0.043	0.085
3	27 ± 0.2 ; 161 ± 6	**250**	**average**	**3.069**	**0.121**	**0.229**	**1.536**	**1.085**
			2 SE	0.160	0.003	0.007	0.029	0.046
4	29 ± 0.2 ; 129 ± 7	**550**	**average**	**2.894**	**0.201**	**0.453**	**1.724**	**1.427**
			2 SE	0.099	0.004	0.016	0.033	0.040
5	27 ± 0.2 ; 68 ± 6	**244**	**average**	**3.059**	**0.230**	**0.445**	**1.589**	**1.469**
			2 SE	0.332	0.007	0.025	0.045	0.071
6	27 ± 0.2 ; 22 ± 3	**172**	**average**	**3.118**	**0.227**	**1.233**	**1.953**	**1.547**
			2 SE	0.228	0.009	0.060	0.092	0.091
7	27 ± 0.2 ; 220 ± 4	**44**	**average**	**2.839**	**0.154**	**0.387**	**1.756**	**1.474**
			2 SE	0.456	0.019	0.048	0.115	0.181
8	27 ± 0.2 ; 0	**6**	**average**	**1.081**	**0.221**	**0.485**	**2.922**	**3.339**
			2 SE	0.130	0.054	0.069	0.196	1.149

Figure 6 presents LA-ICPMS-derived $^{135}Ba/^{138}Ba$ profiles of both shell domains grown during the culture period and the adjacent shell parts secreted before the culturing period. Shell parts secreted during the culturing period can easily be distinguished via their distinctive, ~30-fold higher $^{135}Ba/^{138}Ba$ signature, whereas pre-culture shell domains reflect the natural $^{135}Ba/^{138}Ba$ ratio of ~0.092 (de Laeter et al., 2003). The transition from naturally low to artificially high (spiked) $^{135}Ba/^{138}Ba$ is not sudden, a gradual rise over a shell distance of several µms (varies depending on shell growth rates) can be observed (Fig. 6). The comparison of the Ba isotope ratio profiles of shells 1, 3 and 4 (cultured at 23, 27 and 29°C) reveals that higher culture temperatures - characterized by higher shell growth rates - result in relatively longer 'culturing domains' ranging from ~18 µm at 23°C to ~220 µm at 29°C. The abrupt drop in the $^{135}Ba/^{138}Ba$ ratio in case of shell 3 at a distance of 45 – 50 µm is related to a 15 hour culture interruption during dawn and night of day eight of the experiment, when it was transferred back to the coral reef aquarium, where it continued to grow in seawater characterized by a natural barium isotopic composition. The lowest measured $^{135}Ba/^{138}Ba$ ratio of 0.323 however, does not reach the natural ratio of 0.092 (see below for discussion).

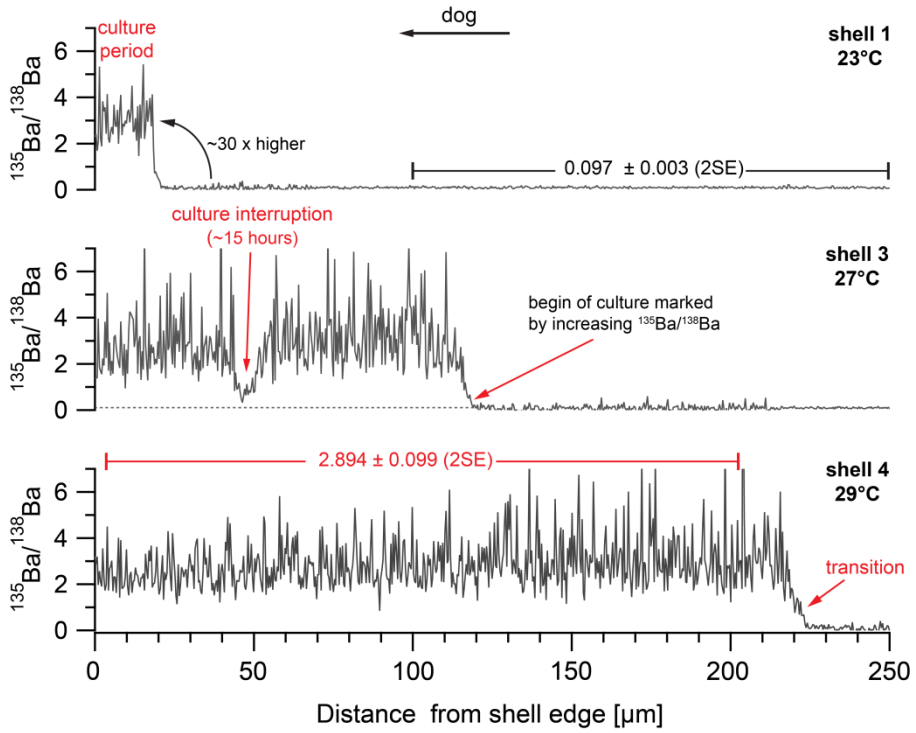

Figure 6. LA-ICPMS derived $^{135}Ba/^{138}Ba$ records of shells 1, 3 and 4. The transition from shell parts with a naturally low $^{135}Ba/^{138}Ba$, secreted before the culture experiment, to shell parts with high $^{135}Ba/^{138}Ba$ signature, is distinct, but gradual, and marks the start of the *Tridacna* culture (indicated by red diagonal arrows). Dog: direction of growth.

Average El/Ca ratios

The presented average El/Ca data for B/Ca, Mg/Ca, Sr/Ca and Ba/Ca for the culture period are illustrated in Fig. 7 and summarized in Table 3. These data are obtained from cultured outer layer shell domains, which exclude the transition period (Fig. 6) and shell parts characterized by peak Mg/Ca ratios (see below). Because temperature and light intensity are related to the shell growth rate, shells secreted in low temperature- and light regimes are on average characterized by a higher 2 SE owing to the on average shorter growth segments (Table 3). In the case of shell 8 (Table 3, Fig. 7C), which has hardly grown, only 6 data points can be attributed to the culture period and these data need to be treated with caution.

Fig. 7A illustrates the averaged El/Ca ratios (B/Ca, Mg/Ca, Sr/Ca and Ba/Ca) obtained from shell parts grown at 23, 25, 27 and 29°C. A decreasing trend with temperature for Mg/Ca, Sr/Ca and Ba/Ca exists for the temperature regimes of 23, 25 and 27°C, with highest El/Ca ratios found for the shell cultured at 23 °C and lowest El/Ca ratios found for the shell cultured at 27°C. The respective averaged El/Ca ratios for the 29°C regime however do not follow this decreasing trend; all El/Ca ratios are higher than the 27°C regime, and also (apart from Sr/Ca) higher than the 25°C regime. While the organisms cultured at 23, 25 and 27°C all received similar light intensities (~162 ± 3 µmol photons/m^2/s, hereafter referred to 100 % light intensity), the *Tridacna* which was cultured at 29°C only received 129 ± 7 µmol photons/m^2/s (79 % light intensity). If corrected for the lower light intensity, all data points for the 29°C regime, may lie as indicated. Fig. 7B presents the El/Ca ratios plotted as a function of light intensity; all shells were cultured at 27°C. A decreasing El/Ca trend with light intensity can be observed for Mg/Ca, Sr/Ca and Ba/Ca, with highest El/Ca ratios found for the shell cultured with lowest light intensity of 22 ± 3 µmol photons/m^2/sec (14 % light intensity) and lowest El/Ca ratios found for the shell cultured at the highest light intensity of 161 ± 6 µmol photons/m^2/sec (100 % light intensity). The light-induced trend in the trace element ratios, especially for Mg/Ca, is even more pronounced than the temperature effect. A clear trend in B/Ca between the different light and temperature regimes is not obvious.

Fig. 7C illustrates the results of the trace element chemistry of shells 7 and 8, both cultured at 27°C under either constant light exposure or constant darkness. The observation that all El/Ca ratios are higher in shell 8 (cultured in complete darkness) compared to the constant light regime (220 ± 4 µmol photons/m^2/sec), confirms the finding from Fig. 7B that an inverse relation exist between light intensity and trace element concentration. It should be noted that organism 7 (27°C, constant light regime) received ~36 % higher light intensities compared to organism 1-3 (27°C, diurnal light cycle regime).

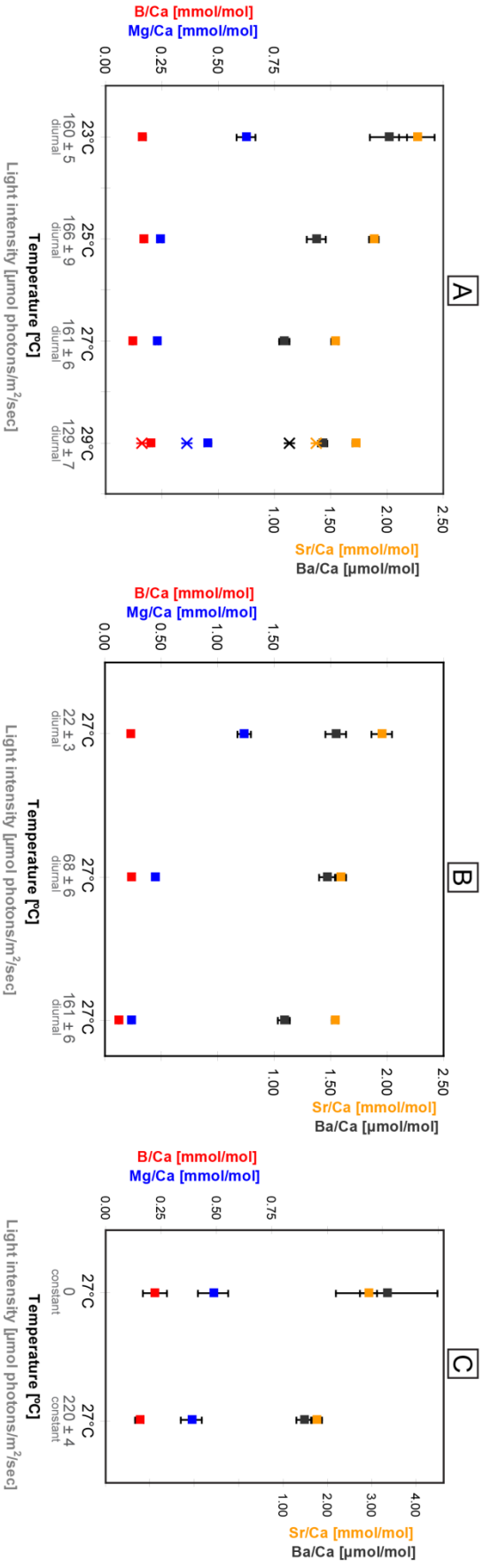

Figure 7. Average B/Ca, Mg/Ca, Sr/Ca and Ba/Ca ratios obtained from shell parts cultured in diurnal light mode at different temperatures A) and light levels B). The scale of the vertical axis for B/Ca and Mg/Ca in B) is two times larger than in A). C) Average B/Ca, Mg/Ca, Sr/Ca and Ba/Ca ratios obtained from shell parts cultured during constant light exposure and constant darkness. El/Ca ratios are shown with 2 SE errors, whereas light intensities are reported with 1 SD error. The 'cross' data points of the 29°C regime in A) represent the respective El/Ca values obtained when corrected for the lower light intensity.

Daily resolved El/Ca records

Figure 8 presents daily trace element cycles for shells 3, 4 and 5. Daily El/Ca cycles could not be resolved for shells 1, 2, 6, 7 and 8. Despite the combination of the slow scan speed (1 µm/s) and short total sweep time (< 350 ms), the spatial resolution is limited by the width of the rectangular ablation spot (3 X 50 µm) (Warter and Müller, 2016). The total thickness of the cultured shell domains for samples 1, 2 and 6 (Fig. 9) imply that daily growth increments in these shells are too thin (<4 µm) to be resolved via ultra-high resolution LA-ICPMS.

The cultured shell part of shell 4 comprises a thickness of ~220 µm and 15 daily growth cycles, with an average width of ~14.5 µm, can be identified (Fig. 8A). Daily compositional variability is best resolved for Mg/Ca and B/Ca. The latter co-vary within the first 190 µm of the profile (Fig 8A). At a distance of 190 – 235 µm, which represents shell growth immediately before and after the start of the culture experiment, the Mg/Ca profile is characterised by distinctively, up to five-fold, higher ratios. Daily Mg/Ca cycles cannot be resolved clearly within this domain. The B/Ca profile, in contrast, does not reveal such an increase in concentration and two daily cycles can be distinguished at a distance 190 – 215 µm (Fig. 8A). Although daily cyclicity is not as clearly resolved for Sr/Ca and Ba/Ca, both profiles reveal significant oscillatory variability in concordance with Mg/Ca and B/Ca.

In the case of shell 3, daily compositional variability is best resolved for Mg/Ca (Fig. 8B), however the daily cycles are less regularly developed compared to those in shell 4. Within the first ~70 µm of the Mg/Ca record, eleven daily cycles, with average widths of only ~7 µm, are clearly recognizable (Fig. 8B). The significant drop in the $^{135}Ba/^{138}Ba$ ratio at a distance of 45 - 50 µm (Fig. 8B) is related to a 15 hour culture interruption on day 8 of the experiment. The organism was transferred back to the coral reef aquarium at ~6 pm, where it continued growing until ~8 am the next morning, before being incorporated into the experiment again. The B/Ca ratio at this distance is, similarly to the $^{135}Ba/^{138}Ba$, characterized by a significant drop of ~40%. However, a clearly resolved daily cycle is identifiable for both Mg/Ca and Sr/Ca at this distance. What is more, the peak Mg/Ca and Sr/Ca (and Ba/Ca) ratios correlate with the trough in $^{135}Ba/^{138}Ba$ and B/Ca, thus allowing identification of day versus night values.

In the case of shell 5, oscillatory trace element variability is best resolved for the co-varying Sr/Ca and Ba/Ca ratios (Fig. 8C). Given that the cultured shell section comprises 125 µm and as such is ~10 µm longer compared to shell 3, the lateral (timely) resolution achieved via ultra-high resolution LA-ICPMS should allow resolving daily cyclicity at higher detail. Similarly to shell 4, the shell part secreted immediately after the start of the experiment is characterized by up to four-fold higher Mg/Ca ratios compared to the shell part secreted later in the stage of the experiment (Fig. 8C). Strikingly, a monotonous increase of Mg/Ca in direction of shell growth can be observed (Fig. 8C), with average Mg/Ca ratios rising from about 0.4 mmol/mol at a

distance of ~100 µm rising to 0.8 mmol/mol at the growing edge (0 µm). A doubling over a distance of ~100 µm can also be observed for the B/Ca profile.

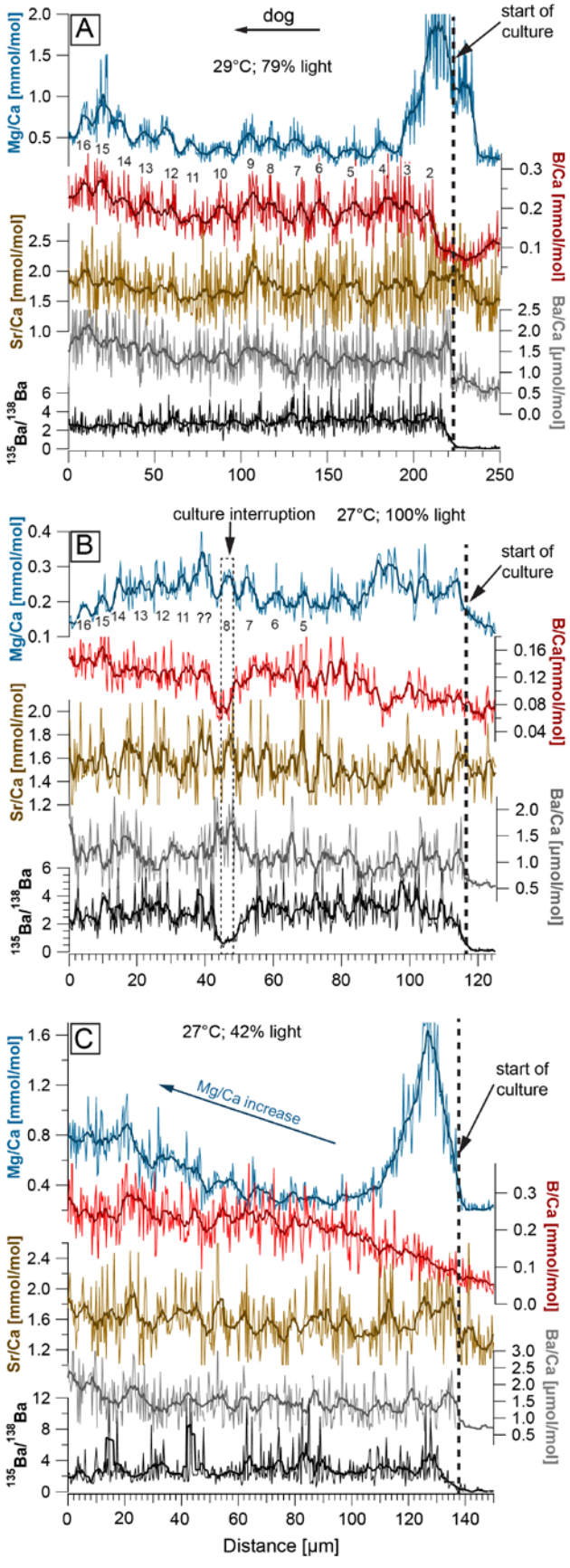

Figure 8. Daily resolved LA-ICPMS profiles for B/Ca, Sr/Ca, Mg/Ca and Ba/Ca in A) shell 4, (29°C; 79 % light intensity, B) shell 3 (27°C and 100 % light intensity) and C) shell 5 (27°C and 42 % light intensity). The dashed lines mark the begin of the culture experiment, identified via the elevated $^{135}Ba/^{138}Ba$ ratios; dog: direction of growth. The numbers within the graphs relate to the number of daily growth cycles countable from the El/Ca profiles. Data smoothing was performed using a 15 point moving average in A and a 10 point moving average in B and C, respectively.

Figure 9 shows the shorter trace element profiles of the *Tridacna* shells 1, 2 and 6. The presented El/Ca profiles are obtained from shell parts secreted under culture conditions only, but overall are too thin to be resolved with regards to daily trace elemental variability. However, some of these records reveal an increase of the trace element ratios i.e. increasing El/Ca ratios in direction of growth. Shell 1, cultured at 23°C, reveals increasing ratios for Mg/Ca and B/Ca that approximately double between early and late formed aragonite through time (Fig. 9A). In case of shell 2, cultured at 25°C, a distinctive rise in Mg/Ca can be observed, with Mg/Ca ratios almost doubling throughout the culture period (Fig. 9B). The Sr/Ca and B/Ca records of shell 2 similarly show an increasing trend with time. Finally, all El/Ca records obtained for shell 6 (cultured at 27°C and 14% light intensity) are characterized by a slight increasing trend throughout the culture period (Fig. 9C).

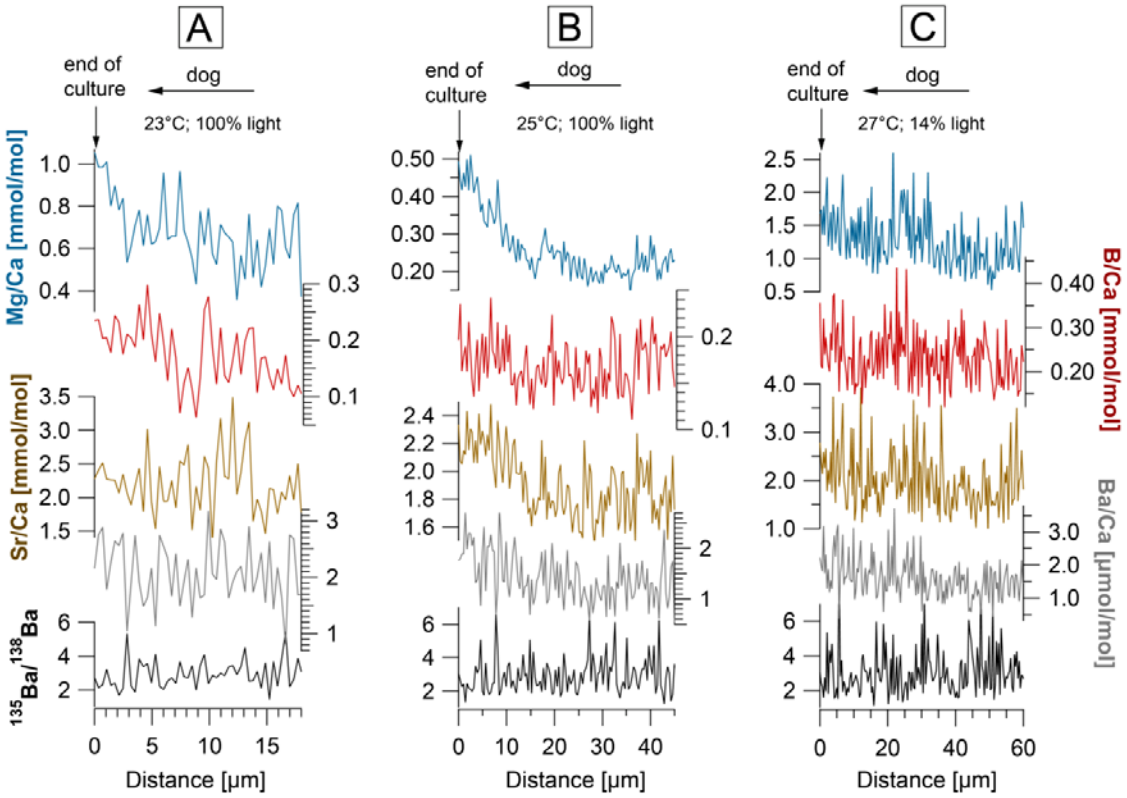

Figure 9. Mg/Ca, B/Ca, Ba/Ca, Sr/Ca and $^{135}Ba/^{138}Ba$ ratio profiles for the cultured shell sections of A) shell 1 (23°C, 100% light intensity), B) shell 2 (25°C, 100% light intensity) and C) shell 6 (27°C, 14% light intensity). Dog: direction of growth.

5.4 Discussion

5.4.1 Organism physiology - Effect of temperature and light intensity on *Tridacna* shell growth

Our results demonstrate that temperature exerts a strong control over shell growth rates of the laboratory cultured *Tridacna crocea*. The highest growth rates were observed during culture in 29°C and 27°C and lowest during the culture in 23°C and 25°C, respectively (Fig. 4 A,C). The difference in total calcification between the highest and lowest temperature regime is distinct, e.g. the *Tridacna* cultured at 29°C calcified about seven times more compared to the organism cultured in 23°C (Table 2, Fig. 6).

The effect of temperature on giant clam growth rates has been investigated in several studies. Hart et al. (1998), who studied *Tridacna crocea, Tridacna derasa* and *Tridacna maxima* at village farms in the Solomon Islands, found - consistent for all three species - increasing growth rates with rising SSTs for a temperature range of 29°C to 31°C. Lucas et al. (1989), who studied juvenile *Tridacna gigas* at Pioneer Bay, Orpheus Island, Australia, reported seasonal growth rate variability, with on average higher growth rates during the warmer summer months. Schwartzmann et al. (2011), similarly reported a positive temperature-growth correlation in *Hippopus hippopus* from New Caledonia. However, this correlation became inverse after surpassing ~27°C. According to the authors the observed growth reduction was related to protective behaviour and/or a stress reaction resulting from exposure to too high temperatures. Temperature-related physiological malfunctioning was also observed for *Tridacna crocea* and *Tridacna squamosa* at Mannai Island, Rayong province, Thailand, during the spring/summer period 2010, which was characterized by exceptionally high SSTs of up to 34°C (Junchompoo et al., 2013). The result of these extreme SSTs, which were up to 5°C higher than average SSTs for the region, was a mass bleaching event and a lethality rate of ca. 40 % (~130 study organisms). The term 'bleaching' refers to the fading or complete loss of the typical iridescent *Tridcana* mantle colour associated with either the expulsion of the symbiotic dinoflagellate algae (zooxanthellae) or the reduction and complete loss of their algal photosynthetic pigments (e.g. Iglesias-Prieto et al., 1992). In the case of corals it has been shown that elevated seawater temperatures and (ultraviolet radiation) not only inhibit the photosynthetic performance of symbiotic dinoflagellates but also ultimately cause the loss of the symbionts via expulsion (Lesser, 1990; Fujise et al., 2014) resulting in coral bleaching. The study by Buck et al. (2002) demonstrates that in combination, increased light intensity and temperature are the main causes for bleaching in giant clams.

Besides the temperature-dependency on shell growth, our results further show light enhanced calcification (LEC) as well as dark decalcification/growth inhibition (Fig. 5). All light experiments were carried out at constant 27°C. The organism cultured within the diurnal light cycle regime, at 100 % light exposure calcified about four times more compared to the shaded

organism that received only 14 % light. Surprisingly, the sample cultured at a light intensity of 42 % showed similar calcification rates to the organism culture at 100 % light intensity (Fig. 4 B, D).

Shading experiments conducted in outdoor tanks on juvenile *Tridacna gigas* (Lucas, 1989) revealed very similar results. Three different light regimes of 10, 50 and 100 % light intensity, respectively, were simulated using shade cloths. The organisms cultured within the 100 % and 50 % light regime, reached similar shell lengths throughout the entire culture period of eight months. On the contrary, the organisms reared under 10 % light exposure only, revealed distinctively, namely~40 % lower growth rates. Moreover, owing to the high mortality rate during the culture period, the experiment had to be aborted after four months. Lucas (1989) concluded that reduced light conditions inhibit shell growth and promote lethality in *T. gigas*, which according to the author demonstrates that "*T. gigas* is an obligate phototroph".

Our findings support a very strong light-dependence on *Tridacna crocea* growth rates. This is demonstrated by the results of the shading experiment as well as the outcome of the culture in complete darkness. This organism calcified very poorly and - after a culture period of 48 hours - even exhibited negative growth rates resulting from aragonite dissolution or at least growth inhibition (Fig. 5). Strikingly, culture under constant lightning also seems to inhibit the growth performance. The organism which was reared under constant light, exposed to 220 µmol photon/m^2/s, calcified only about half as much compared to the *Tridacna*, which was exposed to a natural diurnal light cycle and ~36 % lower light intensities (162 µmol photon/m^2/s). We hypothesize that the interruption of the natural diurnal light cycle negatively affected the organism and/or its symbionts, resulting in decreasing growth rates.

Light enhanced calcification (LEC) is a well known phenomenon occurring in corals (e.g. Goreau, 1959; Tentori and Allemand, 2006; Erez et al., 2011; Cohen et al., 2016), but is poorly documented for giant clams (e.g. Lucas, 1989). Equations (1) and (2), adapted form Erez et al. (2011), describe the main processes commonly associated with LEC.

(1) $Ca^{2+} + 2HCO_3 \leftrightarrow CaCO_3 + CO_2 + H_2O$ (Calcification by host organism)

↓

(2) $CO_2 + H_2O \leftrightarrow CH_2O + O_2$ (Photosynthesis by symbionts)

Owing to their photosynthetic activity, the dinoflagellate symbionts continuously remove CO_2 from the system. The resulting chemical imbalance shifts the equilibrium reaction (1) towards the side of the products, i.e. enhanced calcification. Removal of CO_2 also elevates the pH of the system, which can increase the carbonate ion concentration (CO_3^{2-}) and as such further facilitates precipitation of $CaCO_3$ in the presence of Ca^{2+} (e.g. Cohen et al., 2016). It is also

speculated that LEC in corals is triggered through e.g. the energy contribution of the symbionts (e.g. Erez et al., 2011). This shows that light enhanced calcification is closely coupled to symbiont activity in corals and the same is likely to be true for giant clams.

Ip et al. (2015) suggests that light exposure stimulates the zooxanthellae in *Tridacna squamosa* to produce specific signalling molecules, which in turn increase the activity of the relevant transporters/enzymes that trigger light-enhanced calcification. Holt et al. (2014) further demonstrate that iridescent cells, situated on the surface of the mantle, directly overlie the symbionts of *Tridacna crocea*. These iridocytes distribute photosynthetically productive wavelengths, i.e. the red and blue portions of the visible light, by lateral and forward-scattering of light into the tissue while back-reflecting non-productive wavelengths, i.e. the green and yellow portions of the visible light. This selective bi-functional wavelength scattering allows for sufficient solar energy to reach the symbionts, while also preventing any photodamage of mantle tissue and symbionts. Both studies by Ip et al. (2015) and Holt et al. (2014) highlight the importance of light with regards to survival and growth of these highly specialised organisms.

The relative importance of filter feeding/nutrient availability for *Tridacna* shell growth has been demonstrated in several studies (e.g. Klumpp et al., 1992; Klumpp and Lucas, 1994). Because no food was supplied during the culture period, our results strongly suggest that temperature and light indeed can be considered as primary controls on the observed variation in shell growth rates. However, it must be considered that we introduced a potential 'stress' component by not providing an additional food source.

5.4.2 Trace elemental controls revealed via ultra-high resolution LA-ICPMS

^{135}Ba shell labelling

The presented ^{135}Ba spiking technique (see section 5.3.2) has proven effective in unequivocally identifying aragonite that was secreted during culture condition, from those shell parts that were formed before the start of the experiments (Fig. 6). Cultured shell aragonite exhibits a ^{135}Ba/^{138}Ba ratio that is about 30 times higher compared to shell parts secreted during growth in seawater with the natural ^{135}Ba/^{138}Ba ratio of 0.092 (de Laeter et al., 2003). Isotopic labelling of biogenic carbonates has been successfully applied for the culture of e.g. corals (e.g. Gagnon et al., 2013) and foraminifera (e.g. Evans et al., 2015). The advantage of an isotopic marking of the cultured shell domain is that element concentrations are not modified and owing to the analytical sensitivity and isotope ratio capability of the LA-ICPMS, isotope abundance differences even for low concentration elements such as Ba in aragonite (a few ppm) can be resolved.

Average El/Ca ratios from cultured shell parts – Influence of temperature, light and growth rate

The results of our temperature experiments reveal an inverse relation between the averaged El/Ca values for Mg, Sr and Ba with temperature within the range of 23, 25 and 27°C (Fig 7A). An inverse relation is also observed between these El/Ca ratios with light intensity (Fig. 7B). Our constant dark/light experiment supports these findings, with on average higher Mg, Sr, Ba and B concentrations observed for the cultured shells reared in complete darkness (Fig. 7C). However, shell 7, cultured at 27°C in constant light and moreover exposed to the highest light levels, is not characterized, by the lowest El/Ca ratios, as one would expect. In fact, all its El/Ca ratios are higher compared to shell 3, cultured at 27°C and exposed to diurnal light cycle with about 36 % light exposure during the day. Equally surprisingly, shell 4, cultured at 29°C and characterized by the highest shell growth rates, does not reveal – as one would expect – the lowest El/Ca ratios. Instead, all its El/Ca ratios are higher than the 27°C regime, and even, apart from Sr/Ca, higher than the 25°C regime (Fig. 7A, Table 3). It is important to stress that organism 4 was, due to the experimental set-up, exposed to less light intensity (only ~79 %) compared to the other three organisms within the temperature experiment (Fig. 7A, Table 3). We suggest that the higher than expected El/Ca ratios found for shell 4, partly result from the lower light intensity, which independently from growth rate, affected the geochemical composition of shell. To support this hypothesises the El/Ca ratios of shell 4 have been corrected to a light intensity of 100% (Fig. 7A). The results highlight that while Sr/Ca now follows the overall trend, especially Mg/Ca is still significantly elevated compared to shell 3. This highlights that additional controls, other than external, likely influenced its trace element composition.

The processes and mechanisms which control trace element incorporation in bivalve shells remain largely unknown (Carré et al., 2006). Numerous studies suggest that trace element partitioning into the biogenic carbonate structure depends on the combined effects of biophysiological controls and environmental parameters (e.g. Takesue and van Geen, 2004; Weiner and Dove, 2003). In the case of Mg/Ca partitioning in giant clams, organism metabolism seems to be a controlling factor. An increasing trend in Mg/Ca associated with an ontogenetic growth rate reduction was reported for different *Tridacna* species (e.g. Romanek and Grossman, 1989; Elliot et al., 2009; Warter et al., 2015). Besides, physiological controls have been demonstrated to affect Mg/Ca in *Arctica islandica* (e.g. Schöne et al., 2011) and calcitic bivalves (e.g. Freitas et al., 2005, 2006).

Sr incorporation into aragonite bivalve shells is strongly influenced by shell growth rates (e.g. Carré et al., 2006, Lorrain et al, 2005, Gillikin et al., 2005; Klein et al., 1996 and Stecher et al., 1996). Carré et al. (2006) demonstrated a positive correlation between growth rate and Sr/Ca ratios of *Mesodesma donacium* and *Chione subrugosa* from the Peruvian Coast. Lorrain et al.

(2005) similarly suggested that shell Sr/Ca partitioning in the calcitic *Pecten maximus* is mainly controlled by kinetic effects. Again a positive correlation between SST and Sr/Ca was observed. However, our culture experiments overall reveal a negative relationship between culture temperature and Mg/Ca, Sr/Ca and Ba/Ca. This inverse correlation is in line with results from inorganic precipitation experiments on Mg/Ca and Sr/Ca in aragonite (e.g. Kinsman and Holland, 1969; Gaetani and Cohen, 2006). Our results further demonstrate that trace elemental uptake in giant clams cannot be explained using a simple kinetic model that describes higher El/Ca ratios associated with higher growth rates, as postulated by e.g. Lorrain et al. (2005), because we find overall higher Mg/Ca, Sr/Ca and Ba/Ca ratios in the shells from slower growing *Tridacna crocea* (Table 2 and 3).

Purton et al. (1999), similarly to our finding, reported increasing Sr/Ca ratios with decreasing growth rates in aragonitic mollusks and concluded that metabolism exerts a major control on shell Sr/Ca. What is more, the partition coefficient D_{Sr} ($D_{Sr} = Sr_{aragonite}/Sr_{solution}$) in aragonitic bivalves is ~0.25 (e.g. Gillikin et al., 2005, Takesue and van, Geen, 2004; Poulain et al., 2015) which is far from equilibrium and further confirms the strong biological controls for this proxy. The D_{Sr} of coralline aragonite, for comparison, typically is ~1 (e.g. Gagnon et al., 2013).

Daily trace element variability controls

Figures 8A,B present daily resolved trace elemental cycles obtained from shell 3 and 4, secreted during culture in 29°C and 27°C, respectively and exposed to diurnal light cycle. Because temperature was kept constant within ± 0.2°C over the entire culture period of 16.5 days, we can confidently exclude temperature as a controlling parameter for the daily trace elemental variability. Importantly, shell 3 experienced a ~15 hour culture interruption during the evening/night of day eight in the experiment indicated by a drop in $^{135}Ba/^{138}Ba$, which coincides with both Mg/Ca and Sr/Ca showing the highest respective values of their diurnal cycle (Fig. 6B). Moreover, all organisms were sacrificed at midday on the last day of the culture, which coincides with the trough in El/Ca obtained from the growing edge of these shells (Fig. 8A, B). We therefore conclude that peak concentrations in Mg and Sr correspond to shell growth during night time, i.e. culture during lowest light intensities. This interpretation also matches our observations showing that *Tridacna* aragonite secreted at relatively low light intensity regimes is characterized by elevated El/Ca values (Fig. 7B, C).

Crucially, these findings are in agreement with field observations made by Sano et al. (2012), who imply an inverse relation between Sr/Ca and insolation. They found that real-time, hourly collected data on local insolation variability matched their measured Sr/Ca ratios, with lowest Sr/Ca ratios relating to high insolation intensities.

However, in contrast to this field-experiment, our laboratory culture enabled tight control over all external parameters.

Our experiment was designed in such way that light levels were kept constant throughout the day, i.e. no natural light variability was simulated, apart from the two hours transition time in the morning and evening (see 2.2). This highlights that the observed diurnal El/Ca variability, characterised by striking oscillatory cyclicity, especially for Mg/Ca and B/Ca cannot be controlled solely by light. It is more likely, that the cyclic El/Ca variability reflects diurnal changes in shell growth rates, which supports the finding by Warter and Müller (2016) of a close coupling between daily compositional cycles in B/Ca, Mg/Ca, Sr/Ca and Ba/Ca and the incremental growth pattern.

Bivalve metabolism has been shown to influence shell growth rates as well as the geochemical shell composition. And indeed, several studies report a diurnal metabolic performance of giant clams: Schwartzmann et al. (2011), who performed field observation on the valve-gaping behaviour of the giant clam *Hippopus hippous* from New Caledonia, report a diurnal gaping pattern, with maximal valve opening during daytime, while at night it was reduced to only ~20 %. Furthermore, complete closures regularly occurred at night for short time periods. These findings are in agreement with our observation during the *Tridacna crocea* culture period. During daytime the valves were wide-open and the mantle tissue fully exposed and extended well beyond the upper margin of the shell (overlapping mantle tissue), while during the night, the valves were more apposed and the mantle tissue retracted and less exposed. This gaping behaviour clearly highlights the fact that the clams are more active during the day than during night, which is is further confirmed by the study of Morton (1978), who reported a diurnal rhythm of activity with regards to feeding and digestion in *Tridacna crocea*. In short, feeding occurs during daytime, while digestion occurs at night.

A recent publication by Gutner-Hoch et al. (2016) demonstrated that the scleractinian coral *Acropora eurystoma* calcified – under constant light for 48 hours - in a diurnal rhythmic and cyclic calcification pattern. The authors suggest internal pacemakers, so called ‘circadian clocks’ to regulate the physiology, biochemistry and metabolism of the organism. Such pacemakers are according to the authors coupled to external parameters such as light that initiates calcification and allow the organism to maintain rhythms with a 24 hour periodicity. The authors were, however, not able to disentangle if the regulating mechanisms were triggered endogenously via the coral metabolism and/or via their dinoflagellate symbionts (zooxanthellae). It has been demonstrated that circadian clocks also mediate photosynthetic processes of *Symbiodinium*, both in unicellular cultures and in those living in symbiosis with corals (e.g. Sorek et al., 2013).

The fact that daily, cyclic El/Ca variability is observed in our *Tridcana* shells, which were cultured not only under constant light intensities during the day but also constant temperatures, similarly suggests that their metabolism, growth performance and biochemsitry is subject to an internal endogenous circadian rhythm, which might also mediate the physiological processes described above. The fact that organism 7, cultured in the constant light regime for four days, revealed a much poorer growth performance compared to the diurnal light regime at the same temperature, suggests that the circadian rhythms was disturbed, resulting in an overall lower host and/or symbiont metabolism performance. The almost complete growth inhibition in case of organism 8, cultured in constant darkness (Fig. 5), further confirms a key and initializing role of light towards *Tridacna* shell growth and/or the maintenance of their diurnal activity rhythm.
Finally, Warter and Müller (2016) demonstrate a fortnightly tidal periodicity, superimposed on daily growth cycles in B/Ca, Mg/Ca, Sr/Ca and Ba/Ca of Miocene *Tridacna* shells. It is likely that this fortnightly periodicity is the (direct/or indirect) result of periodic variable light levels, linked to the changing seawater levels. To further test this hypothesis, longer-term laboratory culture experiments, which simulate tidal sea level changes, could be performed along with the culture without a tidal component. An easier approach would be to analyze recent giant clam shells collected from coastal settings exposed/or not exposed to a tidal cyclic sea level changes.

Mg/Ca peaks and increasing El/Ca ratios - Stress indicators?

The daily resolved Mg/Ca profiles of shells 4 and 5 reveal peak ratios for the shell part secreted immediately before and after the start of the culture experiment (Fig. 8A,C). This peak is characterized by Mg/Ca ratios up to five times higher compared to the shell parts secreted later (and ealier) in the stage of the experiment. Lorens and Bender (1980), who performed culture experiments on blue mussel *Mytilus edulis*, equally report highly elevated Mg/Ca ratios for the very initial calcite growth sections, newly secreted from the culture solution. The authors describe this shell section, which is “generally characterized by having the highest Mg/Ca ratio in the shell” as *transition zone*. They hypothesize that *Mytilus edulis* actively controls the Mg activity of the outer extrapallial fluid and that the stress of capture or adjustment to a new environment resulted in a temporary deterioration of the Mg exclusion mechanism. The research team also reports that high Mg/Ca ratios are associated with high organic contents, associated with high sulphur concentrations, and further imply that changes in shell organic matrix content occur as a result of environmental stress. Schöne et al. (2010) also observed a correlation between high Mg concentrations and the organic matrix content. The authors report that organic rich, annual growth lines, in *Arctica islandica* are up to two-to three fold enriched in Mg/Ca and argue that considerable amounts of Mg are bound to the organic matrices rather than the aragonite crystal lattice.

The higher measured Mg/Ca content measured within the 'transition zone' of the *Tridacna* shells, might therefore indicate reduced calcification. Indeed, a decreased growth rate or even growth inhibition can be confirmed via counting the daily growth cycles in Fig. 8A. The B/Ca record reveals 15 well-developed growth cycles; however the culture experiment was performed over a period of 16.5 days. What is more, while the Mg/Ca daily cycles are well-developed for the shell parts secreted later in the stage of the experiment (13 cycles can be counted), daily growth cycles cannot be identified in the Mg/Ca peak domain. We therefore suggest that growth rates initially were significantly lowered directly after the start of the culture, likely related to organism stress during handling or adaption to the new environment. If the anomalously high Mg/Ca ratios indeed present an organism response related to abrupt environmental changes, this proxy could be used to track and date natural disasters such as storm events or men-made ocean pollution, as originally proposed by Lorens and Bender (1980)

Poulain et al. (2015) who performed culture experiments on the aragonitic Manila clam *Ruditapes philippinarum* similarly observed a decrease of daily shell growth rates just after transplantation to the laboratory, associated with high S and Mg concentrations in the shell parts secreted directly after the organism transplantation. The authors also report increasing Mg/Ca ratios throughout the experiment, which however were independent from shell growth rates, which were constant after the first days and also independently from the organic matrices. The authors conclude that the continuously increasing Mg/Ca ratios are not linked to an increasing shell organic matrix content and/or linked to reduced shell growth, and interpreted the rising Mg/Ca ratio as a respond to animal stress and/or pH changes related to internal organism physiology. Similarly to Poulain et al. (2015) increasing Mg/Ca ratios with time are also observed for our cultured *Tridacna crocea* shells (e.g. Fig. 8C, Fig. 9). We exclude the possibility that organic matrices account for the observed increase in El/Ca ratios and - in agreement to Poulain et al. (2015) - interpret the rising El/Ca ratios, most pronounced in Mg/Ca, as a response to organism stress, resulting from e.g. starving or close captivity. Our results further show that insufficient light intensities are likely linked to organism stress too, as revealed by the relatively elevated average El/Ca ratios in case of shell 4, 5, 6 and 8 (Fig. 7A, C).

5.5 Conclusions

Our presented experimental set-up was designed to investigate growth and trace element incorporation into the aragonite shells of giant clams (*Tridacna crocea*) at daily resolution, all cultured under variable, yet tightly controlled temperature and light conditions. It has proven successful in culturing giant clams over a time period of about two weeks and allowed retrieval of appropriately-resolved geochemical signals from the culture period. A clear positive correlation between calcification rate and temperature on the one hand and calcification rate with light intensity on the other hand was observed. However, light seems to play a dominant role: While shell growth occurred in the low temperature (23°C and 25°C), diurnal light regime, no calcification (and possibly even carbonate dissolution) was observed for the culture in constant darkness, but at considerably higher temperatures (27°C).

Ultra-high resolution LA-ICPMS was performed for a detailed investigation of the geochemical signature of cultured shell parts which were unequivocally identifiable following ^{135}Ba isotope labelling of the seawater from which they secreted. Overall, a negative relationship between average values of Mg/Ca, Sr/Ca and Ba/Ca ratio with both temperature and light can be observed. Interestingly, an increasing trend not only in Mg/Ca and Sr/Ca, but also for B/Ca and Ba/Ca can be repeatedly observed throughout the culture period, i. e. in direction of growth. This increase must be related to biophysiological controls because all external parameters were kept constant throughout the entire culture period. Distinct peak ratios in the Mg/Ca record, observed in shell sections secreted directly before and immediately after the start of the experiment, are interpreted to reflect 'stress' events.

Daily trace element cyclicity was resolved within faster-growing shells secreted during culture under the constant 29°C and 27°C diurnal light cycle regime. Because temperature was kept constant at ± 0.2°C throughout the entire experiment, we can exclude temperature as the controlling parameter for daily trace elemental variability. What is more, we demonstrate that relatively high El/Ca ratios correspond to shell growth in darkness, i.e. during night time, which is in agreement to field observations by Sano et al. (2012). However, because light levels were kept constant during day time, light intensity cannot account for the entire range of the El/Ca variability. We suggest that the ambient light accounts only indirectly, via growth rate, for the daily compositional cycles and hypothesize that *Tridacna* physiology and biochemistry is controlled by a circadian rhythm, which is initiated by the external factor light, but endogenously mediated by the giant clam and/or its photosynthetic symbionts.

References

Aharon, P., 1983, 140,00-yr isotope climate record from raised coral reefs New Guinea: Nature, v. 304, p. 720-723.

Aharon, P., 1991, Recorders of reef environment histories - stable isotopes in corals, giant clams and calcareous algae: Coral Reefs, v. 10, p. 71-90.

Aubert, A., Lazareth, C.E., Cabioch, G., Boucher, H., Yamada, T., Iryu, Y., and Farman, R., 2009, The tropical giant clam *Hippopus hippopus* shell, a new archive of environmental conditions as revealed by sclerochronological and $\delta^{18}O$ profiles: Coral Reefs, v. 28, p. 989-998.

Batenburg, S.J., Reichart, G.J., Jilbert, T., Janse, M., Wesselingh, F.P., and Renema, W., 2011, Interannual climate variability in the Miocene: High resolution trace element and stable isotope ratios in giant clams: Palaeogeography, Palaeoclimatology, Palaeoecology, v. 306, p. 75-81.

Beckvar, N., 1981, Cultivation, spawning, and growth of the giant clams *Tridacna gigas, T. derasa,* and *T. squamosa* in Palau, Caroline Islands: Aquaculture, v. 24, p. 21–30.

Bonham, K., 1965, Growth rate of giant clam *Tridacna gigas* at Bikini Atoll as revealed by radioautography: Science, v. 149, p. 300-302.

Buck, B.H., Rosenthal, H., and Saint-Paul, U., 2002, Effect of increased irradiance and thermal stress on the symbiosis of *Symbiodinium microadriaticum* and *Tridacna gigas*: Aquat. Living Resour., v. 15, p. 107–117

Buick, D.P., and Ivany, L.C., 2004, 100 years in the dark: Extreme longevity of Eocene bivalves from Antarctica: Geology, v. 32, p. 921-924.

Butler, P.G., Wanamaker Jr., A.D., Scourse, J.D., Richardson, C.A., and Reynolds. D.J., 2013, Variability of marine climate on the North Icelandic Shelf in a 1357-year proxy archive based on growth increments in the bivalve *Arctica islandica*: Palaeogeography, Palaeoclimatology, Palaeoecology, v. 373, p. 141-151.

Carré, M., Bentaleb, I., Bruguier, O., Ordinola, E., Barrett, N.T., and Fontugne, M., 2006, Calcification rate influence on trace element concentrations in aragonitic bivalve shells: Evidences and mechanisms: Geochimica et Cosmochimica Acta, v. 70, p. 4906-4920.

Cohen, I., Dubinsky, Z., and Erez, J., 2016, Light enhanced calcification in hermatypic corals: New insights from light spectral responses: Frontiers in Marine Science, doi: 10.3389/fmars.2015.00122.

Dame, R.F., 2012, Ecology of Marine Bivalves: An Ecosystem Approach, 2nd edition, Taylor & Francis, London.

De Laeter, J.R., Böhlke, J.K., De Bièvre, P., Hidaka, H., Peiser, H.S., Rosman, K.J.R., and Taylor, P.D.P., 2003, Atomic weights of the elements: Review 2000: Pure and Applied Chemistry, v. 75, p. 683-800.

Elliot, M., Welsh, K., Chilcott, C., McCulloch, M., Chappell, J., and Ayling, B., 2009, Profiles of trace elements and stable isotopes derived from giant long-lived *Tridacna gigas* bivalves: Potential applications in paleoclimate studies: Palaeogeography, Palaeoclimatology, Palaeoecology, v. 280, p. 132-142.

Erez, J., Reynaud, S., Silverman, J., Schneider, K., and Allemand, D., 2011, Coral calcification under ocean acidification and global change: In: Coral reefs: An ecosystem in transition, Dubinsky, Z. and Stambler, N., (editors), Springer, Germany, p. 151–176.

Fatherree, J.W., 2006, Giant clams in the sea and the aquarium: Liquid Medium, Tampa, Florida, 227 pages.

Foster, L.C., Allison, N., Finch A.A., and Andersson C., 2009, Strontium distribution in the shell of the aragonite bivalve *Arctica islandica:* Geochemistry, Geophysics, Geosystems, v. 10 (3), doi: 10.1029/2007GC001915.

Freitas, P.S, Clarke, L.J., Kennedy, H., Richardosn, C.A, and Abrantes, F., 2005, Mg/Ca, Sr/Ca, and stable isotope ($\delta^{18}O$ and $\delta^{13}C$) ratio profiles from the fan mussel *Pinna nobilis*: Seasonal records and temperature relationships: Geochemistry, Geophysics, Geosystems, v. 6 (4), doi: 10.1029/2004GC00872.

Freitas, P.S, Clarke, L.J., Kennedy, H., Richardosn, C.A, and Abrantes, F., 2006, Environmental and biological controls on elemental (Mg/Ca, Sr/Ca and Mn/Ca) ratios in shells of the king scallop *Pecten maximus:* Geochimica et Cosmochimica Acta, v. 70, p. 5119-5133.

Fujise, L., Yamashita, H., Suzuki, G., Sasaki, K., Liao, L.M., Koike, K., 2014, Moderate thermal stress causes active and immediate expulsion of photosynthetically damaged zooxanthellae (*Symbiodinium*) from corals. Plos One, doi:10.1371/journal.pone.0114321.

Gaetani, G.A., and Cohen, A.L., 2006, Element partitioning during precipitation of aragonite from seawater: A framework for understanding paleproxies: Geochimica et Cosmochimica Acta, v. 70, p. 4617-4634.

Gagnon, A.C., Adkins, J.F., Erez, J., Eiler, J.M., Guan, Y., 2013, Sr/Ca sensitivity to aragonite saturation state in cultured subsamples from a single colony of coral: Mechanism of biomineralization during ocean acidification: Geochimica et Cosmochimica Acta, v. 105, p. 240-254.

Gillikin, D.P., Lorrain, A., Navez, J., Taylor, J.W., André, L., Keppens, E., Baeyens, W., and Dehairs, F., 2005, Strong biological controls on Sr/Ca ratios in aragonitic marine bivalve shells: Geochemistry, Geophysics, Geosystems, v. 6 (5), doi: 10.1029/2004GC000874.

Goodwin, D.H., Flessa, K.W., Schöne, B.R., and Dettman, D.L., 2001, Cross-calibration of daily growth increments, stable isotope variation, and temperature in the Gulf of California bivalve mollusk *Chione cortezi:* Implications for paleoenvironmental analysis: Palaios, v. 16, p. 387-398.

Goreau, T., 1959, The physiology of skeleton formation in corals. I. A method for measuring the rate of calcium deposition by corals under different conditions: Biological Bulletin, v.116, p. 59-75.

Gutner-Hoch, E., Schneider, K., Stolarski, J., Domart-Coulon, I., Yam, R., Meibom, A., Shemesh, A., and Levy, O., 2016, Evidence for rhythmicity pacemaker in the calcification process of scleractinian coral: Scientific Reports, doi: 10.1038/srep20191.

Hammer, W.M., and Jones, M.S., 1976, Distribution, burrowing, and growth rates of the clam Tridacna crocea on interior reef flats: Oecologia, v. 24, p. 267-281.

Han, B.-P., Virtanen, M.m Koponen, J., and Straškraba, M., 2000, Effect of photoinhibition on algal photosynthesis: a dynamic model: Journal of Plankton Research, v .22 no.5 p. 865-885.

Hart, A.M., Bell, J.D., and Foyle, T.P., 1998, Growth and survival of the giant clams, *Tridacna derasa*, *T. maxima* and *T. crocea*, at village farms in the Solomon Islands: Aquaculture, v. 165, p. 203-220.

Holt, A.L., Vahidinia, S., Gagnon, Y.L., Morse, D.E., and Sweeney, A.M., 2014, Photosymbiotic giant clams are transformers of solar flux: Journal of the Royal Society Interface, doi.org/10.1098/rsif.2014.0678.

Hori, M., Sano, Y., Ishida, A., Takahata, N., Shirai, K., and Watanabe, T., 2015, Middle Holocene daily light cycle reconstructed from the strontium/calcium ratios of a fossil giant clam shell: Scientific Reports, v. 5, doi: 10.1038/srep08734.

Iglesias-Prieto, R., Matta, J.L., Robins, W.A., and& Trench, R.K., 1992, Photosynthetic responses to elevated temperature in the symbiotic dinoflagellate *Symbiodinium microadriaticum* in culture: Proc. Natl. Acad. Sci. USA, v. 89, p. 10302-10305.

Ip, Y.K., Ching, B., Hiong, K.C., Choo, C.Y.L., Boo, M.V., Wong, W.P., and Chew, S.F., 2015, Light induces changes in activities of Na^+/K^+-ATPase, H^+/K^+-ATPase and glutamine synthetase in tissues involved directly or indirectly in light-enhanced calcification in the giant clam, *Tridacna squamosa*: Frontiers in Physiology, doi: 10.3389/fphys.2015.00068.

Ivany, L.C., Peters, S.C., Wilkinson, B.H., Lohmann, K.C., and Reimer, B.A., 2004, Composition of the early Oligocene ocean from coral stable isotope and elemental chemistry: Geobiology, v. 2, p. 97-106.

Jochum, K.P., Weis, U., Stoll, B., Kuzmin, D., Yang, Q.C., Raczek, I., Jacob, D.E., Stracke, A., Birbaum, K., Frick, D.A., Günther, D., and Enzweiler, J., 2011, Determination of reference values for NIST SRM 610-617 glasses following ISO guidelines: Geostandards and Geoanalytical Research, v. 35, p. 397-429.

Junchompoo, C., Sinrapasan, C., Penpain, C., and Patsorn, N., 2013, Changing seawater temperature effects on giant clams bleaching, Mannai Island, Rayong province, Thailand:

Proceedings of the design symposium on conservation of ecosystem: The 12th SEASTAR2000 workshop, p. 71-76.

Kinsman, D.J.J., Holland, H.D., 1969, The coprecipitation of cations with $CaCO_3$: IV. The coprecipitation of Sr^{2+} with aragonite between 16 and 96 °C: Geochimica et Cosmochimica Acta, v. 33, p. 1-17.

Klein, R.T., Lohmann, K.C., and Thayer, C., 1996, Sr/Ca and $^{13}C/^{12}C$ ratios in skeletal calcite of *Mytilus trossulus*: Covariation with metabolic rate, salinity, and carbon isotopic composition of seawater: Geochimica et Cosmochimica Acta, v. 60, p. 4207-4221.

Klumpp, D.W., Bayne, B.L., and Hawkins, A.J.S., 1992, Nutrition of the giant clam *Tridacna gigas* (L.). I. Contribution of filter feeding and photosynthates to respiration and growth: J. Exp. Mar. Biol. Ecol., v. 155, p. 105-122.

Klumpp, D.W., and Lucas, J.S., 1994, Nutritional ecology of the giant clams *Tridacna tevoroa* and *T. derasa* from Tonga: influence of light on filter-feeding and photosynthesis. Marine Ecology Progress Series, v. 107, p. 147-156.

Klumpp, D.W., Griffiths, C.L., 1994, Contributions of phototrophic and heterotrophic nutrition to the metabolic and growth requirements of four species of giant clam (Tridacnidae): Marine Ecology Progress Series, v. 115, p. 103-115.

Kunzmann, A., 2008, Physiological performance of giant clams (*Tridacna spec*.) in a recirculation system: Proceedings of the 11th International Coral Reef Symposium, Ft. Lauderdale, Florida, 7-11 July 2008.

Lamarck, J.B., 1819a, *Tridacna crocea*: In: Histoire naturelle des animaux sans vertèbres présentant les caractères généraux et particuliers de ces animaux, leur distribution, leurs classes, leurs familles, leurs genres, et la citation des principales espèces qui s'y rapportent, v. 6 (1).

Lesser, H.R., Stochaj, W.R., Tapley, D.W., and Shick, J.M., 1990, Bleaching in coral reef anthozoans: effects of irradiance, ultraviolet radiation, and temperature on the activities of protective enzymes against active oxygen: Coral Reefs, v. 8, p. 225-232.

Longerich, H.P., Günther, D., and Jackson, S.E., 1996, Elemental fractionation in laser ablation inductively coupled plasma mass spectrometry: Fresenius Journal of Analytical Chemistry, v. 355, p. 538-542.

Lorens, R.B., and Bender, M.L., 1980, The impact of solution chemistry on *Mytilus edulis* calcite and aragonite, Geochimica et Cosmuochimica Acta, v. 44, p. 1265-1278.

Lorrain, A., Gillikin, D.P., Paulet, Y.-M., Chauvaud, L., Le Mercier, A., Navez, J., and Luc, A., 2005, Strong kinetic effects on Sr/Ca ratios in the calcitic bivalve: Geology, v. 2005, v. 33, p. 965-968.

Lowenstam, H.A., 1981, Minerals formed by organisms: Science, v. 211, p. 1126 – 1131.

Lucas, J.S., Nash, W.J., Crawford, C.M., and Braley, R.D., 1989, Environmental influences on growth and survival during the ocean-nursery rearing of giant clams, *Tridacna gigas* (L.): Aquaculture, v. 80, p. 45-61.

Marshall, J.F, and McCulloch, M., 2001, Evidence of El Niñio and the Indian Ocean Dipole from Sr/Ca derived SSTs for modern corals at Christmas Island, eastern Indian Ocean: Geophysical Research Letters, v. 28, p. 3453-3456.

Marshall, J.F, and McCulloch, M., 2002, An assessment of the Sr/Ca ratio in shallow water hermatypic corals as a proxy for sea surface temperature: Geochimica et Cosmochimica Acta, v. 66, p. 3263-3280.

Morton, M., 1978, The diurnal rhythm and the processes of feeding and digestion in *Tridacna crocea* (Bivalvia: Tridacnidae): Journal of Zoology, v. 185, p. 371-387.

Müller, W., Shelley, M., Miller, P., and Broude, S., 2009, Initial performance metrics of a new custom-designed ArF excimer LA-ICPMS system coupled to a two-volume laser-ablation cell: Journal of Analytical Atomic Spectrometry, v. 24, p. 209-214.

Paton, C., Hellstrom, J., Paul, B., Woodhead, J., and Hergt, J., 2011, Iolite: Freeware for the visualization and processing of mass spectrometric data: Journal of Analytical Atomic Spectrometry, doi: 10.1039/c1ja10172b.

Pätzold, J., Heinrichs, J.P., Wolschendorf, K., and Wefer, G., 1991, Correlation of stable oxygen isotope temperature record with light attenuation profiles in reef-dwelling *Tridacna* shells: Coral Reefs, v. 10, p. 65-69.

Poulain, C., Gillikin, D.P., Thébault, J., Munaron, J.M., Bohn, M., Robert, R., Paulet, Y.-M., and Lorrain, A., 2015, An evaluation of Mg/Ca, Sr/Ca, and Ba/Ca ratios as environmental proxies in aragonite bivalve shells: Chemical Geology, v. 396, p. 42-50.

Purton, L.M.A., Shields, G.A., Brasier, M.D., and Grime, G.W., 1999, Metabolism controls Sr/Ca ratios in fossil aragonitic mollusks: Geology, v. 27, p. 1083-1086.

Romanek, C.S., and Grossman, E.L., 1989, Stable isotope profiles of *Tridacna maxima* as environmental indicators: Palaios, v. 4, p. 402–413.

Rosewater, J., 1965, The family Tridacnidae in the Indo-Pacific: Indo-Pacific Mollusca, v. 1 (6), 347-394.

Sano, Y., Kobayashi, S., Shirai, K., Takahata, N., Matsumoto, K., Watanabe, T., Sowa, K., and Iwai, K., 2012, Past daily light cycle recorded in the strontium/calcium ratios of giant clam shells: Nature Communications, v. 3, doi: 10.1038/NCOMMS1763.

Schöne, B.R., Lega, J., Flessa, K.W., Goodwin, D.H., and Dettman, D.L., 2002, Reconstructing daily temperatures from growth rates of the intertidal bivalve mollusk *Chione cortezi* (northern Gulf of California, Mexico): Palaeogegrapghy, Palaeoclimatology, Palaeoecology, v. 184, p. 131-146.

Schöne, B.R., Zhang, Z., Jacob, D., Gillikin, D.P., Tütken, T., Garbe-Schönberg, D., McConnaughey, T., and Soldati, A., 2010, Effect of organic matrices on the determination of the trace element chemistry (Mg, Sr, Mg/Ca, Sr/Ca) of aragonitic bivalve shells (*Arctica islandica*) – Comparison of ICP-OES and LA-ICP-MS data: Geochemical Journal, v. 44, p. 23-27.

Schöne, B.R., Zhang, Z., Radermacher, P., Thébault, J., Jacob, D.E., Nunn, E.V., and Maurer, A-.F., 2011, Sr/Ca and Mg/Ca ratios of ontogenetically old, long-lived bivalve shells (*Arctica islandica*) and their function as paleotemperature proxies: Palaeogeography, Palaeoclimatology, Palaeoecology, v. 302, p. 52-64.

Schwartzmann, C., Durrieu, G., Sow, M., Ciret, P., and Lazareth, C.E., 2011, In situ giant clam growth rate behavior in relation to temperature: a one-year coupled study of high-frequency noninvasive valvometry and sclerochronology: Limnology and Oceanography, v. 56 (5), p.1940-1951.

Sinclair, D.J., Kinsley, L.P.J., and McCulloch, M.T., 1998, High resolution analysis of trace elements in corals by laser ablation ICP-MS: Geochimica et Cosmochimica Acta, v. 62, p. 1889-1901.

Sorek, M., Yacobi, Y.Z., Roopin, M., Berman-Frank, I., and Levy, O, 2013, Photosynthetic circadian rhythmicity patterns of *Symbiodinium*, the coral endosymbiotic algae. Proceedings of the Royal Society B - Biological Sciences, doi: 10.1098/rspb.2012.2942.

Stecher, H.A., Krantz, D.E., Lord, C.J., Luther, G.W., and Bock, K.W., 1996, Profiles of strontium and barium in *Mercenaria mercenaria* and *Spisula solidissima* shells: Geochimica et Cosmochimica Acta, v. 60, p. 3445-3456.

Takesue, R. K. and van Geen, A., 2004, Mg/Ca, Sr/Ca, and stable isotopes in modern and Holocene Protothaca staminea shells from a northern California coastal upwelling region: Geochimica and Cosmochimica Acta, v. 68, p. 3845-3861.

Tentori, E., and Allemand, D., 2006, Light-enhanced calcification and dark decalcification in isolates of the soft coral *Cladiella sp*. during tissue recovery: Biological Bulletin, v. 211, p. 193-202.

Warter, V., Müller, W., Wesselingh, F.P., Todd, J.A., and Renema, W., 2015, Late Miocene seasonal to sub-decadal climate variability in the Indo-West Pacific (East Kalimantan, Indonesia) preserved in giant clams: Palaios, v. 30, p. 66-82, doi.org/10.2110/palo.2013.061.

Warter, V., and Müller, W, 2016, Daily growth and tidal rhythms in Miocene and modern giant clams revealed via ultra-high resolution LA-ICPMS analysis – A novel methodological approach towards improved sclerochemistry: Palaeogeography, Palaeoclimatology, Palaeoecology, doi:10.1016/j.palaeo.2016.03.019.

Watanabe, T., Suzuki, A., Kawahata, H., Kan, H., and Ogawa, S., 2004, A 60-year isotopic record from a mid-Holocene fossil giant clam *(Tridacna gigas)* in the Ryukyu Islands:

physiological and paleoclimatic implications: Palaeogeography, Palaeoclimatology, Palaeoecology, v. 212, p. 343-354.

Wei, G., Sun, M., Lia, X., and Nie, B., 2000. Mg/Ca, Sr/Ca and U/Ca ratios of a porites coral from Sanya Bay, Hainan Island, South China Sea and their relationships to sea surface temperature. Palaeogeography, Palaeoclimatology, Palaeoecology. V. 162, p. 59–74.

Weiner, S., and Dove, P.M., 2003, An overview of biomineralization processes and the problem of the vital effect: Reviews in Mineralogy and Geochemistry, v. 54, p. 1-29.

Welsh, K., Elliot, M., Tudhope, A., Ayling, B., and Chappell, J., 2011, Giant bivalves (*Tridacna gigas*) as recorders of ENSO variability: Earth and Planetary Science Letters, v. 307, p. 266-270.

Yan, H., Shao, D., Wang, Y., and Sun, L., 2013, Sr/Ca profile of long-lived *Tridacna gigas* bivalves from South China Sea: A new high-resolution SST proxy: Geochimica et Cosmochimica Acta, v. 112, p. 52-65.

Yan, H., Shao, D., Wang, Y., and Sun, L., 2014, Sr/Ca differences within and among three Tridacnidae species from the South China Sea: Implication for paleoclimate reconstruction: Chemical Geology, v. 390, p. 22-31.

Yan, H., Soon, W., and Wang, Y., 2015, A composite sea surface temperature record of the northern South China Sea for the past 2500 years: A unique look into seasonality and seasonal climate changes during warm and cold periods: Earth-Science Reviews, v. 141, p. 122-135.

Yonge, C.M., 1982, Functional morphology and evolution in the Tridacnidae (Mollusca: Bivalvia: Cardiacea): Records of the Australian Museum, v. 33 (17), p. 735–777.

Chapter 6: Synopsis, Critical evaluation, Conclusions

This chapter provides a synopsis of the research results obtained in Chapters 3, 4 and 5, evaluates the research findings critically, suggests future research directions and presents overall conclusions.

6. 1 Research Synopsis

This study evaluates the extent to which giant clams (*Tridacna spp*.) record and preserve in their aragonite shells any (palaeo)environmental variability they are exposed to during lifetime.

Three successive case studies investigate the geochemical composition of giant clam shells, using high-resolution LA-ICPMS analysis as the key in-situ analytical method, yet each study has a different focus: Case study one (Chapter 3) investigates the preservation of two Late Miocene giant clams and presents seasonally-resolved $\delta^{18}O$ and El/Ca and proxy records from pristine shell aragonite, which provide insight into Late Miocene seasonal SST variability of East Kalimantan, Indonesia. The second case study (Chapter 4) introduces a novel methodological approach for ultra-high resolution LA-ICPMS analysis, which enables to investigate daily and tidal-cyclic trace element variability in Miocene and Recent giant clam shells. The final case study (Chapter 5) combines the laboratory culture of *Tridacna crocea* and the application of ultra-high resolution LA-ICPMS analysis. Daily resolved trace elemental records from cultured shell portions allow disentangling the relative contribution of environmental versus biophysiological controls on trace element incorporation.

Considered together, the results of the three application studies presented herein provide the framework for a significantly improved interpretation of highly time-resolved proxy data in giant clams. Our approach of combining laboratory culture experiments and in-situ ultra-high resolution analysis opens up new perspectives for the detailed investigation of giant clams as (palaeo)environmental archives.

6.2 Evaluating the proxy record

6.2.1 Diagenesis

Chapter 3 (Warter et al., 2015) reveals that although diagenetic alteration strongly affected the shell exteriors of two Late Miocene giant clam shells from East Kalimantan, Indonesia, the shell interiors were to a large extent excellently preserved and proxy records obtained from pristine aragonite were used for palaeoenvironmental reconstructions. This highlights on the one hand that giant clams are suitable 'deep-time' palaeoclimate archives, and on the other hand that *external* shell alteration does not necessarily reflect the overall shell preservation. Considering the immediate demand for suitable fossils for palaeoclimate reconstructions (and chronostratigraphic studies), especially from periods pre-dating the Pleistocene epoch, external shell alteration should not be treated as an exclusionary criterion, especially during field sampling.

The study also highlights that a meticulous screening procedure, via combined usage of macroscopic and microscopic observations, XRD, SEM/CL imaging, and LA-ICPMS trace elemental screening has proven effective in detecting diagenetic shell alteration in the case of the two Miocene giant clams. The trace element screening reveals significant compositional differences between the El/Ca ratios of primary shell aragonite compared to diagenetically affected shell domains. El/Ca ratios obtained from diagenetically altered zones are therefore not suited for the reconstructions of primary palaeoenvironmental conditions during the time of shell formation. XRD analysis is used routinely to assess the preservation of fossil carbonates. Several studies however reveal that this technique has limitations, such as overlapping spectral peaks for pristine and secondary aragonite, which renders this technique, at least partly, insufficient for a diagenetic assessment (e.g. Griffiths et al., 2013; Gothmann et al., 2015, Warter et al., 2015). Warter et al. (2015) further revealed that hand-drilling of pristine aragonite resulted in the conversion of meta-stable pristine aragonite to calcite, detectable in the XRD spectrum, while no aragonite-calcite transition occurred when preparing powdered samples via grinding; thus the detected calcite is the result of a sampling artifact. This must be recognized to avoid misinterpretations.

Diagenetic alteration also affects modern biogenic carbonates, as it has been demonstrated in the case of the aragonite coral skeleton of *Siderastrea radians* (Griffiths et al., 2013). Marcano et al. (2015) equally reported early diagenesis of the aragonitic venerid bivalve *Retrotapes andrilloru.* The authors found that the outer layer of the shell was characterized by anomalously high Sr concentrations and lower than expected $^{87}Sr/^{86}Sr$ ratios, which were not in agreement with the isotopic signature of the ambient porewater. Very similar results are reported by Marshall et al. (in prep.), who investigate the Sr concentration and isotopic composition of a fossil *Tridacna* shell. The authors report that within the aragonitic inner layer micro-cracks occur, which are

characterized by up to seven-fold higher Sr concentrations compared to the 'non-crack aragonite' and lower than expected $^{87}Sr/^{86}Sr$ ratios with an resulting age estimate that does not fit with the magnestotratigraphic age model. In contrast, the Sr isotope compositions of the two Late Miocene shells investigated in Chapter 3 are identical within error and moreover support the corresponding biostratigraphic age estimates (Tortonian) from the Bontang area, which further indicates that pristine aragonite with the original Late Miocene geochemical signature was preserved.

Both studies by Marcano et al. (2015) and Marshall et al. (in prep.) highlight the importance of a thorough and detailed preservation assessment procedure, as was performed in the case of our two Late Miocene giant clam shells (Chapter 3). Overall *Tridacna* shells are perfectly suited for palaeoclimate reconstructions, because of their 1) high shell growth rate, which allows resolving daily trace element variability, 2) longevity, which allows resolving tidal-cyclic and seasonal variability and 3) excellent shell preservation potential, which enables 'deep-time' palaeoenvironmenal investigations (e.g. Batenburg et al., 2011; Warter et al., 2015).

6.2.2 Biophysiology

Previous studies provide inconsistent conclusions about the potential of bivalves as palaeoenvironmental archives. While it is well-documented that species specific physiological effects play a major role with regards to proxy element incorporation into the biogenic carbonate of bivalves (e.g. Klein et al., 1996; Carré et al., 2006; Freitas et al., 2005), their exact contributions to the geochemical composition are difficult to quantify, which complicates proxy based environmental reconstructions (e.g. Schöne et al., 2011).

Chapter 3 investigates seasonally resolved Late Miocene proxy records. This study (Warter et al., 2015) demonstrates that the Mg/Ca time-series profile reflects not only an environmental (SST), but also a biophysiological component. This is revealed by the increasing trend in Mg/Ca with ontogenetic age, which is likely to be associated with a growth rate reduction of the organism, as it has been reported for giant clams and other bivalves (e.g. Elliot et al., 2009). Models can be applied to detrend ontogentically caused variations in shell growth rates (e.g. Scourse et al., 2006; Stott et al., 2010), but age-detrended corrections of the proxy record, aimed to remove the physiological component, prove to be more complicated. Schöne et al. (2011) for instance detrended and standardized Sr/Ca and Mg/Ca records from *Arctica islandica*, but even after this correction only 40 % of the trace elemental variability could be explained via the variability of the calcification temperature. Moreover, the authors report that species-specific El/Ca trends, related to ontogeny, were not consistent in fast-growing shell portions and further argue that the absolute influences of vital effects change through organism ontogeny. The study by Schöne et al. (2011) highlights that without knowing the exact contribution of 'vital effects',

any reliable paleoenvironmental interpretation based on such 'physiology influenced' proxy records remains elusive.

Chapter 5 presents daily resolved trace elemental records from laboratory cultured *Tridacna crocea* shells. The cultivation experiments were designed to disentangle environmental from biophysiological controls, by keeping a close control over the external factors temperature, light and seawater chemistry. The results reveal that both temperature and light influence shell growth rates as well as the average B/Ca, Mg/Ca, Sr/Ca and Ba/Ca composition. However, these proxy records are also under further physiological control: Even though all external parameters were kept constant throughout the entire culture period, increasing El/Ca ratios were repeatedly observed for individual shells. Moreover, distinct peak ratios in the Mg/Ca record exist in shell portions secreted immediately before and after the start of the experiment and are interpreted as additional 'physiological stress' indices. If the anomalously high Mg/Ca ratios indeed present an organisms' response related to abrupt environmental changes, this proxy could be used to track and date natural disasters such as storm events or men-made ocean pollution, as originally proposed by Lorens and Bender (1980). Moreover, such distinct El/Ca ratios could potentially be used as 'anchor points' to link proxy records from contemporaneous species to produce continuous, multi-generation, 'master sclerochemical' records.

Daily trace elemental cycles were resolved within faster-growing shells secreted under constant temperature and we can therefore confidently exclude temperature as the controlling factor for daily trace element variability. The ambient light intensity however cannot account for the entire range of the observed El/Ca variability, because light was kept constant during the day. We argue that the endogenous metabolism of the giant clam and/or its symbionts regulate the shell calcification and the trace elemental incorporation.

Our results reveal the necessity to distinguish between environmental and physiological controls when interpreting El/Ca proxy records. Moreover, different physiological artifacts, such as the ontogenetic growth rate reduction probably linked organism metabolism and the associated increase in Mg/Ca (Chapter 3), 'physiological stress' as indicated by the anomalously high Mg/Ca ratios and/or the monotonously increasing B/Ca, Mg/Ca, Sr/Ca and Ba/Ca ratios, as well as a daily metabolic rhythm which governs the daily cyclic trace element variability, best resolved in Mg/Ca and B/Ca, exist and must be considered. Chapter 4 (Warter and Müller, 2016), demonstrates a fortnightly tidal periodicity, superimposed on daily growth cycles in B/Ca, Mg/Ca, Sr/Ca and Ba/Ca of two Miocene *Tridacna* shells. Given that light plays a key initiating role with regards to *daily* trace element variability, the tidal-cyclic El/Ca variability may directly or indirectly results from varying light levels, related to e.g. changing seawater levels. However, it is more likely that interplaying endogenous and external controls account for the tidal-cyclic El/Ca oscillations in the giant clam shells.

Further in-detail studies, combining controlled *Tridacna* culture experiments and the acquisition of daily resolved proxy records are certainly required to gain a full understanding of the biophysiological role with respect to (daily and tidal-cyclic) trace elemental chemistry in giant clams.

6.2.3 Reconstructed Miocene palaeoenvironmental variability

The quantitative palaeoclimate reconstructions presented in Chapter 3 are based on the seasonally-resolved $\delta^{18}O$ records of two Late Miocene shells in tandem with the corresponding qualitative Mg/Ca profiles. In contrast to trace elemental records, the stable oxygen isotope signature in bivalve shells, including *Tridacna spp*., is generally considered a robust proxy for palaeoenvironmental variability (e.g. Elliot et al., 2003; Gillikin et al., 2005; Welsh et al., 2011), also due to the fact that they secrete their shells close to isotopic equilibrium with seawater (e.g. Romanek and Grossman, 1989; Aharon, 1991; Elliot et al., 2009), which is not true in the case of coral skeletons. Furthermore, the ontogenetically-related growth reduction of *Tridacna spp*. does not reduce the reliability with which temperature and $\delta^{18}O_{sw}$ variability can be reconstructed (e.g. Welsh et al., 2011). However, because the stable isotope signature in biogenic carbonates depends not only on the calcification temperature but also on the isotopic composition of the ambient seawater, which co-varies with salinity (e.g. Gillikin et al., 2005), problems for this technique arise in the case of calcifying organisms that live in coastal settings, which are likely influenced by salinity fluctuations via e.g. fluvial runoff. Furthermore, $\delta^{18}O$-derived palaeo SST estimates are based on an assumed $\delta^{18}O_{sw}$ value, and this assumption automatically introduces an uncertainty to the palaeo SST reconstructions.

Our two Late Miocene shells, derived from the coastline of East Kalimantan, were potentially subjected to riverine influence from the Mahakam delta, a fluvio-deltaic system that already existed during the Miocene (e.g. Rösler et al., 2015). However, we assume that shell formation took place under relatively constant sea-surface salinity (SSS), owing to the fact that both shells were collected within a rich and diverse fossil coral community. Salinity variations are known to negatively impact on the relationship between corals and their symbionts (e.g. Moberg et al. 1997; Mayfield and Gates, 2007), for which reason the occurrence of coral reefs is usually taken to indicate stable euhaline conditions. Furthermore, the good qualitative agreement between the Mg/Ca record and the stable oxygen isotope time-series profile in case of LGS1 (Chapter 3) suggests that $\delta^{18}O_{shell}$ mainly mirrors SST. Because quantitative palaeotemperature reconstructions have a built-in uncertainty owing to the unknown $\delta^{18}O_{sw}$ values, a more achievable objective is to calculate temperature seasonalities.

The $\delta^{18}O$-derived Late Miocene seasonality estimates (Chapter 3) exceed the modern-day seasonality in the Makassar Strait two- to threefold. Palynological studies of sediments obtained

from shelf and deepwater exploration wells from the Kutai Basin (East Kalimantan) provide in contrast evidence for an everwet Late Miocene climate with minimal evidence for seasonality (Morley and Morley, 2011). It is not possible to decipher the causes of our relatively high seasonality estimates, but it should be considered that the resolution of our time-series records cannot be matched using pollen records. The fact that the seasonally-resolved records of both *Tridacna* shells span only eight years of growth each highlights the need for more and longer proxy records from the region to increase the statistical significance. Still, the study by Warter et al (2015) demonstrates that the giant clam derived $\delta^{18}O$ is a suitable palaeo SST proxy, corroborating studies by e.g. Batenburg et al. (2011), Welsh et al. (2011) and Driscoll et al. (2014), who reconstructed ENSO variability based on multi-decadal stable oxygen isotope records from *Tridacna spp*.

LA-ICPMS-derived *daily* El/Ca records of the two Late Miocene shells (Chapter 4) complement the lower resolution (weeks-months) $\delta^{18}O$-records (Chapter 3) in that way that tidal periodicity can be detected. More specifically, 24 tidal cycles, each composed of on average 14-15 daily cycles, were detected within one year of growth. Although at the current state of knowledge it is not possible to determine exactly which external or endogenous parameters control the Late Miocene tidal cyclic trace element variability, these records provide important qualitative information of the palaeohabitat of these giant clams. Tidal-cyclic trace element variability was not detected in the case of a modern *Tridacna sqamosa* shell from Sabah, Malaysia, which might indicate that the modern specimen was not exposed to a tidally-controlled environmental setting that influenced its shell chemistry. To further test this hypothesis, longer-term laboratory culture experiments, which simulate tidal sea level changes, could be performed along with the culture without a tidal component. A simpler approach would be to analyze recent giant clam shells collected from coastal settings exposed/or not exposed to a tidal cyclic sea level changes.

Overall, the existence and detectability of a ~14-15 day tidal periodicity within (trace) elemental records might help to improve and facilitate age estimations, where conventional sclerochronological methods are limited. The possibility of obtaining long-term, daily resolved (trace) element profiles allows investigation of daily trace elemental variability changes through time, which might also make an important contribution towards studies on the history of the Earth's rotation (cf. Wells, 1963; Kahn and Pompea, 1978).

6.3 Conclusions

- Giant clams (*Tridacna spp.*) can be considered ideal palaeoenvironmental archives, owing to their superior potential to preserve the original shell geochemical signature even in 'deep' geological time.
- A combined usage of XRD, SEM/CL imaging and LA-ICPMS trace elemental screening has proven effective at detecting pristine versus diagenetically altered shell domains in fossil *Tridacna spp*. shells.
- Based on two Late Miocene $\delta^{18}O$ time-series records, a seasonal SST variability of 2.7 ± 2.1 and 4.6 ± 1.7 °C, was reconstructed, which exceeds modern-day seasonality in the Makassar Strait (Indonesia) two- to threefold.
- A novel approach for ultra-high resolution LA-ICPMS analysis was developed, which enables resolution of <10 µm *daily* compositional variability in B/Ca, Mg/Ca, Sr/Ca and Ba/Ca preserved within microscopically visible daily growth increments in the aragonitic structure of modern and Miocene giant clams.
- Year-long, daily resolved LA-ICPMS records of B/Ca, Mg/Ca, Sr/Ca and Ba/Ca, reveal the existence of a Late Miocene tidal cyclicity, characterized by a fortnightly recurrent periodic pattern.
- An experimental set-up is presented which allows the culture of *Tridacna crocea* under variable, yet tightly controlled temperature and light conditions.
- Alkalinity measurements quantify both temperature and light influence on shell growth rates.
- Ultra-high resolution LA-ICPMS analysis reveals that both temperature and light influence trace elemental incorporation into shell aragonite of *Tridacna crocea*, yet we also demonstrate that biophysiology plays a major role with respect to trace elemental incorporation.
- Daily-resolved trace element variability within relatively fast-growing shells reveals that elevated El/Ca ratios correspond to shell growth in darkness, but because light levels were kept constant throughout the day, light intensity cannot account for the entire range of the El/Ca variability.
- We hypothesize that *Tridacna* physiology and biochemistry is controlled by a circadian rhythm, which is initiated by the external factor light, but endogenously mediated by the giant clam and/or its photosynthetic symbionts.

References

Aharon, P., 1991, Recorders of reef environment histories - stable isotopes in corals, giant clams and calcareous algae: Coral Reefs, v. 10, p. 71-90.

Batenburg, S.J., Reichart, G.J., Jilbert, T., Janse, M., Wesselingh, F.P., and Renema, W., 2011, Interannual climate variability in the Miocene: High resolution trace element and stable isotope ratios in giant clams: Palaeogeography, Palaeoclimatology, Palaeoecology, v. 306, p. 75-81.

Carré, M., Bentaleb, I., Bruguier, O., Ordinola, E., Barrett, N.T., and Fontugne, M., 2006, Calcification rate influence on trace element concentrations in aragonitic bivalve shells: Evidences and mechanisms: Geochimica et Cosmochimica Acta, v. 70, p. 4906-4920.

Driscoll, R., Elliot, M., Russon, T., Welsh, K., Yokoyama, Y., and Tudhope, A., 2014, ENSO reconstructions over the past 60ka using giant clams (*Tridacna sp.*) from Papua New Guinea: Geophysical Research Letters, v. 41, p. 6819-6825.

Elliot, M., deMenocal, P.B., Linsley, B.K., and Howe, S.S., 2003, Environmental controls on the stable isotopic composition of *Mercenaria mercenaria*: Potential application to paleoenvironmental studies: Geochemistry, Geophysics, Geosystems, v. 4, doi:10.1029/2002GC000425, 2003.

Elliot, M., Welsh, K., Chilcott, C., McCulloch, M., Chappell, J., and Ayling, B., 2009, Profiles of trace elements and stable isotopes derived from giant long-lived *Tridacna gigas* bivalves: Potential applications in paleoclimate studies: Palaeogeography, Palaeoclimatology, Palaeoecology, v. 280, p. 132-142.

Freitas, P., Clarke, J., Kennedy, H., Richardosn, C., and Abrantes, F., 2005, Mg/Ca, Sr/Ca, and stable isotope ($\delta^{18}O$ and $\delta^{13}C$) ratio profiles from the fan mussel *Pinna nobilis*: Seasonal records and temperature relationships: Geochemistry, Geophysics, Geosystems, v. 6 (4), doi: 10.1029/2004GC00872.

Gillikin, D.P., De Ridder, F., Ulens, H., Keppens, E., Baeyensa, W., and Dehairs, F., 2005, Assessing the reproducibility and reliability of estuarine bivalve shells (*Saxidomus giganteus*) for sea surface temperature reconstruction: Implications for paleoclimate studies: Palaeogeography, Palaeoclimatology, Palaeoecology, v. 228, p. 70- 85.

Gothmann, A., Stolarski, J., Adkins, J.F., Schoene, B., Dennis, K.L., Schrag, D.P., Mazur, M., and Bender, M.L., 2015, Fossil corals as an archive of secular variations in seawater chemistry since the Mesozoic: Geochimica et Cosmochimica Acta, v. 160, p. 188-208.

Griffiths, N., Müller, W., Johnson, K.G., and Aguilera, O.A., 2013, Evaluation of the effect of diagenetic cements on element/Ca ratios in aragonitic Early Miocene (~ 16 Ma) Caribbean corals: Implications for 'deep-time' palaeo-environmental reconstructions: Palaeogeography, Palaeoclimatology, Palaeoecology, v. 369, p. 185-200.

Kahn, P.G.K., and Pompea, S.M., 1978, Nautiloid growth rhythms and dynamical evolution of the Earth–Moon system: Nature, v. 275, p. 606- 611.

Klein, R.T., Lohmann, K.C., and Thayer, C., 1996, Sr/Ca and $^{13}C/^{12}C$ ratios in skeletal calcite of *Mytilus trossulus*: Covariation with metabolic rate, salinity, and carbon isotopic composition of seawater: Geochimica et Cosmochimica Acta, v. 60, p. 4207-4221.

Lorens, R.B., and Bender, M.L., 1980, The impact of solution chemistry on *Mytilus edulis* calcite and aragonite, Geochimica et Cosmuochimica Acta, v. 44, p. 1265-1278.

Marcano, M.C., Frank, T.D., Mukasa, S.B., Lohmann, K.C., and Taviano, M., 2015, Diagenetic incorporation of Sr into aragonitic bivalve shells: implications for chronostratigraphic and palaeoenvironmental interpretations: The Depositional Record, v. 1, p. 38–52.

Marshall, N., Manning, C., Novak, V., Warter, V., Renema, W., Anczkiewicz, R., Flecker, R., and Müller, W., in preparation, Navigating the waters of strontium isotope stratigraphy from the Miocene of Borneo.

Mayfield, A., and Gates, R., 2007, Osmoregulation in anthozoan-dinoflagellate symbiosis: Comparative Biochemistry and Physiology A, v. 147, p. 1-10.

Moberg, F., Nystrom, M., Kautsky, N., Tedengren, M. and Jarayabhand, P., 1997, Effects of reduced salinity on the rates of photosynthesis and respiration in the hermatypic corals *Porites lutea* and *Pocillopora damicornis*: Marine Ecology Progress Series, v. 157, p. 53-59.

Morley, R.J., and Morley , H.P., 2011, Neogene climate history of the Makassar Straits, Indonesia: Geological Society, London, Special Publications, v. 355; p. 319-332.

Romanek, C.S., and Grossman, E.L., 1989, Stable isotope profiles of Tridacna maxima as environmental indicators: PALAIOS, v. 4, p. 402–413.

Rösler, A., Pretković, V., Novak., V., Renema, W., and Braga, J.C., 2015, Coralline algae from the Miocene Mahakam Delta (East Kalimantan, Southeast Asia): Palaios, v. 30, p. 83-93.

Schöne, B.R., Zhang, Z., Radermacher, P., Thébault, J., Jacob,D.E., Nunn, E.V., and Maurer, A-F., 2011, Sr/Ca and Mg/Ca ratios of ontogenetically old, long-lived bivalve shells (*Arctica islandica*) and their function as paleotemperature proxies: Palaeogeography, Palaeoclimatology, Palaeoecology, v. 302, p. 52-64.

Scourse, J., Richardson, C., Forsythe, G., Harris, I., Heinemeier, J., Fraser, N., Briffa, K., Jones, P., 2006, First cross-matched floating chronology from the marine fossil record: data from growth lines of the long-lived bivalve mollusc *Arctica islandica*: The Holocene, v. 16, p. 967-974.

Stott, K.J., Austin, W.E.N., Sayer, M.D.J, Weidman, C.R., Cage, A.G. and Wilson, R.J.S., 2010, The potential of *Arctica islandica* growth records to reconstruct coastal climate in northwest Scotland, UK: Quaternary ScienceReviews, v. 29, p. 1602–1613.

Warter, V., Müller, W., Wesselingh, F.P., Todd, J.A., and Renema, W., 2015, Late Miocene seasonal to sub-decadal climate variability in the Indo-West Pacific (East Kalimantan, Indonesia) preserved in giant clams: Palaios, v. 30, p. 66-82, doi.org/10.2110/palo.2013.061.

Warter, V., and Müller, W., 2016, Daily growth and tidal rhythms in Miocene and modern giant clams revealed via ultra-high resolution LA-ICPMS analysis – A novel methodological approach towards improved sclerochemistry: Palaeogeography, Palaeoclimatology, Palaeoecology, doi:10.1016/j.palaeo.2016.03.019.

Welsh, K., Elliot, M., Tudhope, A., Ayling, B., Chappell, J., 2011, Giant bivalves (*Tridacna gigas*) as recorders of ENSO variability: Earth Planetary Science Letters, v. 307, p. 266-270.

Wells, J.W., 1963, Coral growth and geochronometry: Nature, v. 197, p. 448-950.

Contents of Appendix:

The attached DVD contains two excel spread sheets which relate to Chapter 3 (Warter et al., 2015) and Chapter 4 (Warter and Müller, 2016).

Appendix I (Warter et al., 2015):

Electronic Table A and B. B/Ca, Mg/Ca and Sr/Ca and $\delta^{18}O$ and $\delta^{13}C$ data sets corresponding to Fig. 9 (Table A) and Fig. 10 (Table B).

Supplementary data to this article can be found online at

http://www.sepm.org/pages.aspx?pageid5332

Appendix II (Warter and Müller, 2016):

Electronic Table S1 - S6. Complete LA-ICPMS data sets corresponding to the element/Ca profiles presented in Fig. 3, 5, 6, 7 and S3.

Supplementary data to this article can be found online at

http://dx.doi.org/10.1016/j.palaeo.2016.03.019